Aus der Orthopädischen Klinik und Poliklinik, Universitätsmedizin Rostock
(Direktor: Prof. Dr. med. Wolfram Mittelmeier)

Untersuchungen zu den Einflüssen von niederfrequenten elektrischen Wechselfeldern auf die Differenzierung humaner Osteoblasten und deren indirekter Effekt auf die Osteoklastogenese

Kumulative Dissertation
zur Erlangung des akademischen Grades
Doctor rerum humanarum (Dr. rer. hum.)
an der Medizinischen Fakultät der Universität Rostock

vorgelegt von
Franziska Sahm
aus Rostock
geb. am 26.06.1992 in Neubrandenburg

Rostock, 09.02.2023

https://doi.org/10.18453/rosdok_id00004573

Gutachter:

PD Dr. rer. hum. habil. Dipl. Biol. Anika Jonitz-Heincke, Universitätsmedizin Rostock, Orthopädische Klinik und Poliklinik, Forschungslabor für Biomechanik und Implantattechnologie (FORBIOMIT)

Prof. Dr.med. Rüdiger Köhling, Universitätsmedizin Rostock, Oscar Langendorff Institut für Physiologie

Dr.-Ing. Rainer Detsch, Friedrich-Alexander-Universität Erlangen-Nürnberg, Technische Fakultät, Department Werkstoffwissenschaften (WW), Lehrstuhl für Werkstoffwissenschaften (Biomaterialien)

Jahr der Einreichung: 2023
Jahr der Verteidigung: 2023

Inhalt

1 Einleitung

Knochen kann sich als Organ dauerhaft umbauen und erneuern, weshalb alle 10 Jahre von einer kompletten Regeneration des menschlichen Skelettes ausgegangen wird [1,2]. Störungen in den Knochenumbauprozessen können diese Selbstheilungseigenschaft verringern. Es wird angenommen, dass ca. 1,9 % bis 4,9 % der weltweiten Knochenbrüche nur schlecht oder gar nicht heilen [3]. Eine verbreitete Krankheit, hervorgerufen durch Störungen im Knochenstoffwechsel, ist die Osteoporose. Dabei verringert sich unter anderem die Knochenmineraldichte, die Knochenfestigkeit ist beeinträchtigt und die Knochenbeweglichkeit vermindert. Derzeit sind etwa 200 Millionen Menschen weltweit davon betroffen, wobei durchschnittlich jede zweite Frau und jeder vierte Mann über 50 Jahre eine osteoporotische Fraktur erleiden kann [4]. Die Herausforderung besteht darin, die Knochenregeneration bei Osteoporose und Knochenbrüchen zu unterstützen und die Einheilung notwendiger Implantate, z. B. künstlicher Gelenke, zu verbessern [5,6]. Eine Möglichkeit, dies zu erreichen, ist die Applikation externer elektrischer Felder [7].

1.1 Knochenumbau

Knochenaufbau und -abbau sind die beiden grundlegenden Prozesse des Knochenumbaus und somit essenziell für die Regeneration der Knochenstruktur [8]. Die entscheidenden Zelltypen sind die Osteoblasten und Osteoklasten (Abb. 1). Erstere differenzieren sich aus mesenchymalen Stammzellen und sind für die Bildung von Matrixproteinen und mineralisierter Knochenmatrix verantwortlich [8]. Durch die Sekretion von Kollagen I und nicht-kollagenen Proteinen wie Bone-Sialoprotein und Osteopontin (OPN) entsteht zunächst eine nicht mineralisierte extrazelluläre Matrix, das Osteoid [1]. Die Mineralisierung dieser komplexen Struktur ist die Grundlage für die späteren mechanischen Eigenschaften des Knochens. Während der Mineralisierung des Osteoids bilden sich Hydroxylapatitkristalle in Vesikeln der Osteoblastenmembran, die sich nach dem Durchbrechen der Vesikel in die extrazelluläre Matrix ausbreiten und zwischen den Kollagenfibrillen ablagern [9]. Durch die Expansion des Gewebes werden Osteoblasten in die Knochenmatrix eingeschlossen und können weiter in Osteozyten differenzieren [8]. Osteozyten agieren als Mechanosensoren im Knochen und sind Impulsgeber für Knochenumbauprozesse. Mit ihren langen und verzweigten zellulären Fortsätzen bilden sie ein komplexes Netz durch den Knochen, wodurch die Signaltransduktion zu benachbarten Zellen möglich ist. Durch das Ausschütten von Signalstoffen durch die Osteozyten wird die Aktivität von Osteoblasten und Osteoklasten beeinflusst [10]. Letztere sind die Antagonisten der Osteoblasten und resorbieren die Knochenmatrix, was zur Freisetzung von Knochenproteinen führt. Die Ansäuerung der Knochenmatrix führt zur Zersetzung der anorganischen Komponenten, wobei die Carboanhydrase II (CA2) eines der wichtigsten Enzyme für die Regulierung des sauren pH-Wertes ist. Durch die Freisetzung von Enzymen wie Cathepsin K (CTSK) und Matrix-Metallopeptidase 9 (MMP-9) werden die organischen Komponenten des Knochens abgebaut [11]. Osteoklasten entstehen aus dem Zusammenschluss mononuklearer Zellen der

hämatopoetischen Stammzelllinie zu multinuklearen Zellen. Verschiedene Signalkaskaden können diese Differenzierung aktivieren, wobei zwei Signalwege eine übergeordnete Rolle einnehmen: der Receptor activator of NF-κB (RANK)-Receptor activator of NF-κB ligand (RANKL)-Osteoprotegerin (OPG)-Signalweg und der Macrophage colony-stimulating factor (M-CFS)-Colony stimulating factor 1 receptor (CSF1R)-Signalweg [1,8] (Abb. 1). Nur mittels einer erfolgreichen Aktivierung der Osteoklastenvorläuferzellen ist eine Regeneration des Knochengewebes möglich.

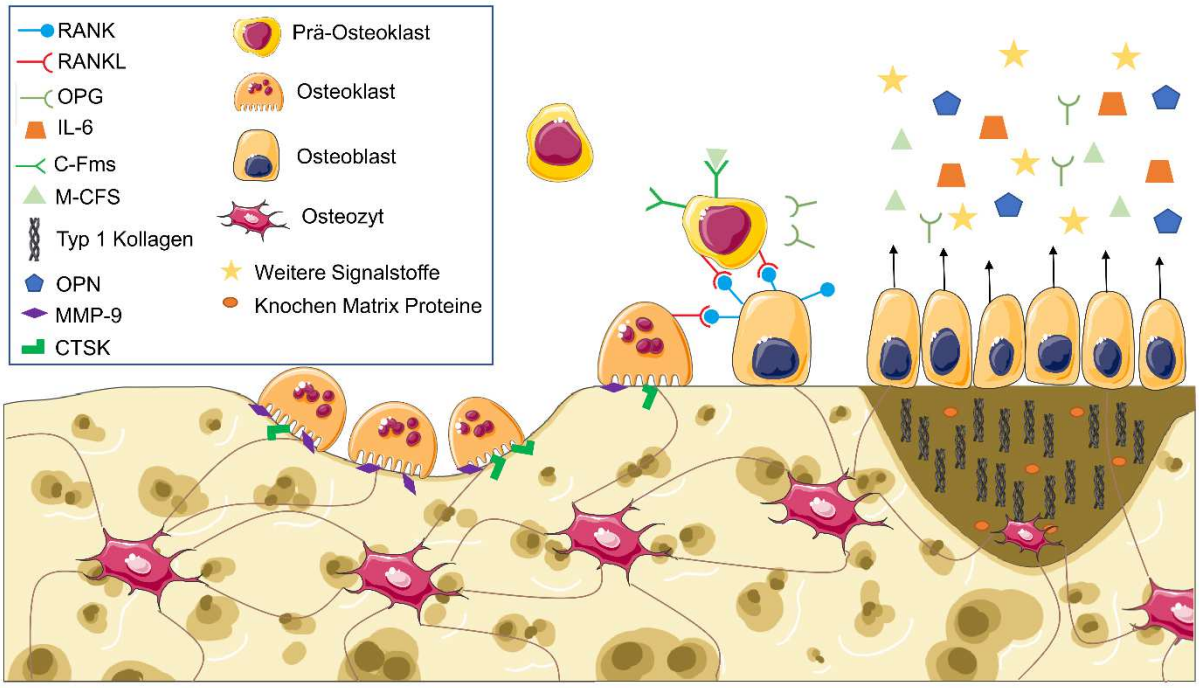

Abbildung 1: Schematische Darstellung des Knochenumbaus mit Prä-Osteoklasten, Osteoklasten, Osteoblasten und Osteozyten inklusive Signaltransduktionswegen. Osteoblasten bauen neue Knochenmatrix auf und produzieren Zytokine sowie weitere Signalstoffe, die unter anderem mit den Osteoklasten und den Prä-Osteoklasten interagieren. Osteoklasten geben Enzyme für die Degradation der extrazellulären Matrix ab. Osteozyten sind in der Knochenstruktur integriert bzw. werden durch die neu gebildete Matrix der Osteoblasten eingemauert. Die zellulären Fortsätze dienen der Signaltransduktion unter den Zellen. Einzelne Bilder von Servier Medical Art (http://smart.servier.com/, Zugriff am 08/06/2022) lizensiert mit Creative Commons Attribution 3.0 Unported License (https://creativecommons.org/licenses/by/3.0/).

1.2 Knochenregeneration mittels elektrischer Stimulation

Das Entstehen endogener elektrischer Felder im Knochen durch mechanische Belastung wurde von Fukada und Yasuda 1957 als eine Form des piezoelektrischen Effekts beschrieben [12]. Durch die Einwirkung externer mechanischer Belastungen wird der Knochen elastisch verformt, wodurch sich die elektrische Polarisation im Knochen verändert und ein elektrisches Feld entsteht [13] (Abb. 2). Bei der Dehnung des Knochens entstehen positive Ladungen, wodurch die Knochenresorption angeregt wird. Die Kompression des Knochens, aber auch Knochenverletzungen und Mikrofrakturen führen zu negativen Ladungen und zur Knochenformation [14–16]. Durch das Anlegen von äußerer elektrischer Ladung kann dieser Prozess umgekehrt werden, was als inverser piezoelektrischer Effekt bezeichnet wird. Die Applikation elektrischer Felder kann somit für die aktive Knochenheilung genutzt werden [17]. In klinischen Anwendungen der elektrischen Stimulation (ES) wurden positive Effekte in der

Knochenheilung von Pseudoarthrosen, Knöchel- und Fußgelenksverbindungen, Wirbelsäulenfusionen und Hüftkopfnekrosen beobachtet [15,17,18].

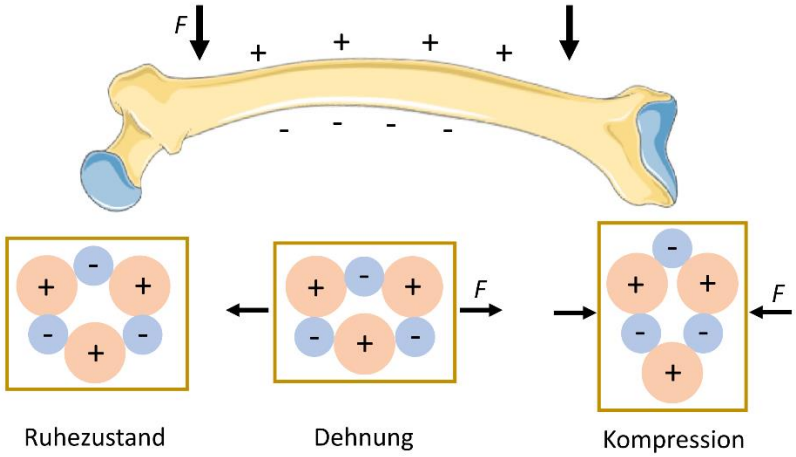

Abbildung 2: Schematische Darstellung des Piezoeffekts im Knochen. Durch Krafteinwirkungen (*F*) werden Dehnung und Kompression des Knochens hervorgerufen, wodurch sich positive und negative Ladungen an der Oberfläche des piezoelektrischen Materials ausbilden. Die Polarisation entsteht durch die Verschiebungen der Ladungen, hervorgerufen durch die mechanische Belastung (nach [19,20]). Die Knochen-Darstellung stammt von Servier Medical Art (http://smart.servier.com/, Zugriff am 27/01/2022), lizensiert mit Creative Commons Attribution 3.0 Unported License (https://creativecommons.org/licenses/by/3.0/).

Es wird angenommen, dass Knochenzellen externe elektrische Signale wahrnehmen können [7]. Durch ES kann ein verändertes Migrations-, Proliferations-, Differenzierungs- und Aktivitätsverhalten der Knochenzellen beobachtet werden. Osteoblastische Zellen zeigen eine Erhöhung in der Produktion von Signalproteinen, der extrazellulären Matrix und Mineralisierungsprozessen [21–24]. Bei osteoklastischen Zellen konnten erhöhte Apoptoseraten sowie eine verringerte Osteoklastenbildung beobachtet werden [25–28]. Es wird vermutet, dass durch die ES die Neuanordnung und Diffusion elektrisch geladener Moleküle, Lipidstrukturen und Membranrezeptoren hervorgerufen wird und somit weitere intrazelluläre Reaktionen ausgelöst werden [24,29,30]. Eine andere Hypothese beschreibt die mögliche Reorganisation des Zytoskeletts durch ES und die Beeinflussung von spannungsgesteuerten Ionenkanälen, wobei der Calcium-Kanal eine zentrale Rolle bei der Untersuchung zellulärer Reaktionen einnimmt [24,31,32].

1.3 Anwendung elektrischer Stimulation

Um die Erzeugung elektrischer Felder und somit den Einfluss der ES auf Knochenumbauprozesse zu untersuchen, gibt es verschiedene Ansätze. Die ES kann durch induktive, kapazitive oder direkte Kopplung erfolgen. Bei der induktiven Kopplung werden gepulste elektromagnetische Felder über eine oder zwei Magnetspulen abgegeben, die über dem Knochendefekt oder den Knochenzellen platziert werden. Werden die Elektroden auf der Haut oberhalb des Knochendefekts oder ohne Kontakt zum Zellkulturmedium angebracht, wird von einer kapazitiven Kopplung gesprochen. Bei der direkten Kopplung werden die Elektroden invasiv auf den betroffenen Knochen oder in direktem Kontakt zu den Zellen und dem Zellkulturmedium platziert [15]. Häufig kommen für die ES von Knochen bzw. Knochenzellen direkte Stimulationssysteme mit Gleichstrom zur Anwendung [7]. Die

Verwendung von Gleichstrom kann jedoch zu unerwünschten Nebeneffekten wie einer Veränderung des pH-Wertes, der Anhäufung geladener Proteine an der Elektrodenoberfläche, der Bildung schädlicher faradayscher Nebenprodukte wie Wasserstoffperoxid und freien Metallionen sowie weiteren elektrochemischen Reaktionen führen [22,29,33,34]. Durch das Anlegen eines biphasischen Stroms, wie Wechselstrom, können diese unerwünschten Nebeneffekte vermindert werden [7].

2 Motivation und Fragestellung

Trotz klinischer Erfolge sind die grundlegenden zellulären Prozesse der Wirkungsweise von ES auf Knochenumbauprozesse noch nicht vollständig verstanden. Ein besseres Grundlagenverständnis ist jedoch notwendig, um klinische Anwendungen zu verbessern, effektiv auf Patienten abzustimmen und Heilungschancen zu erhöhen. In bisherigen In-vitro-Studien wurde eine Vielzahl unterschiedlicher Stimulationseinheiten und Stimulationsparameter verwendet, was eine Vergleichbarkeit dieser Studien sowohl untereinander als auch mit klinischen Arbeiten erschwert [35].

Die in dieser Dissertation beschriebenen elektrischen Stimulationseinheiten beruhen auf dem klinisch eingesetzten ASNIS-III s Schraubensystem, um eine Vergleichbarkeit mit In-vivo-Versuchen beizubehalten. Das Schraubensystem wurde modifiziert und für die In-vitro-Stimulation angepasst [36–38] [I, II]. Die erste In-vitro-Studie im Rahmen der vorliegenden Arbeit diente dem Vergleich verschiedener Eingangsspannungen und Stimulationsintervalle für die ES und deren Einfluss auf Osteoblasten. Weiterhin wurden Zellen in direktem Kontakt mit der Elektrode und in weiterer Entfernung untersucht, um den periprothetischen Spalt nachzubilden [I]. Der Einfluss der unterschiedlichen Positionierung der Zelle zur Stimulationseinheit wurde in [II] weiter vertieft, indem zwei verschiedene Abstände zur Elektrode gewählt wurden. Zudem lag der Fokus auf einer langfristigen Stimulation, um das Mineralisierungsverhalten und mögliche Langzeiteffekte von ES zu untersuchen. In-vitro-Langzeitstimulationen sind von besonderer Bedeutung, um eine bessere Vergleichbarkeit mit länger laufenden In-vivo-Studien zu erzeugen. Mithilfe einer Transkriptomanalyse sollten mögliche Signalkaskaden aufgezeigt werden, welche die Grundlage für weiterführende, zukünftige Studien bilden [II].

Da Knochenregeneration nicht nur von Osteoblasten, sondern auch von Osteoklasten abhängig ist, ist eine Untersuchung beider Zelltypen für ein besseres Verständnis der durch ES beeinflussten Knochenumbauprozesse essenziell. Deshalb wurde in einer dritten Studie der mögliche Einfluss der sekretierten Proteine der Osteoblasten auf osteoklastäre Zellen und Vorläuferzellen untersucht [III]. Somit konnten mögliche Veränderungen im Aktivitäts- und Differenzierungsverhalten der Zellen in Abhängigkeit vom Differenzierungsstatus während der Osteoklastogenese aufgezeigt werden [III].

Um eine bessere Vergleichbarkeit zu verschiedenen Studien zur ES zu gewährleisten, wurden experimentelle Validierungen der elektrischen Felder durchgeführt, und ein automatisiertes 3D-Validierungssystem wurde implementiert. Die somit gewonnenen Daten sind wichtig, um

numerische Simulationen von elektrischen Feldern zu verbessern und eine Vereinheitlichung von Parametern in Zellkultursystemen zu gewährleisten [II, IV].
Ziel dieser Arbeit ist es, mit den In-vitro-Stimulationssystemen Erkenntnisse über die Wirkung von elektrischen Feldern auf die zelluläre Aktivität und Differenzierung von Knochenzellen zu erhalten. Dafür wurden direkt gekoppelte, niederfrequente Wechselfelder appliziert. Durch die Verwendung einer Wechselspannung wurden mögliche Nebeneffekte durch die ES auch im Hinblick auf spätere klinische Anwendungen vermieden.

3 Material und Methoden

Die verwendeten Verbrauchsmaterialien und Geräte sowie die Protokolle sind im Detail mit den Herstellerangaben in den Publikationen [I] bis [IV] aufgeführt.

3.1 Zellkultur

Alle Zellen und Versuchsreihen wurden unter Standardkulturbedingungen bei 37 °C, 5 % CO_2 und 21 % O_2 kultiviert.
Humane Prä-Osteoblasten wurden aus Femurköpfen von Patienten isoliert, die einen Hüftgelenkersatz erhielten [39]. Zuvor wurde die Zustimmung der Patienten nach Genehmigung durch die lokale Ethikkommission (Registrierungsnummer A 2010-0010) eingeholt. Die Zellen wurden isoliert, kultiviert und bis zum Beginn der Versuchsreihen kryokonserviert. Prä-Ostoblasten in der dritten Passage wurden für die Zellkultivierung verwendet [I-III]. Die Kultivierung erfolgte in Dulbecco's Modified Eagle Medium (DMEM) ohne $CaCl_2$, um die Proliferation anzuregen, unter Zugabe von 10 % fötalem Kälberserum, 1 % Amphotericin B, 1 % Penicillin-Streptomycin und 1 % HEPES Puffer. Ascorbinsäure (finale Konzentration: 50 µg/ml), β-Glycerophosphat (finale Konzentration: 10 mM) und Dexamethason (finale Konzentration: 100 nM) wurden als Differenzierungsfaktoren hinzugefügt. Für die Untersuchung der Mineralisierungsprozesse wurde $CaCl_2$ in einer Konzentration von 1,8 mM hinzugefügt.
Humane mononukleare Zellen des peripheren Blutes (PBMCs) wurden aus *Buffy-Coats* von anonymisierten Vollblutspenden des Instituts für Transfusionsmedizin der Universitätsmedizin Rostock gewonnen (Ethikvotum A2011-140). Die Zellen wurden isoliert und für 7 d im Roswell Park Memorial Institute (RPMI) 1640 Medium mit 2 % fötalem Kälberserum, 2 % Glutamin und 1 % Penicillin-Streptomycin kultiviert. Es wurden 100.000 Zellen in jedes Well einer 48-Well-Platte gesät und in PBMCs oder Prä-Osteoklasten unterteilt [III].

3.2 Elektrische Stimulation

3.2.1 Stimulationssysteme

Für die Stimulationsexperimente wurden zwei verschiedene Stimulationssysteme verwendet: ein 1-Well-System und ein 6-Well-System, wobei das 6-Well-Stimulationssystem eine Weiterentwicklung des 1-Well-Systems darstellt (Abb. 3). Beide Systeme bestehen aus zwei Ti-6Al-4V Elektroden, die durch einen Isolator aus Polyetheretherketon voneinander getrennt

sind. Im 1-Well-System besitzen die Elektroden eine Prismenform mit einer angerauten Oberfläche (*Rz*: 21.38 ± 4.67 µm [36]), um die Kultivierung von Zellen auf der Elektrode zu ermöglichen [36]. Durch die Größe der Elektrode ist ein speziell angefertigtes Kultivierungsgefäß notwendig. Zellen können auf der Elektrode und unter der Elektrode auf dem Gefäßboden kultiviert werden (Abb. 3A) [I]. Um den Durchsatz zu erhöhen, wurde das System verkleinert, und die Größe wurde auf eine handelsübliche 6-Well-Zellkulturplatte angepasst. Dabei wurde für die Elektroden eine zylindrische Form gewählt (Abb. 3B). Durch die Elektrodenhalterung konnten zwei verschiedene Abstände zum Boden der Zellkulturplatte eingestellt werden, um zwei verschiedene elektrische Felder zu erzeugen. Eine Kultivierung auf der Elektrode war im 6-Well-System nicht möglich [II].

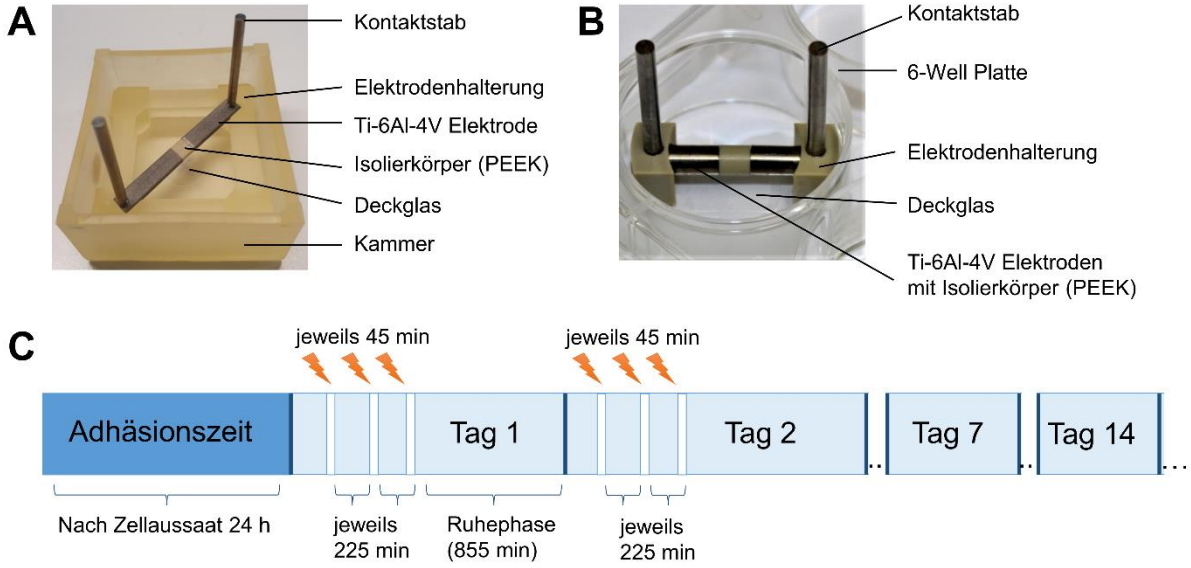

Abbildung 3: Darstellung der elektrischen Stimulationssysteme und des Stimulationsprotokolls **(A)** 1-Well-Stimulationssystem mit größeren, prismenförmigen Ti-6Al-4V Elektroden, Isolierkörper aus Polyetheretherketon (PEEK) und einer dazu entwickelten Kultivierungskammer [36]. **(B)** 6-Well-Stimulationssystem mit zylindrischen Ti-6Al-4V Elektroden und Isolierkörper aus PEEK für die Verwendung in einer Standard-6-Well-Zellkulturplatte [37] [II]. **(C)** Stimulationsprotokoll der nicht-kontinuierlichen Stimulation. Nach 24 h Adhäsionszeit wird an jedem darauffolgenden Tag 3 x 45 min stimuliert.

3.2.2 Stimulationsprotokolle

Für die ES im 1-Well-Stimulationssystem wurden humane Osteoblasten auf Kollagen-beschichtete Deckgläser (Durchmesser: 12 mm) mit einer Dichte von $2{,}2 \times 10^4$ Zellen/cm^2 und auf Ti-6Al-4V-Elektroden mit einer Dichte von $3{,}0 \times 10^4$ Zellen/cm^2 ausgesät. Es wurden eine Frequenz von 20 Hz und Wechselspannungen von 0,2 V, 1,4 V und 2,8 V verwendet. Alle Einheiten der verwendeten Spannungen sind als V≡V_{eff} (Volt Effektivwert) angegeben. Die Spannung wurde 3 x 45 min/d mit 225 min Pause zwischen den Stimulationen (0,2 V, 1,4 V, 2,8 V, Abb. 3C) oder kontinuierlich mit 1,4 V (kont. 1,4 V) über 1, 3 und 7 d angelegt. Als Kontrollen dienten Osteoblasten auf Elektroden und Deckgläsern, bei denen keine Spannung angelegt wurde [I].

Im 6-Well-System wurde eine Wechselspannung von 0,7 V und 20 Hz angelegt, und die Zellen wurden ebenso auf Kollagen-beschichtete Deckgläser gesät. Die Zelldichte betrug

1,7 x 10^4 Zellen/cm^2. Durch das Variieren des Elektrodenhalters von 1 mm und 3 mm Abstand zwischen den Elektroden und dem Boden der Zellkulturplatte entstanden zwei unterschiedliche elektrische Felder [II]. Dadurch wurde der in vivo vorliegende periprothetische Spalt zwischen Elektrode und umgebendem Gewebe imitiert. Stimuliert wurde 3 x 45 min/d mit 225 min Pause zwischen den Stimulationen für 1, 3, 7, 14, 21, 28 und 31 d (Abb. 3C) [II]. Als Kontrolle dienten Osteoblasten, die für denselben Zeitraum mit dem gleichen System ohne das Anlegen elektrischer Felder kultiviert wurden.

3.3 Indirekte Stimulation

Für die indirekte Stimulation wurden Zellkulturüberstande von Osteoblasten gesammelt, die 7, 14 und 21 d mit 0,7 V und 20 Hz mit dem 6-Well-Stimulationssystem stimuliert wurden. Diese werden als elektrisch stimulierte Osteoblasten (ESO) bezeichnet. Die dazugehörigen Kontrollen sind die nicht elektrisch stimulierten Osteoblasten (NSO), die für denselben Zeitraum mit dem gleichen System ohne das Anlegen elektrischer Felder kultiviert wurden. Zellüberstände von verschiedenen Spenderzellen wurden gepoolt und 1:1 mit frischem RPMI 1640 Medium gemischt.

Für die indirekte Stimulation wurden die erhaltenen PBMCs zunächst weitere 72 h kultiviert und die Prä-Osteoklasten 14 d mit 25 ng/ml M-CSF und 50 ng/ml RANK differenziert. Die Inkubation mit den Osteoblasten-Überständen erfolgte jeweils über 48 h [III].

3.4 Biochemische Nachweismethoden

3.4.1 Viabilität

Die Viabilität der Zellen wurde mittels des WST-1 Assays bestimmt und auf die jeweilige Kontrolle bezogen. Zuvor wurde das WST-1 Reagenz 1:10 mit RPMI vermischt und 30 min bei 37 °C und 5 % CO_2 inkubiert. Der entstandene Farbumschlag wurde bei 450 nm quantifiziert [III].

3.4.2 Genexpressionsanalysen

Für die Genexpressionsanalysen wurde zunächst die RNA stimulierter und unstimulierter Zellen isoliert. Dies erfolgte zum einen durch Lyse mit TriReagent® und anschließende Isolation mit dem Direct-zol™ RNA MiniPrep Kit gemäß den Anweisungen des Herstellers [I]. Zum anderen wurde das peqGOLD Total RNA Kit für die RNA-Isolation verwendet [II, III]. Die erhaltene RNA wurde mittels des High Capacity cDNA Reverse Transcription Kit in cDNA umgeschrieben. Die Analyse der Expression verschiedener Gene erfolgte mit dem innuMIX qPCR MasterMix SyGreen Kit. Die verwendeten Primersequenzen sind den jeweiligen Veröffentlichungen zu entnehmen [I-III].

3.4.3 Transkriptomanalyse

Für die Transkriptomanalyse wurde ein RNA-Pool von 3 Osteoblasten-Spendern erstellt, die 7 d oder 28 d unter Verwendung des 1 mm Abstandes stimuliert wurden. Zudem wurde die jeweilige Kontrolle mitgeführt. Die Analyse erfolgte durch ATLAS Biolabs. Die Auswertung erfolgte wie in [II] beschrieben in Kooperation mit dem Lehrstuhl für Modellierung und

Simulation, Universität Rostock. Für 55335 RNA-Transkripte wurden die Fold-Change-Werte bestimmt und die normalisierten, logarithmierten Werte für die weitere Auswertung verwendet. MiRNA und Transkripte mit fehlender Genbeschreibung oder GO-Annotation, die sich auf biologische oder molekulare Funktionen beziehen, wurden für die Signalwegsbestimmung nicht berücksichtigt. Die *Pathway Enrichment Analysis* wurde mit dem g:profiler und EnrichmentMap-Pipeline durchgeführt. Der daraus resultierenden *gene enrichment map* wurde mit Cytoscape Version 3.9.1 visualisiert [II].

3.4.4 Bestimmung von Zytokinen im Zellkulturüberstand

Die Konzentrationen des Typ I C-terminalen Collagen Propeptide (CICP) und Osteopontin (OPN) wurden aus dem Überstand mithilfe von Enzyme-linked Immunosorbent Assay (ELISA) untersucht. Weitere Analysen von Zytokinen erfolgten mit humanen BioLegend's LEGENDplex™ Multiplex Assays [II].

Die gemessenen Proteinkonzentrationen wurden auf die jeweilige Gesamtprotein-konzentration bezogen, die mit dem Qubit Protein Assay Kit bestimmt wurde [III].

3.4.5 Mineralisierungskapazität

Die Mineralisierungskapazität von langzeitstimulierten Prä-Osteoblasten wurde auf den Zellen bestimmt [II]. Dafür wurde der Zellmonolayer zunächst mit PFA fixiert und mit deoinisiertem H_2O gewaschen. Die mineralisierte extrazelluläre Matrix wurde mit Alizarin-Rot angefärbt und getrocknet, und es wurden Fotos vom jeweiligen Deckglas erstellt. Die Auswertung erfolgte durch die Bestimmung des Anteils der angefärbten Matrix mittels Image J Fiji [II].

3.4.6 Statistik

Für die statistische Auswertung der Versuche wurde GraphPad PRISM (GraphPad Software, San Diego, CA, USA) verwendet. Die genauen statistischen Tests sind den jeweiligen Veröffentlichungen zu entnehmen. *P*-Werte kleiner als 0,05 wurden als signifikant eingestuft. Die Daten wurden in *Boxplots* und *Heatmaps* dargestellt. In den Boxplots wurden der Median, das 25 %- und 75 %-Quartil sowie die Whisker für das Minimum und Maximum dargestellt. Die *Heatmaps* zeigen den Median, während eine Hochregulierung mit einem höheren Median als entsprechende Kontrolle in blau und eine Herabregulierung mit einem niedrigeren Median in orange dargestellt ist.

3.5 Experimentelle Validierung und numerische Simulation elektrischer Wechselfelder

Die automatisierte Validierung und Simulation erfolgten in Kooperation mit dem Institut für Allgemeine Elektrotechnik, Universität Rostock. Es wurde das elektrische Feld des 6-Well-Systems mit 0,7 V, 20 Hz und 1 mm Abstand untersucht. Die manuelle Messung erfolgte mit einer monopolaren Platin-/Iridium-Elektrode und einem Raster mit Abständen von je 2 mm zwischen den Messpunkten. Die detaillierte Beschreibung der Durchführung ist im Anhang dargestellt. Die Durchführung der numerischen Simulation ist in Studie [II] und die Auswertung der automatischen Messung in [IV] veröffentlicht.

4 Ergebnisse

4.1 Untersuchung der Auswirkungen verschiedener elektrischer Wechselfelder auf die Differenzierung von Osteoblasten [I]

Um optimale Stimulationsbedingungen für die Differenzierung von Osteoblasten zu identifizieren, wurden elektrische Spannungen von 0,2 V, 1,4 V und 2,8 V für eine Stimulation von 3 x 45 min/d verwendet. Zudem wurde für 1,4 V eine diskontinuierliche Stimulation von 3 x 45 min/d mit einer kontinuierlichen Stimulation verglichen. Für die Untersuchungen wurden humane Prä-Osteoblasten auf der Stimulationselektrode sowie unterhalb der Elektrode auf einem mit Kollagen I beschichteten Deckglas gesät. Die vollständigen Ergebnisse sind der Publikation [I] zu entnehmen.

Es wurden keine signifikanten Unterschiede in der Morphologie und Zellzahl beobachtet [I]. Ein Einfluss der Stimulation zeigte sich jedoch in den Genexpressionsdaten von Kollagen I (*COL1A1*) und Alkalischer Phosphatase (*ALPL*) (Abb. 4). Zellen, die mit 0,2 V auf der Elektrode stimuliert wurden, wiesen eine Hochregulierung von ALPL nach 1 d und von COL1A1 nach 3 d Stimulation auf. Eine Spannung von 1,4 V führte zu einer signifikanten Erhöhung von *COL1A1* und *ALPL* nach 3 d in Zellen, die auf dem Deckglas stimuliert wurden. Die kontinuierliche Stimulation mit 1,4 V zeigte keine erhöhten Genexpressionsdaten im Vergleich zur diskontinuierlichen Stimulation. Im Vergleich zur Kontrolle verringerte sich die *ALPL*-Expression der Zellen auf dem Deckglas signifikant nach 7 d. Am auffälligsten war die Stimulation mit 2,8 V mit einer erhöhten Expression von *COL1A1* und *ALPL* in Zellen auf der Elektrode nach 1 d Stimulation und einer verminderten Expression nach 3 und 7 d. Ebenso konnte ein mit der Zeit abnehmender Verlauf in der Genexpression von *COL1A1* und *ALPL* für Osteoblasten auf dem Deckglas beobachtet werden (Abb. 4).

Die kontinuierliche Stimulation zeigte gegenüber der diskontinuierlichen Stimulation keine Vorteile, daher wurden weiterführende Versuche mit einer Stimulation von 3 x 45 min/d durchgeführt. Stimulationen mit 1,4 V und 0,2 V erzielten Erhöhungen in der Expression von Differenzierungsgenen in Osteoblasten und in den dazugehörigen Proteinkonzentrationen [I]. Für weiterführende Stimulationsstudien wurde eine gemittelte Eingangsspannung von 0,7 V gewählt.

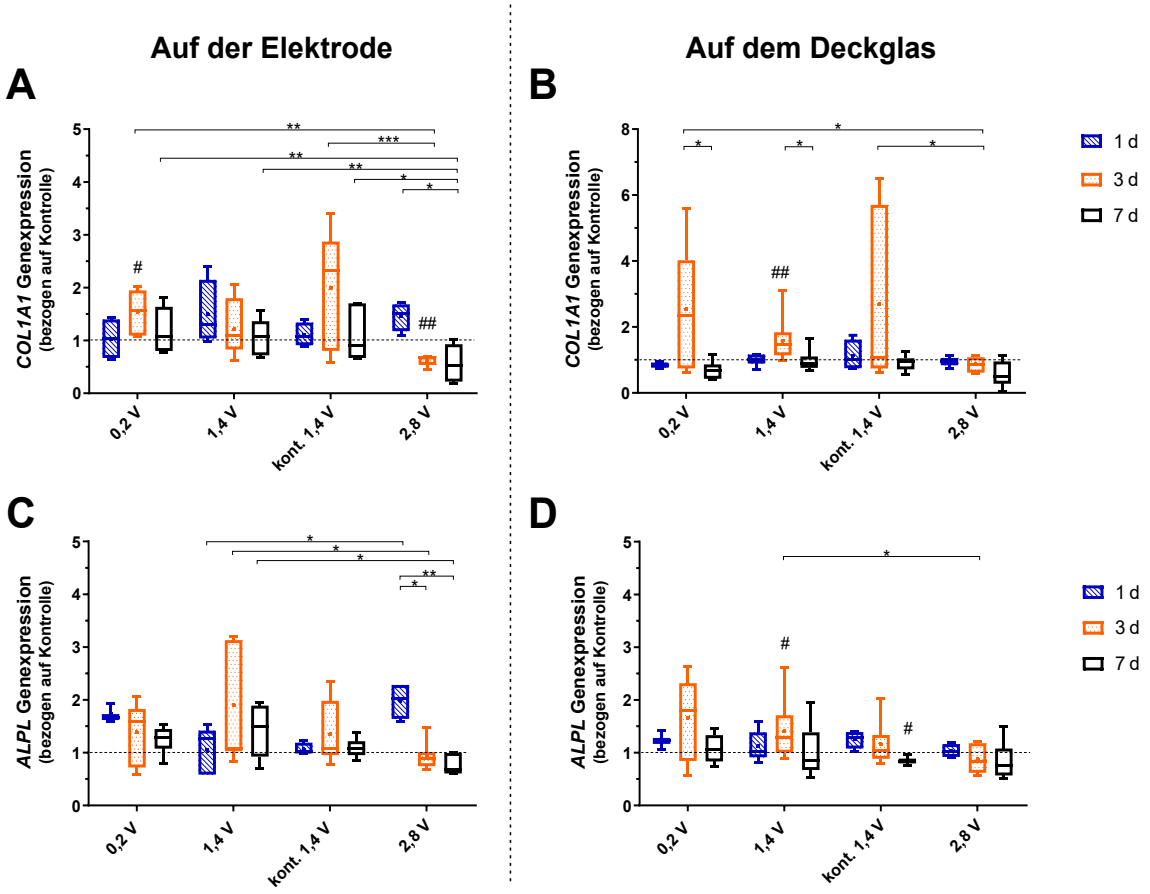

Abbildung 4: Genexpressionsdaten bezogen auf die unstimulierte Kontrolle. Zellen wurden auf T-i6Al-4V (A, C) oder auf kollagenbeschichteten Deckgläsern (B, D) kultiviert. $2^{-\Delta\Delta Ct}$ Werte wurden für Kollagen I (*COL1A1*; A, B), Alkalische Phosphatase (*ALPL*; C, D) nach 1, 3 und 7 d erhoben [$n \geq 3$]. Die 0,2 V-, 1,4 V- und 2,8 V-Gruppen wurden 3 × 45 min und die kont. 1.4 V-Gruppe kontinuierlich mit 1,4 V stimuliert. # zeigt signifikante Unterschiede zwischen der stimulierten Gruppe und der Kontrollgruppe an: # $p < 0{,}05$ und ## $p < 0{,}01$ (Wilcoxon-Test), * zeigt signifikante Unterschiede zwischen den Stimulationsgruppen an: * $p < 0{,}05$, ** $p < 0{,}01$, *** $p < 0{,}001$ (Two-Way ANOVA).

4.2 Langzeitstimulation von Osteoblasten über 31 Tage [II]

Die Langzeitstimulation von Osteoblasten erfolgte mit dem 6-Well-Stimulationssystem mit den zuvor bestimmten Stimulationsparametern. Die ausführlichen Ergebnisse sind in Publikation [II] dargestellt.

4.2.1 Zellvitalität und Mineralisierung

Durch das Einstellen von zwei unterschiedlichen Abständen zwischen dem Zellkulturplattenboden und der Elektrode war es möglich, zwei verschiedene elektrische Feldstärken zu erzeugen. Der kleine Abstand von 1 mm führte zu einem größeren elektrischen Feld (HEF) mit einem simulierten elektrischen Feld von bis zu 150 V/m. Der größere Abstand von 3 mm führte zu einem kleineren elektrischen Feld (LEF) mit einem simulierten elektrischen Feld mit bis zu 100 V/m [II]. Es konnte eine erhöhte Vitalität der Osteoblasten nach 1 d für das HEF und nach 3 d für das LEF beobachtet werden. Ab 3–31 d wirkten sich die Stimulationen nicht auf die Zellvitalität aus [II]. Dafür konnte mit fortschreitender Kultivierung eine zunehmende Mineralisierung auf den Zellen festgestellt werden (Abb. 5). Im Vergleich

zur unstimulierten Kontrolle wurden vermehrte Calciumablagerungen bei der Verwendung des LEF gefunden. Erhöhte Mengen konnten nach 7, 14, 21, 28 und 31 d beobachtet werden, wobei der Unterschied zur Kontrolle nach 14, 28 und 31 d signifikant war. Zellen, die mit dem HEF stimuliert wurden, zeigten keine signifikant erhöhte Mineralisierungskapazität (Abb. 5).

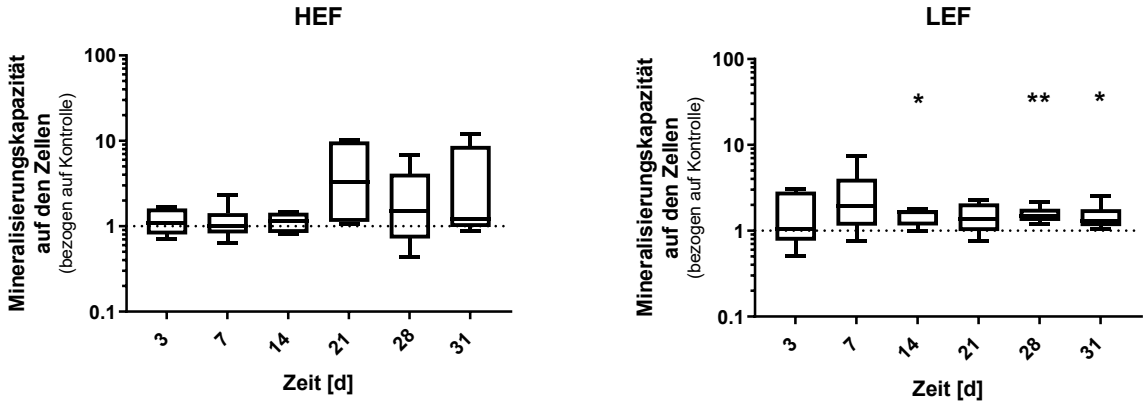

Abbildung 5: Mineralisierungsverhalten von humanen Osteoblasten unter ES. Osteoblasten wurden über 31 d mit zwei verschiedenen elektrischen Feldern (höheres elektrisches Feld – HEF, niedrigeres elektrisches Feld – LEF) und ohne ES (Kontrolle) stimuliert. Die Analysezeitpunkte waren 3, 7, 14, 21, 28 und 31 d, wobei die Untersuchungen 20 h nach Beginn des letzten Stimulationsintervalls durchgeführt wurden. Zur Bestimmung der Menge der Calciumablagerungen wurde diese mit Alizarin-Rot angefärbt und fotografiert. Der Anteil des gefärbten Bereiches wurde mit ImageJ bestimmt und auf die Kontrolle bezogen [$n \geq 5$]. Die signifikanten Unterschiede zwischen der jeweiligen Stimulationsgruppe und der Kontrolle wurden mit dem gepaarten t-Test (normalverteilt) oder Wilcoxon-Test (nicht normalverteilt) bestimmt. * zeigt signifikante Unterschiede zwischen den stimulierten Gruppen und den Kontrollgruppen: * $p < 0{,}05$, ** $p < 0{,}01$.

4.2.2 Proteinbestimmung in den Zellüberständen

Um die Bildung des Osteoids zu untersuchen, wurde CICP in den Überständen der stimulierten Osteoblasten nachgewiesen. Eine Hochregulierung von CICP konnte durch die Stimulation mit dem HEF nach 1 und 3 d festgestellt werden. Das LEF führte zu einer tendenziellen Herabregulation von CICP nach 31 d. Weiterhin erfolgte die Analyse von OPN, Osteoprotegerin (OPG), Interleukin-6 (IL-6) und des Dickkopf-verwandten Proteins 1 (DKK-1) in den Überständen (Abb. 6A). Zellen, die mit dem HEF stimuliert wurden, zeigten eine signifikant erhöhte Konzentration von OPG und IL-6 nach 14 und 21 d im Vergleich zur unstimulierten Kontrolle. Eine signifikant höhere Konzentration von OPN konnte ebenso nach 21 d gemessen werden. Die Stimulation mit dem LEF führte zu einer Veränderung in der OPN- und OPG-Konzentration, die schon nach 3 d Stimulation beobachtet wurde. Nach 7 d war OPG leicht erhöht, DKK-1 zudem signifikant hochreguliert. OPN wies nach 14 d Stimulation mit LEF eine signifikant verringerte Konzentration auf. Nach 31 d war OPN signifikant und IL-6 tendenziell herunterreguliert (Abb. 6A).

4.2.3 Transkriptomanalyse

Eine Transkriptomanalyse erfolgte nach 7 d und 28 d Stimulation, um einen besseren Überblick über regulierte Gene zu erhalten. Die Aktivität verschiedener Signalwege in Abhängigkeit zur Stimulationszeit konnte nachgewiesen werden (Abb. 6B). Die Stimulation über 7 d führte unter anderem zu einer Herunterregulierung verschiedener Signal- und G-

Protein-gekoppelter Rezeptoren (GPCR). Die Stoffwechselprozesse von Prostaglandin, Eicosanoid, ungesättigten Fettsäuren und Prostanoid wurden hochreguliert. Nach einer Stimulation über 28 d konnte eine verstärkte zelluläre Reaktion auf Stimuli und Stress nachgewiesen werden. Zudem nahmen unterschiedliche Lokalisierung- und Lokomotions-Reaktionen sowie Bewegungsreaktionen von Zell- oder subzellulären Komponenten zu (Abb. 6B).

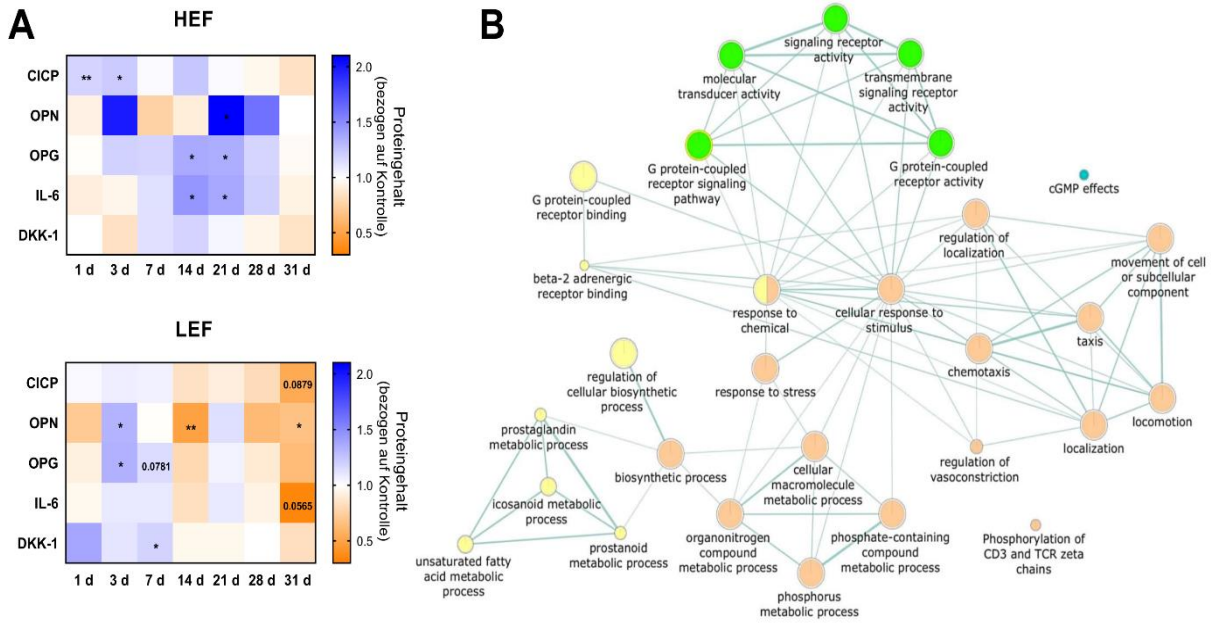

Abbildung 6: Sekretion von Proteinen durch Osteoblasten und Transkriptomanalyse von 7 d und 28 d HEF. Die Osteoblasten wurden insgesamt über 31 d stimuliert (höheres elektrisches Feld (HEF), niedrigeres elektrisches Feld (LEF), Kontrolle), wobei die Tests 20 h nach Beginn des letzten Stimulationsintervalls durchgeführt und auf die nicht stimulierte Kontrolle bezogen wurden. (**A**) Die Proteingehalte wurden aus dem Überstand ermittelt, auf den Gesamtproteingehalt des Überstands bezogen und zur Kontrolle ins Verhältnis gesetzt. Die Ergebnisse sind als Mediane in *Heatmaps* dargestellt, wobei die Herabregulierung in orange [< 1], die Hochregulierung in blau [> 1] und eine ähnliche Proteinkonzentration wie bei der Kontrolle in weiß [= 1] gekennzeichnet ist [$n \geq 5$]. Die signifikanten Unterschiede zwischen der jeweiligen Stimulationsgruppe und der Kontrolle wurden mit dem gepaarten t-Test (normalverteilt) oder dem Wilcoxon-Test (nicht normalverteilt) bestimmt. * zeigt signifikante Unterschiede zwischen den stimulierten Gruppen und den Kontrollgruppen: * $p < 0{,}05$, ** $p < 0{,}01$. (**B**) Transkriptomanalyse der isolierten RNA von 7 d und 28 d HEF und Kontrolle, ausgewertet nach den durch ES beeinflussten Signalwegen. Jeder Kreis steht für eine bestimmte molekulare oder biologische Funktion, und die Linien stellen die Anzahl der sich überschneidenden Gene dar. Gelbe und orangefarbene Kreise stehen für hochregulierte molekulare oder biologische Funktionen nach 7 (gelb) bzw. 28 d (orange) HEF-Stimulation. Grüne und blaue Kreise stehen für herunterregulierte molekulare oder biologische Funktionen nach 7 (grün) bzw. 28 d (blau) HEF-Stimulation.

4.3 Einfluss der indirekten Stimulation auf die Osteoklastogenese [III]

Die Überstände aus dem Langzeitversuch mit 0,7 V wurden für die indirekte Stimulation von Osteoklasten-Vorläufern und Prä-Osteoklasten verwendet. Gesammelt wurden die Überstände nach Stimulation mit dem HEF und LEF nach 7, 14 und 21 d. Als Kontrolle dienten die Überstände der unstimulierten Osteoblasten. Hierdurch sollte der Einfluss der elektrisch stimulierten Osteoblasten auf die Osteoklastogenese untersucht werden. Als Osteoklasten-Vorläufer wurden PBMCs untersucht und als Prä-Osteoklasten dienten PBMCs, die zuvor 14 d mit RANKL und M-CSF stimuliert wurden. Ausführliche Ergebnisse mit den HEF-Medien sind der Publikation [III] zu entnehmen. Aufgrund der geringeren Zellantwort wurden die Daten zu den LEF-Medien nicht veröffentlicht. Teile der Daten sind in Abbildung 7, 8 und 9 dargestellt.

4.3.1 Zellviabilität

Die Viabilität der PBMCs reduzierte sich durch den Einfluss der 7 d HEF- und LEF-Medien signifikant. Die Kultivierung mit den 14 d Überständen führte unter Verwendung der LEF-Überstände zu einer signifikanten Reduktion der Viabilität, die Reduktion der Viabilität von 14 d HEF war nicht signifikant. Überstände der 21 d ESO hatten keinen Einfluss auf die Viabilität der PBMCs. Die Caspase-8 (*CASP8)* Genexpression war unverändert. Prä-Osteoklasten wiesen keine Veränderung in der Viabilität nach der Kultivierung mit Überständen der 7 d und 14 d ESO auf. Mit den 21 d ESO-Medien konnte eine Erhöhung der Viabilität beobachtet werden. Die *CASP8* Genexpression war mit 21 d HEF signifikant herunterreguliert (Abb. 7).

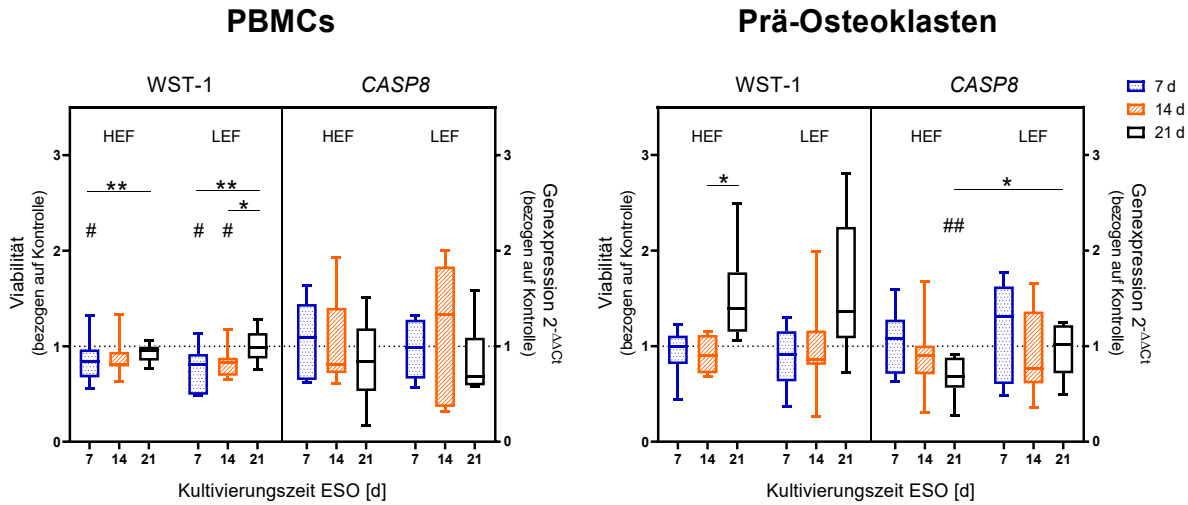

Abbildung 7: Relative Viabilität und *CASP8* Genexpression von PBMCs und Osteoklasten nach 48 h Inkubation mit gepooltem Überstand von Osteoblasten, die zuvor über 7, 14 und 21 d mit einem höheren elektrischen Feld (HEF), einem niedrigeren elektrischen Feld (LEF) und ohne elektrische Stimulation (Kontrolle) kultiviert wurden. Die Viabilität wurde mittels WST-1 Assay analysiert und, wie die *CASP8* Genexpression, auf die unstimulierte Kontrollgruppe der Osteoblasten bezogen [$n = 8$]. Die Signifikanzen wurden anhand der Zwei-Wege-ANOVA mit Tukey ermittelt. # zeigt signifikante Unterschiede zwischen den stimulierten Gruppen und den Kontrollgruppen an: # $p < 0,05$, ## $p < 0,01$; * zeigt signifikante Unterschiede zwischen den Stimulationszeitpunkten an: * $p < 0,05$, ** $p < 0,01$.

4.3.2 Expression von Osteoklastenmarkern bei PBMCs

Weiterhin wurden verschiedene Osteoklastenmarker untersucht. PBMCs, die mit 7 und 14 d HEF-Überständen kultiviert wurden, zeigten höhere Genexpressionen der tartratresistenten sauren Phosphatase Typ 5b (*ACP5*) im Vergleich zu 21 d. Ebenfalls war *MMP-9* nach der Kultivierung mit 7 d höher exprimiert als mit 21 d Medium. *CTSK* war im Vergleich zur Kontrolle nach 7 d signifikant erhöht. Die *RANK*-Expression wies wie bei *ACP5* einen signifikanten Unterschied zwischen 14 d und 21 d auf. Zudem unterschied sich die *RANK*-Expression zwischen den beiden elektrischen Feldern: 14 d HEF führte zu einer Erhöhung von *RANK* im Vergleich zu 14 d LEF. Mit dem 21 d Medium wurde dieser Effekt umgekehrt: PBMCs mit 21 d LEF zeigten eine höhere Expression von *RANK* im Vergleich zu PBMCs, die mit 21 d HEF-Überständen kultiviert wurden (Abb. 8). Das LEF-Medium begünstigte mit 7 d die

Überexpression von *ACP5* mit einem signifikanten Abfall bei 14 d sowie eine Erhöhung von *CTSK* mit 7 d im Vergleich zum 14 d Medium.

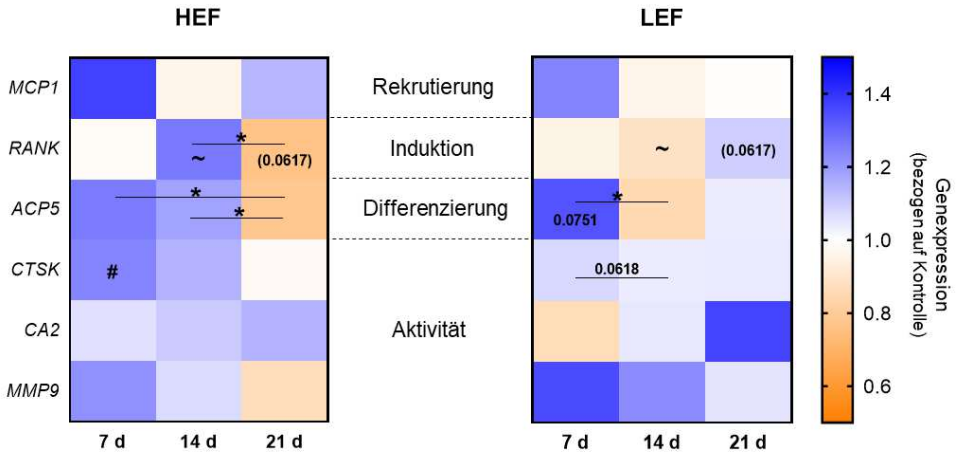

Abbildung 8: Genexpressionsdaten bezogen auf die unstimulierte Kontrolle. PBMCs wurden 48 h mit gepoolten Überständen von Osteoblasten inkubiert, die zuvor über 7, 14 und 21 d mit einem höheren elektrischen Feld (HEF), einem niedrigeren elektrischen Feld (LEF) und ohne elektrische Stimulation (Kontrolle) kultiviert wurden [n = 8]. Die Ergebnisse sind als Mediane in *Heatmaps* dargestellt, wobei die Herabregulierung in orange [< 1], die Hochregulierung in blau [> 1] und eine ähnliche Genexpression wie bei der Kontrolle in weiß [= 1] gekennzeichnet ist. Die Signifikanzen wurden mithilfe des Two-Way-ANOVA mit Tukey ermittelt. # zeigt signifikante Unterschiede zwischen den Stimulationen und der Kontrolle an: # $p < 0{,}05$; * zeigt signifikante Unterschiede zwischen den Stimulationszeitpunkten an: * $p < 0{,}05$; ~ zeigt signifikante Unterschiede zwischen HEF und LEF an: ~ $p < 0{,}05$.

4.3.3 Expression von Osteoklastenmarkern bei Prä-Osteoklasten

Während bei den PBMCs vermehrt die Genexpression von Induktions- und Differenzierungsmarkern reguliert wurde, konnten bei den Prä-Osteoblasten häufiger Expressionsänderungen bei Genen der Aktivität beobachtet werden. Überstände mit HEF führten zu einer erhöhten Expression von *CA2* und *MMP-9* mit 7 d im Vergleich zu 14 d und 21 d Medium. 7 d Medium führte zudem zu einer signifikant erhöhten Genexpression von *Monocyte chemoattractant protein 1* (*MCP1*) und *MMP-9* im Vergleich zur Kontrolle. Prä-Osteoklasten, die mit 21 d HEF-Medium kultiviert wurden, zeigten eine Reduktion in der Genexpression von *CASP8* und *CA2*. Unterschiede zwischen den elektrischen Feldern konnten in der Expression von *MCP1* festgestellt werden. Die *MCP1*-Expression war bei 7 d HEF signifikant höher als bei 7 d LEF. Die Kultivierung mit 7 d LEF-Medium führte zu einer erhöhten Expression von *CA2* und *MMP-9* im Vergleich zur Kontrolle und dem 14 d LEF-Medium. Das 21 d Medium reduzierte die Genexpression von *RANK* im Vergleich zu 14 d und von *CTSK* im Vergleich zur Kontrolle (Abb. 9).

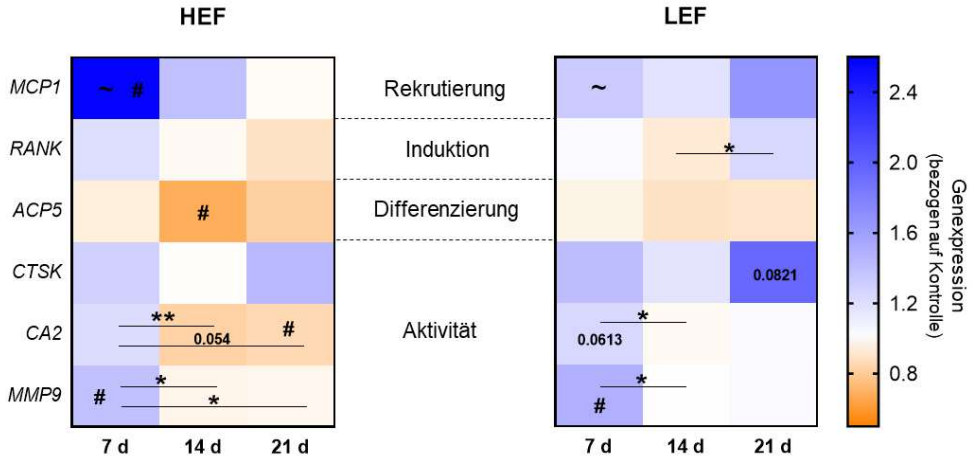

Abbildung 9: Genexpressionsdaten bezogen auf die unstimulierte Kontrolle. Prä-Osteoklasten wurden 48 h mit gepoolten Überständen von Osteoblasten inkubiert, die zuvor über 7, 14 und 21 d mit einem höheren elektrischen Feld (HEF), einem niedrigeren elektrischen Feld (LEF) und ohne elektrische Stimulation (Kontrolle) kultiviert wurden [n = 8]. Die Ergebnisse sind als Mediane in *Heatmaps* dargestellt, wobei die Herabregulierung in orange [< 1], die Hochregulierung in blau [> 1] und eine ähnliche Genexpression wie bei der Kontrolle in weiß [= 1] gekennzeichnet ist. Die Signifikanzen wurden mithilfe des Two-Way-ANOVA mit Tukey ermittelt. # zeigt signifikante Unterschiede zwischen den Stimulationen und der Kontrolle an: # < 0,05; * zeigt signifikante Unterschiede zwischen den Stimulationszeitpunkten an: * p < 0,05, ** p < 0,01; ~ zeigt signifikante Unterschiede zwischen HEF und LEF an: ~ p < 0,05.

4.4 Bestimmung elektrischer Felder [IV]

Um genaue Informationen über die entstehenden elektrischen Felder zu erhalten, wurden Versuche zur numerischen Simulation und experimentellen Validierung durchgeführt. Zur Bestimmung der elektrischen Felder wurden elektrische Potenziale an definierten Positionen innerhalb der Zellkulturplatte gemessen, um weiterführend das elektrische Feld (in V/m) zu berechnen. Diese Daten wurden mit Simulationsdaten verglichen [II, IV].

In Vorarbeiten wurde manuell mit einer Messelektrode das elektrische Potenzial auf dem Wellboden gemessen. Dafür wurde die Konfiguration von 1 mm Abstand, 0,7 V und 20 Hz gewählt. Da davon ausgegangen werden kann, dass das Feld durch den Aufbau der Elektrode symmetrisch verläuft, wurde zunächst nur die Spannung auf einer Seite gemessen. Es konnte ein Feld von bis zu 4 V/m bestimmt werden (Abb. 10A). Da eine zugehörige numerische Simulation jedoch elektrische Felder von bis zu 150 V/m aufzeigte (Abb. 10B) [II] und Temperaturschwankungen sowie manuelle Fehler beim Abtasten der Positionen auf dem Zellkulturplattenboden nicht ausgeschlossen werden konnten, wurde ein automatisierter Prozess zum Messen der Spannung entwickelt. Dafür wurde zunächst ein 3D-Drucker modifiziert, sodass anstelle des Extruders eine Messelektrode platziert werden konnte. Mithilfe des Druckarms war eine dreidimensionale Positionierung der Messelektrode im Well möglich. Durch die Symmetrie der Elektrode konnte im identischen Abstand oberhalb der Elektrode gemessen werden, um die elektrische Feldverteilung auf dem Zellkulturplattenboden zu ermitteln. Der modifizierte 3D-Drucker wurde in einem Wärmeschrank platziert, sodass alle Messungen bei 37 °C vorgenommen werden konnten. Die Temperatur wurde regelmäßig im Medium des Messwells in der Zellkulturplatte überprüft. Somit konnte eine Feldstärke von bis zu 5,2 V/m bestimmt werden [IV] (Abb. 10B).

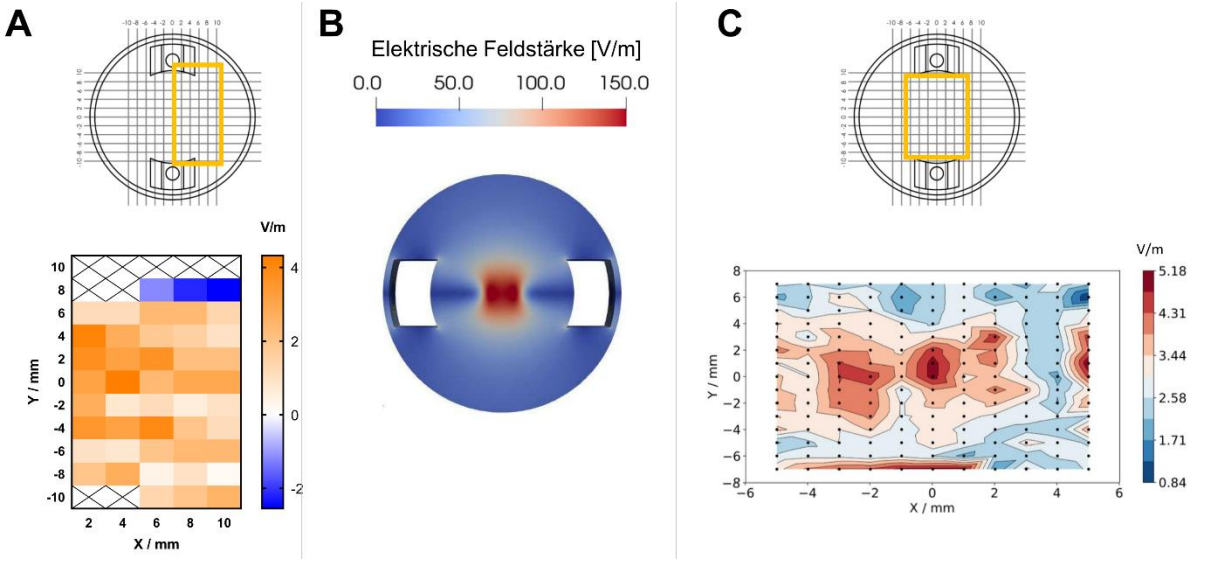

Abbildung 10: Validierung und Simulation des elektrischen Feldes bei einer Eingangsspannung von 0,7 V, 20 Hz und einem Abstand der Feldmessung zur Elektrode von 1 mm. (**A**) Mittelwert der händischen Messungen der Spannung auf dem Zellkulturplattenboden [n = 9]. Gezeigt werden die Positionierung im Well und das errechnete elektrische Feld in V/m. (**B**) Numerische Simulation des elektrischen Feldes auf dem Zellkulturplattenboden in V/m. [II] (**C**) Automatisierte Messung der Spannung oberhalb der Elektrode im selben Abstand wie zwischen der Elektrode und dem Wellboden. Die Messung erfolgte temperiert bei 37 °C mithilfe eines modifizierten 3D-Druckers. Gezeigt werden die Positionierung im Well und das errechnete elektrische Feld in V/m.

5 Diskussion

Die ES von Knochen bietet die Möglichkeit, Osteoporose sowie schlecht heilende oder große Knochendefekte zu behandeln [17]. In In-vivo-Studien, in denen die Knochenheilung mittels ES untersucht wurde, konnte eine Erfolgsrate von 77 % in Tierstudien und 73 % in klinischen Studien beobachtet werden [17]. Mit dieser Dissertation sollte das Grundlagenwissen zu zellulären Reaktionen der Knochenzellen auf elektrische Felder erweitert werden. Dabei standen die veränderte Osteogenese durch direkte ES sowie die Osteoklastogenese durch eine indirekte Kultivierung mit durch ES konditionierte Osteoblastenmedien im Vordergrund. Weiterhin sollten die verwendeten elektrischen Feldstärken charakterisiert werden.

5.1 Einfluss elektrischer Wechselfelder auf die Differenzierung von Osteoblasten

Da Osteoblasten für die Bildung mineralisierter Knochenmatrix verantwortlich sind, stellen sie einen der wichtigsten Zelltypen für die Knochenheilung dar [8]. Ziel ist es, durch die Stimulierung mit elektrischen Feldern die Aktivität und Differenzierung der Osteoblasten zu erhöhen, um eine verbesserte Knochenheilung zu erreichen.

Bei der Untersuchung verschiedener elektrischer Wechselfelder und Stimulationseinheiten zeigten sich Unterschiede zwischen den verwendeten Spannungen sowie zwischen den Stimulationszeiträumen. Stimulationen mit 2,8 V führten nach 1 d zu einer Erhöhung von Differenzierungsmarkern, mit zunehmender Stimulationszeit sank jedoch die Genexpression unter das Kontrolllevel. Dies konnte bei kleineren angelegten Spannungen nicht beobachtet werden, womit sich kleine Felder als vorteilhafter für eine gesteigerte Osteoblastendifferenzierung herausstellten [I]. Es wird deutlich, dass optimale Stimulationsparameter für eine gezielte Aktivierung der Osteoblasten essenziell sind.

Chaudhari et al. [40] zeigten in einer Vergleichsstudie zu variierenden Spannungen und Frequenzen, wie stark die Zellreaktion vom elektrischen Feld abhängig ist. So können unterschiedliche Felder fördernde, aber auch hemmende Wirkungen auf die Aktivität von Osteoblasten haben [40].

Die Analyse verschiedener Zeitpunkte während der Stimulation zeigte die Abhängigkeit der Zellreaktion von der Stimulationsdauer [I]. Su et al. sowie de Sousa verdeutlichten in Studien mit kapazitiven Systemen die Variation der Expression und Freisetzung von Differenzierungsfaktoren über einen Zeitverlauf von bis zu 28 d [41,42]. Da in Studie [I] nur die Stimulation bis 7 d beobachtet wurde und nur wenige Langzeitstudien mit direkten Wechselfeldern existieren [7,43], wurde der Versuchszeitraum auf 31 d erweitert, und verschiedene Untersuchungszeitpunkte während der Stimulation wurden hinzugefügt [II]. Ein Fokus lag dabei auf der zeitlichen Aufnahme der mineralisierten Matrix, da Mineralisierungsprozesse der Osteoblasten erst mit fortgeschrittener Kultivierungszeit zu beobachten sind [44–46]. Zudem wird in Studien zur ES oft kein Zeitverlauf der Mineralisierung aufgezeichnet, sondern diese beinhalten nur eine Endpunktbestimmung [42,43]. Deshalb wurde dies in Veröffentlichung [II] integriert.

Die zwei unterschiedlichen Abstände zur Elektrode, die in der Langzeitstimulation verwendet wurden, führten zu einem HEF und einem LEF [II]. Es traten vereinzelt erste *Nodule*-Bildungen nach 3 bzw. 7 d auf, wobei eine signifikante Erhöhung der Mineralisierungskapazität bei LEF nach 14, 28 und 31 d beobachtet werden konnte. Parallel zu dem signifikanten Anstieg der Mineralisierungsmenge konnte eine Verringerung der OPN-Konzentration beobachtet werden. War OPN hingegen hochreguliert bzw. ähnlich zur Kontrolle, war die Mineralisierungskapazität nicht beeinflusst. Dieser kohärente Trend zwischen Mineralisierung und OPN und die daraus vermutete regulatorische Wirkung von OPN auf die Mineralisierungsmenge lassen sich anhand der gemessenen Menge des Alkalischen Phosphatase Proteins weiter vertiefen. OPN besitzt im phosphorylierten Zustand eine hemmende Wirkung auf Mineralisierungsprozesse, was mit den Beobachtungen in Studie [II] korreliert [47]. Da die Alkalische Phosphatase Menge nicht durch die Stimulation verändert wurde [II], kann von keiner erhöhten Dephosphorylierung des OPN ausgegangen werden. Somit lässt sich vermuten, dass phosphoryliertes OPN vorlag, das zur Regulation der Mineralisierung beitrug.

Das HEF führte zu keiner signifikanten Veränderung der Mineralisierung, jedoch zu einer länger andauernden erhöhten Freisetzung von Signalproteinen wie OPG und IL-6. Beide Proteine sind an Knochenumbauprozessen beteiligt [1,48,49]. OPG reguliert das Knochenwachstum positiv durch das RANKL/RANK/OPG-System, indem es RANKL blockiert. Es kann durch mechanische und elektrische Einwirkungen aktiviert werden [50–54]. IL-6 nimmt eine kontroverse Rolle in Knochenumbauprozessen ein, da es Osteoblasten und Osteoklasten aktivieren oder deaktivieren kann, vermutlich in Abhängigkeit des Differenzierungsstadiums der Zellen und des Einflusses anderer Zytokine [55,56]. Es lässt sich somit vermuten, dass ES

in Abhängigkeit der Feldstärke die Mineralisierung über geringere elektrische Felder oder die Zytokinfreisetzung durch größere Felder und damit die Kommunikation zwischen verschiedenen Zelltypen begünstigt.

Auch andere Forschungsgruppen konnten unter Verwendung elektrischer Felder verstärkte Differenzierung und Mineralisierung von Osteoblasten beobachten [57–60]. McCullen et al. verglichen die Feldstärken 100 V/m, 300 V/m und 500 V/m. Sie zeigten eine starke Zunahme in der Mineralisierung mit 100 V/m, eine nicht veränderte Mineralisierung mit 300 V/m und eine Reduzierung im Vergleich zur unstimulierten Kontrolle bei 500 V/m [57]. In anderen Studien wurde unter Verwendung kapazitiv gekoppelter Felder die Zunahme der mineralisierten Matrixbildung oder die gesteigerte Differenzierung von Osteoblasten mit sehr geringen Feldstärken beobachtet [58–60]. Somit ist zu vermuten, dass niedrige elektrische Felder die Differenzierung und Mineralisierung von Osteoblasten fördern. Die in Studie [II] verwendeten elektrischen Felder waren, nach experimentellen Überprüfungen, mit bis zu 5 V/m deutlich niedriger als die Felder von McCullen et al.. Es ist jedoch hervorzuheben, dass durch die numerische Simulation in der eigenen Studie [II] zunächst von einer ähnlichen Feldstärke mit 150 V/m ausgegangen werden konnte. Da bei McCullen et al. keine messtechnische Überprüfung der Feldstärken vorliegt, ist eine Abweichung zwischen realen und simulierten Feldstärken ebenso möglich [57]. Dies verdeutlicht die Notwendigkeit einer experimentellen Validierung der verwendeten elektrischen Felder, da eine starke Diskrepanz zwischen Simulation und Messdaten vorliegen kann. In der Literatur wird oft keine experimentelle Überprüfung der elektrischen Feldstärken beschrieben, weshalb davon ausgegangen werden kann, dass die beschrieben Feldstärken geringer ausfallen als durch numerische Simulationen berechnet.

Es sind weiterführende Studien bezüglich der Zellwahrnehmung der elektrischen Signale und zur Signalweiterleitung von Nöten, um die Wirkungsweise geringer elektrischer Felder besser zu verstehen. Eine aktuelle Hypothese stellt die Wahrnehmung der elektrischen Signale durch Zytoskelett-Strukturen, Mikrofilamente oder das primäre Cilium dar [24,61]. Es ist ebenso möglich, dass elektrische Felder auf die Zellmembran wirken, z. B. durch eine Reorganisation der Lipidstrukturen in der Membran, Umverteilungen der Zelloberflächenrezeptoren oder Strukturveränderungen von Membranproteinen, insbesondere spannungsgesteuerte Ionenkanäle wie Calcium-Kanäle [24,32,62]. Calcium-Ionen nehmen eine zentrale Rolle ein, denn durch die Freisetzung von intrazellulärem Ca^{2+} durch ES erhöht sich das freie Ca^{2+} in der Zelle, aktiviert somit den Calcium/Calmodulin-Signalweg und löst die Zelldifferenzierung aus [24]. Mittels einer Transkriptomanalyse war es möglich, durch ES angesprochene Signalwege nach 7 d und 28 d in den Osteoblasten mit LEF zu untersuchen [II]. So konnten nach 7 d eine reduzierte Expression von GPCR und eine erhöhte Expression von Eicosanoiden nachgewiesen werden. Eicosanoide sind wichtige Signalproteine, die hauptsächlich durch GPCR in der Zellmembran erkannt werden [63]. Da die Expression der GPCR in den Osteoblasten selbst herunter reguliert war, ist eine mögliche Aktivierung anderer Zelltypen durch die ESO denkbar.

Ebenso ist es möglich, dass Kernrezeptoren in den Osteoblasten selbst auf die Eicosanoide reagieren und somit Proliferations- und Differenzierungsprozesse aktivieren [64]. Dies könnte im Zusammenhang mit den vermehrt beobachteten Mineralisierungsprozessen stehen. Nach 28 d wurden Gene reguliert, die besonders für die Bewegung von Zellen oder subzellulären Komponenten verantwortlich sind [II]. Dies unterstreicht unter anderem die Annahme, dass das Zytoskelett eine entscheidende Rolle in der Signalwahrnehmung und -weiterleitung elektrischer Signale spielt [24].

5.2 Indirekter Einfluss stimulierter Osteoblasten auf die Osteoklastogenese

Durch die ES der Osteoblasten werden Signalmoleküle freigesetzt, die wiederum andere Zelltypen beeinflussen. Von besonderem Interesse ist die Stimulation osteoklastärer Vorläufer und differenzierter Osteoklasten. Als Gegenspieler der Osteoblasten sind Osteoklasten für den Knochenabbau zuständig und somit essenziell für Knochenumbauprozesse und eine gesunde Knochenheilung [8]. Die Überstände der elektrisch stimulierten Osteoblasten aus Studie [II] wurden nach 7, 14 und 21 d gesammelt und für die indirekte Stimulation der PBMCs und Prä-Osteoklasten verwendet.

Auffällig bei der indirekten Kultivierung ist die unterschiedliche Viabilität der beiden Zelltypen (Abb. 7). PBMCs zeigten eine verringerte Viabilität mit 7 und 14 d Medium, Prä-Osteoklasten eine erhöhte Viabilität mit 21 d Medium. Dies könnte auf den unterschiedlichen Differenzierungsgrad der Zellen zurückzuführen sein. PBMCs bestehen aus multipotenten Progenitorzellen mit einer hohen Variabilität bei der Differenzierung in verschiedene Zelltypen, aber auch mit einer hohen Proliferationsrate [65,66]. Durch eine vermehrte Differenzierung, die durch die Genexpression von *ACP5* nachgewiesen werden kann (Abb. 8), wurde vermutlich die Proliferation vermindert und somit die Viabilität verringert, da weniger Zellen für den Umsatz des WST-1 Reagenz zur Verfügung standen. Prä-Osteoklasten waren hingegen vordifferenziert und besaßen somit nicht die Möglichkeit der erhöhten Proliferation oder Differenzierung [66]. Bei den Prä-Osteoklasten konnte eine erhöhte Aktivität durch eine gesteigerte Genexpression von *CTSK*, *CA2* und *MMP-9* (Abb. 9) besonders nach 7 d festgestellt werden. Nach 21 d war diese nicht vorhanden, jedoch eine negative Regulierung des Apoptose-Markers *CASP8* bei HEF [67]. Durch die unveränderte Aktivität der Prä-Osteoklasten mit dem 21 d Medium und der verringerten *CASP8*-Expression lässt sich eine erhöhte Proliferation und somit eine erhöhte Viabilität vermuten. Zukünftige Zell-Zyklus-Untersuchungen können gezieltere Aussagen über die Proliferationskapazitäten und Differenzierungsstadien der Zellen ermöglichen [66].

Bei beiden Zelltypen zeigte sich mit den 7 d Medien keine Regulation der *RANK*-Expression, jedoch eine Hochregulation der Expression von *ACP5* bei den PBMCs oder *CTSK*, *CA2* und *MMP-9* bei den Prä-Osteoklasten. Die indirekt durch die ES hervorgerufene Differenzierung und Aktivität der Zellen scheint somit nicht auf den Differenzierungsfaktor *RANKL*, dem Liganden für den RANK-Rezeptor, zurückzuführen zu sein [68]. Diese Annahme der RANKL-RANK-unabhängigen Differenzierung kann durch die Studie von Lei et al. [69] untermauert

werden, da in direkt elektrisch stimulierten Makrophagen eine Hemmung der RANKL-induzierten Osteoklastogenese nachgewiesen werden konnte. In Studie [III] kann ebenso von einem RANK-RANKL-unabhängigen Signalweg ausgegangen werden, wobei vermutlich eine Regulation über TNF-α erfolgte. TNF-α ist unter anderem ein möglicher Mediator für eine erhöhte Osteoklastogenese [70–72] und konnte in erhöhten Konzentrationen in den Überständen der ESO nachgewiesen werden [III]. Weiterhin wird diese Hypothese durch die verringerte IFN-β- und IL-10-Konzentration bestärkt, beides Antagonisten der Osteoklastogenese. Beide Zytokine konnten vermehrt im 7 d Medium der NSO detektiert werden, jedoch nicht im ESO-HEF-Medium [III], was für eine verminderte Differenzierung und Aktivierung mit dem Kontrollmedium spricht. Obwohl nach 14 d diese Mediatoren auch im ESO-Medium nachweisbar waren, konnte weiterhin eine Induktion der osteoklastischen Differenzierungs- und Aktivitätsmarker nachgewiesen werden. Dies könnte auf die erhöhte Konzentration von IL-6, aber auch auf die stark erhöhte Konzentration des TNF-α-Proteins im ESO-HEF-Medium zurückzuführen sein [III]. Vermutlich sind jedoch auch andere Mediatoren von Bedeutung, die in der Studie [III] nicht berücksichtigt wurden. Eine umfänglichere Analyse von Signalproteinen, aber auch von extrazellulären Vesikeln könnte Aufschluss über weitere Details der Zell-Zellkommunikation geben.

Auffällig war, dass das HEF und LEF zu ähnlichen, aber nicht denselben Zellreaktionen in den PBMCs und Prä-Osteoklasten führten. So zeigten sich signifikante Unterschiede z. B. in der Expression von *MCP1*, *CASP8* oder *RANK*. Gleichzeitig konnten mit dem LEF weniger signifikante Änderungen in den PBMCs und Prä-Osteoklasten erzeugt werden als mit HEF-Überständen. Dies könnte die anfänglich aufgestellte These unterstützen, dass LEF die Mineralisierung und HEF die Knochenumbauprozesse fördern. Weiterführende Untersuchungen der Zellmedien, aber auch mit Co-Kulturen von Osteoblasten und Osteoklasten sind unerlässlich, um diese Vermutung zu stützen.

5.3 Experimentelle Validierung und Simulation der elektrischen Felder

Sowohl in In-vitro- als auch in In-vivo-Versuchen fehlen häufig genaue Angaben zu den applizierten elektrischen Feldern. Da die Verwendung unterschiedlicher Stimulationssysteme und -parameter verschiedene Zellreaktionen hervorrufen kann, ist ein Vergleich zwischen verschiedenen Studien nur sehr begrenzt möglich [24,73,74]. Ein solcher Vergleich ist jedoch unerlässlich, um die Zellreaktionen bei ES übersichtlich darstellen und das daraus entstehende Wissen nutzen zu können, um die Behandlung von Patienten mit Knochendefekten zu verbessern [75]. Eine Vergleichbarkeit kann über das Ermitteln der applizierten elektrischen Feldstärken ermöglicht werden [76,77]. Oftmals wird dies in Studien jedoch nicht bestimmt und experimentell überprüft, sondern nur simuliert oder angenommen [41,42,78–80]. Gundersen und Greenebaum veröffentlichten drei Methoden für die experimentelle Bestimmung des elektrischen Feldes [81]. In Vorversuchen zur Studie [IV] wurde die Methode des Messens der lokalen Spannungsverteilung in der Stimulationskammer gewählt, um die Größe des elektrischen Feldes abschätzen zu können. Dabei ähnelte das elektrische Feld der

manuellen Messung in der Größenordnung dem elektrischen Feld, das automatisiert gemessen wurde. Das in der Simulation berechnete Feld war hingegen ca. 30-fach größer als das experimentelle. Somit ist davon auszugehen, dass in der Berechnung des elektrischen Feldes durch die numerische Simulation Parameter nicht berücksichtigt wurden, welche die reale Feldstärke beeinträchtigen. Ursachen können z. B. das Entstehen einer Doppelschicht um die Elektrode während der Stimulation, die Korrosion an der Elektrode oder Ablagerungen an der Elektrode durch Medienbestandteile wie das Bilden einer Mineralisierungsschicht um die Elektrode sein. Weiterführende Versuche mit höheren Frequenzen wurden vorgenommen, um die Diskrepanz zwischen der Messung und der Simulation detailliert zu untersuchen [IV]. Es zeigte sich, dass der Unterschied zwischen Simulation und Messung mit einer höheren Frequenz deutlich geringer ist als mit kleineren Frequenzen [IV]. Dies verdeutlicht die Wichtigkeit einer experimentellen Überprüfung des elektrischen Feldes, um präzise Daten über dessen Stärke zu erlangen. Weiterführende Studien sollten erfolgen, um mögliche Parameter zu identifizieren, die zu einer Veränderung des elektrischen Feldes führen.

5.4 Ausblick

Die in der vorliegenden Arbeit generierten Erkenntnisse zur ES von Knochenzellen bieten eine Grundlage für weiterführende Untersuchungen. Direkte Co-Kultivierungsmodelle unter der Verwendung von Gerüststrukturen (*Scaffolds*) sind angeraten, um eine knochenähnliche Matrix zu erhalten, verschiedene Zelltypen gleichzeitig zu stimulieren und die daraus entstehende Interaktion der Zelltypen zu beobachten. Zudem wäre eine Vordifferenzierung von Osteoblasten zu Osteozyten im *Scaffold* denkbar, mit anschließender Besiedelung von Osteoblasten- und Osteoklasten-Vorläuferzellen. Die damit erhöhte Komplexität des Zellaustausch würde eine bessere Vergleichbarkeit zu In-vivo-Studien bieten.

Neben der Entwicklung einer Co-Kultur sind weiterführende Analysen zur Signalwahrnehmung von elektrischen Feldern durch Knochenzellen ein relevantes Forschungsziel. Das Verständnis zur Wahrnehmung und Weiterleitung der elektrischen Signale durch die Zelle ist notwendig, um Stimulationsparameter optimal anpassen zu können. Durch ein solches Grundlagenverständnis kann die Forschung zur ES von Knochen vorangebracht und letztendlich die klinische Anwendung am Patienten verbessert werden. Mittels der Durchführung einer Lebendzell-Bildgebung unter ES könnten Aufnahmen von kurz- und langzeitstimulierten Zellen generiert werden, mit denen z. B. Veränderungen im Calcium-Flux, im Zytoskelett, in Zellorganellen und in der Membran erfasst werden könnten. Ebenso könnten damit relevante Rezeptoren der Signalwahrnehmung, wie Piezo 1 und 2, analysiert werden [82].

Durch die Versuche zur Validierung und Simulation der elektrischen Felder hat sich die Relevanz der experimentellen Messung applizierter elektrischer Felder gezeigt. In zukünftigen Versuchen sollte eine konstante Stromstärken- und Spannungsmessung während der Stimulation erfolgen, um Erkenntnisse über die Intensität und eventuelle Schwankungen der

elektrischen Felder zu erlangen. Zudem sollten mögliche Ablagerungen und Korrosionsvorgänge an den Stimulationselektroden ermittelt werden. Die Bestimmung der Feldverteilung in stimulierten 3D-Strukturen und -Geweben gewährleistet eine bessere Vergleichbarkeit mit In-vivo-Studien, die für eine zukünftige verbesserte klinische Anwendung notwendig ist.

6 Zusammenfassung

Die ES von Knochen ist eine Methode, mit der die Knochenregeneration verbessert und Knochendefekte behandelt werden können. Trotz der erfolgreichen klinischen Anwendung bestehen offene Fragen bezüglich der Wirkungsweise elektrischer Felder auf Knochenzellen. In der vorliegenden Arbeit wurde daher der Einfluss elektrischer Felder auf humane Osteoblasten untersucht, und deren indirekte Wirkung auf die Osteoklastogenese analysiert.
Mithilfe spezieller In-vitro-Stimulationssysteme war es möglich, die Differenzierung und Aktivität humaner Osteoblasten unter ES zu untersuchen und eine Vergleichbarkeit mit einem vorliegenden In-vivo-Stimulationssystem herzustellen. Höhere Eingangsspannungen führten zu höheren elektrischen Feldern und zu einer Herunterregulierung der Genexpression von osteoblastischen Differenzierungsmarkern über die Zeit. Beim Vergleich von kontinuierlicher und diskontinuierlicher ES konnte kein Vorteil der kontinuierlichen Stimulation beobachtet werden. Deshalb wurde in dieser Arbeit für die Untersuchung von Langzeiteffekten eine diskontinuierliche Stimulation von 3 x 45 min und einer Eingangsspannung von 0,7 V gewählt. Durch das Einstellen zwei unterschiedlicher Abstände der Elektrode zum Boden der Zellkulturplatte war es möglich, die Varianz des Abstands der Elektroden zum umgebenden Knochen nachzubilden. Bei den entstehenden elektrischen Feldern stellte sich das LEF als fördernd für eine erhöhte Mineralisierung heraus. Die Untersuchung von Signalproteinen zeigte eine erhöhte Sekretion mit LEF nach 3 und 7 d, mit dem HEF nach 14 und 21 d. Für eine tiefergreifende Analyse möglicher Signalkaskaden während der ES wurde eine Transkriptomanalyse durchgeführt. Es konnte gezeigt werden, dass unterschiedliche Zeitpunkte der ES die Expression unterschiedlicher Gene anregen. Nach 7 d wurde eine Regulation von GPCR und Eicosanoiden nachgewiesen, die im Zusammenhang mit Proliferations- und Differenzierungsprozessen stehen kann. Nach 28 d waren Gene hochreguliert, die für die Bewegung der Zellen und subzellulären Komponenten verantwortlich sind.
Die Untersuchung zur Beeinflussung der Osteoklastogenese durch Überstände von elektrisch stimulierten Osteoblasten zeigte eine variierende Reaktion in der Zellviabilität in Abhängigkeit des Differenzierungsstadiums der Zellen. Überstände bei der Applikation von HEF führten zu stärker ausgeprägten Veränderungen in der Expression osteoklastärer Gene als Überstände bei der Applikation von LEF. Daher lässt sich vermuten, dass höhere Felder eine stärkere Regulation der Knochenumbauprozesse anregen, kleinere Felder hingegen eher Mineralisierungsprozesse unterstützen. Weiterhin war eine Erhöhung der Genexpression

vermehrt nach der Kultivierung mit 7 d Medien feststellbar, was suggeriert, dass die ersten Tage der ES entscheidend für die Interaktion von Osteoblasten und Osteoklasten sind.
Mit der Entwicklung eines Versuchsaufbaus zur experimentellen Validierung elektrischer Felder war es möglich, die entstehenden Feldstärken zu bestimmen und mit Simulationsdaten zu vergleichen. Es konnte beobachtet werden, dass bei kleinen elektrischen Feldern die Varianz zwischen Mess- und Simulationsdaten sehr groß war. Weiterführende Untersuchungen zu verschiedenen Stimulationsparametern, die das elektrische Feld verändern, sind notwendig, um numerische Simulationen zu verbessern. Auch eine messtechnische Überprüfung der elektrischen Felder ist essenziell, um verschiedene Studien miteinander vergleichen zu können.

7 Literaturverzeichnis

1. Rucci, N. Molecular Biology of Bone Remodelling. *Clin Cases Miner Bone Metab* **2008**, *5*, 49–56.
2. Manolagas, S.C. Birth and Death of Bone Cells: Basic Regulatory Mechanisms and Implications for the Pathogenesis and Treatment of Osteoporosis*. *Endocr Rev* **2000**, *21*, 115–137, doi:10.1210/edrv.21.2.0395.
3. Wildemann, B.; Ignatius, A.; Leung, F.; Taitsman, L.A.; Smith, R.M.; Pesántez, R.; Stoddart, M.J.; Richards, R.G.; Jupiter, J.B. Non-Union Bone Fractures. *Nat Rev Dis Primers* **2021**, *7*, 57, doi:10.1038/s41572-021-00289-8.
4. de Martinis, M.; Sirufo, M.M.; Polsinelli, M.; Placidi, G.; di Silvestre, D.; Ginaldi, L. Gender Differences in Osteoporosis: A Single- Center Observational Study. *World Journal of Men's Health* **2020**, *38*, 2287–4690, doi:10.5534/WJMH.200099.
5. Sözen, T.; Özışık, L.; Başaran, N.Ç. An Overview and Management of Osteoporosis. *Eur J Rheumatol* **2017**, *4*, 46–56, doi:10.5152/eurjrheum.2016.048.
6. Bou Monsef, J.; Parekh, A.; Osmani, F.; Gonzalez, M. Failed Total Hip Arthroplasty. *JBJS Rev* **2018**, *6*, e3, doi:10.2106/JBJS.RVW.17.00140.
7. deVet, T.; Jhirad, A.; Pravato, L.; Wohl, G.R. Bone Bioelectricity and Bone-Cell Response to Electrical Stimulation: A Review. *Crit Rev Biomed Eng* **2021**, *49*, 1–19, doi:10.1615/CritRevBiomedEng.2021035327.
8. Florencio-Silva, R.; Sasso, G.R. da S.; Sasso-Cerri, E.; Simões, M.J.; Cerri, P.S. Biology of Bone Tissue: Structure, Function, and Factors That Influence Bone Cells. *Biomed Res Int* **2015**, *2015*, 421746, doi:10.1155/2015/421746.
9. Orimo, H. The Mechanism of Mineralization and the Role of Alkaline Phosphatase in Health and Disease. *J Nippon Med Sch* **2010**, *77*, 4–12, doi:10.1272/jnms.77.4.
10. Capulli, M.; Paone, R.; Rucci, N. Osteoblast and Osteocyte: Games without Frontiers. *Arch Biochem Biophys* **2014**, *561*, 3–12, doi:10.1016/j.abb.2014.05.003.
11. Wambo, T.O.; Chen, L.Y.; McHardy, S.F.; Tsin, A.T. Molecular Dynamics Study of Human Carbonic Anhydrase II in Complex with Zn(2+) and Acetazolamide on the Basis of All-Atom Force Field Simulations. *Biophys Chem* **2016**, *214–215*, 54–60, doi:10.1016/j.bpc.2016.05.006.
12. Fukada, E.; Yasuda, I. On the Piezoelectric Effect of Bone. *J Physical Soc Japan* **1957**, *12*, 1158–1162, doi:10.1143/JPSJ.12.1158.
13. Hohmann, M. 4.8 Der piezoelektrische Effekt. In *Bewegungsapparat Hund, Funktionelle Anatomie, Biomechanik und Pathophysiologie*; Georg Thieme Verlag: Stuttgart, 2015; p. 41 ISBN 9783131980014.
14. Bassett, C.A.L.; Becker, R.O. Generation of Electric Potentials by Bone in Response to Mechanical Stress. *Science (1979)* **1962**, *137*, 1063–1064, doi:10.1126/science.137.3535.1063.

15. Griffin, M.; Bayat, A. Electrical Stimulation in Bone Healing: Critical Analysis by Evaluating Levels of Evidence. *Eplasty* **2011**, *11*, e34.
16. Black, J.L. Electrical Stimulation: Its Role in Growth, Repair and Remodeling of the Musculoskeletal System 1986.
17. Bhavsar, M.B.; Han, Z.; DeCoster, T.; Leppik, L.; Costa Oliveira, K.M.; Barker, J.H.; Oliveira, K.M.C.; Bhavsar, M.B.; Barker, J.H.; Han, Z.; et al. Electrical Stimulation-Based Bone Fracture Treatment, If It Works so Well Why Do Not More Surgeons Use It? *European Journal of Trauma and Emergency Surgery* **2020**, *46*, 245–264, doi:10.1007/s00068-019-01127-z.
18. Ellenrieder, M.; Tischer, T.; Kreuz, P.C.; Fröhlich, S.; Fritsche, A.; Mittelmeier, W. Arthroskopisch Gestützte Behandlung Der Aseptischen Hüftkopfnekrose [Arthroscopically Assisted Therapy of Avascular Necrosis of the Femoral Head]. *Oper Orthop Traumatol* **2013**, *25*, 85–94, doi:10.1007/s00064-011-0072-4.
19. Yang, C.; Ji, J.; Lv, Y.; Li, Z.; Luo, D. Application of Piezoelectric Material and Devices in Bone Regeneration. *Nanomaterials* **2022**, *12*, 4386, doi:10.3390/nano12244386.
20. Mishra, S.; Unnikrishnan, L.; Nayak, S.K.; Mohanty, S. Advances in Piezoelectric Polymer Composites for Energy Harvesting Applications: A Systematic Review. *Macromol Mater Eng* **2019**, *304*, 1800463, doi:10.1002/mame.201800463.
21. Portan, D. V; Deligianni, D.D.; Papanicolaou, G.C.; Kostopoulos, V.; Psarras, G.C.; Tyllianakis, M. Combined Optimized Effect of a Highly Self-Organized Nanosubstrate and an Electric Field on Osteoblast Bone Cells Activity. *Biomed Res Int* **2019**, *2019*, 7574635, doi:10.1155/2019/7574635.
22. Ercan, B.; Webster, T.J. The Effect of Biphasic Electrical Stimulation on Osteoblast Function at Anodized Nanotubular Titanium Surfaces. *Biomaterials* **2010**, *31*, 3684–3693, doi:10.1016/j.biomaterials.2010.01.078.
23. dos Santos, M.P.S.; Marote, A.; Santos, T.; Torrão, J.; Ramos, A.; Simões, J.A.O.; da Cruz E Silva, O.A.B.; Furlani, E.P.; Vieira, S.I.; Ferreira, J.A.F. New Cosurface Capacitive Stimulators for the Development of Active Osseointegrative Implantable Devices. *Sci Rep* **2016**, *6*, doi:10.1038/srep30231.
24. Leppik, L.; Oliveira, K.M.C.; Bhavsar, M.B.; Barker, J.H. Electrical Stimulation in Bone Tissue Engineering Treatments. *Eur J Trauma Emerg Surg* **2020**, *46*, 231–244, doi:10.1007/s00068-020-01324-1.
25. Creecy, C.M.; O'Neill, C.F.; Arulanandam, B.P.; Sylvia, V.L.; Navara, C.S.; Bizios, R. Mesenchymal Stem Cell Osteodifferentiation in Response to Alternating Electric Current. *Tissue Eng Part A* **2013**, *19*, 467–474, doi:10.1089/ten.TEA.2012.0091.
26. Detsch, R.; Boccaccini, A.R. The Role of Osteoclasts in Bone Tissue Engineering. *J Tissue Eng Regen Med* **2015**, *9*, 1133–1149, doi:10.1002/term.1851.

27. Rubin, J.; McLeod, K.J.; Titus, L.; Nanes, M.S.; Catherwood, B.D.; Rubin, C.T. Formation of Osteoclast-like Cells Is Suppressed by Low Frequency, Low Intensity Electric Fields. *Journal of Orthopaedic Research* **1996**, *14*, 7–15, doi:10.1002/jor.1100140104.
28. Shankar, V.S.; Simon, B.J.; Bax, C.M.R.; Pazianas, M.; Moonga, B.S.; Adebanjo, O.A.; Zaidi, M. Effects of Electromagnetic Stimulation on the Functional Responsiveness of Isolated Rat Osteoclasts. *J Cell Physiol* **1998**, *176*, 537–544, doi:10.1002/(SICI)1097-4652(199809)176:3<537::AID-JCP10>3.0.CO;2-X.
29. Balint, R.; Cassidy, N.J.; Cartmell, S.H. Electrical Stimulation: A Novel Tool for Tissue Engineering. *Tissue Eng Part B Rev* **2012**, *19*, 48–57, doi:10.1089/ten.teb.2012.0183.
30. Chen, C.; Bai, X.; Ding, Y.; Lee, I.-S. Electrical Stimulation as a Novel Tool for Regulating Cell Behavior in Tissue Engineering. *Biomater Res* **2019**, *23*, 25, doi:10.1186/s40824-019-0176-8.
31. Babona-Pilipos, R.; Liu, N.; Pritchard-Oh, A.; Mok, A.; Badawi, D.; Popovic, M.R.; Morshead, C.M. Calcium Influx Differentially Regulates Migration Velocity and Directedness in Response to Electric Field Application. *Exp Cell Res* **2018**, *368*, 202–214, doi:10.1016/j.yexcr.2018.04.031.
32. Rems, L.; Kasimova, M.A.; Testa, I.; Delemotte, L. Pulsed Electric Fields Can Create Pores in the Voltage Sensors of Voltage-Gated Ion Channels. *Biophys J* **2020**, *119*, 190–205, doi:10.1016/j.bpj.2020.05.030.
33. Srirussamee, K.; Xue, R.; Mobini, S.; Cassidy, N.J.; Cartmell, S.H. Changes in the Extracellular Microenvironment and Osteogenic Responses of Mesenchymal Stem/Stromal Cells Induced by in Vitro Direct Electrical Stimulation. *J Tissue Eng* **2021**, *12*, 204173142097414, doi:10.1177/2041731420974147.
34. Guette-Marquet, S.; Roques, C.; Bergel, A. Theoretical Analysis of the Electrochemical Systems Used for the Application of Direct Current/Voltage Stimuli on Cell Cultures. *Bioelectrochemistry* **2021**, *139*, 107737, doi:10.1016/j.bioelechem.2020.107737.
35. Zimmermann, J.; Budde, K.; Arbeiter, N.; Molina, F.; Storch, A.; Uhrmacher, A.M.; van Rienen, U. Using a Digital Twin of an Electrical Stimulation Device to Monitor and Control the Electrical Stimulation of Cells in Vitro. *Front Bioeng Biotechnol* **2021**, *9*, 1149, doi:10.3389/fbioe.2021.765516.
36. Dauben, T.J.; Ziebart, J.; Bender, T.; Zaatreh, S.; Kreikemeyer, B.; Bader, R. A Novel *In Vitro* System for Comparative Analyses of Bone Cells and Bacteria under Electrical Stimulation. *Biomed Res Int* **2016**, *2016*, 1–12, doi:10.1155/2016/5178640.
37. Hiemer, B.; Krogull, M.; Bender, T.; Ziebart, J.; Krueger, S.; Bader, R.; Jonitz-Heincke, A. Effect of Electric Stimulation on Human Chondrocytes and Mesenchymal Stem Cells under Normoxia and Hypoxia. *Mol Med Rep* **2018**, *18*, 2133–2141, doi:10.3892/mmr.2018.9174.
38. Hiemer, B.; Ziebart, J.; Jonitz-Heincke, A.; Grunert, P.C.; Su, Y.; Hansmann, D.; Bader, R. Magnetically Induced Electrostimulation of Human Osteoblasts Results in Enhanced

Cell Viability and Osteogenic Differentiation. *Int J Mol Med* **2016**, *38*, 57–64, doi:10.3892/ijmm.2016.2590.

39. Lochner, K.; Fritsche, A.; Jonitz, A.; Hansmann, D.; Mueller, P.; Mueller-hilke, B.; Bader, R. The Potential Role of Human Osteoblasts for Periprosthetic Osteolysis Following Exposure to Wear Particles. **2011**, 1055–1063, doi:10.3892/ijmm.2011.778.
40. Chaudhari, S.D.; Sharma, K.K.; Marchetto, J.J.; Hydren, J.R.; Burton, B.M.; Moreno, A.P. Modulating OPG and TGF-B1 MRNA Expression via Bioelectrical Stimulation. *Bone Rep* **2021**, *15*, 101141, doi:10.1016/j.bonr.2021.101141.
41. Su, C.-Y.; Fang, T.; Fang, H.-W. Effects of Electrostatic Field on Osteoblast Cells for Bone Regeneration Applications. *Biomed Res Int* **2017**, *2017*, 7124817, doi:10.1155/2017/7124817.
42. de Sousa, B.M.; Correia, C.R.; Ferreira, J.A.F.; Mano, J.F.; Furlani, E.P.; Soares dos Santos, M.P.; Vieira, S.I. Capacitive Interdigitated System of High Osteoinductive/Conductive Performance for Personalized Acting-Sensing Implants. *NPJ Regen Med* **2021**, *6*, 80, doi:10.1038/s41536-021-00184-6.
43. Supronowicz, P.R.; Ajayan, P.M.; Ullmann, K.R.; Arulanandam, B.P.; Metzger, D.W.; Bizios, R. Novel Current-Conducting Composite Substrates for Exposing Osteoblasts to Alternating Current Stimulation. *J Biomed Mater Res* **2001**, *59*, 499–506, doi:10.1002/jbm.10015.
44. Coelho, M.J.; Fernandes, M.H. Human Bone Cell Cultures in Biocompatibility Testing. Part II: Effect of Ascorbic Acid, β-Glycerophosphate and Dexamethasone on Osteoblastic Differentiation. *Biomaterials* **2000**, *21*, 1095–1102, doi:10.1016/S0142-9612(99)00192-1.
45. Nefussi, J.-R.; Boy-Lefevre, M.L.; Boulekbache, H.; Forest, N. Mineralization in Vitro of Matrix Formed by Osteoblasts Isolated by Collagenase Digestion. *Differentiation* **1985**, *29*, 160–168, doi:10.1111/j.1432-0436.1985.tb00310.x.
46. Serguienko, A.; Wang, M.Y.; Myklebost, O. Real-Time Vital Mineralization Detection and Quantification during In Vitro Osteoblast Differentiation. *Biol Proced Online* **2018**, *20*, 14, doi:10.1186/s12575-018-0079-4.
47. Jono, S.; Peinado, C.; Giachelli, C. Phosphorylation of Osteopontin Is Required for Inhibition of Vascular Smooth Muscle Cell Calcification. *J Biol Chem* **2000**, *275*, 20197–20203, doi:10.1074/jbc.M909174199.
48. Si, J.; Wang, C.; Zhang, D.; Wang, B.; Hou, W.; Zhou, Y. Osteopontin in Bone Metabolism and Bone Diseases. *Medical Science Monitor* **2020**, *26*, e919159, doi:10.12659/MSM.919159.
49. Einhorn, T.A.; Gerstenfeld, L.C. Fracture Healing: Mechanisms and Interventions. *Nat Rev Rheumatol* **2015**, *11*, 45–54, doi:10.1038/nrrheum.2014.164.
50. Boyce, B.F.; Xing, L. Functions of RANKL/RANK/OPG in Bone Modeling and Remodeling. *Arch Biochem Biophys* **2008**, *473*, 139–146, doi:10.1016/j.abb.2008.03.018.

51. Yamaguchi, M. RANK/RANKL/OPG during Orthodontic Tooth Movement. *Orthod Craniofac Res* **2009**, *12*, 113–119, doi:10.1111/j.1601-6343.2009.01444.x.
52. Tobeiha, M.; Moghadasian, M.H.; Amin, N.; Jafarnejad, S. RANKL/RANK/OPG Pathway: A Mechanism Involved in Exercise-Induced Bone Remodeling. *Biomed Res Int* **2020**, *2020*, 6910312, doi:10.1155/2020/6910312.
53. Fonseca, J.H.; Bagne, L.; Meneghetti, D.H.; Santos, G.M.T.; Esquisatto, M.A.M.; Andrade, T.A.M.; Amaral, M.E.C.; Felonato, M.; Caetano, G.F.; Santamaria, M.; et al. Electrical Stimulation: Complementary Therapy to Improve the Performance of Grafts in Bone Defects? *J Biomed Mater Res B Appl Biomater* **2019**, *107*, 924–932, doi:10.1002/jbm.b.34187.
54. Stephan, M.; Zimmermann, J.; Klinder, A.; Sahm, F.; van Rienen, U.; Kämmerer, P.W.; Bader, R.; Jonitz-Heincke, A. Establishment and Evaluation of an In Vitro System for Biophysical Stimulation of Human Osteoblasts. *Cells* **2020**, *9*, 1995, doi:10.3390/cells9091995.
55. Blanchard, F.; Duplomb, L.; Baud'huin, M.; Brounais, B. The Dual Role of IL-6-Type Cytokines on Bone Remodeling and Bone Tumors. *Cytokine Growth Factor Rev* **2009**, *20*, 19–28, doi:10.1016/j.cytogfr.2008.11.004.
56. Feng, W.; Liu, H.; Luo, T.; Liu, D.; Du, J.; Sun, J.; Wang, W.; Han, X.; Yang, K.; Guo, J.; et al. Combination of IL-6 and SIL-6R Differentially Regulate Varying Levels of RANKL-Induced Osteoclastogenesis through NF-KB, ERK and JNK Signaling Pathways. *Sci Rep* **2017**, *7*, 41411, doi:10.1038/srep41411.
57. McCullen, S.D.; McQuilling, J.P.; Grossfeld, R.M.; Lubischer, J.L.; Clarke, L.I.; Loboa, E.G. Application of Low-Frequency Alternating Current Electric Fields Via Interdigitated Electrodes: Effects on Cellular Viability, Cytoplasmic Calcium, and Osteogenic Differentiation of Human Adipose-Derived Stem Cells. *Tissue Eng Part C Methods* **2010**, *16*, 1377–1386, doi:10.1089/ten.tec.2009.0751.
58. Brighton, C.T.; Okereke, E.; Pollack, S.R.; Clark, C.C. In Vitro Bone-Cell Response to a Capacitively Coupled Electrical Field. The Role of Field Strength, Pulse Pattern, and Duty Cycle. *Clin Orthop Relat Res* **1992**, 255–262.
59. Fitzsimmons, R.J.; Farley, J.; Adey, W.R.; Baylink, D.J. Embryonic Bone Matrix Formation Is Increased after Exposure to a Low-Amplitude Capacitively Coupled Electric Field, in Vitro. *Biochimica et Biophysica Acta (BBA) - General Subjects* **1986**, *882*, 51–56, doi:10.1016/0304-4165(86)90054-1.
60. Rubin, C.T.; Donahue, H.J.; Rubin, J.E.; McLeod, K.J. Optimization of Electric Field Parameters for the Control of Bone Remodeling: Exploitation of an Indigenous Mechanism for the Prevention of Osteopenia. *Journal of Bone and Mineral Research* **1993**, *8*, S573–S581, doi:10.1002/jbmr.5650081327.
61. Cai, S.; Bodle, J.C.; Mathieu, P.S.; Amos, A.; Hamouda, M.; Bernacki, S.; McCarty, G.; Loboa, E.G. Primary Cilia Are Sensors of Electrical Field Stimulation to Induce

Osteogenesis of Human Adipose-Derived Stem Cells. *FASEB J* **2017**, *31*, 346–355, doi:10.1096/fj.201600560R.

62. Zhang, J.; Li, M.; Kang, E.-T.; Neoh, K.G. Electrical Stimulation of Adipose-Derived Mesenchymal Stem Cells in Conductive Scaffolds and the Roles of Voltage-Gated Ion Channels. *Acta Biomater* **2016**, *32*, 46–56, doi:10.1016/j.actbio.2015.12.024.
63. Calder, P.C. Eicosanoids. *Essays Biochem* **2020**, *64*, 423–441, doi:10.1042/EBC20190083.
64. Chinetti, G.; Fruchart, J.-C.; Staels, B. Peroxisome Proliferator-Activated Receptors (PPARs): Nuclear Receptors at the Crossroads between Lipid Metabolism and Inflammation. *Inflammation Research* **2000**, *49*, 497–505, doi:10.1007/s000110050622.
65. Zhang, M.; Huang, B. The Multi-Differentiation Potential of Peripheral Blood Mononuclear Cells. *Stem Cell Res Ther* **2012**, *3*, 48, doi:10.1186/scrt139.
66. Ruijtenberg, S.; van den Heuvel, S. Coordinating Cell Proliferation and Differentiation: Antagonism between Cell Cycle Regulators and Cell Type-Specific Gene Expression. *Cell Cycle* **2016**, *15*, 196–212, doi:10.1080/15384101.2015.1120925.
67. Fritsch, M.; Günther, S.D.; Schwarzer, R.; Albert, M.-C.; Schorn, F.; Werthenbach, J.P.; Schiffmann, L.M.; Stair, N.; Stocks, H.; Seeger, J.M.; et al. Caspase-8 Is the Molecular Switch for Apoptosis, Necroptosis and Pyroptosis. *Nature* **2019**, *575*, 683–687, doi:10.1038/s41586-019-1770-6.
68. Borciani, G.; Montalbano, G.; Baldini, N.; Cerqueni, G.; Vitale-Brovarone, C.; Ciapetti, G. Co-Culture Systems of Osteoblasts and Osteoclasts: Simulating in Vitro Bone Remodeling in Regenerative Approaches. *Acta Biomater* **2020**, *108*, doi:10.1016/j.actbio.2020.03.043.
69. Lei, Y.; Su, J.; Xu, H.; Yu, Q.; Zhao, M.; Tian, J. Pulsed Electromagnetic Fields Inhibit Osteoclast Differentiation in RAW264.7 Macrophages via Suppression of the Protein Kinase B/Mammalian Target of Rapamycin Signaling Pathway. *Mol Med Rep* **2018**, *18*, 447–454, doi:10.3892/mmr.2018.8999.
70. Kim, N.; Kadono, Y.; Takami, M.; Lee, J.; Lee, S.-H.; Okada, F.; Kim, J.H.; Kobayashi, T.; Odgren, P.R.; Nakano, H.; et al. Osteoclast Differentiation Independent of the TRANCE–RANK–TRAF6 Axis. *Journal of Experimental Medicine* **2005**, *202*, 589–595, doi:10.1084/jem.20050978.
71. Mun, S.H.; Ko, N.Y.; Kim, H.S.; Kim, J.W.; Kim, D.K.; Kim, A.-R.; Lee, S.H.; Kim, Y.-G.; Lee, C.K.; Lee, S.H.; et al. Interleukin-33 Stimulates Formation of Functional Osteoclasts from Human CD14+ Monocytes. *Cellular and Molecular Life Sciences* **2010**, *67*, 3883–3892, doi:10.1007/s00018-010-0410-y.
72. Kobayashi, K.; Takahashi, N.; Jimi, E.; Udagawa, N.; Takami, M.; Kotake, S.; Nakagawa, N.; Kinosaki, M.; Yamaguchi, K.; Shima, N.; et al. Tumor Necrosis Factor α Stimulates Osteoclast Differentiation by a Mechanism Independent of the Odf/Rankl–Rank

Interaction. *Journal of Experimental Medicine* **2000**, *191*, 275–286, doi:10.1084/jem.191.2.275.

73. Griffin, M.; Iqbal, S.A.; Sebastian, A.; Colthurst, J.; Bayat, A. Degenerate Wave and Capacitive Coupling Increase Human MSC Invasion and Proliferation While Reducing Cytotoxicity in an In Vitro Wound Healing Model. *PLoS One* **2011**, *6*, e23404, doi:10.1371/journal.pone.0023404.
74. Bique, A.M.; Kaivosoja, E.; Mikkonen, M.; Paulasto-Kröckel, M. Choice of Osteoblast Model Critical for Studying the Effects of Electromagnetic Stimulation on Osteogenesis in Vitro. *Electromagn Biol Med* **2016**, *35*, 353–364, doi:10.3109/15368378.2016.1138124.
75. Nicksic, P.J.; Donnelly, D.T.; Hesse, M.; Bedi, S.; Verma, N.; Seitz, A.J.; Shoffstall, A.J.; Ludwig, K.A.; Dingle, A.M.; Poore, S.O. Electronic Bone Growth Stimulators for Augmentation of Osteogenesis in In Vitro and In Vivo Models: A Narrative Review of Electrical Stimulation Mechanisms and Device Specifications. *Front Bioeng Biotechnol* **2022**, *10*, doi:10.3389/fbioe.2022.793945.
76. Ryan, C.N.M.; Doulgkeroglou, M.N.; Zeugolis, D.I. Electric Field Stimulation for Tissue Engineering Applications. *BMC Biomed Eng* **2021**, *3*, 1, doi:10.1186/s42490-020-00046-0.
77. Thrivikraman, G.; Boda, S.K.; Basu, B. Unraveling the Mechanistic Effects of Electric Field Stimulation towards Directing Stem Cell Fate and Function: A Tissue Engineering Perspective. *Biomaterials* **2018**, *150*, 60–86, doi:10.1016/j.biomaterials.2017.10.003.
78. Leppik, L.; Bhavsar, M.B.; Oliveira, K.M.C.; Eischen-Loges, M.; Mobini, S.; Barker, J.H. Construction and Use of an Electrical Stimulation Chamber for Enhancing Osteogenic Differentiation in Mesenchymal Stem/Stromal Cells In Vitro. *J Vis Exp* **2019**, doi:10.3791/59127.
79. Srirussamee, K.; Mobini, S.; Cassidy, N.J.; Cartmell, S.H. Direct Electrical Stimulation Enhances Osteogenesis by Inducing Bmp2 and Spp1 Expressions from Macrophages and Preosteoblasts. *Biotechnol Bioeng* **2019**, *116*, 3421–3432, doi:10.1002/bit.27142.
80. Rohde, M.; Ziebart, J.; Kirschstein, T.; Sellmann, T.; Porath, K.; Kühl, F.; Delenda, B.; Bahls, C.; van Rienen, U.; Bader, R.; et al. Human Osteoblast Migration in DC Electrical Fields Depends on Store Operated Ca2+-Release and Is Correlated to Upregulation of Stretch-Activated TRPM7 Channels. *Front Bioeng Biotechnol* **2019**, *7*, 422, doi:10.3389/fbioe.2019.00422.
81. Gundersen, R.; Greenebaum, B. Low-Voltage ELF Electric Field Measurements in Ionic Media. *Bioelectromagnetics* **1985**, *6*, 157–168, doi:10.1002/bem.2250060207.
82. Whasil, L.; A., L.H.; Yong, C.; Hee, L.S.; A., Z.N.; L., M.A.; Jason, W.; N., B.K.; Jeffrey, C.; Stefan, Z.; et al. Synergy between Piezo1 and Piezo2 Channels Confers High-Strain Mechanosensitivity to Articular Cartilage. *Proceedings of the National Academy of Sciences* **2014**, *111*, E5114–E5122, doi:10.1073/pnas.1414298111.

8 Liste der Publikationen zur kumulativen Dissertation

Für die kumulative Dissertation wurden folgende Publikationen herangezogen:

[**I**] **Sahm, F.**; Ziebart, J.; Jonitz-Heincke, A.; Hansmann, D.; Dauben, T.; Bader, R. Alternating Electric Fields Modify the Function of Human Osteoblasts Growing on and in the Surroundings of Titanium Electrodes. *Int J Mol Sci.* **2020** Sep 22;21(18), 6944, doi: 10.3390/ijms21186944.
Impact Factor: 6,208 (2022)

[II] **Sahm, F.**; Freiin Grote, V.; Zimmermann, J.; Haack, F.; Uhrmacher, A.M.; van Rienen, U.; Bader, R.; Detsch, R.; Jonitz-Heincke, A. Long-Term Stimulation with Alternating Electric Fields Modulates the Differentiation and Mineralization of Human Pre-Osteoblasts. *Front Physiol* **2022**, 13, doi:10.3389/fphys.2022.965181.
Impact Factor: 4,755 (2022)

[**III**] **Sahm, F.**; Jakovljevic, A.; Bader, R.; Detsch, R.; Jonitz-Heincke, A. Is There an Influence of Electrically Stimulated Osteoblasts on the Induction of Osteoclastogenesis? *Appl. Sci*. **2022**, 12, 11840, doi.org/10.3390/app122211840.
Impact Factor: 2,838 (2022)

[**IV**] Zimmermann, J.; **Sahm, F.**; Arbeiter, N.; Bathel, H.; Song, Z.; Bader, R.; Jonitz-Heincke, A.; Rienen, U. Experimental and Numerical Methods to Ensure Comprehensible and Replicable Alternating Current Electrical Stimulation Experiments. *Bioelectrochemistry* **2023**, 108395, doi:10.1016/j.bioelechem.2023.108395.
Impact Factor: 5,76 (2022)

International Journal of
Molecular Sciences

MDPI

Article

Alternating Electric Fields Modify the Function of Human Osteoblasts Growing on and in the Surroundings of Titanium Electrodes

Franziska Sahm [1,*], Josefin Ziebart [1,*], Anika Jonitz-Heincke [1], Doris Hansmann [1], Thomas Dauben [2] and Rainer Bader [1]

[1] Biomechanics and Implant Technology Research Laboratory, Department of Orthopaedics, Rostock University Medical Centre, 18057 Rostock, Germany; anika.jonitz-heincke@med.uni-rostock.de (A.J.-H.); doris.hansmann@med.uni-rostock.de (D.H.); rainer.bader@med.uni-rostock.de (R.B.)

[2] Institute for Medical Microbiology, Virology and Hygiene, University Medical Center, Schillingallee 70, 18057 Rostock, Germany; thomas.dauben@uni-jena.de

* Correspondence: Franziska.sahm@med.uni-rostock.de (F.S.); josefin.ziebart@googlemail.com (J.Z.); Tel.: +49-0381-4949336 (J.Z.)

Received: 11 September 2020; Accepted: 19 September 2020; Published: 22 September 2020

Abstract: Endogenous electric fields created in bone tissue as a response to mechanical loading are known to influence the activity and differentiation of bone and precursor cells. Thus, electrical stimulation offers an adjunct therapy option for the promotion of bone regeneration. Understanding the influence of electric fields on bone cell function and the identification of suitable electrical stimulation parameters are crucial for the clinical success of stimulation therapy. Therefore, we investigated the impact of alternating electric fields on human osteoblasts that were seeded on titanium electrodes, which delivered the electrical stimulation. Moreover, osteoblasts were seeded on collagen-coated coverslips near the electrodes, representing the bone stock surrounding the implant. Next, 0.2 V, 1.4 V, or 2.8 Vwere applied to the in vitro system with 20 Hz frequency. After one, three, and seven days, the osteoblast morphology and expression of osteogenic genes were analysed. The actin organisation, as well as the proliferation, were not affected by the electrical stimulation. Changes in the gene expression and protein accumulation after electrical stimulation were voltage-dependent. After three days, the osteogenic gene expression and alkaline phosphatase activity were up to 2.35-fold higher following the electrical stimulation with 0.2 Vand 1.4 Von electrodes and coverslips compared to controls. Furthermore, collagen type I mRNA, as well as the amount of the C-terminal propeptide of collagen type I were increased after the stimulation with 0.2 Vand 1.4 V, while the higher electrical stimulation with 2.8 Vled to decreased levels, especially on the electrodes.

Keywords: alternating current; electrical stimulation; electric field; osteoblasts; bone remodelling; osteoblasts differentiation factors; osteogenesis

1. Introduction

The implantation of a total hip replacement is a common surgery which is being performed with increasing frequency due to the rising age of the global population [1]. Surgery is indicated in the case of trauma, osteoarthritis, avascular necrosis of the femoral head, or bone loss resulting from tumours [2–5]. In a study by Springer et al., it was observed that about 10% of all patients sustained a loosening of the implant in the 15-year period after the surgery [6]. Notably, 80% of these cases represent aseptic loosening, although there is strong evidence regarding the high percentage of false-negative microbiologic results due to the insensitivity of the method [7,8]. To avoid aseptic loosening, a promising option for the enhancement of early and stable implant fixation is the application

of electrical stimulation as an adjunct therapy, during the critical phase after surgery. Bone formation and bone remodelling are known to be triggered by the application of mechanical loads on the bone tissue [9]. Since Fukada and Yasuda discovered that endogenous electrical fields arise in bone through the application of mechanical force, a lot of research and clinical applications have been done in the field of electrical stimulation [10]. The use of the inverse piezoelectric effect to improve bone formation by electrical stimulation (ES) is already utilised as an adjunct therapy with good levels of evidence for non-unions, ankle/foot unions, spinal fusions, and necrosis of the femoral head [11–13]. ES can be applied by direct, capacitive, or inductive coupling. Thereby, electric fields are delivered by direct or alternating current. Using a direct coupling system, electrodes and power supply are placed invasively on the affected bone and therefore can lead to the risk of infection, soft tissue irritation, and a second surgical procedure for electrode removal after bone healing/regeneration. Capacitive coupling, using electrodes attached to the skin above the bone defect, is non-invasive ES. However, skin irritation can occur during capacitive coupled electrical stimulation and the application of high voltages is necessary to induce appropriate electric fields inside the bone tissue. Inductive coupling delivers the pulsed electromagnetic fields (PEMFs) via one or two magnetic coils placed over the bone defect and therefore induce an electrical field through PEMFs while connected to an outer current supply [11]. Another option for the application of ES after joint arthroplasty is the integration of devices for electrical stimulation into the endoprosthetic implant. A possible design of such an implant has been described previously [14,15]. The advantages of this method are the possibility of direct electrical stimulation at the desired site of the bone regeneration and the need for low patient compliance.

The effect of direct current (DC) and PEMFs on osteoblasts and mesenchymal stem cells has been demonstrated in vitro in several studies, showing an increase in proliferation, differentiation factors like osteocalcin, osteopontin, and Runt-related transcription factor 2 (RunX2), an increased alkaline phosphatase (ALP) activity, and calcium deposition [16–23]. However, research on electric fields generated through alternating current (AC) is less common but interesting, since the application of AC reduces corrosion processes at the electrodes that contribute to particular wear generation and metal ions release on the implant surface [24]. Besides this advantage of AC, it leads to a reduction in the pH shifts and gas formation, which would otherwise lead to tissue irritation. In our previous work, we have established an in vitro system for the alternating current stimulation where bone cells can be cultivated on top of rough electrodes made of Ti6Al4V [25]. These represent the surface of an endoprosthetic implant that delivers ES. Thereby, osteoblasts were cultivated in small distances to the electrodes on collagen-coated glass coverslips in order to approach physiological growth conditions in an implant's surroundings. Hence, the effects of AC stimulation on contact and distant osteogenesis could be investigated with the in vitro stimulation system. In the present study, the influence of different voltages resulting in varying electric fields were analysed in order to determine the suitable voltages for the application in AC stimulation.

2. Results

2.1. Influence of Alternating Electric Fields on Osteoblast Morphology

The viability of human osteoblasts, after their exposure to alternating electric fields for three and seven days, was ensured by actin staining following the strongest stimulation protocols, which were 1.4 Vcontinuous and 2.8 Vintermittent electrical stimulations (ES). The cell morphology, intensity, and orientation of actin fibres were unchanged after ES, compared to the unstimulated controls on collagen-coated coverslips (Figure 1a) and titanium electrodes (Figure 1b) at both time points. The dimensions of osteoblasts growing on rough Ti6Al4V electrodes were smaller than those growing on collagen-coated coverslips due to the rough surface. However, the osteoblasts were able to proliferate on the electrodes, showing a higher cell density after seven days, compared to the three-day time point, and formed a confluent cell layer on both the rough surface of the electrode and the smooth surfaces of the collagen-coated coverslip under control and ES conditions.

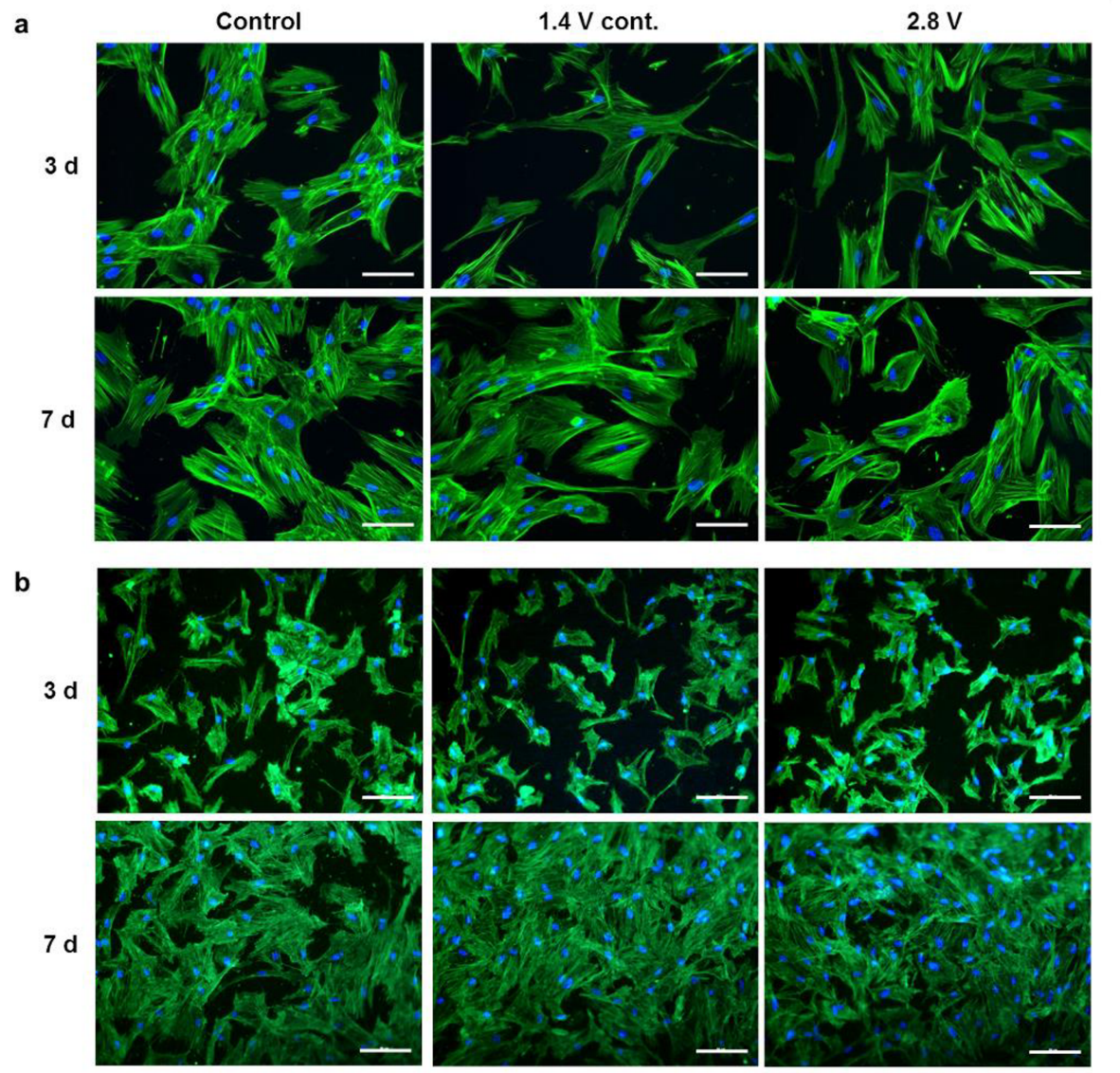

Figure 1. Actin staining of human osteoblasts on collagen-coated coverslips (**a**) and Ti6Al4V electrodes (**b**) in unstimulated cells, after electrical stimulation (ES) with 1.4 Vcont. and 2.8 Vafter three and seven days. The 2.8 Vgroup was stimulated 3 × 45 min per day, while the 1.4 Vcont. group was stimulated continuously with 1.4 V. The scale measures 50 µm.

2.2. *Effects of Alternating Electric Fields on Osteoblastic Proliferation*

Electrical stimulation showed no significant influence on the proliferation of human osteoblasts during seven days of stimulation using different applied electrical fields. Furthermore, the proliferation was not changed through the intensity of the electrical field acting on the cells. Cells cultivated on the electrode showed similar proliferation as cells cultured on collagen-coated coverslips on the bottom of the well (Figure 2).

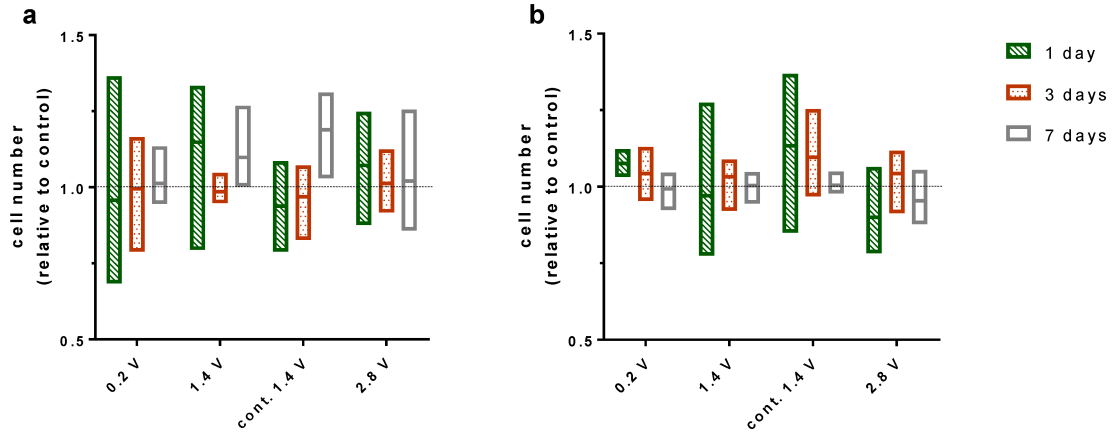

Figure 2. Cell number of osteoblasts cultured one, three, and seven days with and without electrical stimulation counted via ImageJ. Cell number is displayed relative to the control for each time point. For this experiment, 0.2V, 1.4 V, and 2.8 Vgroups were stimulated 3 × 45 min per day while the cont. 1.4 Vgroup was stimulated continuously with 1.4 V. Cells grown on Ti6Al4V electrodes (**a**) and collagen-coated coverslips (**b**). $n = 3$.

2.3. Effects of Alternating Electric Fields on Osteogenic Gene Expression

Three genes for osteogenic differentiation, collagen 1 (*COL1A1*), alkaline phosphatase (*ALP*), and osteocalcin (*BGLAP*) were examined. *COL1A1* and *ALP* were expressed at every time point for each ES. *BGLAP* expression could be detected after three and seven days of cultivation.

COL1A1 expression in human osteoblasts on Ti6Al4V electrodes was mainly downregulated through stimulation with 2.8 Vover time. After one day of cultivation with 2.8 V, the gene expression was slightly upregulated but dropped significantly after seven days ($p = 0.0190$). Further, after three days, the gene expression was significantly downregulated compared to 0.2 Vand 1.4 Vcontinuous stimulation ($p = 0.0044$, $p = 0.0004$, respectively) and compared to the unstimulated control ($p = 0.0078$). The same progression could be observed for the cultivation with 2.8 Vover seven days, as the gene expression for ES with 0.2 V, 1.4 V, and continuously 1.4 Vwas significantly higher compared to 2.8 V ($p = 0.0089$, $p = 0.0027$, $p = 0.0299$, respectively) (Figure 3a). The expression of *ALP* showed similarities to the *COL1A1* gene expression from cells grown on electrodes. Cells stimulated with 2.8 Vexpressed a higher amount of *ALP* after one day of stimulation but reduced their expression after three days ($p = 0.0460$) and seven days ($p = 0.0061$) of cultivation. Compared with the data from ES using 1.4 V, cells stimulated with 2.8 Vexpressed significantly less *ALP* after three days ($p = 0.0178$) and seven days ($p = 0.0337$) (Figure 3c). *BGLAP* expression of cells growing on electrodes was significantly lower after ES with 2.8 Vcompared to ES with 0.2 Vafter three days ($p = 0.0166$) (Figure 3e).

Cells growing on coverslips showed less change in the gene expression of *COL1A1*, *ALP*, and *BGLAP* after ES compared to cells growing on electrodes. *COL1A1* expression was increased after three days for ES with 0.2 V, 1.4 V, and continuous 1.4 V. Thereby, the increase after three days of stimulation with 1.4 Vwas significant ($p = 0.0078$). Furthermore, the decrease of the *COL1A1* expression from three to seven days was significant for 0.2 Vand 1.4 V($p = 0.0369$, $p = 0.0218$, respectively). Cells grown under ES with 2.8 Vfor three days expressed significantly less *COL1A1* compared to cells with 0.2 V($p = 0.0319$) and continuous 1.4 V($p = 0.0386$) (Figure b). As for the electrodes, cells growing on coverslips showed a similar expression behaviour of *ALP* and *COL1A1*. ES with 1.4 Vled to a significant increase in *ALP* expression after three days compared to the unstimulated control ($p = 0.0319$) and the stimulation with 2.8 V($p = 0.0155$). As for *COL1A1*, the expression of *ALP* decreases under ES with 2.8 Vwith time. Furthermore, a stimulation with continuous 1.4 Vled to decreased *ALP* expression after seven days ($p = 0.0313$) (Figure 3d). No significant change of *BGLAP* expression could be observed for the cultivation under electrical stimulation (Figure 3f).

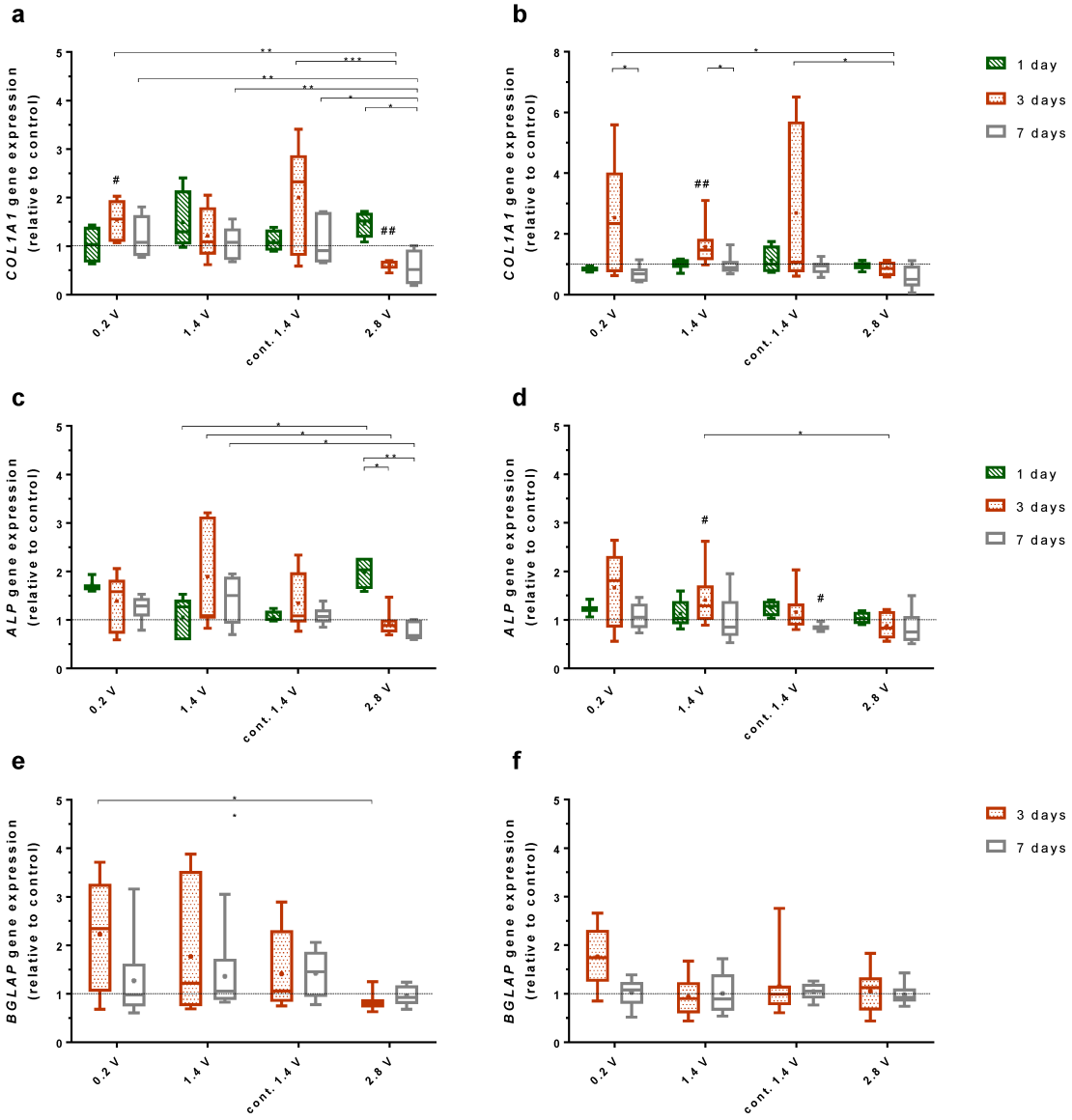

Figure 3. $2^{-\Delta\Delta Ct}$ values for the gene expression of collagen type I (*COL1A1*; **a**,**b**), alkaline phosphatase (*ALP*; **c**,**d**), and osteocalcin (*BGLAP*; **e**,**f**) after electrical stimulation, compared to the unstimulated controls for the same time points. Cells were cultured on Ti6Al4V electrodes (**a**,**c**,**d**) and collagen-coated coverslips (**b**,**d**,**f**) for one, three, and seven days. The 0.2V, 1.4 V, and 2.8 Vgroups were stimulated 3 × 45 min per day, while the cont. 1.4 Vgroup was stimulated continuously with 1.4 V. # indicates significant differences between the stimulated and control groups: # $p < 0.05$ and ## $p < 0.01$ (Wilcoxon matched pair test), * indicates significant differences between stimulation groups: * $p < 0.05$, ** $p < 0.01$, *** $p < 0.001$ (two-way ANOVA). $n \geq 3$.

2.4. Effects of Alternating Electric Fields on Osteogenic Mediators

De novo synthesis of collagen type I of the osteoblasts growing on both the electrodes and coverslips was evaluated by the detection of the propeptide of collagen type I (C1CP) in the cell culture supernatant. A significant increase in the C1CP synthesis was found after ES with 1.4 V($p = 0.0391$), while 2.8 Vstimulation significantly decreased the C1CP synthesis after three days of ES ($p = 0.0059$), as compared to the unstimulated controls (Figure 4). Differences between both stimulation groups were significant ($p = 0.0056$). Further, the amount of C1CP differed significantly between the stimulation with continuous 1.4 Vand 2.8 V($p = 0.0095$) after three days. No changes in the C1CP synthesis were detected after seven days of ES compared to the unstimulated cells or between the different stimulation groups.

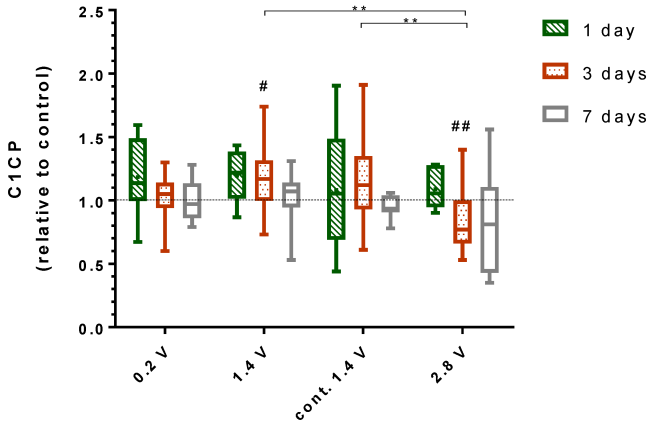

Figure 4. Collagen type 1 propeptide (C1CP) synthesised by human osteoblasts growing on electrodes and coverslips for one, three, and seven days. Peptide concentrations were determined from cell culture supernatant with and without electrical stimulation, and values are displayed relative to the unstimulated control for each time point. For this experiment, 0.2V, 1.4 V, and 2.8 Vgroups were stimulated 3 × 45 min per day, while the cont. 1.4 Vgroup was stimulated continuously with 1.4 V. # indicates significant differences between the stimulated and control groups: # $p < 0.05$ and ## $p < 0.01$ (Wilcoxon matched pair test), * indicates significant differences between stimulation groups: ** $p < 0.01$ (two-way ANOVA). $n \geq 6$.

The alkaline phosphatase (ALP) activity from cells growing on electrodes was significantly elevated after their exposure to 0.2 V, 1.4 V, and continuous 1.4 Vcompared to 2.8 V($p = 0.0004$, $p = 0.0003$, $p = 0.0002$, respectively) (Figure 5a). After seven days of stimulation, this trend was continued for 0.2 Vand 1.4 Vcompared to 2.8 V($p = 0.0002$, $p = 0.0005$, respectively). Seven days after exposure to 1.4 Vcontinuous stimulation, the ALP activity decreased significantly ($p = 0.0313$). Further, ES with 2.8 Vreduced the ALP activity on the electrodes significantly after three days ($p = 0.0313$) and non-significantly after seven days.

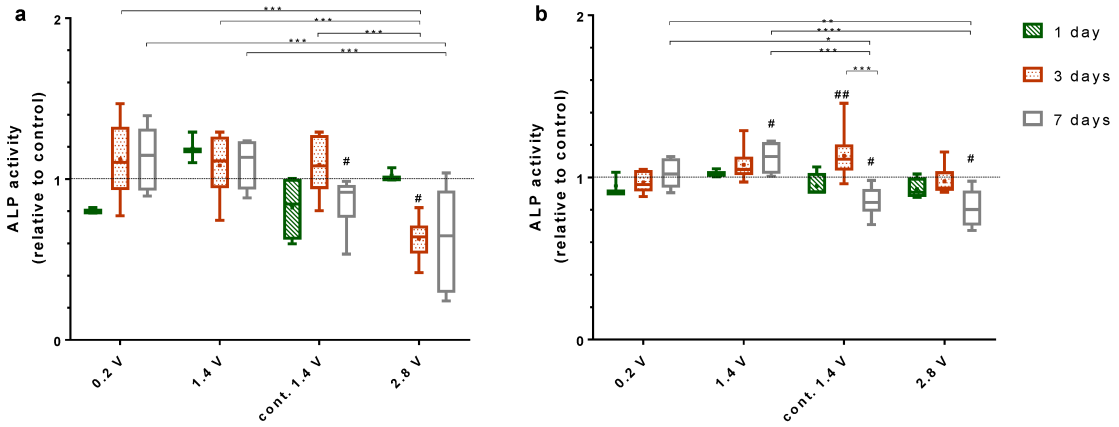

Figure 5. Alkaline phosphatase activity (ALP) of human osteoblasts growing on electrodes (**a**) and coverslips (**b**) with and without electrical stimulation. Results are displayed relative to the unstimulated controls after one, three, and seven days. For this experiment, 0.2 V, 1.4 V, and 2.8 Vgroups were stimulated 3 × 45 min per day, while the cont. 1.4 Vgroup was stimulated continuously with 1.4 V. # indicates significant differences between the stimulated and control groups: # $p < 0.05$ and ## $p < 0.01$ (Wilcoxon matched pair test), * indicates significant differences between stimulation groups: * $p < 0.05$, ** $p < 0.01$, *** $p < 0.001$ and **** $p < 0.0001$ (two-way ANOVA). $n \geq 3$.

Cells cultivated on collagen-coated coverslips with a stimulation of 0.2 Vand 1.4 Vshowed increasing ALP activity over time (Figure 5b). After seven days, the ALP activity for ES with 1.4 Vincreased significantly compared to the control ($p = 0.0313$). Furthermore, the ES with 0.2 Vand 1.4 Vled to a significant rise in ALP activity after seven days compared to ES with continuous 1.4 V($p = 0.0276$, $p = 0.0001$, respectively) and 2.8 V($p = 0.0044$, $p < 0.0001$). Cells stimulated continuously with 1.4 Vinitially showed a significant increase in ALP activity after three days ($p = 0.0078$), though the ALP activity decreased significantly after seven days compared to three days ($p = 0.0001$) and the unstimulated control ($p = 0.0313$). A similar significant decrease could be observed for cells cultivated over seven days with 2.8 VES ($p = 0.0313$).

3. Discussion

In the present in vitro study, we investigated the response of human osteoblasts to alternating electric fields when seeded directly on the rough surface of Ti6Al4V electrodes, modelling an implant surface equipped with an AC stimulator for bone cell growth on the implant. In these experiments, the osteoblasts were also seeded at a short distance to the electrodes on collagen-coated coverslips to evaluate the effects of electrostimulation on bone cells growing in the tissue surrounding the implant.

Staining the cytoskeleton of the osteoblasts with phalloidin showed no effect of electrical stimulation with 2.8 Vor continuous stimulation with 1.4 Von actin organisation. The cells were able to maintain a spread phenotype and proliferate evenly on electrodes, demonstrating that the osteoblast viability was not deteriorated by the electrical stimulation applied in our study. Quantification of the stained nuclei of the osteoblasts could equally show that the amount of cells on the electrodes and coverslips was not reduced by ES.

Effects of ES on osteoblast functions were highly voltage-dependent. While 0.2 Vand 1.4 Vresulted in enhanced expression of the key mediators involved in bone formation (C1CP, and ALP), 2.8 Vreduced the osteoblast function. Applying the same voltage, the continuous stimulation was not found to be superior to an intermittent stimulation (3 × 45 min per day), having even a negative effect on the expression of the investigated mediators, such as ALP after seven days, as compared to the unstimulated controls. Considering the required energy supply of the electrically active implants, shorter stimulation periods are also preferable over continuous stimulation. Compared to the three-day stimulation period, the positive effects of ES on the osteoblast function were slightly diminished after seven days of ES, as the C1CP concentration as well as the *COL1A1* gene expression dropped from three to seven days. On the other hand, ALP activity was constant or even rose over time. Su et al. showed that the gene and mediator expression of differentiation factors can vary over time when using capacitive ES [26]. Therefore, it would be interesting to cultivate the cells over a longer time period to survey possible fluctuations of the osteogenic markers under ES. Further, as various differentiation factors are expressed on different time points throughout osteoblasts differentiation, it is possible that other factors which were not examined were positive influenced through ES [27].

Although significant effects dependent on the applied AC voltage could be demonstrated in our study, these effects were relatively small. The sensitivity of human osteoblasts from different patients to ES was subjected to high variances. Since human osteoblasts were pre-differentiated during the cultivation before conducting the experiments, cells might have reached a high differentiation state, thereby further limiting the effects of ES. Therefore, the use of mesenchymal stem cells with a high differentiation capacity might elicit more pronounced effects from the applied AC voltages, considering that implant ingrowth is not only realised by the pre-existing osteoblasts but also by the immigrating precursor cells that undergo differentiation into the osteogenic lineage. The influence of AC on mesenchymal stem cells has been investigated by Hronik-Tupaj et al. [28]. In this previous study, the human bone marrow-derived stem cells were exposed to a 2 V/m AC field with a frequency of 60 kHz for 40 min per day [28]. The researchers found an increase in *COL1A1* and *ALP* transcripts on day 15 and 20, which were associated with an increase in heat shock protein 27 transcripts and a higher metabolic activity as compared to the unstimulated controls. However, collagen fibres and calcium deposition

were not increased in stimulated samples, compared to the control samples [28]. McCullen et al. stimulated adipose-derived stem cells with very high AC fields ranging from 1–1000 V/cm at 1 Hz frequency for four hours per day [29]. The cell viability and attachment were maintained at a maximum of 10 V/cm. While 1 V/cm increased the calcium deposition as compared to the controls on day 28, the rise in intracellular calcium was first seen when 10 or 100 V/cm was applied [29].

Further, the substrate in which the cells are electrically stimulated by ES is important for the ES effects. In a previous study, human osteoblasts cultured on three-dimensional collagen scaffolds and stimulated with a magnetic field and an additional alternating electric field strongly increased the collagen synthesis [30]. The effects could be due to a coupled mechanical stimulation induced by the piezoelectric properties of the collagen scaffold [31]. However, the osteoblast function was also increased during the electromagnetic stimulation when cultured in a non-piezoelectric three-dimensional matrix using a similar test set-up [32]. Jin and Kim exposed the osteoblast-like MG-63 cells to AC fields (5.5 V/m, 60 Hz, 30 min per day) during culture on a different polycaprolactone (PCL)-based scaffold [33]. They found elevated ALP activity and calcium deposition after ES on day 14, with the highest effects apparent in MG-63 cells seeded on PCL scaffolds that included β-tricalcium phosphate [33]. The conductive polypyrrole (PPY)/PCL scaffold used by Zhang et al. led to an increased cell proliferation compared to pure PCL scaffolds, with both scaffolds under electrical stimulation (0–250 μA, DC) [34]. In our present study, we stimulated the human osteoblasts on collagen-coated coverslips to supply a physiologic surface. Three-dimensional conductive scaffolds, such as bioceramic scaffolds [35,36], conductive hydrogels [37], or biodegradable polymers as polyaniline scaffolds [38], can be implemented in further studies to approach better physiologic conditions in order to adjust the electrical field distribution during electrical stimulation. A limitation of our present study is that the complex in vivo situation, including the interplay of different bone and precursor cells interacting via cell contacts and various cytokines and growth factors, has not been considered. Therefore, a co-cultivation of different osteogenic cells, like osteoblasts, osteoclasts, and bone marrow stem cells, should be applied in future experiments to understand the interplay between different cell types under ES. Additionally, scaffolds can be used to not only mimic the three-dimensional tissue structure but also reflect the possible replacement material which can be used in surgery.

4. Materials and Methods

4.1. Isolation and Cultivation of Human Osteoblasts

Human primary osteoblasts were isolated from the femoral heads of patients undergoing primary total hip replacement under sterile conditions, as previously described [39]. The samples were collected with the consent of the patients, following an approval by the Local Ethical Committee (Registration number: A 2010-0010, approval date: 27 January 2017). The donor cells used in the experiments were obtained from 26 females (age: 69.1 ± 11.8 years) and 25 males (age: 66.0 ± 9.9 years).

Isolated cells were cultured in Dulbecco's Modified Eagle Medium (DMEM, PAN-Biotech, Aidenbach, Germany), containing 10% fetal calf serum (FCS, PAN-Biotech, Aidenbach, Germany), 1% amphotericin B, 1% penicillin-streptomycin, and 1% Hepes buffer (all: Sigma-Aldrich, Munich, Germany) under standard cell culture conditions (5% CO_2 and 37 °C). Ascorbic acid (final concentration: 50 μg/mL), β-glycerophosphate (final concentration: 10 mM), and dexamethasone (final concentration: 100 nM) (all: Sigma-Aldrich, Munich, Germany) were added to the cell culture medium to promote osteogenic differentiation. For the cell experiments, osteoblasts in passage three were seeded on rat tail collagen coated coverslips (diameter: 12 mm, Neuvitro, Vancouver, WA, USA) with a density of 2.2×10^4 cells/cm^2 and on Ti6Al4V electrodes with a density of 3.0×10^4 cells/cm^2 due to the roughness and the enlarged surface of the electrodes. To survey the actin staining in single cells, osteoblasts were also seeded in a lower density (i.e., 4.4×10^3 cells/cm^2 on Ti6Al4V electrodes and 1.5×10^4 cells/cm^2 on collagen-coated coverslips) to ensure a closer observation of the actin cytoskeleton and a good staining quality. After adhering for 30 min at room temperature, 30 mL of cell culture medium containing

osteogenic additives were added, and the stimulation system was incubated under standard cell culture conditions for 12 h prior to electrical stimulation.

4.2. Electrical Stimulation Protocol

The in vitro stimulation system for the application of the AC voltage was designed according to the Asnis IIIs screw system used for in vivo electrical stimulation of femoral heads in humans [40]. The structure of the in vitro system and the resulting field distribution in the chamber have been described previously [25]. The electrical stimulation (ES) was started 12 h after the cell seeding. Different electrical fields were induced with 0.2, 1.4, or 2.8 Vroot mean square voltages, with a frequency of 20 Hz as a sinusoidal signal. The resulting electrical fields with a maximum of 1.4 V/m, 17 V/m, and 41 V/m were determined as previously described [25]. The ES was carried out using a Metrix GX 305 and GX310 function generator (Metrix Electronics, Bramley, Hampshire, UK). The AC voltage was applied three times a day for 45 min with 225 min breaks between stimulations (0.2 V, 1.4 V, 2.8 V), or continuously with 1.4 V(1.4 Vcont.) for a total period of one, three, or seven days. Cells were cultivated under standard cell culture conditions. For unstimulated controls, chambers were similarly prepared without a connection to the function generator.

4.3. Actin Staining

Actin cytoskeleton was stained to evaluate the cell morphology, stress fibre formation, and orientation in order to exclude harmful effects of ES. Osteoblasts were washed with phosphate buffered saline (PBS, Merck KGaA, Darmstadt, Germany) and fixed in 4% paraformaldehyde for 10 min at room temperature (RT). Cells were washed in PBS and incubated with 0.5% Triton-X (Merck KGaA, Darmstadt, Germany) in PBS for five minutes at RT for permeabilisation. Afterwards, the osteoblasts were rinsed with PBS and incubated with 100 nM Acti-stain 488 fluorescent phalloidin (Cytoskeleton, Denver, CO, USA) for 30 min at RT, protected from light. The osteoblasts were washed three times with PBS, and the cell nuclei were stained with diamidino-2-phenylindole dihydrochloride (DAPI, Merck KGaA, Darmstadt, Germany) for 5 min. The images were captured with a Leica DMI 6000 (Leica Microsystems, Wetzlar, Germany) with 200× magnification.

4.4. Cell Proliferation

The cell numbers were quantified using DAPI, as described above, or Hoechst 33342 reagent (Thermo Fisher Scientific, Waltham, MA, USA). For the staining with Hoechst 33342, the reagent was diluted in culture medium in a concentration of 8 mg/L and cells were incubated 15 min in the dark under standard cell culture conditions. The images were captured with a Leica DMI 6000 (Leica Microsystems, Wetzlar, Germany) with 200× magnification and evaluated with the open source ImageJ software.

4.5. Gene Expression Analysis

For the isolation of total RNA, the osteoblasts were lysed in TriReagent® (Zymo Research, Freiburg, Germany) and the samples were stored at −70 °C. Total RNA was extracted using Direct-zol™ RNA MiniPrep Kit (Zymo Research) according to the manufacturer's instructions. Next, 50 ng of RNA from cells stimulated for one day or 100 ng of RNA from cells stimulated three and seven days were used for the cDNA synthesis with a High Capacity cDNA Reverse Transcription Kit (Applied Biosystems, Forster City, CA, USA). Semi-quantitative real-time polymerase chain reaction (PCR) for collagen type 1 (*COL1A1*, forward primer: 5′-ACGAAGACATCCCACCAATC-3′, reverse primer: 5′-AGATCACGTCATCGCACAAC-3′), alkaline phosphatase (*ALP*, forward primer: 5′-CATTGTGACCACCACGAGAG-3′, reverse primer: 5′-CCATGATCACGTCAATGTCC-3′), and osteocalcin (*BGLAP*, forward primer: 5′-TCAGCCAACTCGTCACAGTC-3′, reverse primer: 5′-GGTGCAGCCTTTGTGTCC-3′) was performed in triplicates using innuMIX qPCR MasterMix SyGreen (Analytik Jena AG, Jena, Germany). Ct-values were normalised to the

house-keeping gene hypoxanthine guanine phosphoribosyl transferase (*HPRT,* forward primer: 5′-CCCTGGCGTCGTGATTAGTG-3′, reverse primer: 5′-TCGAGCAAGACGTTCAGTCC-3′) and analysed by the $2^{-\Delta\Delta ct}$ method [41]. The resulting gene expression is presented as the $2^{-\Delta\Delta Ct}$ value.

4.6. Collagen Type I Synthesis

The collagen type I (COL I) synthesis was investigated by the detection of the C-terminal propeptide of collagen type I (C1CP), which is released into the supernatant and directly correlates to the COL I protein biosynthesis. Supernatants containing propeptides released from osteoblasts while growing on electrodes and coverslips were collected after the experiments and stored at −20 °C until the analysis by an enzyme-linked immunosorbent assay (ELISA) (MicroVue™ CICP EIA, QUIDEL, Quidel Corporation, San Diego, CA, USA). The supernatants were treated according to the manufacturer's instructions, and the absorbance was measured at a wavelength of 405 nm using Opsys MR microplate reader (Dynex Technologies, Denkendorf, Germany).

4.7. ALP Activity

For quantifying the alkaline phosphatase activity (ALP), the cells were washed with tris buffered saline two times and lysed in distilled water containing 1% Triton-X and 1% phenylmethylsulfonyl fluoride (PMSF) for 10 min at RT. The cell lysates were incubated with 1 mM p-nitrophenyl phosphate, 100 mM 2-amino-2-methyl-1-propanol, and 5 mM $MgCl_2$ in distilled water for one hour at 37 °C, and the reaction was stopped with 2 M NaOH. Absorbance of the solution was detected at 405 nm in a microplate reader (Tecan, Maennedorf, Switzerland).

4.8. Data Illustration and Statistical Analysis

Each test was conducted with osteoblasts obtained from at least three and up to twelve patients. The data are depicted as box plots showing the medians, 25th and 75th percentile, and the minimum and the maximum. For quantification of the cell proliferation, floating bars depicting the minimum, median, and the maximum value were used because of the small sample number (n = 3). Data from the samples exposed to the ES were compared to the unstimulated controls and are depicted as a fold change. Statistical testing was done with GraphPad Prism 7 (GraphPad Software, La Jolla, CA, USA). Differences to the controls were statistically analysed by Wilcoxon matched pairs test using raw data. For gene expression, delta Ct values were compared using Wilcoxon matched pairs test and two-way ANOVA. Differences between the different ES groups and time points were analysed by two-way ANOVA using data normalised to the controls. The level of significance was set to $p < 0.05$.

5. Conclusions

Our in vitro system exclusively enables the electrical stimulation of bone cells growing on a model implant surface, thereby delivering electrical stimulation of the electrodes and the surroundings in one experiment. Suitable and inappropriate AC voltages for low-frequency bone stimulation were identified, as higher electrical stimulation with 2.8 Vsignificantly reduced osteogenic differentiation factors. The efficiency of short-term ES, as opposed to continuous stimulation, has been demonstrated, supporting clinical approaches using temporary ES due to its practicability.

Author Contributions: Conceptualization: J.Z., F.S. and A.J.-H.; methodology: J.Z., F.S., and D.H.; software: T.D.; resources: R.B.; data curation: F.S. and J.Z.; writing—original draft preparation: F.S. and J.Z; writing—review and editing: A.J.-H. and R.B.; visualization: F.S. and J.Z; supervision: A.J.-H. and R.B.; project administration: A.J.-H. and R.B.; funding acquisition: A.J.-H. and R.B. All authors have read and agreed to the published version of the manuscript.

Funding: This research was funded by the German Research Foundation (DFG) via the GRK 1505 welisa, DFG JO 1483/1-1, and CRC 1270 ELAINE.

Acknowledgments: We gratefully acknowledge Martin Krogull, Vivica Freiin Grote, and Marie-Luise Sellin for their technical support.

Conflicts of Interest: The authors declare no conflict of interest. The funders had no role in the design of the study; in the collection, analyses, or interpretation of data; in the writing of the manuscript, or in the decision to publish the results.

References

1. Cross, M.; Smith, E.; Hoy, D.; Nolte, S.; Ackerman, I.; Fransen, M.; Bridgett, L.; Williams, S.; Guillemin, F.; Hill, C.L.; et al. The global burden of hip and knee osteoarthritis: Estimates from the Global Burden of Disease 2010 study. *Ann. Rheum. Dis.* **2014**, *73*, 1323–1330. [CrossRef]
2. Bordini, B.; Stea, S.; De Clerico, M.; Strazzari, S.; Sasdelli, A.; Toni, A. Factors affecting aseptic loosening of 4750 total hip arthroplasties: Multivariate survival analysis. *BMC Musculoskelet. Disord.* **2007**, *8*, 69. [CrossRef] [PubMed]
3. Hailer, N.P.; Garellick, G.; Kärrholm, J. Uncemented and cemented primary total hip arthroplasty in the Swedish Hip Arthroplasty Register. *Acta Orthop.* **2010**, *81*, 34–41. [CrossRef] [PubMed]
4. Hooper, G.J.; Rothwell, A.G.; Stringer, M.; Frampton, C. Revision following cemented and uncemented primary total hip replacement. *J. Bone Jt. Surg. Br.* **2009**, *91*, 451–458. [CrossRef] [PubMed]
5. Corten, K.; Bourne, R.B.; Charron, K.D.; Au, K.; Rorabeck, C.H. What works best, a cemented or cementless primary total hip arthroplasty?: Minimum 17-year followup of a randomized controlled trial. *Clin. Orthop. Relat. Res.* **2011**, *469*, 209–217. [CrossRef]
6. Springer, B.D.; Fehring, T.K.; Griffin, W.L.; Odum, S.M.; Masonis, J.L. Why revision total hip arthroplasty fails. *Clin. Orthop. Relat. Res.* **2009**, *467*, 166–173. [CrossRef] [PubMed]
7. Nilsdotter-Augustinsson, Å.; Briheim, G.; Herder, A.; Ljunghusen, O.; Wahlström, O.; Öhman, L. Inflammatory response in 85 patients with loosened hip prostheses: A prospective study comparing inflammatory markers in patients with aseptic and septic prosthetic loosening. *Acta Orthop.* **2007**, *78*, 629–639. [CrossRef] [PubMed]
8. Bori, G.; Soriano, A.; García, S.; Gallart, X.; Casanova, L.; Mallofre, C.; Almela, M.; Martínez, J.A.; Riba, J.; Mensa, J. Low sensitivity of histology to predict the presence of microorganisms in suspected aseptic loosening of a joint prosthesis. *Mod. Pathol.* **2006**, *19*, 874–877. [CrossRef]
9. Wolff, J. Das Gesetz der Transformation der Knochen [The law of bone remodeling, translated by P. Maquet and R. Furlong]. *A Hirshwald* **1892**, *1*, 1–152.
10. Fukada, E.; Yasuda, I. On the Piezoelectric Effect of Bone. *J. Phys. Soc. Jpn.* **1957**, *12*, 1158–1162. [CrossRef]
11. Griffin, M.; Bayat, A. Electrical Stimulation in Bone Healing: Critical Analysis by Evaluating Levels of Evidence. *Eplasty* **2011**, *11*, e34. [PubMed]
12. Bhavsar, M.B.; Han, Z.; DeCoster, T.; Leppik, L.; Costa Oliveira, K.M.; Barker, J.H. Electrical stimulation-based bone fracture treatment, if it works so well why do not more surgeons use it? *Eur. J. Trauma Emerg. Surg.* **2020**, *46*, 245–264. [CrossRef] [PubMed]
13. Ellenrieder, M.; Tischer, T.; Kreuz, P.C.; Fröhlich, S.; Fritsche, A.; Mittelmeier, W. Arthroskopisch gestützte Behandlung der aseptischen Hüftkopfnekrose [Arthroscopically assisted therapy of avascular necrosis of the femoral head]. *Oper. Orthop. Traumatol.* **2013**, *25*, 85–94. [CrossRef] [PubMed]
14. Ebner, C.; Su, Y.; Zimmermann, U.; von Rienen, U.; Bader, R. A novel concept for active electrical stimulation of the osseointegration of an uncemented total hip stem. *Biomed. Eng. Tech.* **2014**, *59*, S1162.
15. Schmidt, C.; Zimmermann, U.; van Rienen, U. Modeling of an optimized electrostimulative hip revision system under consideration of uncertainty in the conductivity of bone tissue. *IEEE J. Biomed. Health Inform.* **2015**, *19*, 1321–1330. [CrossRef]
16. Mobini, S.; Leppik, L.; Barker, J.H. Direct current electrical stimulation chamber for treating cells in vitro. *Biotechniques* **2016**, *60*, 95–98. [CrossRef]
17. Hu, W.-W.; Hsu, Y.-T.; Cheng, Y.-C.; Li, C.; Ruaan, R.-C.; Chien, C.-C.; Chung, C.-A.; Tsao, C.-W. Electrical stimulation to promote osteogenesis using conductive polypyrrole films. *Mater. Sci. Eng. C Mater. Biol. Appl.* **2014**, *37*, 28–36. [CrossRef]
18. Meng, S.; Zhang, Z.; Rouabhia, M. Accelerated osteoblast mineralization on a conductive substrate by multiple electrical stimulation. *J. Bone Miner. Metab.* **2011**, *29*, 535–544. [CrossRef]

19. Zhai, M.; Jing, D.; Tong, S.; Wu, Y.; Wang, P.; Zeng, Z.; Shen, G.; Wang, X.; Xu, Q.; Luo, E. Pulsed electromagnetic fields promote in vitro osteoblastogenesis through a Wnt/β-catenin signaling-associated mechanism. *Bioelectromagnetics* **2016**, *37*, 152–162. [CrossRef]
20. Fassina, L.; Visai, L.; Benazzo, F.; Benedetti, L.; Calligaro, A.; De Angelis, M.G.C.; Farina, A.; Maliardi, V.; Magenes, G. Effects of Electromagnetic Stimulation on Calcified Matrix Production by SAOS-2 Cells over a Polyurethane Porous Scaffold. *Tissue Eng.* **2006**, *12*, 1985–1999. [CrossRef]
21. Luo, F.; Hou, T.; Zhang, Z.; Xie, Z.; Wu, X.; Xu, J. Effects of Pulsed Electromagnetic Field Frequencies on the Osteogenic Differentiation of Human Mesenchymal Stem Cells. *Orthopedics* **2012**, *35*, e526–e531. [CrossRef] [PubMed]
22. Wang, J.; An, Y.; Li, F.; Li, D.; Jing, D.; Guo, T.; Luo, E.; Ma, C. The effects of pulsed electromagnetic field on the functions of osteoblasts on implant surfaces with different topographies. *Acta Biomater.* **2014**, *10*, 975–985. [CrossRef] [PubMed]
23. Eischen-Loges, M.; Oliveira, K.M.C.; Bhavsar, M.B.; Barker, J.H.; Leppik, L. Pretreating mesenchymal stem cells with electrical stimulation causes sustained long-lasting pro-osteogenic effects. *PeerJ* **2018**, *6*, e4959. [CrossRef] [PubMed]
24. Yan, Y.; Neville, A.; Dowson, D. Biotribocorrosion—An appraisal of the time dependence of wear and corrosion interactions: I. The role of corrosion. *J. Phys. D Appl. Phys.* **2006**, *39*, 3200–3205. [CrossRef]
25. Dauben, T.J.; Ziebart, J.; Bender, T.; Zaatreh, S.; Kreikemeyer, B.; Bader, R. A Novel In Vitro System for Comparative Analyses of Bone Cells and Bacteria under Electrical Stimulation. *Biomed Res. Int.* **2016**, *2016*, 5178640. [CrossRef]
26. Su, C.-Y.; Fang, T.; Fang, H.-W. Effects of Electrostatic Field on Osteoblast Cells for Bone Regeneration Applications. *Biomed Res. Int.* **2017**, *2017*, 7124817. [CrossRef]
27. Rutkovskiy, A.; Stensløkken, K.-O.; Vaage, I.J. Osteoblast Differentiation at a Glance. *Med. Sci. Monit. Basic Res.* **2016**, *22*, 95–106. [CrossRef]
28. Hronik-Tupaj, M.; Rice, W.L.; Cronin-Golomb, M.; Kaplan, D.L.; Georgakoudi, I. Osteoblastic differentiation and stress response of human mesenchymal stem cells exposed to alternating current electric fields. *Biomed. Eng. Online* **2011**, *10*, 9. [CrossRef]
29. McCullen, S.D.; McQuilling, J.P.; Grossfeld, R.M.; Lubischer, J.L.; Clarke, L.I.; Loboa, E.G. Application of low-frequency alternating current electric fields via interdigitated electrodes: Effects on cellular viability, cytoplasmic calcium, and osteogenic differentiation of human adipose-derived stem cells. *Tissue Eng. Part C Methods* **2010**, *16*, 1377–1386. [CrossRef]
30. Grunert, P.C.; Jonitz-Heincke, A.; Su, Y.; Souffrant, R.; Hansmann, D.; Ewald, H.; Krüger, A.; Mittelmeier, W.; Bader, R. Establishment of a Novel In Vitro Test Setup for Electric and Magnetic Stimulation of Human Osteoblasts. *Cell Biochem. Biophys.* **2014**, *70*, 805–817. [CrossRef]
31. Wieland, D.C.F.; Krywka, C.; Mick, E.; Willumeit-Romer, R.; Bader, R.; Kluess, D. Investigation of the inverse piezoelectric effect of trabecular bone on a micrometer length scale using synchrotron radiation. *Acta Biomater.* **2015**, *25*, 339–346. [CrossRef] [PubMed]
32. Hiemer, B.; Ziebart, J.; Jonitz-Heincke, A.; Grunert, P.C.; Su, Y.; Hansmann, D.; Bader, R. Magnetically induced electrostimulation of human osteoblasts results in enhanced cell viability and osteogenic differentiation. *Int. J. Mol. Med.* **2016**, *38*, 57–64. [CrossRef] [PubMed]
33. Jin, G.; Kim, G. The effect of sinusoidal AC electric stimulation of 3D PCL/CNT and PCL/β-TCP based bio-composites on cellular activities for bone tissue regeneration. *J. Mater. Chem. B* **2013**, *1*, 1439. [CrossRef]
34. Zhang, J.; Li, M.; Kang, E.-T.; Neoh, K.G. Electrical stimulation of adipose-derived mesenchymal stem cells in conductive scaffolds and the roles of voltage-gated ion channels. *Acta Biomater.* **2016**, *32*, 46–56. [CrossRef] [PubMed]
35. Shie, M.-Y.; Fang, H.-Y.; Lin, Y.-H.; Lee, A.K.-X.; Yu, J.; Chen, Y.-W. Application of piezoelectric cells printing on three-dimensional porous bioceramic scaffold for bone regeneration. *Int. J. Bioprinting* **2019**, *5*, 210. [CrossRef]
36. Polley, C.; Distler, T.; Detsch, R.; Lund, H.; Springer, A.; Boccaccini, A.R.; Seitz, H. 3D Printing of Piezoelectric Barium Titanate-Hydroxyapatite Scaffolds with Interconnected Porosity for Bone Tissue Engineering. *Materials* **2020**, *13*, 1773. [CrossRef]
37. Distler, T.; Boccaccini, A.R. 3D printing of electrically conductive hydrogels for tissue engineering and biosensors-A review. *Acta Biomater.* **2020**, *101*, 1–13. [CrossRef]

38. Qazi, T.H.; Rai, R.; Boccaccini, A.R. Tissue engineering of electrically responsive tissues using polyaniline based polymers: A review. *Biomaterials* **2014**, *35*, 9068–9086. [CrossRef]
39. Lochner, K.; Fritsche, A.; Jonitz, A.; Hansmann, D.; Mueller, P.; Mueller-hilke, B.; Bader, R. The potential role of human osteoblasts for periprosthetic osteolysis following exposure to wear particles. *Int. J. Mol. Med.* **2011**, 1055–1063. [CrossRef]
40. Su, Y.; Souffrant, R.; Kluess, D.; Ellenrieder, M.; Mittelmeier, W.; van Rienen, U.; Bader, R. Evaluation of electric field distribution in electromagnetic stimulation of human femoral head. *Bioelectromagnetics* **2014**, *35*, 547–558. [CrossRef]
41. Livak, K.J.; Schmittgen, T.D. Analysis of relative gene expression data using real-time quantitative PCR and the $2^{(-\Delta\Delta CT)}$ method. *Methods* **2001**, *25*, 402–408. [CrossRef] [PubMed]

frontiers | Frontiers in Physiology

TYPE Original Research
PUBLISHED 30 September 2022
DOI 10.3389/fphys.2022.965181

OPEN ACCESS

EDITED BY
Laurence Vico,
Institut National de la Santé et de la Recherche Médicale (INSERM), France

REVIEWED BY
Donata Iandolo,
Ecole des Mines de Saint-Étienne, France
Marco P. Soares Dos Santos,
University of Aveiro, Portugal

*CORRESPONDENCE
Franziska Sahm,
franziska.sahm@uni-rostock.de
Anika Jonitz-Heincke,
anika.jonitz-heincke@med.uni-rostock.de

SPECIALTY SECTION
This article was submitted to Skeletal Physiology, a section of the journal Frontiers in Physiology

RECEIVED 09 June 2022
ACCEPTED 13 September 2022
PUBLISHED 30 September 2022

CITATION
Sahm F, Freiin Grote V, Zimmermann J, Haack F, Uhrmacher AM, van Rienen U, Bader R, Detsch R and Jonitz-Heincke A (2022), Long-term stimulation with alternating electric fields modulates the differentiation and mineralization of human pre-osteoblasts.
Front. Physiol. 13:965181.
doi: 10.3389/fphys.2022.965181

Long-term stimulation with alternating electric fields modulates the differentiation and mineralization of human pre-osteoblasts

Franziska Sahm[1]*, Vivica Freiin Grote[1], Julius Zimmermann[2], Fiete Haack[3], Adelinde M. Uhrmacher[3], Ursula van Rienen[2,4,5], Rainer Bader[1], Rainer Detsch[6] and Anika Jonitz-Heincke[1]*

[1]Biomechanics and Implant Technology Research Laboratory, Department of Orthopedics, Rostock University Medical Centre, Rostock, Germany, [2]Chair of Theoretical Electrical Engineering, Institute for General Electrical Engineering, University of Rostock, Rostock, Germany, [3]Institute for Visual and Analytic Computing, University of Rostock, Rostock, Germany, [4]Department Life, Light and Matter, University of Rostock, Rostock, Germany, [5]Department Ageing of Individuals and Society, University of Rostock, Rostock, Germany, [6]Department of Materials Science and Engineering, Institute of Biomaterials, Friedrich Alexander-University Erlangen-Nuremberg, Erlangen, Germany

Biophysical stimulation by electric fields can promote bone formation in bone defects of critical size. Even though, long-term effects of alternating electric fields on the differentiation of osteoblasts are not fully understood. Human pre-osteoblasts were stimulated over 31 days to gain more information about these cellular processes. An alternating electric field with 0.7 V_{rms} and 20 Hz at two distances was applied and viability, mineralization, gene expression, and protein release of differentiation factors were analyzed. The viability was enhanced during the first days of stimulation. A higher electric field resulted in upregulation of typical osteogenic markers like osteoprotegerin, osteopontin, and interleukin-6, but no significant changes in mineralization. Upregulation of the osteogenic markers could be detected with a lower electric field after the first days of stimulation. As a significant increase in the mineralized matrix was identified, an enhanced osteogenesis due to low alternating electric fields can be assumed.

KEYWORDS

pre-osteoblasts, differentiation, electric stimulation, alternating fields, long-term stimulation, bone remodeling

1 Introduction

Understanding bone remodeling processes becomes more important as the global population is getting older. The percentage of the world population aged over 65 years is presumed to rise from 14.3% in 2020 to 25.3% in 2050 to 33% in 2080, more than doubling within the next 60 years (United Nations, Department of Economic and Social Affairs, 2019). Hence, characteristics of aging will affect the quality of their life. Typical problems

during aging, such as the wear and tear of joints, can lead to limited physical mobility. The reduction of bone density and impaired healing capacities result in a higher risk of bone fractures and hip arthroplasty (Maier et al., 2016; Carvalho et al., 2021). Thus, unharmed bone healing and remodeling processes are essential for the successful regeneration and osseointegration of artificial joints (Gruber et al., 2006).

Currently, severe complications occur while healing in 5–10% of bone fractures and 1–5% of joint replacements with a revision rate of less than 5% beyond 10 years for total hip replacements (Crawford and Murray, 1997; Buza and Einhorn, 2016; Khan et al., 2016; Ferguson et al., 2018). One possibility to enhance osseointegration and to increase the early and stable fixation of bone implants are biophysical and mechanotransduction processes, particularly the stimulation with exogenous electric fields (Bhavsar et al., 2020; Hao et al., 2021). After applying mechanical loading, Fukada and Yasuda discovered endogenous electric fields in bone (Fukada and Yasuda, 1957). The described piezoelectricity can be reversed. It is already successfully used in different electrical stimulation systems for bone non-unions, ankle and foot unions, spinal fusions, and necrosis of the femoral head (Griffin and Bayat, 2011; Ellenrieder et al., 2013; Bhavsar et al., 2020).

Several studies were conducted *in vitro* to understand the underlying processes. At the cellular level, the exogenously generated electric fields induce various electrocoupling mechanisms that cause asymmetric redistribution or diffusion of electrically charged molecules on the cell membrane, activating numerous downstream signaling cascades (Balint et al., 2012; Chen et al., 2019). Another effector mechanism may be related to cell membrane depolarization through direct activation of voltage-gated Ca^{2+} ion channels (Babona-Pilipos et al., 2018; Leppik et al., 2020). In addition, the inverse piezoelectric effect is widely discussed: an electrical stimulus leads to mechanical strain, resulting in either direct reorganization of cytoskeletal filaments or interfering with cellular processes regulated by the cytoskeleton (Leppik et al., 2020). Recent *in vitro* studies on electrical stimulation demonstrate the pro-healing potential of osseous cells following electrical stimulation. In general, cell behavior can be influenced with respect to migration, proliferation, differentiation, formation of extracellular matrix, and mineralization (Leppik et al., 2020). For osteoblastic cells, the influence on phenotype expression and differentiation factors, like alkaline phosphatase (ALP), collagen type 1 and calcium deposition, could be demonstrated (Ercan and Webster, 2010; dos Santos et al., 2016; Portan et al., 2019). These findings were obtained using a variety of different test systems, including approaches for capacitive, inductive, magnetic, or direct coupling of the electric fields (Thrivikraman et al., 2018; Leppik et al., 2020). However, most studies focus on pulsed electromagnetic fields, whereas only a few studies exist on direct coupling (deVet et al., 2021). Furthermore, mainly direct current signals are used, accompanied by significant side effects due to electrochemical reactions on the electrode (Thrivikraman et al., 2018). The application of alternating fields can prevent such chemical reactions and further could act as a pump to move ions and waste to and from cells in the absence of vessels. (Balint et al., 2012; deVet et al., 2021).

The stimulation system used for direct coupling of alternating electric fields is based on the ASNIS IIIs screw system. The clinically used electrode system served as the basis for designing an electrode which can be used for *in vitro* studies but still has similarities to the *in situ* used stimulation device (Hiemer et al., 2018). This should help to improve the applicability of *in vitro* gained results. As studies mainly focused on short-term stimulation up to 7–14 days, current research focuses on the influence of long-term stimulation on the differentiation and mineralization behavior of osteoblastic cells up to 31 days (Sahm et al., 2020; deVet et al., 2021). The present study aimed to clarify how the initial induction of osteogenic differentiation can be maintained over a more extended stimulation period using the direct stimulation device. As *in vivo* studies and clinical applications often last longer than 14 days, the present study extended investigation of cell effects up to 31 days. In this context, the study by McCullen et al. (2010) already proves that prolonged stimulation over 14 days increases the mineralization capacity and the release of calcium in adipogenic stem cells and thus osteogenic differentiation (McCullen et al., 2010). de Sousa et al. (2021) analyzed the protein synthesis of osteonectin and collagen type 1 of osteoblasts under the influence of high frequencies using a capacitive coupled system over 28 days and revealed significant changes at different time points (de Sousa et al., 2021). With the following study a broader spectrum of differentiation factors and signaling molecules should be analyzed using a direct stimulation system with low alternating electrical fields. A more detailed observation of the mineralization processes was done to receive further information about the calcium deposition under electric stimulation over time. To reveal new signaling cascades which might be influenced through the electric stimulation, a transcriptome analyses of cells stimulated over 7 and 28 days was performed.

2 Materials and methods

2.1 Isolation and cultivation of human primary pre-osteoblasts

Human primary pre-osteoblasts were isolated from patients undergoing total hip replacement as described previously (Lochner et al., 2011). Femoral heads were

collected under sterile conditions with the patients' consent, following approval by the Local Ethical Committee (Registration number: A 2010-0010, approval date: 27 January 2017). In brief, the spongiosa was isolated and digested with collagenase a and dispase (both: Roche, Basel, Switzerland). The cell suspension was filtered and centrifuged for further purification. Afterward, it was transferred in cell culture flask and cultivated in Dulbecco's Modified Eagle Medium (DMEM, PAN-Biotech, Aidenbach, Germany) without calcium, containing 10% fetal calf serum (FCS, PAN-Biotech, Aidenbach, Germany), 1% amphotericin B, 1% penicillin-streptomycin, and 1% HEPES buffer (all: Sigma-Aldrich, Munich, Germany). $CaCl_2$ was reduced to enhance proliferation and to maintain the immature stage of the osteoblasts. Ascorbic acid (final concentration: 50 µg/mL), β-glycerophosphate (final concentration: 10 mM), and dexamethasone (final concentration: 100 nM) (all: Sigma-Aldrich, Munich, Germany) were added to the cell culture medium to prevent cells from dedifferentiation and promoting the osteogenic stage of the cells (Coelho and Fernandes, 2000). All cultivation steps were performed under standard cell culture conditions (5% CO_2 and 37°C). After two passages, ALP activity was tested on a random basis to ensure the pre-osteoblastic cell stage. The cells were stored in liquid nitrogen until usage.

For the stimulation experiments, pre-osteoblasts from a total of 19 different donors, ten females (age: 72.3 ± 8.68 years) and nine males (age: 73.3 ± 6.3 years) were thawed and cultured for another passage using the same medium and osteogenic additives (ascorbic acid, β-glycerophosphate, dexamethasone) as described above. 30,000 cells, each from a different donor, were seeded on a rat tail collagen-coated coverslip (diameter: 15 mm, Neuvitro Corporation, Vancouver, WA, United States) placed in the center of a 6-well plate. After adhering for 30 min at room temperature, 5 mL of cell culture medium was added. The medium contained the osteogenic additives with the addition of 200 mg/L $CaCl_2$ for activating mineralization processes and promote further cell differentiation into mature osteoblasts during stimulation (Coelho and Fernandes, 2000). This medium composition was used for all experiments.

2.2 Electrical stimulation protocol

An *in vitro* setup for a 6-well cell culture plate, developed earlier by our working group, was used to analyze the influence of electrical stimulation on pre-osteoblasts (Hiemer et al., 2018). The stimulation system is based on the clinically used ASNIS IIIs screw system, which is a semi-invasive bone formation stimulating implant. In this system, two electrodes separated by an insulator are integrated into a screw that can be implanted into the femoral head. The system can be used to apply electromagnetic fields with an additional alternating electric field between 5 and 70 V/m, and its operation is based on the bipolar induction screw system (BISS) (Mittelmeier et al., 2004). The electric field delivered with the stimulation parameters is expected to stimulate the peri-implant bone tissue and thus accelerate bone regeneration (Grunert et al., 2014; Su et al., 2014). This electrode arrangement was appropriately adapted for cell culture to induce the alternating electric fields directly without the use of a magnetic coil. The miniaturization further allows a reduction in the volume of medium used, which can significantly increase the concentration of secreted proteins for further protein analysis.

Each electrode for the direct electrical stimulation comprises two Ti6Al4V cylindrical electrodes, separated by a 5 mm long insulator made of polyetheretherketone (PEEK) (Figure 1). The electrode holders were made of PEEK and can generate a 1 mm or 3 mm gap between the electrodes and the coverslips positioned on the well bottom. Thus, it is possible to generate two different electric fields: a higher electric field with the 1 mm gap and a lower one with a 3 mm gap. Voltage was applied over the Ti6Al4V contact rods using a Metrix GX 305 and GX 310 function generator (Metrix Electronics, Bramley, Hampshire, United Kingdom). The electrical stimulation started 24 h after cell seeding. A sinusoidal signal with 0.7 V_{rms} and a frequency of 20 Hz was used. The 1 mm and the 3 mm gaps were used to mimic the periprosthetic gap between the electrode and the surrounding tissue *in vivo*. The AC voltage was applied three times a day for 45 min with 225 min breaks between stimulations and a longer 855 min break. Electrical stimulation was done using the two different gaps, and unconnected electrodes were used for the unstimulated controls. For each time point and assay, the matching unstimulated control, cultured the same amount of time as the stimulated cells, served as a control. Gene expression data were generated from day 1 to day 28 to gather information about changes in transcription directly after the stimulation was started. The mineralization was analyzed from day 3 to day 31 as mineralization processes are only detectable at later time points. The metabolic activity and the protein release in the medium were observed at each time point. Samples were taken always 20 h after the last stimulation interval was started. All cultivation steps were implemented using standard cell culture conditions as mentioned above. The medium was exchanged every 7 days.

2.3 Electric field simulation

Two distances between the electrode and the well bottom were used to generate two different electric fields. The small distance of 1 mm led to a higher electric field (HEF) and the

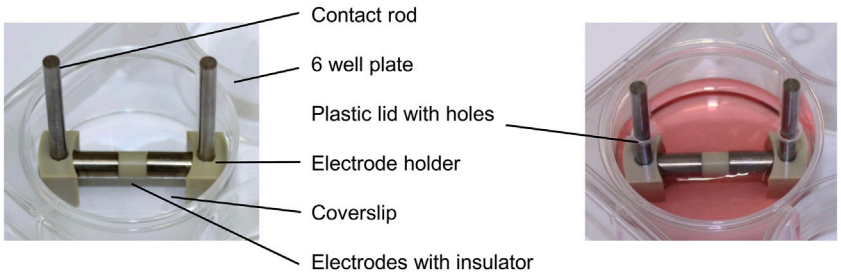

FIGURE 1
Electrical stimulation device without and with culture medium in a 6-well plate consisting of contact rods, electrode holders, and the electrodes connected over an insulator.

3 mm to a lower electric field (LEF). Numerical simulations were performed to get a first idea of the magnitudes of the LEF and HEF. The electric field strength was computed using the Finite Element Method (FEM). Laplace's equation was solved on the cell culture medium domain. The height of the cell culture medium in the center of the well was estimated by visual inspection. In this work, we did not consider the meniscus arising due to capillary effects at the well's walls and the electrode holder. The numerical solution was post-processed to obtain the total current through the medium. Convergence was ensured by locally refining the mesh and applying adaptive mesh refinement. More detailed explanations of the underlying theoretical and numerical approach can be found in an earlier publication (Zimmermann J et al., 2021). The simulations were performed using NGSolve (Schöberl et al., 2014) and the Netgen mesh generator (Schöberl, 1997). COMSOL Multiphysics was employed to verify the correctness of the results.

2.4 Cell viability

The cell viability was determined after 1, 3, 7, 14, 21, 28, and 31 days of stimulation, each 20 h after the last stimulation interval started. The coverslips with the cells were transferred from the 6-well plate to a 12-well plate. The water-soluble tetrazolium salt (WST-1) assay (Takara, Gothenburg, Sweden) was used in a ratio of 1:10 with DMEM and transfused on the cells. The reagent was incubated over 45 min at 37°C and 5% CO_2. 100 µL of the solution were transferred as duplicates into a 96-well plate. The color change was quantified using the multimode plate reader Infinite 200 pro (Tecan Group Ltd., Maennedorf, Switzerland) at a wavelength of 450 nm and a reference filter of 630 nm. The WST-1 and DMEM solution blank was carried along with each series and subtracted from the measured values.

2.5 Assessment of alkaline phosphatase activity

The activity of the intracellularly generated ALP was analyzed after 1, 3, 7, 14, 21, and 28 days of stimulation, each 20 h after the last stimulation interval started. The cells were washed twice using TRIS buffer (50 mM, pH = 8.0) lysed with 1% Triton X and 1% phenylmethylsulfonyl fluoride (both: Merck, Darmstadt, Germany) for 10 min. A solution containing 10 mM 4-Nitrophenylphosphat (AppliChem, Darmstadt, Germany), 100 mM 2-amino-2-methyl-1,3-propanediol (Sigma-Aldrich, Munich, Germany), and 5 mM magnesium chloride (Merck, Darmstadt, Germany) was added to the lysate and incubated over 1 h at 37°C and 5% CO_2. The reaction was stopped with a 2 M sodium hydroxide solution, and the absorption was measured at 405 nm with multimode plate reader Infinite 200 pro (Tecan Group Ltd., Maennedorf, Switzerland). A blank served as an internal control and was subtracted from each value.

2.6 Gene expression analysis

Gene expression was analyzed after 1, 3, 7, 14, 21, and 28 days of stimulation, each 20 h after the last stimulation interval started. Coverslips with the cells were transferred from a 6-well to a 12-well plate and lysed with the peqGOLD Total RNA Kit (VWR International GmbH, Darmstadt, Germany), following the manufacturer's instructions, to analyze the expression of genes associated with osteogenic differentiation. The purified RNA was eluted with 25 µL of sterile RNase-free water (Carl Roth GmbH & Co. KG, Karlsruhe, Germany) and RNA concentration was determined using the plate reader Infinite 200 pro. The High Capacity cDNA Reverse Transcription Kit (Thermo Fisher Scientific, Waltham, MA, United States) was used for the transcription of 100 ng RNA into complementary DNA (cDNA) following the manufacturer's instructions. The program was run at 25°C for 10 min, 37°C for 120 min and 85°C for 15 s. The cDNA was diluted 1:1 with nuclease

TABLE 1 Primer sequences for the genes of interest.

Gene	Sequence
Alkaline phosphatase (ALPL)	For: 5′-CATTGTGACCACCACGAGAG-3′
	Rev: 5′-CCATGATCACGTCAATGTCC-3′
Alpha-1 type I collagen (COL1A1)	For: 5′-ACGAAGACATCCCACCAATC-3′
	Rev: 5′-AGATCACGTCATCGCACAAC-3′
Caspase 8 (CASP8)	For: 5′-TGTTTTCACAGGTTCTCCTCCTTT-3′
	Rev: 5′-GAGAATATAATCCGCTCCACCTT-3′
Hypoxanthine-guanine phosphoribosyl transferase (HPRT)	For: 5′-CCCTGGCGTCGTGATTAGTG-3′
	Rev: 5′-TCGAGCAAGACGTTCAGTCC-3′
Integrin binding sialoprotein (IBSP)	For: 5′- ATTTTGGGAATGGCCTGTGC-3′
	Rev: 5′- GTCACTACTGCCCTGAACTGG-3′
Bone gamma-carboxyglutamate protein—osteocalcin (BGLAP)	For: 5′-TCAGCCAACTCGTCACAGTC-3′
	Rev: 5′-GGTGCAGCCTTTGTGTCC-3′
Secreted protein acidic and cysteine rich-osteonectin (SPARC)	For: 5′- CTGGACTACATCGGGCCTTG-3′
	Rev: 5′- ATGGATCTTCTTCACCCGCAG-3′
Secreted phosphoprotein 1—osteopontin (SPP1)	For: 5′-AACGCCGACCAAGGAAAACT-3′
	Rev: 5′-GCACAGGTGATGCCTAGGAG-3′
Receptor activator of nuclear factor-kappa-B ligand (RANKL)	For: 5′-TCTTCTATTTCAGAGCGCAGATGG-3′
	Rev: 5′-CTGATGTGCTGTGATCCAACG-3′
Runt-related transcription factor 2 (RUNX2)	For: 5′- CGCCTCACAAACAACCACAG-3′
	Rev: 5′- ACTGCTTGCAGCCTTAAATGAC-3′

free water, and frozen at −20°C until further usage. Samples were thawed on ice for the semi-quantitative reverse transcription-polymerase chain reaction (qPCR). The PCR was done in duplicates using the innuMIX qPCR MasterMix SyGreen Kit (Analytik Jena, Jena, Germany). The samples were heated up to 95°C for 2 min, and a cycle of 40 reruns was processed with 95°C for 5 s and 60–65°C for 25 s. Primers for the genes of interest are listed in Table 1. The delta-delta Ct (ΔΔCt) method was used to evaluate the results (Livak and Schmittgen, 2001). HPRT was used as a housekeeper gene, and the simulation samples were related to the matching control.

2.7 Quantification of the secreted proteins

The supernatants used for the quantification of secreted proteins were collected after 1, 3, 7, 14, 21, 28, and 31 days of stimulation, each 20 h after the last stimulation interval started.

2.7.1 Quantification of secreted procollagen type I and osteopontin

The type I C-terminal collagen pro peptide (CICP), and osteopontin were used as markers for the differentiation capacity of the pre-osteoblasts. The supernatants containing CICP and osteopontin were analyzed using enzyme-linked immunosorbent assays (ELISA). For CICP, the MicroVue CICP ELISA (Quidel, San Diego, CA, United States), and for osteopontin, the Human Osteopontin SimpleStep ELISA Kit (Abcam, Cambridge, United Kingdom) were used. The analyses were done following the manufacturer's instructions, and internal standards served to determine the concentration of each protein. The absorption was measured using a microplate reader (Tecan Trading AG, Maennedorf, Switzerland) at a wavelength of 405 nm. The measured protein concentration was normalized to the total protein content of each supernatant. For this purpose, the Invitrogen Qubit Protein Assay Kit and the Qubit fluorometer Q32857 (both: Thermo Fisher Scientific, Waltham, MA, United States) were used according to the manufacturer's instructions. Included standards were used to quantify the total protein content.

2.7.2 Quantification of the secreted interleukin-6, dickkopf-related protein 1 and osteoprotegerin

Secreted interleukin-6 (IL-6), dickkopf-related protein 1 (DKK-1), and osteoprotegerin (OPG) were analyzed in the supernatant of each sample with a customized human BioLegend's LEGENDplex™ multiplex assay (Biolegend, San Diego, CA, United States) containing antibodies for IL-6, DKK-1, and OPG. Analysis was done following the manufacturer's instructions, and internal standards served to determine the concentration of each protein. The multiplex assay was measured with a BD FACSVerse™ (Becton, Dickinson and Company, Franklin Lakes, NJ, United States) and analyzed with

the LEGENDplex™ Data Analysis Software. The measured protein concentration was normalized to each supernatant's total protein content (see 2.7.1).

2.8 Quantification of mineralization

The amount of calcium phosphate mineralization was determined after 1, 3, 7, 14, 21, 28, and 31 days of stimulation, each 20 h after the last stimulation interval started. The mineralization processes were examined on top of the cells and the surrounding well bottom. The glass coverslips were transferred to a 12-well plate to analyze the amount of calcium nodules on the cell layer. They were washed with PBS, fixed with PFA for 10 min (Grimm med. Logistik GmbH, Torgelow, Germany), and washed with deionized water before staining with 1% alizarin red (Santa Cruz Biotechnology, Dallas, TX, United States). After an incubation of 10 min, the coverslips containing the cell monolayer were rewashed with deionized water to remove the excess dye. The glass coverslips were dried at room temperature overnight. Pictures of the entire coverslip were generated using the digital microscope VHX-6000 (Keyence, Osaka, Japan) with an automatically stitching process of single pictures taken with a 200x magnification. The percentage of the colored surface area of the entire coverslip was determined with the open-source software ImageJ by three different researchers, and the mean value was used to prevent subjective evaluation.

The amount of deposited calcium surrounding the cell-seeded coverslips was analyzed using the remaining 6-well plates (Supplementary Figure S1). After removing the coverslips containing the cells, the well's bottom was washed with deionized water, and the calcium layer was dissolved by adding 2 ml of 0.5 M HCl. After overnight incubation, the pH was neutralized using 2 M NaOH. The calcium concentration was measured with the colorimetric Calcium Assay Kit (Abcam, Cambridge, United Kingdom), and internal standards served to determine the concentration. Measurements without human pre-osteoblast served further as controls for calcium deposition in the LEF or in unstimulated wells (Supplementary Figure S2). The assay was carried out following manufactures instructions, and the measurement was done at a wavelength of 575 nm using a microplate reader (Tecan Trading AG, Maennedorf, Switzerland).

2.9 Transcriptome analysis

The transcriptome analysis was performed by ATLAS Biolabs (Berlin, Germany). Pre-osteoblasts from three different donors were stimulated in duplicates 7 and 28 days with the HEF and without electric stimulation (control). The total RNA of each donor was isolated and afterward pooled from the three donors. The pooling was necessary due to the need of a high RNA amount for the transcriptome analysis and the comparatively low cell number used in the experiments. In the transcriptome analysis data set provided by ATLAS Biolabs, the signal intensity of more than 55,335 annotated probe sets, hence RNA transcripts were determined.

Based on the normalized, logarithmic (basis 2) probe set intensity measured for each transcript in pooled control and HEF stimulated cells, fold change values were calculated for each stimulation time, i.e., for cells stimulated 7 or 28 days.

For pathway analysis the data set was further reduced by removing all transcripts with missing gene description or any GO-annotation referring to biological or molecular functions. Further we concentrated on genes and omitted functional RNA species, such as miRNA.

The pathway enrichment analysis was done using the g:profiler and EnrichmentMap pipeline, as described in Reimand et al. (2019) (Reimand et al., 2019). The version of g:profiler used in this analysis was e105_eg52_p16_e84549f, with database update on 03/01/2022. Only annotated genes were used in the analysis and all queries were issued with the following parameters. The organism h. sapiens was chosen. As data sources, molecular function and biological process of gene ontology (GO) were used as annotations, and KEGG and Reactome were used as pathway data bases. The resulting data annotation set and gene enrichment map (gmt and gem files, respectively) were downloaded and subsequently used for visualization in cytoscape version 3.9.1. (Shannon et al., 2003).

2.10 Display of the data and statistical analysis

The data obtained in this study were depicted related to the unstimulated control (100%) of each time point. Therefore, every graph shows the changes resulting from the electric stimulations compared to the related unstimulated control. The data were shown in heatmaps and individual values with median and the 25%- and 75%-quartile. The heatmaps show the median while an upregulation with a median higher than the related control is shown in blue, a downregulation with a lower median is shown in orange.

The data were statistically analyzed using GraphPad Prism software (GraphPad Software, San Diego, CA, United States). For all experiments, a minimum of five replicates, each from a different donor, were used for each time point. The normal distribution was verified using the Shapiro-Wilk test. The results of each electrical stimulation and their respective control were compared with a paired *t*-test for normal distribution or a Wilcoxon for not normal distribution to identify significances. Differences resulting from stimulation time were analyzed using a one-way ANOVA with Tukey for normal distribution or a

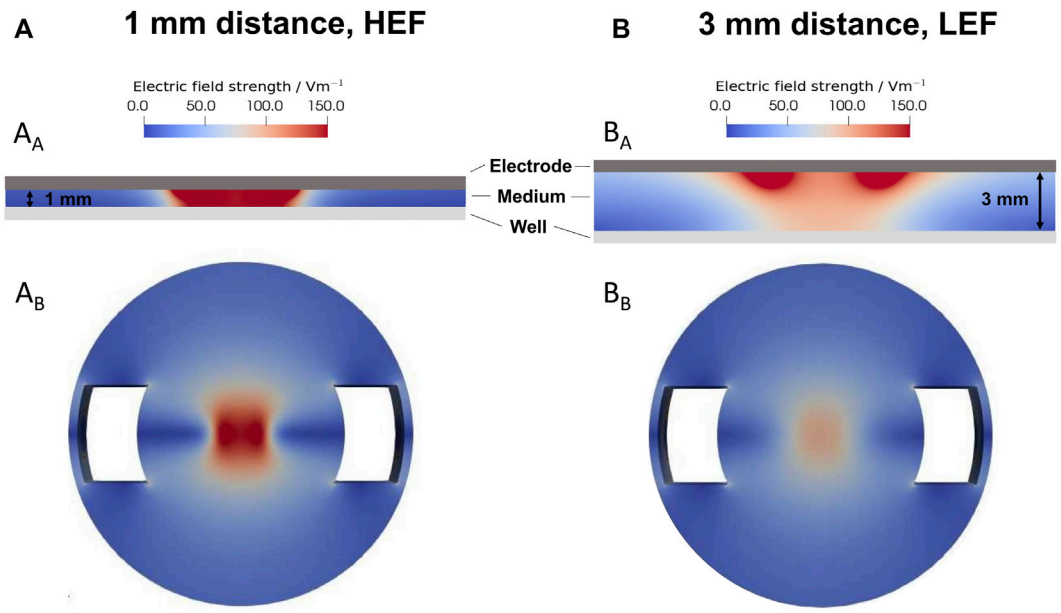

FIGURE 2
Simulation of the electric field using a sinusoidal signal with 20 Hz and 0.7 V_{rms}. **(A)** Distribution of the electric field with a distance of 1 mm, leading to a higher electric field (HEF) **(B)** Distribution of the electric field with a distance of 3 mm, resulting in a lower electric field (LEF). A_A and B_A distribution of the electric field between the electrode and the well's bottom. A_B and B_B electric field distribution on the well's bottom. The 1 mm distance results in a higher electric field up to 150 V/m, and the 3 mm distance results in a lower electric field up to 100 V/m.

Kruskal-Wallis Test with Dunn's for not normal distribution. The results for the two different electric fields were compared with a two-way ANOVA, but no significant changes ($p < 0.05$) could be determined.

3 Results

3.1 Numerical simulation of alternating electric fields

The electric field strengths were simulated for the 1 mm distance (Figure 2A) and the 3 mm distance (Figure 2B) from the electrode to the well's bottom. The smaller gap results in a HEF with up to 150 V/m in the cell medium (Figure $2A_A$) and at the well's bottom (Figure $2A_B$). The larger distance results in a LEF. The electric field strength decreased from approx 150 V/m near the electrode with increasing distance in the medium (Figure $2B_A$). According to the simulation, the electric field on the bottom of the well was a maximum of 100 V/m (Fig. B_B).

The predicted total current through the well was 17.76 mA for the HEF. The current for the LEF was about 5% smaller. In preliminary current measurements, we recorded a current of about 0.77 mA. The measured smaller current can be mainly explained by the impedance of the electrode-electrolyte interface, which we did not consider in our model. Regarding the ratio between the measured and the predicted current, the prevailing electric field in the well could be about 20 times smaller than predicted by the simulations.

3.2 Cell viability

Compared to unstimulated cells, a significant increase in the cell viability of the pre-osteoblasts could be detected 1 day after stimulation for the HEF ($p = 0.0225$) and a slight increase after 3 days for the LEF ($p = 0.0632$). Further stimulation time did not influence the viability. Besides, no significant difference between the electric fields could be detected (Figure 3).

3.3 Gene expression

The gene expression of *COL1A1*, *ALPL*, *RUNX2*, *IBSP*, *SPARC*, *BGLAP*, *SPP1*, *RANKL*, and *CASP8* was analyzed following stimulation with HEF and LEF. The respective gene expression results are summarized in the heatmaps for HEF (Figure 4A) and LEF (Figure 4F). Since Ct values for *RANKL* did not reach the limit of 29, the results were not included in this study.

For cells stimulated with HEF, a slight downregulation for *RUNX2* after 7 days ($p = 0.0541$, Figure 4C) and for *ALPL* mRNA

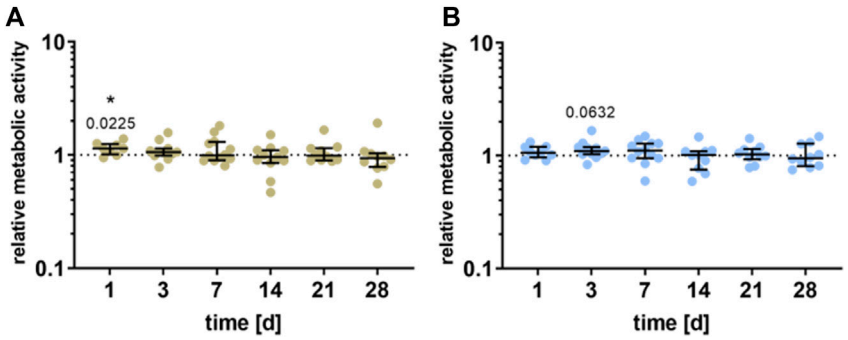

FIGURE 3
Metabolic activity of human pre-osteoblasts undergoing electrical stimulation. Pre-osteoblasts were stimulated over 31 days with two different electric fields [**(A)** higher electric field: HEF and **(B)** lower electric field: LEF] and without electrical stimulation (control). Analysis time points were 1, 3, 7, 14, 21, 28, and 31 days with assays performed 20 h after the last stimulation interval started. Metabolic activity of stimulated pre-osteoblasts related to the unstimulated control, determined *via* WST-1 assay. Results are shown as individual values with median and the 25%- and 75%-quartile to present the distribution of the total results [$n \geq 5$]. *$p < 0.05$: significant differences between the stimulated and control groups.

after 14 days ($p = 0.0519$, Supplementary Figure S3C) was detectable. After 21 days of stimulation, a slight reduction for *IBSP* could be detected (Supplementary Figure S3D) and after 28 days of stimulation, *COL1A1* ($p = 0.0671$) was upregulated (Figure 4B). Pre-osteoblasts stimulated with the HEF showed decreased *CASP8* gene expression ($p = 0.0503$, Supplementary Figure S3A) after 3 days of stimulation. No changes in the expression of *SPARC, BGLAP* and *SPP1* were observed due to the electric stimulation. (Figures 4D,E and Supplementary Figure S3B).

Stimulation with the LEF led to a downregulation of *COL1A1* mRNA on day 3 ($p = 0.061$), and of *RUNX2* on day 7 ($p = 0.0581$, Figures 4G,H). A stimulation over 21 days led to a significant upregulation of *COL1A1* ($p = 0.0285$), *RUNX2* ($p = 0.034$), *SPARC* ($p = 0.0248$), *BGLAP* ($p = 0.0433$) (Figures 4G–J), and a non-significant increase of *SPP1* (Supplementary Figure S3F). The upregulation did not continue until 28 days. Contrary, a significant downregulation of *RUNX2* ($p = 0.0475$) was detected. For cells stimulated with LEF, the mRNA transcription of *ALPL* and *IBSP* was not affected (Supplementary Figures S3G,H). Moreover, the *CASP8* gene expression was not influenced through the electric stimulation during the first days. At day 21 a slight increase in *CASP8* was detectable ($p = 0.0607$). (Supplementary Figure S3E).

3.4 Alkaline phosphatase activity and secretion of proteins

The release of different signaling proteins and the enzyme activity of ALP were analyzed for the two different distances from the electrode. The data are summarized in the heatmaps for HEF (Figure 5A) and LEF (Figure 5H). During the first stimulation days, CICP was significantly upregulated (day 1: $p = 0.0034$, day 3: $p = 0.0104$) following stimulation with HEF. A higher concentration could be detected for OPG and IL-6, with a peak at 14 and 21 and a decline at days 28 and 31. OPG and IL-6 were significantly upregulated during days 14 (OPG: $p = 0.0156$, IL-6: $p = 0.0391$) and 21 (OPG: $p = 0.0158$, IL-6: $p = 0.0117$). Moreover, OPN was significantly increased after 21 days ($p = 0.0243$) compared to the unstimulated control, and the concentration of OPG, IL-6, and DKK-1 dropped until 31 days. The electrical stimulation did not influence the ALP activity. Only after 28 days a slight decrease could be measured ($p = 0.0503$) (Figures 5B–G).

For the stimulation with the LEF, the CICP concentration was not significant influenced during the first days of stimulation but dropped until it reached its lowest value after 31 days ($p = 0.0879$) compared to the unstimulated control. ALP was not significantly influenced by the electrical stimulation but showed a similar downward trend at days 21 and 28 as CICP. The concentration of OPN and OPG was mainly upregulated 3 days (OPN: $p = 0.0427$, OPG $p = 0.0156$) and 7 days (OPG: $p = 0.0781$) after stimulation, and dropped after 14 days (OPN: $p = 0.007$). After 28 and 31 days a similar downturn as for CICP could be detected for OPN ($p = 0.0368$), OPG and IL-6 ($p = 0.0565$). DKK-1 was upregulated after 7 days ($p = 0.0156$) of electrical stimulation (Figures 5I–N).

3.5 Mineralization capacity

The mineralization capacity of the human pre-osteoblastic cells under electrical stimulation was determined by the amount of calcium deposited on the surrounding well (Supplementary Figure S1) and the calcium nodule formation on the cells

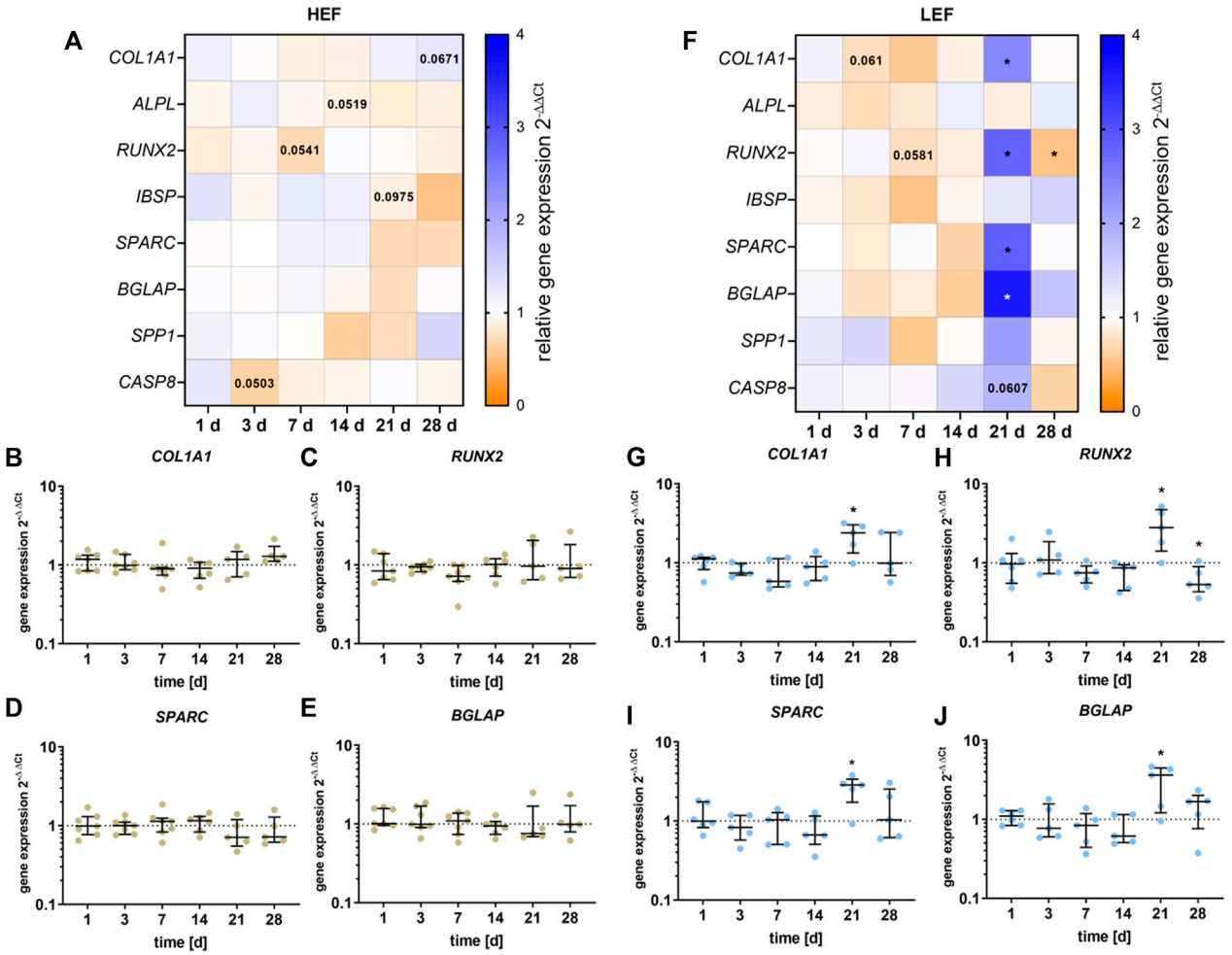

FIGURE 4
Gene expression analysis of osteogenic differentiation marker following stimulation with two different electric field strengths [**(A–E)** higher electric field: HEF, **(F–J)** lower electric field: LEF] related to the unstimulated control. Human pre-osteoblasts were stimulated over 28 days; the analysis time points were 1, 3, 7, 14, 21, and 28 days with assays performed 20 h after the last stimulation interval started. Gene expression rates were acquired *via* qPCR and related to the control using the $2^{-\Delta\Delta Ct}$ method. **(A,F)** Results within heatmaps are shown as medians whereby the downregulation is identified in orange [< 1], the upregulation in blue [> 1], and a similar gene expression as the control in white [= 1]. **(B–E,G–J)** The distribution of the total results [$n \geq 5$] are depicted as individual values with median and the 25%- and 75%-quartile. *$p < 0.05$: significant differences between the stimulated and control groups.

(Figure 6A). Deposition of mineralized matrix increased during cultivation time, both on the cells and the surrounding (Figures 6A–C). Stimulation without cells did not lead to calcium deposition (Supplementary Figures S2A,B). Cells cultivated under HEF showed an upregulation in the calcium nodule formation on the cells after 21 days ($p = 0.0683$) compared to unstimulated controls whereas calcium deposition on the surrounding well was not influenced (Figure 6B). Stimulation with the LEF led to higher precipitation of calcium on the surrounding on days 7 ($p = 0.0736$) and 31 ($p = 0.0743$). The calcium nodule formation was upregulated on day 7 ($p = 0.0625$) and significantly upregulated on days 14 ($p = 0.0260$), 28 ($p = 0.005$), and 31 ($p = 0.0469$) (Figure 6C).

3.6 Transcriptome analysis

Based on the probe intensity in the microarray data, the fold change of each gene transcript between unstimulated control cells and cells with HEF stimulation was estimated after 7 and 28 days, respectively. For the subsequent analysis only, transcripts were considered that have a higher/lower fold change value than 1/-1 (log2), which corresponds to double/halve expression values when comparing control and stimulation.

Interestingly, for most transcripts affected by the stimulation, the expression fold change is clearly distinct for both stimulation times (see Figure 7A). Only for a small set of genes stimulation with HEF induced an up- or downregulation at both time points.

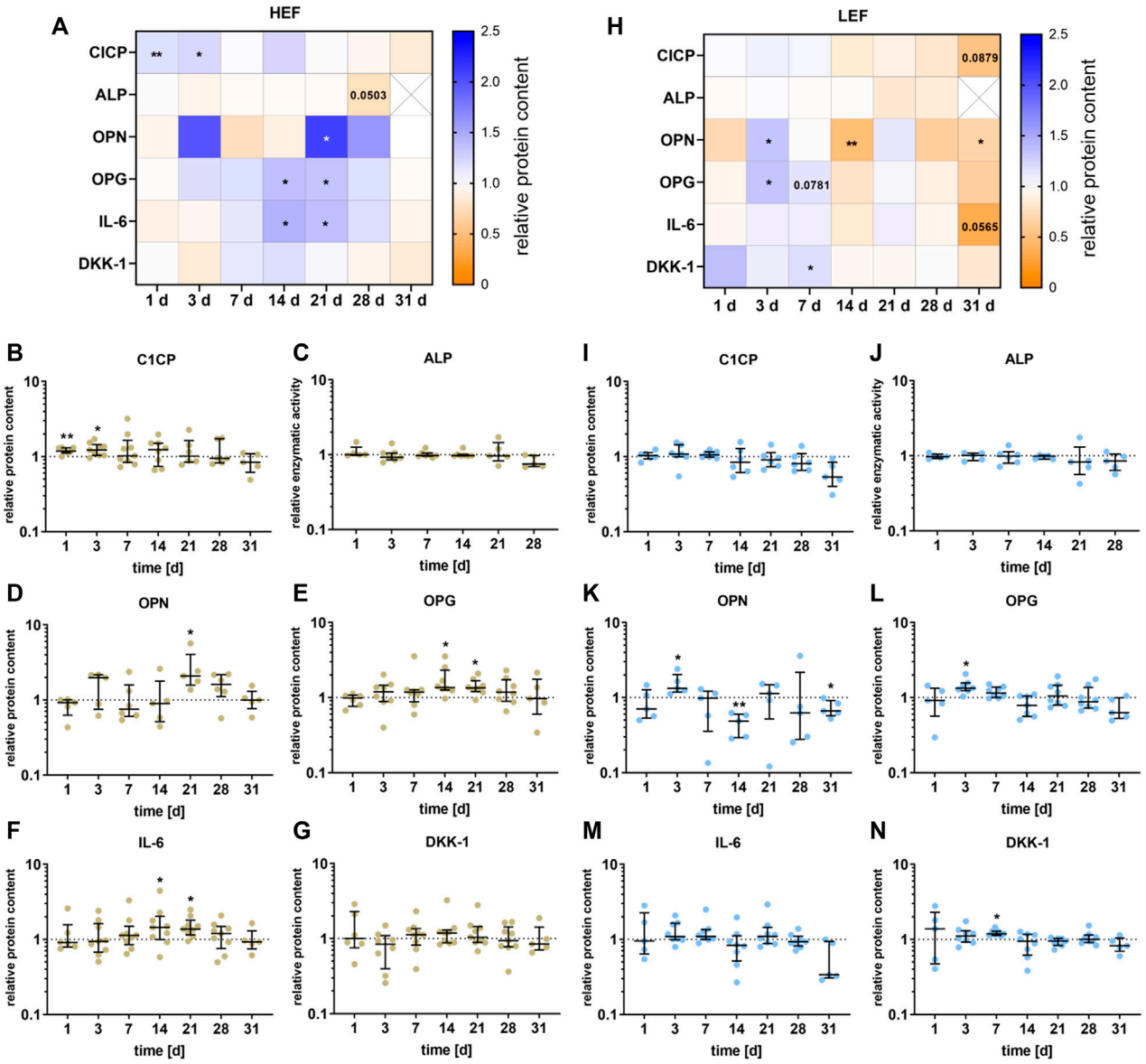

FIGURE 5
Secretion of proteins by pre-osteoblasts stimulated with two different electric field strengths [**(A–G)** higher electric field: HEF, **(H–N)** lower electric field: LEF] related to the unstimulated control. Pre-osteoblasts were stimulated over 31 days. The analysis time points were 1, 3, 7, 14, 21, 28 (for ALP), and 31 days (for CICP, OPN, OPG, IL-6, and DKK-1) with assays performed 20 h after the last stimulation interval started. Protein levels were acquired for CICP, OPN, OPG, IL-6, and DKK-1 from the supernatant and related to the total protein content of the supernatant. The activity level of ALP was generated through the lysis of the cells. The unstimulated control of each time point was used for normalization. **(A,H)** Results within heatmaps are shown as medians whereby the downregulation is identified in orange [< 1], the upregulation in blue [> 1], and a similar protein secretion as the control in white [= 1]. **(B-G, I-N)** The distribution of the total results [$n \geq 5$] are depicted as individual values with median and the 25%- and 75%-quartile. *$p < 0.05$, **$p < 0.01$: significant differences between the stimulated and control groups.

The remaining transcripts either show an up or down-regulated expression after 7 or 28 days of stimulation compared to unstimulated control, but not at both time points. Therefore, the gene expression at day 7 and 28 was considered separately in the pathway enrichment analysis.

The top 10 genes with highest and lowest expression fold changes are shown in Figure 7B. Among other genes, MMP1 and CXCL8 were both upregulated after 7 and 28 days of stimulation. SPX was one of the genes with the highest fold change for 7 days and ACKR4 for 28 days. Different G protein-coupled receptors

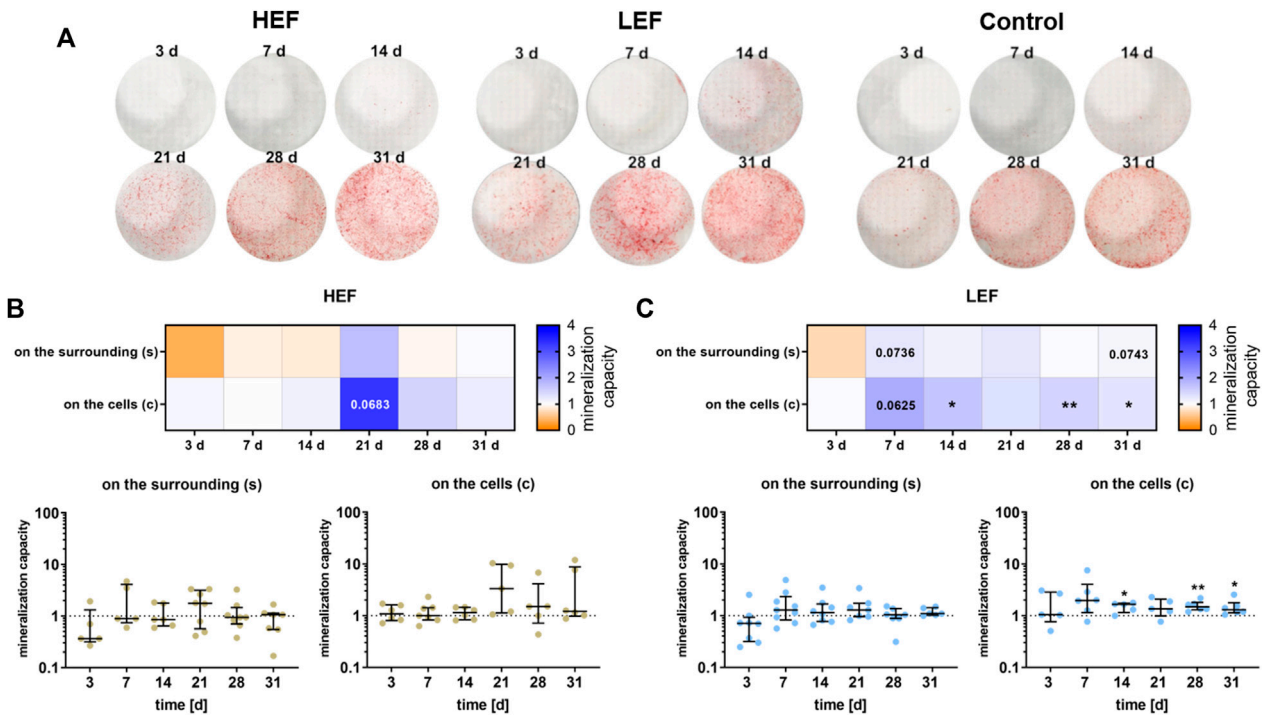

FIGURE 6
Mineralization behavior of human pre-osteoblasts undergoing electrical stimulation. Pre-osteoblasts were stimulated over 31 days with two different electric fields (higher electric field: HEF, lower electric field: LEF) and without electrical stimulation (control). Analysis time points were 3, 7, 14, 21, 28, and 31 days with assays performed 20 h after the last stimulation interval started. **(A)** Calcium nodule formation on the cells after electrical stimulation with HEF, LEF, and without electrical stimulation colored with alizarin red. **(B,C)** Evaluation of the mineralization behavior for HEF **(B)** and LEF **(C)** relative to the mineralization behavior of the unstimulated control. The amount of calcium nodule formation was determined after alizarin staining of the cells grown on coverslips (c) by proportioning the colored areas to the uncolored areas using ImageJ. The concentration of the calcium deposition on the surrounding (s) was determined after dissolving the mineralized matrix with HCl with the colorimetric Calcium Assay Kit. The unstimulated control of each time point was used for normalization. Results within heatmaps are shown as medians whereby the downregulation is identified in orange [< 1], the upregulation in blue [> 1], and a similar mineralization capacity as the control in white [= 1]. The distribution of the total results [$n \geq 5$] are depicted as individual values with median and the 25%- and 75%-quartile. *$p < 0.05$, **$p < 0.01$: significant differences between the stimulated and control groups.

were up- or downregulated e.g., OR5H14, OR52I2, OR2T29, OR1J1, and ORC6.

To gain an overview over the different cell responses revealed through the transcriptome analysis, a pathway enrichment analysis was created with separate lists for day 7 and day 28 containing all genes with distinct expression fold change (i.e., higher/lower fold change value than 1/-1 (log2)). Both gene lists were separately used as input for pathway enrichment analysis and to create gene enrichment maps with the help of g:profiler web-service. The resulting network shown in Figure 7C combines both gene enrichment maps of day 7 and day 28. It depicts all GO terms of molecular and biological functions that were overrepresented in the provided gene lists and further provides color-coded information, whether the associated genes were down- or upregulated. The network underlines the activation of different pathways by varying time points. Seven days stimulation led to a regulation of the binding, signaling pathway and activity of G protein-coupled receptors. Further, the metabolic processes of prostaglandin, eicosanoid, unsaturated fatty acids and prostanoid were upregulated. The stimulation over 28 days resulted in, among others, an increased cellular response to stimulus and stress, and different localization, locomotion reactions as well as an increase in the movement of cell or subcellular component. (Figure 7C).

4 Discussion

Electrical stimulation is known to influence bone healing processes and increase bone formation *in vivo*. Bhavsar et al. compared animal and clinical studies and revealed a positive influence of electrical stimulation in 77% of the animal studies and 73% of the clinical ones (Bhavsar et al., 2020).

Despite this availability of studies, the underlying cellular processes are not yet fully understood. While there is a substantial amount of data on short-term electric field

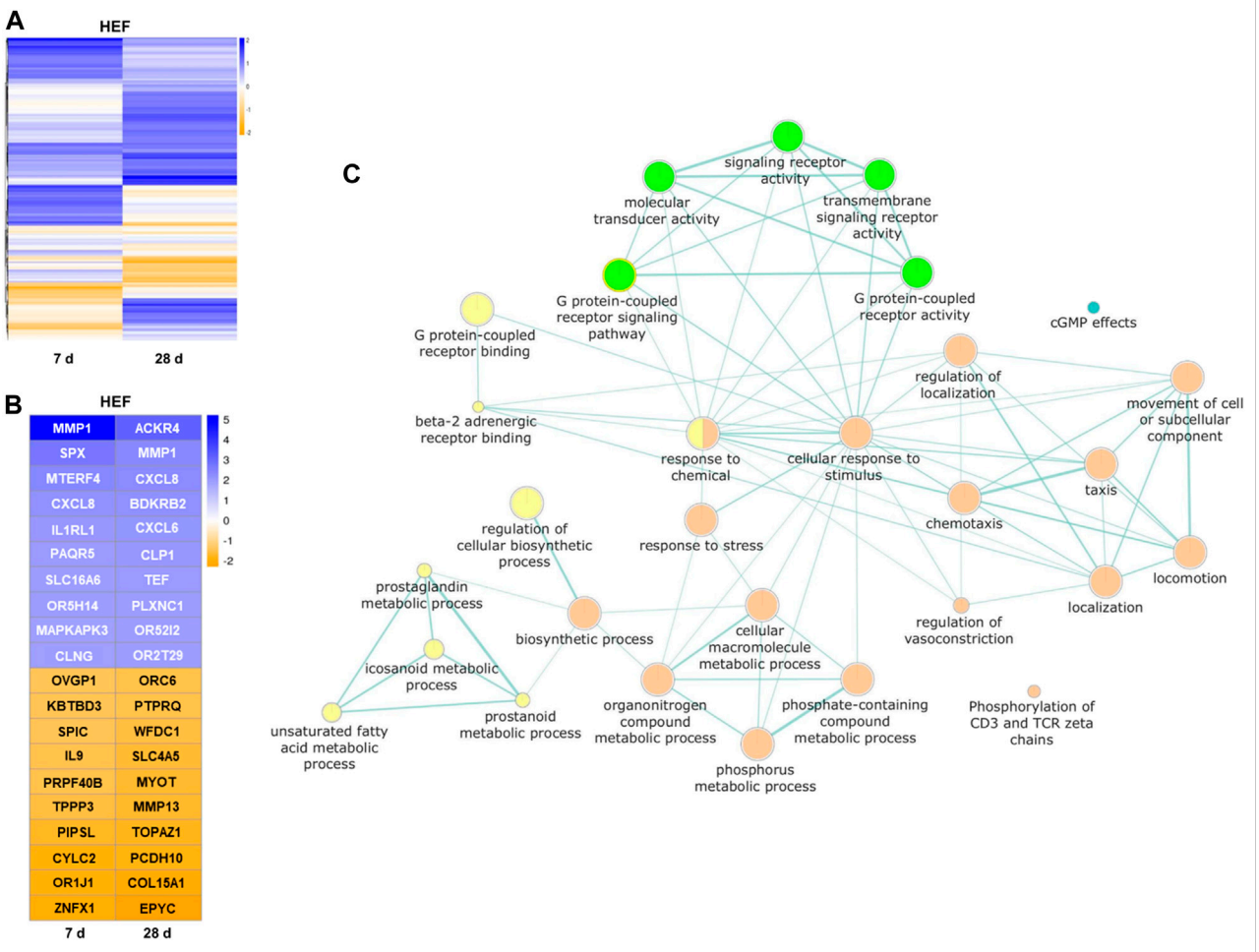

FIGURE 7
Results of the transcriptome analysis. **(A)** Heatmap of all genes with higher/lower fold change value than 1/-1 (log2), compared between unstimulated control cells and HEF stimulated cells after 7 and 28 days. **(B)** Heatmap of top 10 genes with highest and lowest fold changes (log2) each day. **(C)** Pathways influenced by the electric stimulation. Each node (circle) represents a distinct molecular or biological function, and edges (green lines) represent the number of overlapping genes, determined using a similarity coefficient (Shannon et al., 2003). Yellow and orange circles represent upregulated molecular or biological functions after 7 (yellow) and 28 days (orange) of HEF stimulation, respectively. Green and blue circles represent downregulated molecular or biological functions after 7 (green) and 28 days (blue) of HEF stimulation, respectively.

exposure studies (Supronowicz et al., 2001; Creecy et al., 2013; Bique et al., 2016), there is a lack of knowledge on the biological response in long-term *in vitro* studies using directly coupled alternating electrical fields. Therefore, the focus of this research was to stimulate human osteoblasts with alternating electric fields over a period of 31 days to investigate the differentiation and mineralization behavior of the cells at different time points. Due to the chosen setup, we were able to stimulate the cells with two different electric field strengths. In addition, we used a numerical simulation to obtain information about the distributions of the HEF and LEF electric fields used for stimulation. Our main findings in this study were: 1) High alternating electric fields (HEF) induced increased secretion of CICP, OPN, OPG, and IL-6 across different time points. 2) Low alternating electric fields (LEF) induced gene expression of important osteogenic markers at day 21. Moreover, LEF increased the amount of mineralized matrix already after 7 days of stimulation. This increased mineralization was observed throughout the stimulation period. Thus, it can be concluded that directly coupled low-level alternating electric fields promote bone mineralization *in vitro*.

During the first days of stimulation, the cell viability of pre-osteoblasts was slightly increased, and no negative long-term effect was noticable. Similar outcomes were observed by other studies using alternating electric fields with a rise in cell number after 1 day's stimulation or an increase in proliferation after 2 days (Supronowicz et al., 2001; Sahm et al., 2020). Studies with other stimulation systems revealed an influence on the cell

number or metabolic activity during the first days of stimulation and no further change in osteoblast-like cells' proliferation up to 29 days (Hronik-Tupaj et al., 2011; Zhu et al., 2017, 2019; Leppik et al., 2018; Bloise et al., 2020; Konstantinou et al., 2020; de Sousa et al., 2021). Even though these studies used different culture conditions, various stimulation systems and different cell types, a similar trend for the viability of pre-osteoblasts could be observed. As most of the studies analyzed the proliferation or viability, effects on cell apoptosis were not studied. *CASP8* is a widely described apoptotic marker for different cell types (Nicholson, 1999). The downregulation of *CASP8* with HEF after 3 days matches the slightly increased viability during the first days of stimulation. However, the upregulation of *CASP8* at day 21 with LEF was not reflected in the viability. In contrary, at day 21 the gene expression of several differentiation markers was increased. *CASP8* is not only known for its role in the cell death signaling but also has been shown to be important for the differentiation of the macrophage lineage (Kang et al., 2004). Furthermore, in osteoblastic cells, it was found that a reduction of *CASP8* transcripts decreased the expression of the osteogenic genes *BGLAP* and *PHEX* (phosphate-regulating neutral endopeptidase, X-linked gene) (Kratochvílová et al., 2020). Therefore, it can be assumed that an increase in *CASP8* mRNA following stimulation with LEF led to an increase to the investigated differentiation factors (*BGLAP, SPARC, COL1A1*) in our study. However, further work is required to evaluate a direct correlation between these signal cascades.

Besides *CASP8,* stimulation with LEF induced the mRNA transcription of *COL1A1*, *RUNX2*, *SPARC*, *BGLAP,* and *SPP1* after 21 days. These genes are involved in the induction of bone matrix formation and differentiation of osteoblasts (Bruderer et al., 2014). RUNX2 is one of the initial markers for osteogenic differentiation and decisive for the progression of pre-osteoblasts into active osteoblasts. During this differentiation process, RUNX2 is essential for the expression of bone matrix proteins like collagen 1, osteopontin, osteocalcin, and osteonectin (Huang et al., 2007; Rucci, 2008; Bruderer et al., 2014). Accordingly to Supronowicz et al. (2001) the detectable overexpression after 21 days suggests a promoting effect of electric fields on the further development of pre-osteoblasts into mature osteoblasts and for the further formation of mineralized bone matrix (Supronowicz et al., 2001). Also other studies observed a similar upregulation of osteogenic gene expression but with earlier upregulations after 7, 14, or 21 days (Hronik-Tupaj et al., 2011; Creecy et al., 2013; Wechsler et al., 2016; Zhu et al., 2017). Different stimulation systems, applied frequencies, voltages, or even the cell type origin or cultivation conditions can trigger different gene expressions at different time points (Griffin et al., 2011; Bique et al., 2016; Leppik et al., 2020). Chaudhari et al. examined the *OPG* expression using a variety of frequencies and voltages and revealed up- and downregulations of *OPG* depending on the electric field strength (Chaudhari et al., 2021). This observation can be supported with our result obtained for the secretion of OPG by the pre-osteoblasts stimulated with different electric field strengths. Besides OPG, the HEF upregulated the protein synthesis rate of IL-6, OPN and DKK-1 after 14 or 21 days of stimulation. A similar trend was detected for the LEF at an earlier stage, as the upregulation started already after the first day of stimulation. The cells seem to react differently to the varying electric field strengths underlining the importance of an optimal electric field used for stimulating bone cells.

Moreover, LEF caused a significant upregulation of the mineralized matrix after 14, 28, and 31 days of stimulation. During these days, the amounts of the investigated proteins were not influenced or even downregulated, suggesting a promoting effect on the mineralization capacity. In particular, our data demonstrate the correlation of secreted OPN on the mineralization capacity of pre-osteoblasts following stimulation with LEF. OPN in its phosphorylated state inhibits mineralization processes (Jono et al., 2000), and as the amount of ALP did not vary during stimulation, phosphorylated OPN can be assumed. When comparing mineralization and OPN release, a coherent trend becomes apparent. Is OPN upregulated or similar to the control, the mineralization capacity is not upregulated. The amount of mineralized matrix increases significantly when OPN is downregulated, confirming the regulatory effect of OPN on mineralization during electric stimulation (Jono et al., 2000). The increased deposition of mineralized matrix was detectable not only on the cell-seeded coverslips but also outside of them in the surrounding wells. It is likely that secreted microvesicles, which include Ca^{2+} and P_i ions (Bourne et al., 2021), are circulated throughout the well. At those sites where type 1 collagen has been deposited, crystallization of CaP then occurs (Bourne et al., 2021). We assume that osteoblastic deposition of a collagen matrix is not only limited to the coverslips, so that a clear mineralization can also be detected in the complete well. Moreover, as described before, the regulation of the mineralization layer seems to be dependent on the alkaline phosphatase activity and OPN secretion.

HEF, on the contrary, did not affect the mineralization processes to the same extent as LEF did, but led to a prolonged and later upregulation of secreted protein levels of OPG, IL-6, OPN, and DKK-1. These proteins are known to be involved in bone remodeling processes (Rucci, 2008; Einhorn and Gerstenfeld, 2015; Si et al., 2020). OPG is known for its influence on bone growth through the RANKL/RANK/OPG signaling system (Boyce and Xing, 2008). OPN can influence progenitor cells like mesenchymal stem cells, hematopoietic stem cells and osteoclast migration and adhesion (Walker et al., 2010; Si et al., 2020). A common underlying mechanism triggered by the electrical stimulation for DKK-1 and IL-6 may be the Wnt signaling pathway, as both are known to be involved in this pathway (Malysheva et al., 2016). DKK-1 is mainly known for inhibiting osteoblastic function but can also

play a role in the mineralization processes of mature osteoblasts (Westendorf et al., 2004; van der Horst et al., 2005). IL-6 has a controversial role in bone remodeling processes as it can activate or deactivate osteoblasts and osteoclasts, probably depending on the presence of other cytokines and the differentiation stage of the cells (Blanchard et al., 2009; Feng et al., 2017). Because these proteins were upregulated in HEF over a longer stimulation time than in LEF, a stronger influence of HEF on bone remodeling and possibly on bone resorption processes can be assumed. Further studies are necessary to prove this assumption. The cultivation of osteoclast-like cells with the supernatants generated from stimulated osteoblasts or the simultaneous stimulations in co-cultures may give insights into the activation and differentiation of osteoclasts through the released cytokines. The interaction between osteoblast and osteoclast is important to understand the up- and downregulation of cytokines which are essential for promoting healing rates in stimulated bone. A 3D printed scaffold can generate a surrounding to study the crosstalk between different cells like osteoblasts, osteoclast or endothelial cells (Sieberath et al., 2020; Kanwar and Vijayavenkataraman, 2021). It would allow the differentiation of osteoblasts into osteocytes, as 3D systems are necessary for generating osteocytes *in vitro* (Sawa et al., 2019). Further, a 3D system would enable better comparison between *in vitro* and *in vivo* conditions to increase knowledge about the influence of electrical stimulation on bone remodeling processes. Future *in vivo* studies are necessary to confirm the assumptions made through this study and to examine crosstalk between different cell types. One conceivable application would be the insertion of an electrically active stimulation device into an artificial hip stem or the use in bone defects of critical size (Zimmermann U et al., 2021). As *in vivo* processes are more complex through the interplay of different cells, the fluid flow and the bone matrix, it can be that the observed effects are diminished, unchanged or intensified. *In vivo* analysis of the healing process under electrical stimulation using sensors like the bioMEMS are possible to generate more data about the optimal stimulation conditions for increasing bone healing rates under electric stimulation *in vivo* (McGilvray et al., 2015).

To identify fundamental key factors and signaling pathways, which are the link between the external field and the increased differentiation, further studies are needed. The calcium-sensing receptor and channels like piezo 1 and 2 seems to be key factors which might be involved in the signal transduction (Lee et al., 2014; Cianferotti et al., 2015). A first try to reveal the underlying signaling cascades was done by the transcriptome analysis of cells stimulated 7 and 28 days with the HEF. The comparison between the early and late time point emphasizes the importance of a long-time stimulation *in vitro* as different gene expression profiles were observed. Under electric stimulation, the gene expression changed depending on the stimulation time. The gene expression profile of the 7 day stimulation revealed an increase in the metabolic processes of eicosanoids like prostaglandin and prostanoid and a reduction of the G protein-coupled receptor (GPCR) activity. Eicosanoids are known to be important signaling molecules and are mainly recognized by cell membrane GPCRs (Calder, 2020). As the GPCR activity was reduced, the enhanced eicosanoids processes might suggest an increase in the cell communication with other cell types triggered through the electric stimulation. Another possible target could be nuclear receptors in the cells like the peroxisome proliferator-activated receptors which are known to be involved in proliferation and differentiation processes (Chinetti et al., 2000). The 28 days stimulation led to an increase in cellular responses to stimulus, stress and to an activation and regulation of locomotion, localization and movement. The influence of electrical stimulation in the movement and migration of the cells is mainly known for direct current and electromagnetic field stimulation (Ferrier et al., 1986; Mycielska and Djamgoz, 2004; Zhang et al., 2018). As the influence of alternating electric fields on the migration was not yet described, further research needs to be done regarding long-term stimulation with alternating fields and the observation of the movement of the cell or subcellular components. In the conjunction with the enhanced migration, the transcriptome analysis revealed increased chemotaxis and taxis. It can be assumed that released chemokines influence the migration behavior not only for the osteoblastic cells but also for other cells types. The increased gene expression of osteoblastic differentiation factors at day 21 might be the possible trigger for further chemotaxis and migration. These observations underline the importance of co-culture models to understand the interplay between different cell types. The implemented transcriptome analysis is, through the pooling of analyzed samples, just a first insight. Further investigations regarding the gene expression profiles are necessary. More time points can give a better understanding on how the electric stimulation is changing the signaling cascades over time. Analysis from cells 24 h after the start of the electric stimulation might reveal cascades which are involved in the proliferation. Advanced timings are important to understand cell signaling which is fundamental for the increased mineralization.

In order to achieve more comprehensive comparability between studies, the specification of the electric field and validation of the utilized fields should be sought after. With information about the applied electric fields, research data can be put in the proper context, and the optimal electric field for bone regeneration may be identified. The numerical simulation of the electric fields used in our study is the first attempt to estimate the field resulting from the used parameters. One limitation of the numerical simulations is the assumption that the electrode-electrolyte interface

impedance does not affect the current density distribution on the electrode surface. At low frequencies such as 20 Hz, an electrochemical double layer may arise on the electrode, reducing the electric field in the surrounding. Moreover, the model makes the postulation of an electrochemically inert and stable system. Due to the cells, the progressive mineralization processes, and the electric field, electrochemical reactions in the system might occur. These electrochemical reactions would influence the electric field as well. Furthermore, electrochemical reactions on the electrode could lead to corrosion on the surface of the electrode, resulting in reduced field strengths. The first steps in addressing these issues have been made and will be refined in future research (Zimmermann J et al., 2021). Measurements with electrochemical impedance spectroscopy, local measurements of the induced voltage in the medium, and the constant documentation of the current and the voltage during stimulation will give more information about the electric field strength and possible confounding factors. Investigations about probable corrosion processes or deposits on the surface of the Ti6Al4V during electrical stimulation could answer if electrochemical reactions on the electrode arise and how strongly they influence the electric field strength. This is also important when thinking about future *in vivo* applications. *In vivo* devices may need to be controllable as the electric field is reduced by the deposition of extracellular matrix. With an adjustable device, a desired electric field can be kept constant over time by increasing parameters such as frequency or voltage. Despite a presumed reduction of the simulated field strengths during stimulation in this study, the percentage difference between the fields will remain the same. Thus, it can be assumed that the two electrode configurations with different distances will always lead to different electric fields with constant ratios.

5 Conclusion

In conclusion, our study demonstrates the importance of long-term stimulation for a better understanding of the effects of electric fields on osteoblastic cells. The impact of electrical stimulation on the cells can change as time progresses, so experiments on long-term stimulation are essential. The metabolic activity was promoted during the first days of stimulation, gene expression and protein release changed over time. The electrical stimulation with low frequency alternating electric fields activated the osteogenic differentiation of pre-osteoblast and influenced bone remodeling processes. The LEF led to an increase in the mineralization capacity over time until 31 days. In contrast, HEF did not influence the mineralization but led to a later but longer-lasting increase in the bone remodeling markers OPN, OPG, IL-6, and DKK-1. This could predict a higher efficiency in bone formations due to lower electric fields. Further experiments with immune cells and osteoclasts should be performed to understand better the influence of the released cytokines and the crosstalk between different cell types and the resulting bone remodeling processes under long-term electrical stimulation. With increased studies of electric field strengths *in vitro* and *in vivo* through validation and simulation of field distribution, more information on optimal stimulation parameters can be obtained.

Data availability statement

The datasets generated during the current study are available from the corresponding author on reasonable request.

Ethics statement

The studies involving human participants were reviewed and approved by Medical Departmend University Rostock, Local Ethical Committee (Registration number: A 2010-0010, approval date: 27 January 2017). The patients/participants provided their written informed consent to participate in this study.

Author contributions

Conceptualization: FS and AJ-H; data curation: FS and VFG; simulation: JZ; pathway enrichment analysis: FH; formal analysis: FS, JZ, FH; funding acquisition: AJ-H, RD, UV, and RB; methodology: FS and VFG. project administration: AJ-H; Resources: AJ-H and RB; supervision: AJ-H and RB; visualization: FS, AJ-H, JZ, FH; writing—original draft preparation: FS, JZ, FH; writing—review and editing: VFG, JZ, UV, FH, AJ-H, RD, and RB. All authors have read and agreed to the published version of the manuscript.

Funding

This work was supported by the Deutsche Forschungsgemeinschaft (DFG, German Research Foundation)—JO 1483/1-1, and SFB 1270/1,2 - 299150580.

Acknowledgments

We gratefully acknowledge Doris Hansmann, Vivien Krebs, Wendy Bergmann, and Michael Müller (from the Core Facility for Cell Sorting and Cell Analysis, Rostock University Medical Centre) for their technical support.

Conflict of interest

The authors declare that the research was conducted in the absence of any commercial or financial relationships that could be construed as a potential conflict of interest.

Publisher's note

All claims expressed in this article are solely those of the authors and do not necessarily represent those of their affiliated organizations, or those of the publisher, the editors and the reviewers. Any product that may be evaluated in this article, or claim that may be made by its manufacturer, is not guaranteed or endorsed by the publisher.

Supplementary material

The Supplementary Material for this article can be found online at: https://www.frontiersin.org/articles/10.3389/fphys.2022.965181/full#supplementary-material

References

Babona-Pilipos, R., Liu, N., Pritchard-Oh, A., Mok, A., Badawi, D., Popovic, M. R., et al. (2018). Calcium influx differentially regulates migration velocity and directedness in response to electric field application. *Exp. Cell Res.* 368, 202–214. doi:10.1016/j.yexcr.2018.04.031

Balint, R., Cassidy, N. J., and Cartmell, S. H. (2012). Electrical stimulation: A novel tool for tissue engineering. *Tissue Eng. Part B Rev.* 19, 48–57. doi:10.1089/ten.teb.2012.0183

Bhavsar, M. B., Han, Z., DeCoster, T., Leppik, L., Costa Oliveira, K. M., Barker, J. H., et al. (2020). Electrical stimulation-based bone fracture treatment, if it works so well why do not more surgeons use it? *Eur. J. Trauma Emerg. Surg.* 46, 245–264. doi:10.1007/s00068-019-01127-z

Bique, A. M., Kaivosoja, E., Mikkonen, M., and Paulasto-Kröckel, M. (2016). Choice of osteoblast model critical for studying the effects of electromagnetic stimulation on osteogenesis *in vitro*. *Electromagn. Biol. Med.* 35, 353–364. doi:10.3109/15368378.2016.1138124

Blanchard, F., Duplomb, L., Baud'huin, M., and Brounais, B. (2009). The dual role of IL-6-type cytokines on bone remodeling and bone tumors. *Cytokine Growth Factor Rev.* 20, 19–28. doi:10.1016/j.cytogfr.2008.11.004

Bloise, N., Patrucco, A., Bruni, G., Montagna, G., Caringella, R., Fassina, L., et al. (2020). *In vitro* production of calcified bone matrix onto wool keratin scaffolds via osteogenic factors and electromagnetic stimulus. *Mater. (Basel)* 13, 3052. doi:10.3390/ma13143052

Bourne, L. E., Wheeler-Jones, C. P., and Orriss, I. R. (2021). Regulation of mineralisation in bone and vascular tissue: A comparative review. *J. Endocrinol.* 248 (2), R51–R65. doi:10.1530/JOE-20-0428

Boyce, B. F., and Xing, L. (2008). Functions of RANKL/RANK/OPG in bone modeling and remodeling. *Arch. Biochem. Biophys.* 473, 139–146. doi:10.1016/j.abb.2008.03.018

Bruderer, M., Richards, R. G., Alini, M., and Stoddart, M. J. (2014). Role and regulation of RUNX2 in osteogenesis. *Eur. Cell. Mat.* 28, 269–286. doi:10.22203/ecm.v028a19

Buza, J. A., III, and Einhorn, T. (2016). Bone healing in 2016. *Clin. Cases Min. Bone Metab.* 13, 101–105. doi:10.11138/ccmbm/2016.13.2.101

Calder, P. C. (2020). Eicosanoids. *Essays Biochem.* 64, 423–441. doi:10.1042/EBC20190083

Carvalho, M. S., Alves, L., Bogalho, I., Cabral, J. M. S., and da Silva, C. L. (2021). Impact of donor age on the osteogenic supportive capacity of mesenchymal stromal cell-derived extracellular matrix. *Front. Cell Dev. Biol.* 9, 747521. doi:10.3389/fcell.2021.747521

Chaudhari, S. D., Sharma, K. K., Marchetto, J. J., Hydren, J. R., Burton, B. M., and Moreno, A. P. (2021). Modulating OPG and TGF-β1 mRNA expression via bioelectrical stimulation. *Bone Rep.* 15, 101141. doi:10.1016/j.bonr.2021.101141

Chen, C., Bai, X., Ding, Y., and Lee, I.-S. (2019). Electrical stimulation as a novel tool for regulating cell behavior in tissue engineering. *Biomater. Res.* 23, 25. doi:10.1186/s40824-019-0176-8

Chinetti, G., Fruchart, J.-C., and Staels, B. (2000). Peroxisome proliferator-activated receptors (PPARs): Nuclear receptors at the crossroads between lipid metabolism and inflammation. *Inflamm. Res.* 49, 497–505. doi:10.1007/s000110050622

Cianferotti, L., Gomes, A. R., Fabbri, S., Tanini, A., and Brandi, M. L. (2015). The calcium-sensing receptor in bone metabolism: From bench to bedside and back. *Osteoporos. Int.* 26, 2055–2071. doi:10.1007/s00198-015-3203-1

Coelho, M. J., and Fernandes, M. H. (2000). Human bone cell cultures in biocompatibility testing. Part II: Effect of ascorbic acid, β-glycerophosphate and dexamethasone on osteoblastic differentiation. *Biomaterials* 21, 1095–1102. doi:10.1016/S0142-9612(99)00192-1

Crawford, R. W., and Murray, D. W. (1997). Total hip replacement: Indications for surgery and risk factors for failure. *Ann. Rheum. Dis.* 56, 455–457. doi:10.1136/ard.56.8.455

Creecy, C. M., O'Neill, C. F., Arulanandam, B. P., Sylvia, V. L., Navara, C. S., and Bizios, R. (2013). Mesenchymal stem cell osteodifferentiation in response to alternating electric current. *Tissue Eng. Part A* 19, 467–474. doi:10.1089/ten.TEA.2012.0091

de Sousa, B. M., Correia, C. R., Ferreira, J. A. F., Mano, J. F., Furlani, E. P., Soares dos Santos, M. P., et al. (2021). Capacitive interdigitated system of high osteoinductive/conductive performance for personalized acting-sensing implants. *NPJ Regen. Med.* 6, 80. doi:10.1038/s41536-021-00184-6

deVet, T., Jhirad, A., Pravato, L., and Wohl, G. R. (2021). Bone bioelectricity and bone-cell response to electrical stimulation: A review. *Crit. Rev. Biomed. Eng.* 49, 1–19. doi:10.1615/CritRevBiomedEng.2021035327

dos Santos, M. P. S., Marote, A., Santos, T., Torrão, J., Ramos, A., Simões, J. A. O., et al. (2016). New cosurface capacitive stimulators for the development of active osseointegrative implantable devices. *Sci. Rep.* 6, 30231. doi:10.1038/srep30231

Einhorn, T. A., and Gerstenfeld, L. C. (2015). Fracture healing: Mechanisms and interventions. *Nat. Rev. Rheumatol.* 11, 45–54. doi:10.1038/nrrheum.2014.164

Ellenrieder, M., Tischer, T., Kreuz, P. C., Fröhlich, S., Fritsche, A., and Mittelmeier, W. (2013). [Arthroscopically assisted therapy of avascular necrosis of the femoral head]. *Oper. Orthop. Traumatol.* 25, 85–94. doi:10.1007/s00064-011-0072-4

Ercan, B., and Webster, T. J. (2010). The effect of biphasic electrical stimulation on osteoblast function at anodized nanotubular titanium surfaces. *Biomaterials* 31, 3684–3693. doi:10.1016/j.biomaterials.2010.01.078

Feng, W., Liu, H., Luo, T., Liu, D., Du, J., Sun, J., et al. (2017). Combination of IL-6 and sIL-6R differentially regulate varying levels of RANKL-induced osteoclastogenesis through NF-κB, ERK and JNK signaling pathways. *Sci. Rep.* 7, 41411. doi:10.1038/srep41411

Ferguson, R. J., Palmer, A. J. R., Taylor, A., Porter, M. L., Malchau, H., and Glyn-Jones, S. (2018). Hip replacement. *Lancet* 392, 1662–1671. doi:10.1016/S0140-6736(18)31777-X

Ferrier, J., Ross, S. M., Kanehisa, J., and Aubin, J. E. (1986). Osteoclasts and osteoblasts migrate in opposite directions in response to a constant electrical field. *J. Cell. Physiol.* 129, 283–288. doi:10.1002/jcp.1041290303

Fukada, E., and Yasuda, I. (1957). On the piezoelectric effect of bone. *J. Phys. Soc. Jpn.* 12, 1158–1162. doi:10.1143/JPSJ.12.1158

Griffin, M., and Bayat, A. (2011). Electrical stimulation in bone healing: Critical analysis by evaluating levels of evidence. *Eplasty* 11, e34.

Griffin, M., Iqbal, S. A., Sebastian, A., Colthurst, J., and Bayat, A. (2011). Degenerate wave and capacitive coupling increase human MSC invasion and proliferation while reducing cytotoxicity in an *in vitro* wound healing model. *PLoS One* 6, e23404. doi:10.1371/journal.pone.0023404

Gruber, R., Koch, H., Doll, B. A., Tegtmeier, F., Einhorn, T. A., and Hollinger, J. O. (2006). Fracture healing in the elderly patient. *Exp. Gerontol.* 41, 1080–1093. doi:10.1016/j.exger.2006.09.008

Grunert, P. C., Jonitz-Heincke, A., Su, Y., Souffrant, R., Hansmann, D., Ewald, H., et al. (2014). Establishment of a novel *in vitro* test setup for electric and magnetic stimulation of human osteoblasts. *Cell biochem. Biophys.* 70, 805–817. doi:10.1007/s12013-014-9984-6

Hao, Z., Xu, Z., Wang, X., Wang, Y., Li, H., Chen, T., et al. (2021). Biophysical stimuli as the fourth pillar of bone tissue engineering. *Front. Cell Dev. Biol.* 9, 790050. doi:10.3389/fcell.2021.790050

Hiemer, B., Krogull, M., Bender, T., Ziebart, J., Krueger, S., Bader, R., et al. (2018). Effect of electric stimulation on human chondrocytes and mesenchymal stem cells under normoxia and hypoxia. *Mol. Med. Rep.* 18, 2133–2141. doi:10.3892/mmr.2018.9174

Hronik-Tupaj, M., Rice, W. L., Cronin-Golomb, M., Kaplan, D. L., and Georgakoudi, I. (2011). Osteoblastic differentiation and stress response of human mesenchymal stem cells exposed to alternating current electric fields. *Biomed. Eng. Online* 10, 9. doi:10.1186/1475-925X-10-9

Huang, W., Yang, S., Shao, J., and Li, Y.-P. (2007). Signaling and transcriptional regulation in osteoblast commitment and differentiation. *Front. Biosci.* 12, 3068–3092. doi:10.2741/2296

Jono, S., Peinado, C., and Giachelli, C. (2000). Phosphorylation of osteopontin is required for inhibition of vascular smooth muscle cell calcification. *J. Biol. Chem.* 275, 20197–20203. doi:10.1074/jbc.M909174199

Kang, T.-B., Ben-Moshe, T., Varfolomeev, E. E., Pewzner-Jung, Y., Yogev, N., Jurewicz, A., et al. (2004). Caspase-8 serves both apoptotic and nonapoptotic roles. *J. Immunol.* 173, 2976–2984. doi:10.4049/jimmunol.173.5.2976

Kanwar, S., and Vijayavenkataraman, S. (2021). Design of 3D printed scaffolds for bone tissue engineering: A review. *Bioprinting* 24, e00167. doi:10.1016/j.bprint.2021.e00167

Khan, M., Osman, K., Green, G., and Haddad, F. S. (2016). The epidemiology of failure in total knee arthroplasty: Avoiding your next revision. *Bone Jt. J.* 98-B, 105–112. doi:10.1302/0301-620X.98B1.36293

Konstantinou, E., Zagoriti, Z., Pyriochou, A., and Poulas, K. (2020). Microcurrent stimulation triggers MAPK signaling and TGF-β1 release in fibroblast and osteoblast-like cell lines. *Cells* 9, 1924. doi:10.3390/cells9091924

Kratochvílová, A., Vesela, B., Ledvina, V., Svandova, E., Kleparnik, K., Dadakova, K., et al. (2020). Osteogenic impact of pro-apoptotic caspase inhibitors in MC3T3-E1 cells. *Sci. Rep.* 10, 7489. doi:10.1038/s41598-020-64294-9

Lee, W., Leddy, H. A., Chen, Y., Lee, S. H., Zelenski, N. A., McNulty, A. L., et al. (2014). Synergy between Piezo1 and Piezo2 channels confers high-strain mechanosensitivity to articular cartilage. *Proc. Natl. Acad. Sci. U. S. A.* 111, E5114–E5122. doi:10.1073/pnas.1414298111

Leppik, L., Oliveira, K. M. C., Bhavsar, M. B., and Barker, J. H. (2020). Electrical stimulation in bone tissue engineering treatments. *Eur. J. Trauma Emerg. Surg.* 46, 231–244. doi:10.1007/s00068-020-01324-1

Leppik, L., Zhihua, H., Mobini, S., Thottakkattumana Parameswaran, V., Eischen-Loges, M., Slavici, A., et al. (2018). Combining electrical stimulation and tissue engineering to treat large bone defects in a rat model. *Sci. Rep.* 8, 6307. doi:10.1038/s41598-018-24892-0

Livak, K. J., and Schmittgen, T. D. (2001). Analysis of relative gene expression data using real-time quantitative PCR and the 2(-Delta Delta C(T)) Method. *Methods* 25, 402–408. doi:10.1006/meth.2001.1262

Lochner, K., Fritsche, A., Jonitz, A., Hansmann, D., Mueller, P., Mueller-hilke, B., et al. (2011). The potential role of human osteoblasts for periprosthetic osteolysis following exposure to wear particles. *Int. J. Mol. Med.* 28 (6), 1055–1063. doi:10.3892/ijmm.2011.778

Maier, G. S., Kolbow, K., Lazovic, D., and Maus, U. (2016). The importance of bone mineral density in hip arthroplasty: Results of a survey asking orthopaedic surgeons about their opinions and attitudes concerning osteoporosis and hip arthroplasty. *Adv. Orthop.* 2016, 8079354. doi:10.1155/2016/8079354

Malysheva, K., de Rooij, K., Lowik, C. W., Baeten, D. L., Rose-John, S., Stoika, R., et al. (2016). Interleukin 6/wnt interactions in rheumatoid arthritis: Interleukin 6 inhibits Wnt signaling in synovial fibroblasts and osteoblasts. *Croat. Med. J.* 57, 89–98. doi:10.3325/cmj.2016.57.89

McCullen, S. D., McQuilling, J. P., Grossfeld, R. M., Lubischer, J. L., Clarke, L. I., and Loboa, E. G. (2010). Application of low-frequency alternating current electric fields via interdigitated electrodes: Effects on cellular viability, cytoplasmic calcium, and osteogenic differentiation of human adipose-derived stem cells. *Tissue Eng. Part C Methods* 16, 1377–1386. doi:10.1089/ten.tec.2009.0751

McGilvray, K. C., Unal, E., Troyer, K. L., Santoni, B. G., Palmer, R. H., Easley, J. T., et al. (2015). Implantable microelectromechanical sensors for diagnostic monitoring and post-surgical prediction of bone fracture healing. *J. Orthop. Res.* 33, 1439–1446. doi:10.1002/jor.22918

Mittelmeier, W., Lehner, S., Kraus, W., Matter, H. P., Gerdesmeyer, L., and Steinhauser, E. (2004). BISS: Concept and biomechanical investigations of a new screw system for electromagnetically induced internal osteostimulation. *Arch. Orthop. Trauma Surg.* 124 (2), 86–91. doi:10.1007/s00402-003-0594-9

Mycielska, M. E., and Djamgoz, M. B. A. (2004). Cellular mechanisms of direct-current electric field effects: Galvanotaxis and metastatic disease. *J. Cell Sci.* 117, 1631–1639. doi:10.1242/jcs.01125

Nicholson, D. W. (1999). Caspase structure, proteolytic substrates, and function during apoptotic cell death. *Cell Death Differ.* 6, 1028–1042. doi:10.1038/sj.cdd.4400598

Portan, D. V., Deligianni, D. D., Papanicolaou, G. C., Kostopoulos, V., Psarras, G. C., and Tyllianakis, M. (2019). Combined optimized effect of a highly self-organized nanosubstrate and an electric field on osteoblast bone cells activity. *Biomed. Res. Int.* 2019, 7574635. doi:10.1155/2019/7574635

Reimand, J., Isserlin, R., Voisin, V., Kucera, M., Tannus-Lopes, C., Rostamianfar, A., et al. (2019). Pathway enrichment analysis and visualization of omics data using g:Profiler, GSEA, Cytoscape and EnrichmentMap. *Nat. Protoc.* 14, 482–517. doi:10.1038/s41596-018-0103-9

Rucci, N. (2008). Molecular biology of bone remodelling. *Clin. Cases Min. Bone Metab.* 5, 49–56.

Sahm, F., Ziebart, J., Jonitz-Heincke, A., Hansmann, D., Dauben, T., and Bader, R. (2020). Alternating electric fields modify the function of human osteoblasts growing on and in the surroundings of titanium electrodes. *Int. J. Mol. Sci.* 21, 69444–E7013. doi:10.3390/ijms21186944

Sawa, N., Fujimoto, H., Sawa, Y., and Yamashita, J. (2019). Alternating differentiation and dedifferentiation between mature osteoblasts and osteocytes. *Sci. Rep.* 9, 13842. doi:10.1038/s41598-019-50236-7

Schöberl, J., Arnold, A., Erb, J., Melenk, J. M., and Wihler, T. P. (2014). *C++11 implementation of finite elements in NGSolve*. Report number: 30/2014. Vienna, Austria: Vienna University of Technology.

Schöberl, J. (1997). NETGEN an advancing front 2D/3D-mesh generator based on abstract rules. *Comput. Vis. Sci.* 1, 41–52. doi:10.1007/s007910050004

Shannon, P., Markiel, A., Ozier, O., Baliga, N. S., Wang, J. T., Ramage, D., et al. (2003). Cytoscape: A software environment for integrated models of biomolecular interaction networks. *Genome Res.* 13, 2498–2504. doi:10.1101/gr.1239303

Si, J., Wang, C., Zhang, D., Wang, B., and Zhou, Y. (2020). Osteopontin in bone metabolism and bone diseases. *Med. Sci. Monit.* 26, e919159e919159. doi:10.12659/MSM.919159

Sieberath, A., Della Bella, E., Ferreira, A. M., Gentile, P., Eglin, D., and Dalgarno, K. (2020). A comparison of osteoblast and osteoclast *in vitro* Co-culture models and their translation for preclinical drug testing applications. *Int. J. Mol. Sci.* 21, 912. doi:10.3390/ijms21030912

Su, Y., Souffrant, R., Kluess, D., Ellenrieder, M., Mittelmeier, W., van Rienen, U., et al. (2014). Evaluation of electric field distribution in electromagnetic stimulation of human femoral head. *Bioelectromagnetics* 35 (8), 547–558. doi:10.1002/bem.21879

Supronowicz, P. R., Ajayan, P. M., Ullmann, K. R., Arulanandam, B. P., Metzger, D. W., and Bizios, R. (2001). Novel current-conducting composite substrates for exposing osteoblasts to alternating current stimulation. *J. Biomed. Mat. Res.* 59, 499–506. doi:10.1002/jbm.10015

Thrivikraman, G., Boda, S. K., and Basu, B. (2018). Unraveling the mechanistic effects of electric field stimulation towards directing stem cell fate and function: A tissue engineering perspective. *Biomaterials* 150, 60–86. doi:10.1016/j.biomaterials.2017.10.003

United Nations, Department of Economic and Social Affairs (2019). *World Population Prospects 2019,Old-age dependency ratio (ratio of population aged 65+ per 100 population 15-64*. New York, US: United Nations.

van der Horst, G., van der Werf, S. M., Farih-Sips, H., van Bezooijen, R. L., Löwik, C. W. G. M., and Karperien, M. (2005). Downregulation of Wnt signaling by increased expression of dickkopf-1 and -2 is a prerequisite for late-stage osteoblast differentiation of KS483 cells. *J. Bone Min. Res.* 20, 1867–1877. doi:10.1359/JBMR.050614

Walker, C. G., Dangaria, S., Ito, Y., Luan, X., and Diekwisch, T. G. H. (2010). Osteopontin is required for unloading-induced osteoclast recruitment and modulation of RANKL expression during tooth drift-associated bone remodeling, but not for super-eruption. *Bone* 47, 1020–1029. doi:10.1016/j.bone.2010.08.025

Wechsler, M. E., Hermann, B. P., and Bizios, R. (2016). Adult human mesenchymal stem cell differentiation at the cell population and single-cell levels under alternating electric current. *Tissue Eng. Part C Methods* 22, 155–164. doi:10.1089/ten.TEC.2015.0324

Westendorf, J. J., Kahler, R. A., and Schroeder, T. M. (2004). Wnt signaling in osteoblasts and bone diseases. *Gene* 341, 19–39. doi:10.1016/j.gene.2004.06.044

Zhang, Y., Yan, J., Xu, H., Yang, Y., Li, W., Wu, H., et al. (2018). Extremely low frequency electromagnetic fields promote mesenchymal stem cell migration by increasing intracellular Ca(2+) and activating the FAK/Rho GTPases signaling pathways *in vitro*. *Stem Cell Res. Ther.* 9, 143. doi:10.1186/s13287-018-0883-4

Zhu, B., Li, Y., Huang, F., Chen, Z., Xie, J., Ding, C., et al. (2019). Promotion of the osteogenic activity of an antibacterial polyaniline coating by electrical stimulation. *Biomater. Sci.* 7, 4730–4737. doi:10.1039/c9bm01203f

Zhu, S., Jing, W., Hu, X., Huang, Z., Cai, Q., Ao, Y., et al. (2017). Time-dependent effect of electrical stimulation on osteogenic differentiation of bone mesenchymal stromal cells cultured on conductive nanofibers. *J. Biomed. Mat. Res. A* 105, 3369–3383. doi:10.1002/jbm.a.36181

Zimmermann, J., Budde, K., Arbeiter, N., Molina, F., Storch, A., Uhrmacher, A. M., et al. (2021). Using a digital twin of an electrical stimulation device to monitor and control the electrical stimulation of cells *in vitro*. *Front. Bioeng. Biotechnol.* 9, 765516. doi:10.3389/fbioe.2021.765516

Zimmermann, U., Ebner, C., Su, Y., Bender, T., Bansod, Y. D., Mittelmeier, W., et al. (2021). Numerical simulation of electric field distribution around an instrumented total hip stem. *Appl. Sci. (Basel).* 11, 6677. doi:10.3390/app11156677

applied sciences

MDPI

Article

Is There an Influence of Electrically Stimulated Osteoblasts on the Induction of Osteoclastogenesis?

Franziska Sahm [1,*], Ana Jakovljevic [1], Rainer Bader [1], Rainer Detsch [2] and Anika Jonitz-Heincke [1,*]

[1] Biomechanics and Implant Technology Research Laboratory, Department of Orthopedics, Rostock University Medical Centre, 18057 Rostock, Germany
[2] Department of Materials Science and Engineering, Institute of Biomaterials, Friedrich-Alexander University Erlangen-Nuremberg, 91058 Erlangen, Germany
* Correspondence: franziska.sahm@uni-rostock.de (F.S.); anika.jonitz-heincke@med.uni-rostock.de (A.J.-H.); Tel.: +49-381-494-9306 (A.J.-H.)

Abstract: Bone is a highly dynamic tissue characterized mainly by the interactions of osteoblasts and osteoclasts. When the healing ability of bone regeneration is disturbed, targeted biophysical stimulations such as electrical stimulation are applied. In this study the indirect effects of electrically stimulated human osteoblasts on osteoclastogenesis were investigated to better understand detailed cellular interactions. Therefore, two different cell developmental stages were examined: peripheral blood mononuclear cells (PBMCs) as precursors and pre-osteoclasts as differentiated cells. Previously, over a 21-day period, human osteoblasts were stimulated with a low-frequency alternating electric field. The supernatants were collected and used for an indirect co-culture of PBMCs and pre-osteoclasts. The cellular viability and the induction of differentiation and activity were analyzed. Further, the secretion of relevant osteoclastic markers was examined. Supernatants of 7 d and 14 d stimulated osteoblasts led to a decrease in the viability of PBMCs and an increased number of cells containing actin ring structures. Supernatants from osteoblasts stimulated over 7 d induced PBMC differentiation and pre-osteoclastic activation. Furthermore, pre-osteoclasts showed varying mRNA transcripts of MCP-1, ACP5, CA2, and CASP8 when cultivated with media from osteoblasts. Supernatants from day 21 did not influence PBMCs at all but increased the viability of pre-osteoclasts. We could show that different time points of stimulated osteoblasts have varying effects on the cells and that changes can be observed due to the differentiation stages of the cells. Through the effects of the indirect stimulation, it was possible to underline the importance of studying not only osteoblastic differentiation and mineralization behavior under electric stimulation but also analyzing changes in osteoclastogenesis and the activity of osteoclasts.

Keywords: indirect co-culture; biophysical stimulation; alternating electric fields; PBMCs; pre-osteoclasts; osteoclastogenesis; bone remodeling

Citation: Sahm, F.; Jakovljevic, A.; Bader, R.; Detsch, R.; Jonitz-Heincke, A. Is There an Influence of Electrically Stimulated Osteoblasts on the Induction of Osteoclastogenesis? *Appl. Sci.* **2022**, *12*, 11840. https://doi.org/10.3390/app122211840

Academic Editor: Rossella Bedini

Received: 6 October 2022
Accepted: 15 November 2022
Published: 21 November 2022

1. Introduction

Electrical stimulation is a frequently used medical application to treat different disorders in nerves, muscles, and cardiac tissue, and it can play an essential role in wound healing [1]. Since Fukada and Yasuda described the piezoelectric properties of bone, research has been conducted using externally applied electric fields to improve bone healing [2,3]. Animal studies and even clinical applications of electric stimulation devices revealed positive effects on bone regeneration; however, the fundamental cellular processes are still not fully understood [3,4].

There are different possibilities to apply electric fields, such as capacitive coupling, inductive coupling with pulsed electromagnetic fields (PEMF), and direct coupling. For the capacitive coupling, electrodes are placed outside of the tissue or the cell culture plate, avoiding possible side reactions with the environment. Due to the barriers between the

stimulated cells and the electrodes, electrical signals are reduced, resulting in the need for high voltages. PEMF are applied by placing a conductive coil over the tissue of interest or the cell culture. While current flows through the coil, an electromagnetic field arises. The pulsed signals are used to mimic natural voltage potentials. The third type, often used in in vitro studies, is direct coupling. During direct stimulation, the electrodes are placed in contact with the tissue or cell culture medium [5,6]. Due to this direct contact, the biocompatibility of the materials used is essential. Furthermore, the direct current (DC) can lead to a rise in temperature, changes in the pH, the accumulation of charged proteins on the electrode, and harmful faradic by-products such as hydrogen peroxide and free metal ions from the used electrode [1,7,8]. Biphasic electrical stimulation such as alternating current (AC) can avoid these effects.

Several studies have already used alternating electric fields to stimulate osteoblasts, but little is known about the effect on osteoclastogenesis and osteoclast-like cells [7,9–11]. A balance between bone resorption through the activation of osteoclasts and bone formation through osteoblast activity is essential for bone regeneration [12,13]. Therefore, studies regarding the differentiation of macrophages and the activity and formation of osteoclasts under electrical fields are essential. Among the few studies regarding this issue, most use PEMF or sometimes direct stimulation with DC [14–19]. Stimulation via PEMF leads to a decrease in cell numbers, an increased apoptotic rate, and reduced osteoclast formation [14,16,19,20]. Stimulation with DC revealed different migration behaviors of osteoblasts and osteoclasts as they moved in opposite directions during stimulation [18]. There are no studies yet on the effects of direct alternating fields. The situation is similar regarding studies of the influence of electrical stimulation on macrophages generated out of peripheral blood mononuclear cells (PBMCs) and possible osteoclast precursors. Electrical stimulation is mainly performed with PEMF, and in some cases with DC, revealing both anti-inflammatory and pro-inflammatory effects with low-frequency electromagnetic field stimulation [21,22]. Furthermore, reduced proliferation, higher apoptosis rates, and altered migration behavior of macrophages were observed under PEMF and DC [23–25]. Due to the mentioned problem of monophasic stimulation, analyses with alternating electrical fields are necessary.

Studies regarding human macrophages and osteoclasts are as crucial as studies on osteoblasts in understanding fundamental bone remodeling processes under electric stimulation. Indirect and direct co-culture systems allow the investigation of the interaction and interplay between these cell types [26]. These cellular interactions could even be shown in an osteoid model, i.e., non-mineralized bone tissue [27]. In general, secreted cytokines and released factors modify the cell reaction of each cell type; thus, the crosstalk can change cell behavior in comparison to mono-cultured cells [28]. Shankar et al. revealed the importance of a co-culture system between osteoblasts and osteoclasts while observing the influence of PEMF [17]. Changes in differentiation and the bone-resorption capability of osteoclasts were observed after incubating cells with a medium derived from PEMF-stimulated osteocytes [29].

Therefore, in our present study, the effect of electrically stimulated human osteoblasts on osteoclast formation processes was investigated. The aim of our study was to gain a better understanding of the effects of cytokines released by electrically stimulated osteoblasts with alternating electric fields on osteoclastogenesis (Figure 1). Consequently, the indirect influence of electric stimulation on the viability and differentiation of PBMCs and osteoclast-progenitor cells was investigated. Study data should help to understand the activation of PBMCs and pre-osteoclasts in the periphery of electrically active bone implants by releasing cytokines from osteoblasts in direct proximity to the electrical field.

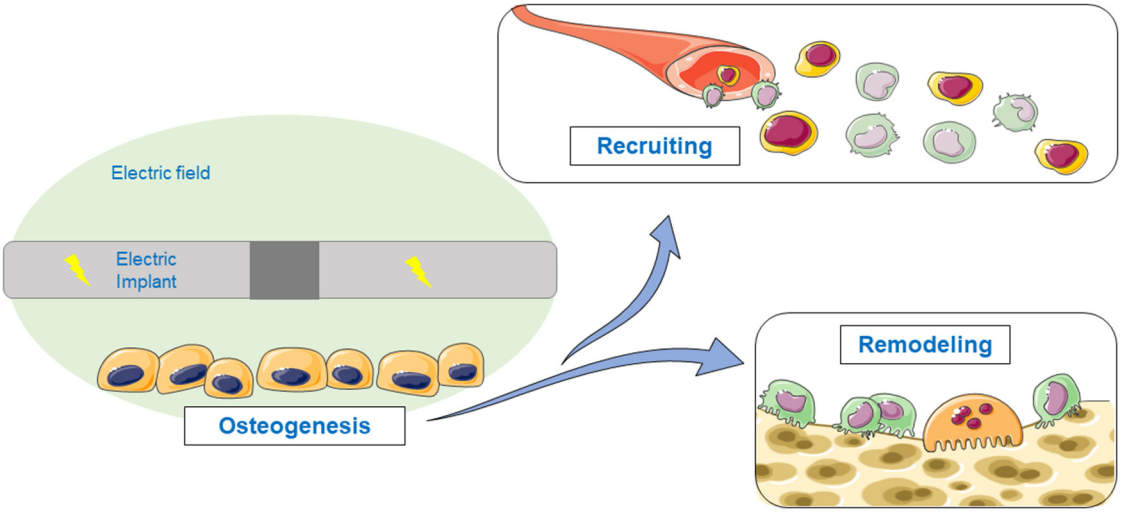

Figure 1. Schematic overview of the study aim. Stimulated osteoblasts produce signaling molecules that influence osteoclastogenesis through recruiting and remodeling processes. Single pictures were used from Servier Medical Art (http://smart.servier.com/, accessed on 14 June 2022).

2. Materials and Methods

The setup used to analyze the indirect influence of electrically stimulated osteoblasts on osteoclastogenesis is shown in a graphical overview in Figure 2. A detailed description of each step can be found in the following sections.

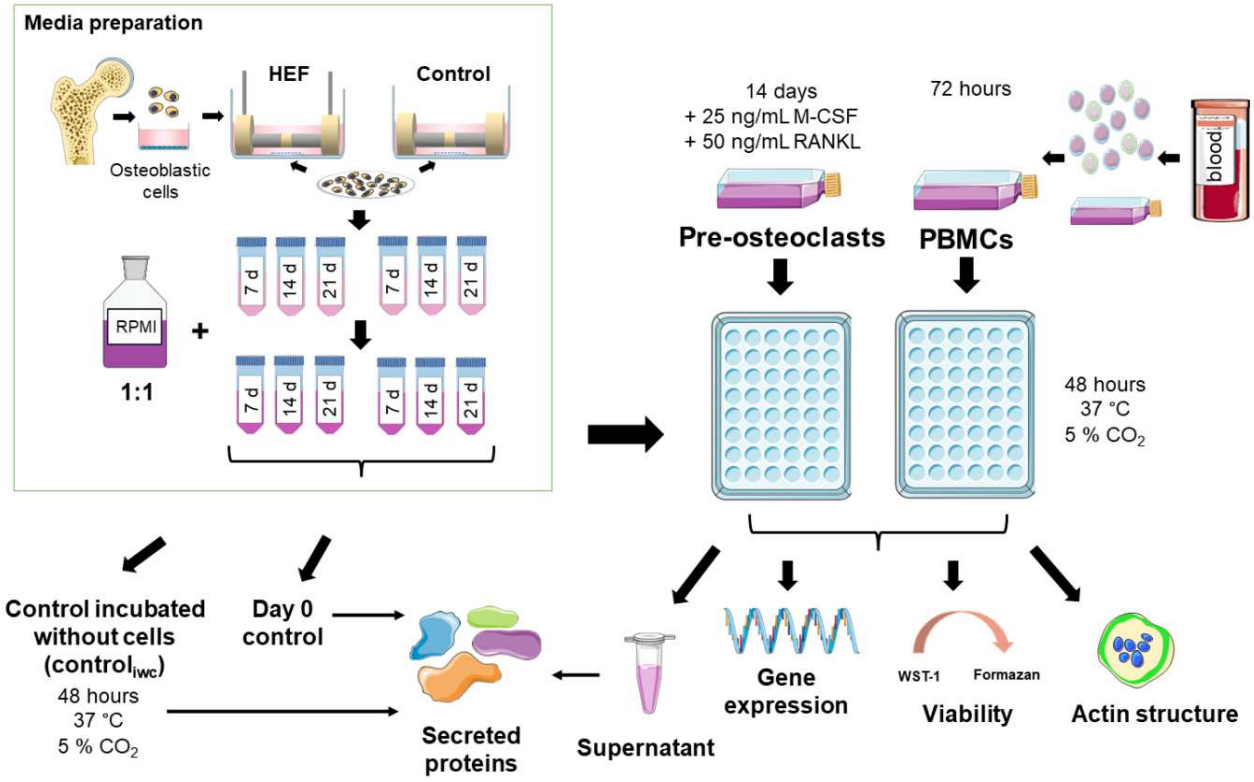

Figure 2. Schematic overview of the used methods. Single pictures were used from Servier Medical Art (http://smart.servier.com/, accessed on 23 May 2022) or bioicons (https://bioicons.com/, 23 May 2022).

2.1. Electrical Stimulation of Human Primary Osteoblasts

Human primary osteoblasts were isolated, cultivated, and electrically stimulated for the experiments, as previously described by Sahm et al. [30]. In brief, spongiosa was isolated from femoral heads allocated from patients undergoing total hip replacement (registration number: A 2010-0010, approval date: 27 January 2017). After digestion with collagenase a and dispase (both: Roche, Basel; Switzerland), the cell suspension was purified through filtration and centrifugation steps. The cells were cultivated in a cell culture flask with Dulbecco's Modified Eagle Medium without $CaCl_2$ to increase proliferation (DMEM, PAN-Biotech, Aidenbach, Germany), containing 10% fetal calf serum (FCS, PAN-Biotech, Aidenbach, Germany), 1% amphotericin B, 1% penicillin-streptomycin, and 1% HEPES buffer (all: Sigma-Aldrich, Munich, Germany). Ascorbic acid (final concentration: 50 µg/mL), β-glycerophosphate (final concentration: 10 mM), and dexamethasone (final concentration: 100 nM) (all: Sigma-Aldrich, Munich, Germany) were added to bring cells to a similar stage of differentiation. The cells were kept in cell culture under standard cell culture conditions (5% CO_2 and 37 °C) until the second passage and stored in liquid nitrogen until use.

For the electrical stimulation experiment, osteoblasts from seven different human donors (four females (age: 77.25 ± 2.21 years), three males (age: 73 ± 9.54 years)) were thawed and cultured for another passage at 37°C and 5% CO_2. Rat tail collagen-coated coverslips (diameter: 15 mm, Neuvitro Corporation, Vancouver, WA, USA) were placed in a 6-well plate, and 30,000 cells were seeded on each coverslip. The cells adhered for 30 min, and 5 mL of cell culture medium (Dulbecco's Modified Eagle Medium (DMEM w/o calcium)) was added with 10% fetal calf serum (FCS, both: PAN-Biotech, Aidenbach, Germany), 1% amphotericin B, 1% penicillin-streptomycin, and 1% HEPES buffer (all: Sigma-Aldrich, Munich, Germany) containing the osteogenic additives ascorbic acid (final concentration: 50 µg/mL), β-glycerophosphate (final concentration: 10 mM), dexamethasone (final concentration: 100 nM) (all: Sigma-Aldrich, Munich, Germany) and $CaCl_2$ (final concentration: 1.8 mmol/L) for mineralization. An in vitro stimulation electrode was used, which was designed similarly to the clinically used ASNIS III s-series stimulation screw system [31,32]. The electrode consists of two 14 mm Ti6Al4V cylindrical electrodes separated by a 5 mm long insulator made of polyetheretherketone. The detailed stimulation protocol can be found as described by Sahm et al. [30]. The stimulation electrodes were placed in each well. In addition to the electrically stimulated osteoblasts (ESO), unconnected electrodes served as a control (non-stimulated osteoblasts—NSO). A sinusoidal signal with 0.7 V_{rms} and 20 Hz was applied 24 h after cell seeding using a Metrix GX 305 and GX310 function generator (Metrix Electronics, Bramley, Hampshire, UK). The distance between the electrode and the well bottom was 1 mm, which leads to an electric field of approximately 150 V/m in the cell medium and the well bottom under the center of the electrode [30]. The alternating current was applied 3 × 45 min/d with 225 min breaks between stimulations and a longer 855 min break between the last and the first new stimulation. This was performed to keep comparability with clinical studies [31]. The supernatant was collected and refreshed after 7, 14, and 21 days. The supernatant was collected 20 h after the last stimulation interval had started. It was centrifuged, pooled, and frozen for indirect stimulation.

2.2. Isolation and Differentiation of Peripheral Blood Mononuclear Cells

Peripheral blood mononuclear cells (PBMCs) were isolated from buffy coats from eight anonymous donors using SepMate™-50 mL tubes and Histopaque®-107, following manufacturers' instructions. The approval was obtained by the Local Ethical Committee (registration number: A2011-140, approval date: 24 November 2021). The generated cells were resuspended in Roswell Park Memorial Institute (RPMI) 1640 medium (PAN™-Biotech GmbH, Aidenbach, Germany) containing 10% fetal calf serum, 2% glutamine, and 1% penicillin-streptomycin. After seven days of culture in suspension cell culture flasks to increase the number of mononuclear cells (Greiner bio-one GmbH, Frickenhausen, Germany), the cells

were harvested [33]. Nonadherent cells were transferred into a 50 mL centrifugation tube; adherent cells were incubated twice over 10–15 min with cold PBS and then gently scraped from the bottom of the flask. Cells were pooled, centrifuged at 120× *g* for 8 min, and counted with trypan blue. A total of 100,000 viable cells were plated in each well of a 48-well plate to form a monolayer on the bottom of the well. Each donor was divided into "PBMCs" and "pre-osteoclasts".

2.3. Indirect Stimulation

For the experiments, PBMCs were cultured for 72 h until further use and osteoclasts were cultured for 14 d with the above-mentioned medium supplemented with 25 ng/mL Macrophage Colony-Stimulating Factor (M-CSF) and 50 ng/mL Receptor Activator of Nuclear Factor-κB Ligand (RANKL) (both: PreproTech EC, London, UK). Medium was refreshed for the "pre-osteoclasts" after 5 and 10 d.

To analyze the indirect influence of electric stimulation by released mediators, PBMCs and pre-osteoclasts were cultivated for 48 h with the supernatants of the stimulated osteoblasts over 48 h. The media from the ESO and the NSO were used after the stimulation time points of 7 d, 14 d, and 21 d. The pooled supernatants were mixed 1:1 with fresh RPMI 1640 containing 2% fetal calf serum, 2% glutamine, and 1% penicillin-streptomycin.

2.4. Cell Viability

To determine cell viability after 48 h, the supernatant was removed and replaced with a suspension of the water-soluble tetrazolium salt (WST-1, Roche GmbH, Grenzach-Wyhlen, Germany) in the medium. Therefore, the WST-1 reagent was diluted 1:10 with RPMI 1640 and transfused into the cells. Diluted WST-1 reagent without cells served as a blank. After an incubation time of 30 min at 37 °C and 5% CO_2, 100 µL of the solution was transferred as duplicates into a 96-well plate. The color change was quantified using the Infinite 200 pro multimode plate reader (Tecan Group Ltd., Maennedorf, Switzerland) at a wavelength of 450 nm and a reference filter of 630 nm. The blank was subtracted from the values of each sample.

2.5. Actin-DAPI Staining

Fluorescence images were used to visualize the cell morphology and confirm the osteoclastic differentiation of the pre-osteoclasts via the formation of actin rings. After 48 h of incubation, cells were fixed with 4% paraformaldehyde (Grimm MED Logistik GmbH, Torgelow, Germany) for 10 min at room temperature (RT), washed with phosphate-buffered saline (PBS, Sigma-Aldrich Chemie GmbH, Taufkirchen, Germany), and permeabilized with 1:200 diluted Triton X (Merck KGaA, Darmstadt, Germany) for 5 min. After another rinsing step with PBS, Acti-stain™ 488 (Cytoskeleton, Inc., Denver, CO, USA) was diluted 1:140 with PBS to a concentration of 100 nM and transferred onto the cells. The cells were incubated in the dark for 30 min and washed 3 x with PBS afterward. The 4′,6-Diamidin-2-phenylin-dol (DAPI, Merck KGaA, Darmstadt, Germany) reagent was diluted 1:1000 with PBS, and cells were incubated with the solution for 5 min in the dark. A final rinse with PBS completed the staining process before the plates were stored at 4 °C, protected from light until further use. The images were captured using FITC (EX480/30, DM505, BA535/45) and DAPI (EX375/28, DM415, BA460/60) fluorescent filters with the Nikon Eclipse TS100 microscope and the Nikon digital sight DS-2Mv camera (all: Nikon GmbH, Duesseldorf, Germany). The superimposition of the images was performed with Gimp (GNU Image Manipulation Program).

2.6. Gene Expression Analysis

The gene expression of stimulated and unstimulated PBMCs and pre-osteoclasts was analyzed after 48 h incubation time. The RNA was extracted with the peqGOLD Total RNA Kit (VWR International GmbH, Darmstadt, Germany) following the manufacturer's instructions. Cells were lysed with the lysis buffer, and the lysate of the corresponding duplicate determinations was placed together in one column. By adding 25 µL of 60 °C

nuclease-free water (Carl Roth GmbH & Co. KG, Karlsruhe, Germany), the RNA was eluted by centrifugation for 2 min at the highest possible speed. RNA concentration was measured using the Tecan Reader Infinite® 200 Pro, and nuclease-free water was used to determine the blank value. The transcription of 150 ng RNA into complementary DNA (cDNA) was performed using the High Capacity cDNA Reverse Transcription Kit (Thermo Fisher Scientific, Waltham, MA, USA) following the manufacturer's instructions. Afterward, all samples were diluted 1:1 with nuclease-free water and stored at −20 °C for further usage. Semi-quantitative reverse transcription-polymerase chain reaction (qPCR) was performed in duplicate using the innuMIX qPCR MasterMix SyGreen Kit (Analytik Jena, Germany). The primers used in this process are listed in Table 1. The results were evaluated using the delta-delta Ct (ΔΔCt) method [34]. HPRT served as a housekeeper gene, and the stimulated samples were related to the matching non-stimulated osteoclast control from the same time point.

Table 1. Primer sequences for the genes of interest.

Gene	Abbreviation	Sequence
Caspase 8	CASP8	For: TGTTTTCACAGGTTCTCCTCCTTT Rev: GAGAATATAATCCGCTCCACCTT
Receptor Activator of NFκB	RANK	For: AGAAAACCACCAAATGAACCCC Rev: GCCAGAGCCTCATTGATTC
Tartrate Resistant Acid phosphatase 5	ACP5	For: GGGAGATGTGTGAGCCAGTG Rev: GTCCACATGTCCATCCAGGG
Carbonic anhydrase 2	CA2	For: TGGGGTTCACTTGATGGACAA Rev: CAGCACTCTTGCCCTTTGTT
Cathepsin K	CTSK	For: GGAAGCAATTAACAACAAGGTGGA Rev: GGGGCCTACCTTCCCATTC
Matrix Metallopeptidase 9	MMP9	For: ACGCAGACATCGTCATCCAG Rev: AACCGAGTTGGAACCACGAC
Hypoxanthine-Guanine Phosphoribosyl Transferase	HPRT	For: CCCTGGCGTCGTGATTAGTG Rev: TCGAGCAAGACGTTCAGTCC

2.7. Quantification of the Secreted Proteins

Secreted tartrate-resistant acid phosphatase 5 b (TRAP5b), bone morphogenetic protein 2 (BMP2), cystatin C, interferon-β (IFN-β), interleukin 10 (IL-10), interleukin-17A (IL-17A), interleukin-1β (IL-1β), interleukin-4 (IL-4), interleukin-6 (IL-6), interleukin-23 (IL-23), osteopontin (OPN), free active transforming growth factor-β 1 (TGF-β1), and tumor necrosis factor-α (TNF-α) were analyzed out of the supernatant of each sample with a customized human BioLegend's LEGENDplex™ multiplex assay (Biolegend, San Diego, CA, USA). Analysis was performed following the manufacturer's instructions, and internal standards served to determine the concentration of each protein. The volume of used samples, standards, and kit reagents was adjusted to 15 µL. The samples and standards were incubated with the beads overnight. The multiplex assay was measured with a BD FACSVerse™ (Becton, Dickinson and Company, Franklin Lakes, NJ, USA).

To identify the initial concentration of the cytokines secreted by electrically stimulated osteoblasts, the supernatant used for stimulation was diluted 1:1 with RPMI medium, as explained in 3.3. The multiplex assay was measured directly with a BD FACSVerse™. Further, the diluted supernatant was incubated under standard cell culture conditions (5% CO_2 and 37 °C) for 48 h and was then handled as the PBMC and pre-osteoclast samples. This measurement served as an internal control to validate the number of proteins that would be degraded during the 48 h incubation. The internal control was named "control incubated without cells" ($control_{iwc}$).

The total protein content of each supernatant was determined to normalize the protein concentration measured with the LEGENDplex™ multiplex assay. Therefore, the supernatant was analyzed with the Invitrogen Qubit Protein Assay Kit and the Qubit fluorometer Q32857

(both: Thermo Fisher Scientific, Waltham, MA, USA) following manufacturer instructions. The quantification of the total protein content was ensured through included standards.

2.8. Display of the Data and Statistical Analysis

The statistical analysis was performed using GraphPad PRISM (GraphPad Software, San Diego, CA, USA). All experiments were conducted with eight replicates, each from a different donor. The ROUT method was used to identify any outliers. The analysis of the released proteins led to non-detectable amounts of protein for some donors for varying proteins. Therefore, and through the ROUT method, the number of replicates was reduced to $n \geq 7$ for osteoclasts and $n \geq 6$ for the PBMCs. The normal distribution was verified with the Shapiro–Wilk test. The two-way ANOVA with Tukey was used to compare the results of the electric stimulations among each other and with the control, as well as the different time points. *p*-values smaller than 0.05 were included as significant. The data were shown in boxplots and heat maps. Boxplots represented the median, the 25% and 75% quartile, and whiskers for indicating minimum and maximum.

3. Results

3.1. Initial Concentration of Cytokines in the Supernatants

The indirect influence of electric stimulation was analyzed using PBMCs and pre-osteoclasts. The supernatants of electrically stimulated osteoblasts (ESO) and non-stimulated osteoblasts (NSO) were collected after 7 d, 14 d, and 21 d, pooled, and used for the stimulation. The supernatants were diluted 1:1 with RPMI, as described in Section 2.3.

The concentration of possible mediators released by human osteoblasts that might affect the PBMCs and pre-osteoclasts was analyzed before incubating the diluted supernatant with the cells. The protein concentrations of BMP-2, cystatin C, IFN-β, IL-10, IL-1β, IL-6, OPN, TGF-β1, and TNF-α were determined via LEGENDplex™ multiplex assay. No signal was detectable for BMP-2, cystatin C, IL-1β, and OPN. The concentrations for TNF-α, IL-6, IL-10, IFN-β, and TGF-β1 are shown in Table 2. The highest concentration of TNF-α was detectable with the ESO for all time points: about twice as high as with the NSO. The amount of IL-6 rose in the ESO supernatants constant over time. The IL-6 concentration for the NSO peaked at 14 d. IL-10, IFN-β, and TGF-β1 were not detectable for all time points. IL-10 was just determined for 14 d ESO, 7 d NSO, and 21 d NSO. IFN-β was determined for ESO only at 14 d. The IFN-β concentration in the control varied between the stimulation times, with the highest amount at 21 d. The TGF-β1 concentration was only measurable in HEF after 21 d whereas, for the control, it was also measurable at 7 d.

Table 2. Protein concentration of the pooled supernatants of electrically stimulated osteoblasts (ESO) and non-stimulated osteoblasts (NSO) after 7, 14, and 21 days.

	ESO			NSO		
Time [d]	7	14	21	7	14	21
			Pro-osteoclastic			
TNF-α [pg/mg]	6.00	6.20	5.70	2.56	3.27	2.55
			Anti-osteoclastic			
IL-10 [pg/mg]	0.00	0.92	0.00	0.96	0.00	1.47
IFN-β [pg/mg]	0.00	1.48	0.00	1.3	0.76	2.36
			Bone remodeling			
TGF-β1 [pg/mg]	0.00	0.00	0.59	0.69	0.00	0.62
IL-6 [pg/mg]	176.45	213.29	387.33	231.20	318.82	278.55

3.2. Influence of Conditioned Osteoblastic Supernatants on Peripheral Blood Mononuclear Cell (PBMC)

3.2.1. Morphology and Viability

Different cell morphologies were expressed in PBMC cell cultures by treatment with various supernatants. Smaller and larger cell morphologies were seen in all stimulation groups, reflecting the different cell types of PBMCs. A few cells with a green actin ring structure were observed at all stimulation time points with ESO. The NSO showed fewer actin rings on days 7 and 14; stimulation with the 21 d control medium led to a rise in the number of cells with ring structures (Figure 3a,b).

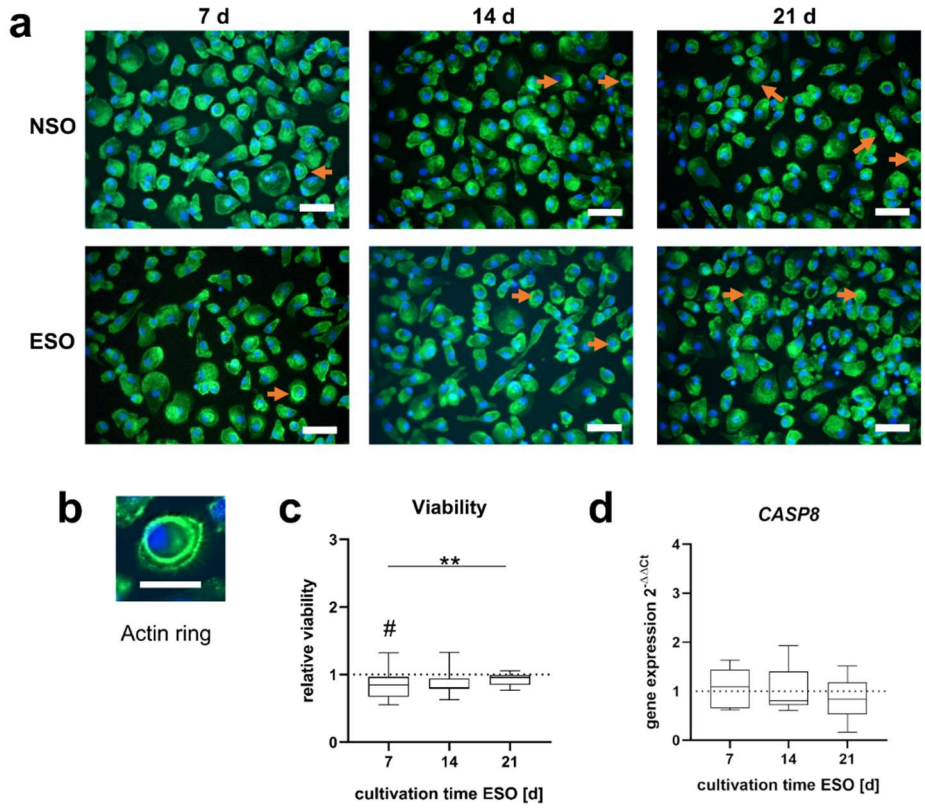

Figure 3. Morphology and viability of PBMCs after 48 h incubation with pooled supernatant of osteoblast stimulated over 7, 14, and 21 d (ESO) and without electric stimulation (NSO). (**a**) Morphology of PBMCs. The actin skeleton is visualized in a green color and the nucleus in blue. Cells with an actin ring structure are highlighted with an orange arrow. The scale bar measures 50 µm. (**b**) PBMC with an actin ring. The scale bar measures 20 µm. (**c**) The viability of ESO PBMCs related to the viability of NSO PBMCs. Significant differences were determined using the two-way ANOVA with Tukey. # indicates significant differences between the stimulated and control groups: # $p < 0.05$. * indicates significant differences between stimulation time points: ** $p < 0.01$ [n = 8]. (**d**) *CASP8* gene expression data with ESO related to NSO PBMCs using the $2^{-\Delta\Delta Ct}$ method. Significant differences were determined using the two-way ANOVA with Tukey [n = 8].

The viability of PBMCs was influenced by indirect stimulation (Figure 3c). The supernatant of ESO obtained after 7 and 14 d reduced the viability of PBMCs compared to the unstimulated control. This reduction was significant after 7 d ($p = 0.036$) and not significant after 14 d ($p = 0.062$). After 21 d of stimulation, the medium had no impact on viability. The rise in viability from 7 d to 21 d was significant ($p = 0.042$) as well. No significant changes were observed in the *CASP8* gene expression (Figure 3d).

3.2.2. Gene Expression

The gene expression of PBMCs stimulated with osteoblastic cell culture supernatants was analyzed for *RANK*, *ACP5*, *CTSK*, *CA2*, and *MMP9*. *RANK* was significantly higher with the 14 d supernatant compared to the 21 d ($p = 0.017$). *ACP5* was significantly enhanced while using the 7 d ($p = 0.025$) and 14 d ($p = 0.025$) supernatants of the ESO compared to the 21 d supernatant (Figure 4a). A similar trend was observable for *CTSK* and *MMP9*. *CTSK* was significantly upregulated with the 7 d ESO supernatant ($p = 0.042$), slightly upregulated with 14 d, and unaffected with 21 d. *MMP9* gene expression showed an upward trend with 7 d and a downward trend with 21 d. The supernatants did not significantly influence the gene expression of *CA2* for ESO (Figure 4a).

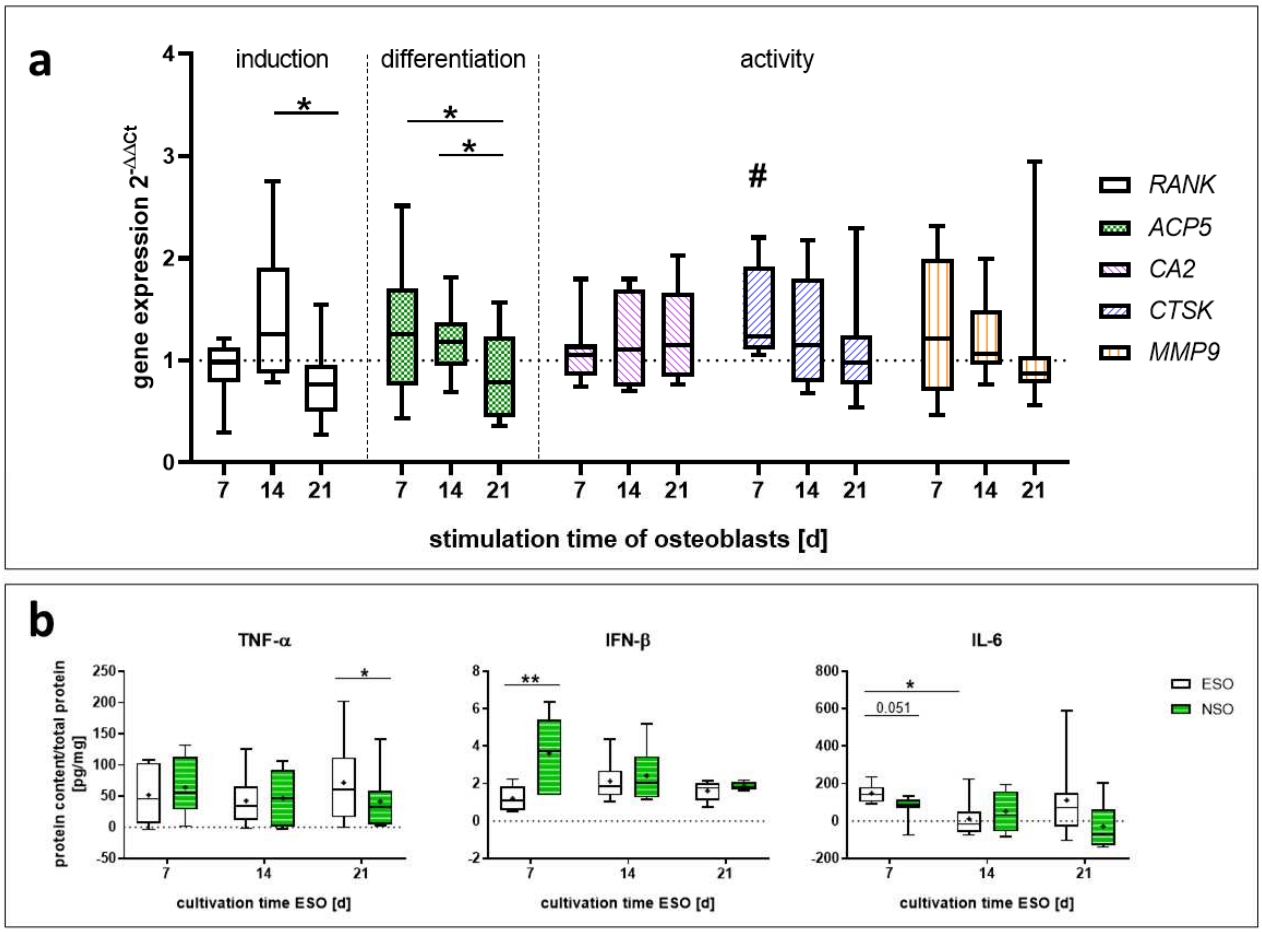

Figure 4. Gene expression and protein data of PBMCs after 48 h incubation with pooled supernatant of osteoblast (ESO) stimulated over 7, 14, and 21 d and without electric stimulation (NSO). (**a**) Gene expression data were related to the NSO using the $2^{-\Delta\Delta Ct}$ method. Boxplots are used to present the distribution of the total results with significant changes [n = 8]. Significant differences were determined using the two-way ANOVA with Tukey. # indicates significant differences between ESO and NSO cultivation: # $p < 0.05$. * indicates significant differences between stimulation time points: * $p < 0.05$. (**b**) The protein concentration was related to the total protein concentration of the supernatant of each sample. Afterward, the respective protein concentration from the $control_{iwc}$ was subtracted. Boxplots are used to present the distribution of the total results [n $\geq$ 6]. Significant differences were determined using the two-way ANOVA with Tukey. * indicates significant differences: * $p < 0.05$, ** $p < 0.01$.

3.2.3. Released Mediators

The amounts of released TRAP5b, BMP-2, cystatin C, IFN-β, IL-1β, -4, -6, -10, -17A, -23, OPN, TGF-β1, and TNF-α were analyzed for PBMCs stimulated with ESO and NSO, and

the control$_{iwc}$. The concentration of the control$_{iwc}$ was subtracted from the concentration of the cultivated PBMCs.

No proteins could be detected for IL-1β, -4, -17A-23, and BMP-2. For OPN, cystatin C, TRAP5b, IL-10, and TGF-β1, no significant changes in the protein concentration could be determined (Figure S1). The concentration of released TNF-α was not influenced by the 7 d and 14 d media (Figure 4b). The 21 d medium led to an increased amount with the ESO compared to the NSO ($p = 0.015$). IFN-β was downregulated for the 7 d medium ($p = 0.0055$). Later stimulation times did not influence the IFN-β release. New IL-6 was mainly produced by cells stimulated with the 7 d medium. The 7 d medium led to an increase in IL-6 compared to the NSO ($p = 0.051$) and the 14 d ESO ($p = 0.023$). The additional stimulation times 14 d and 21 d did not affect the IL-6 concentration (Figure 4b).

3.3. Influence of Conditioned Osteoblastic Supernatants on Pre-Osteoclasts

3.3.1. Morphology and Viability

The morphology of the pre-osteoclasts was visualized through staining of the actin cytoskeleton (Figure 5a,b). The cells were mainly round-shaped and larger than PBMCs. Some cells showed a more intense green glowing actin ring structure. Multinuclear cells with more than three nuclei could not be observed.

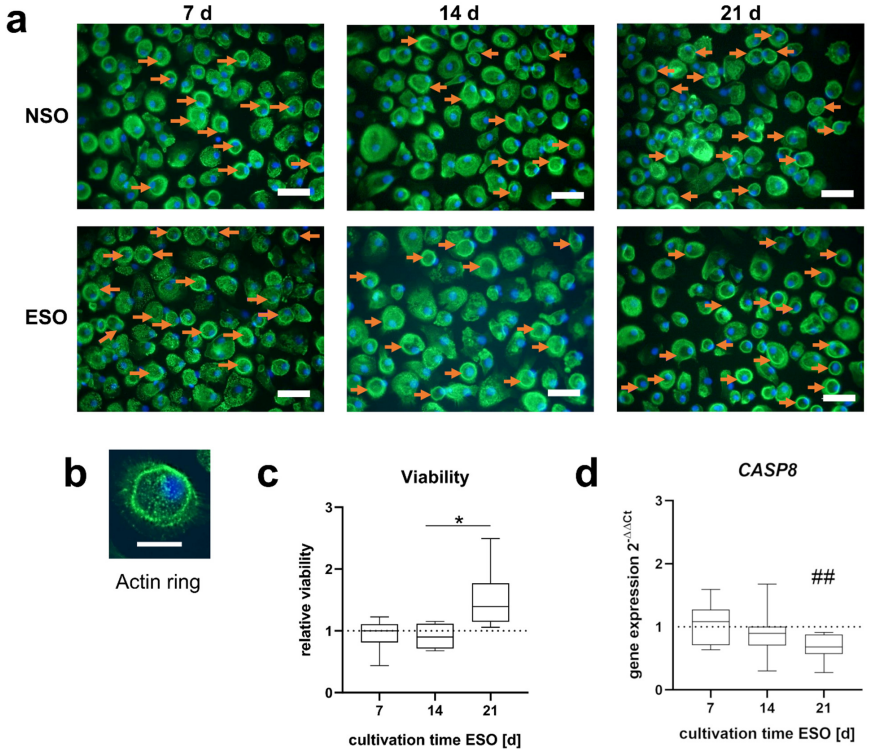

Figure 5. Morphology and viability of pre-osteoclasts after 48 h incubation with pooled supernatant of osteoblast stimulated over 7, 14, and 21 d (ESO) and without electric stimulation (NSO). (**a**) The morphology of PBMCs shows mostly round cell shapes. The actin skeleton is visualized in a green color and the nucleus in blue. Cells with an actin ring structure are highlighted with an orange arrow. The scale bar measures 50 µm. (**b**) Pre-osteoclast with an actin ring. The scale bar measures 20 µm. (**c**) The viability of pre-osteoclasts related to the viability of the control. Significant differences were determined using the two-way ANOVA with Tukey, * indicates significant differences between stimulation time points: * $p < 0.05$ [n = 8]. (**d**) *CASP8* gene expression data with ESO related to NSO PBMCs using the $2^{-\Delta\Delta Ct}$ method. Significant differences were determined using the two-way ANOVA with Tukey, # indicates significant differences between the stimulated and control groups: ## $p < 0.01$ [n = 8].

The 7 d and 14 d media of the stimulated osteoblasts did not influence the viability of the pre-osteoclasts. With the 21 d supernatant, the viability rose compared to 7 d and 14 d. The rise in viability from 14 d to 21 d was significantly higher ($p = 0.012$) (Figure 5c). The *CASP8* expression was reduced with the further stimulation time of the ESO. On day 21 *CASP8* was significantly downregulated compared to NSO ($p = 0.006$) (Figure 5d).

3.3.2. Gene Expression

The gene expression of *RANK*, *ACP5*, *CTSK*, *CA2*, and *MMP9* was determined to analyze the influence of released osteoblastic mediators on pre-osteoclastic differentiation and activity (Figure 6a). The 14 d and 21 d supernatants from ESO led to a downregulation of *ACP5*, which was significant for 14 d ($p = 0.034$). *RANK*, *CA2*, *CTSK*, and *MMP9* were upregulated with the medium of 7 d stimulated osteoblasts and downregulated with 14 d and 21 d media. *RANK* and *CTSK* did not significantly change. The expression of *CA2* was upregulated with 7 d medium and dropped significantly compared to 14 d ($p = 0.0012$) and 21 d ($p = 0.054$). *CA2* was downregulated compared to the control with 21 d ($p = 0.032$). *MMP9* was significantly upregulated with 7 d ESO compared to the control ($p = 0.0462$) and dropped when compared to 14 d ($p = 0.0241$) and 21 d ($p = 0.0469$). In addition, the gene expression of the recruiting marker monocyte chemoattractant protein (*MCP1*) was analyzed (Figure S2). A significant increase in the *MCP1* gene expression could be detected with the 7 d ESO ($p = 0.0455$).

3.3.3. Released Mediators

The release of TRAP5b, BMP-2, cystatin C, IFN-β, IL-1β, -4, -6, -10, -17A, -23, OPN, TGF-β1, and TNF-α were analyzed for the pre-osteoclasts stimulated with ESO and NSO, and the $control_{iwc}$. The concentration of the $control_{iwc}$ was subtracted from the concentration of the cultivated pre-osteoclasts. The data for IFN-β are not shown as no proteins could be detected.

The different stimulation conditions did not significantly influence the concentration of IL-1β, OPN, cystatin C, TRAP5b, TGF-β1, and IL-17A (Figure S3). For TNF-α and IL-6 lower amounts of proteins were detected after the stimulation with pre-osteoclasts compared to the incubated medium without any cells ($control_{iwc}$). As the protein concentrations of the $control_{iwc}$ were subtracted from the protein concentrations of the sample, negative concentrations are shown (Figure 6c).

The concentration of IL-4 was downregulated by 7 d, 14 d, and 21 d ESO media compared to NSO. This downregulation was significant for 7 d ($p = 0.0008$) and for 14 d ($p = 0.0087$). A similar trend was observed for IL-10, IL-23, and BMP-2. The IL-10 concentration was downregulated with 7 d and 14 d ESO media and significantly downregulated for 21 d compared to the NSO ($p = 0.0002$). For IL-23, differences between the ESO and the control were the most pronounced after 7 d ($p = 0.008$) and slighter at 14 d ($p = 0.051$) and 21 ($p = 0.08$). The concentration of BMP-2 was mainly changed through indirect stimulation with the 21 d medium. BMP-2 was reduced with the ESO supernatant ($p = 0.059$) compared to the NSO (Figure 6b).

For TNF-α, the lowest protein amount was detected for the cultivation with 7 d ESO supernatant compared to the NSO ($p < 0.0001$). With 14 d and 21 d, no changes between the ESO and NSO were observed. IL-6 was mainly regulated by the 7 d supernatant; stimulation with ESO led to a significant upregulation of IL-6 compared to NSO ($p = 0.0036$). Media generated after 14 d and 21 d stimulation did not affect the IL-6 release (Figure 6c).

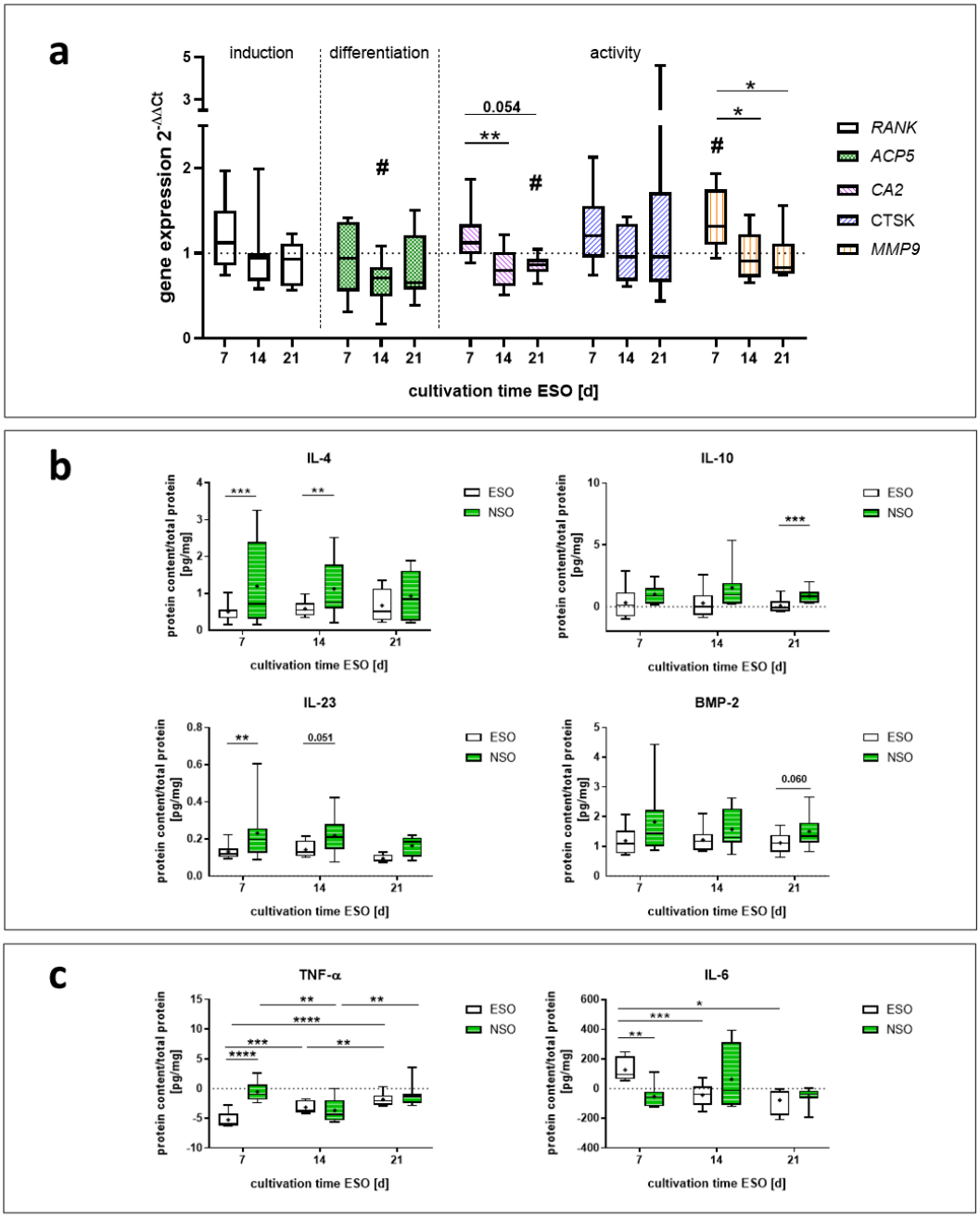

Figure 6. Gene expression and protein data of pre-osteoclasts after 48 h incubation with pooled supernatant of osteoblast (ESO) stimulated over 7, 14, and 21 d and without electric stimulation (NSO). (**a**) Gene expression data were related to the NSO using the $2^{-\Delta\Delta Ct}$ method. Boxplots are used to present the distribution of the total results with significant changes [n = 8]. Significant differences were determined using the two-way ANOVA with Tukey. # indicates significant differences between the ESO and NSO: # $p < 0.05$. * indicates significant differences between stimulation time points: * $p < 0.05$. (**b**, **c**) Protein concentration related to the total protein concentration of the supernatant. The respective protein concentration from the $control_{iwc}$ was subtracted. Boxplots are used to present the distribution of the total results [n ≥ 6]. Significant differences were determined using the two-way ANOVA with Tukey. * indicates significant differences: * $p < 0.05$, ** $p < 0.01$, *** $p < 0.001$, **** $p < 0.0001$. (**b**) Proteins that were produced by the pre-osteoclasts (**c**) proteins that were consumed by the pre-osteoclasts.

4. Discussion

The tailoring of bone remodeling processes through external stimulation is essential for the treatment of osteoporosis, critical-size bone defects, and poorly ingrown artificial joints. Electric stimulation with externally applied electrical fields is one possible treatment method. Positive results have been observed in clinical use in the past, but open questions remain regarding the cellular processes [35]. Various in vitro studies focus on the influence of electric fields on the differentiation of osteoblasts and their bone-forming potential [3]. However, bone healing depends not only on the bone formation capacity of the osteoblast. Bone resorption processes through osteoclasts play an essential role in bone turnover and fracture healing.

Co-cultures between osteoblasts and osteoclasts are essential to verify cellular behavior and interaction, as differences between cells in co-culture and cells in monoculture have been noted [28,36]. Consequently, they improve the comparability of in vitro studies with in vivo studies [37]. The system used in this study gives the first insights into how released cytokines from osteoblasts can influence osteoclastogenesis. With the exchange of the supernatant of stimulated osteoblasts, a study focused on the changes in osteoclast formation, differentiation, and activity through indirect stimulation was possible. However, this study can only make assumptions about the impact on osteogenesis through the feedback of the osteoclasts. Further studies using a trans-well system or 3D scaffolds are important to include the direct exchange and feedback of the cells. Nevertheless, results obtained in this study revealed indirect effects of ESO (Figure 7): (I) Electrical stimulation of osteoblasts resulted in the release of various cytokines that influence osteoclastic differentiation and activation. They respond with an additional release of pro-and anti-inflammatory cytokines. (II) The viability of PBMCs is most influenced by the supernatants from the ESO of the two earlier time points. At the same time, osteoclastogenesis is induced in the cells. (III) Pre-osteoclasts revealed an increased activity when cultivated with 7 d medium, and ESO supernatants at day 21 led to higher viability.

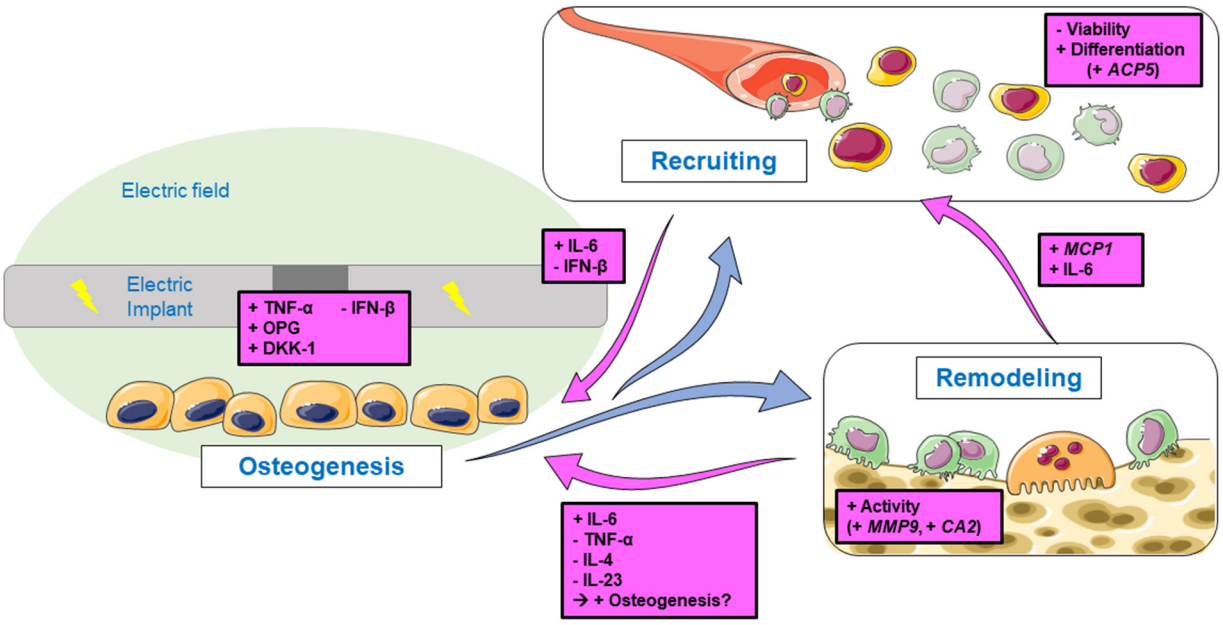

Figure 7. Schematic overview of the aims and results of this study. Stimulated osteoblasts produce signaling molecules that influence osteoclastogenesis through recruiting and remodeling processes. The observed changes in gene expression and protein release of the progenitor cells and osteoclasts-like cells are shown in pink. Single pictures were used from Servier Medical Art (http://smart.servier.com/, accessed on 14 June 2022).

4.1. Differentiation of PBMCs

Monocytes as well as macrophages play an important role in inflammation, homeostasis, tissue development, and injury repair [38]. They have the potential to differentiate into osteoclasts. Therefore, understanding their differentiation potential is important for further information on bone remodeling processes [39]. This study focused on the impact of indirect stimulation with ESO on the induction of PBMC differentiation into osteoclasts. It was possible to initiate osteoclastic differentiation of PBMCs without the external differentiation factors M-CSF and RANKL [28] by using supernatants from stimulated osteoblasts. A higher number of osteoclast-like cells were seen with 7 d and 14 d ESO media, and an increase in *ACP5* gene expression could be observed. Further, a significant upregulation in *CTSK* gene expression could be observed with the 7 d medium, a gene that is an important marker for the activity of osteoclastic cells [40]. As no major changes in the *RANK* gene expression were noticeable, it can be assumed that RANKL was not the key factor for the induced osteoclastogenesis. Studies have shown that other mediators such as TNF-α, TGF-β, and IL-33 have the potential to enhance osteoclast differentiation in the absence of the RANK-RANKL pathway [41–43]. In this study, TNF-α was doubled in the ESO supernatants; thus, the differentiation through TNF-α can be assumed [41,44,45]. Further, Lei et al. revealed the inhibition of RANKL-induced osteoclastogenesis in directly electrically stimulated macrophages, which would underline the assumption of a RANKL-independent differentiation observed in this study [20]. Another argument supporting the hypothesis is the IFN-β concentration, as IFN-β is an anti-osteoclastogenic cytokine [46]. The highest amount of released IFN-β was detectable in PBMCs cultivated with the 7 d NSO medium. Comparing the protein concentration of ESO and NSO proves that, especially after seven days, the presence of osteoclastic antagonists such as IFN-β and IL-10 were present in the NSO medium, but not in the ESO medium. IL-10, like IFN-β, is known for its possible role in inhibiting osteoclast formation [47]. Vice versa, the induction of *ACP5* and *CTSK* mRNA transcripts in PBMCs cultivated with the 7 d ESO medium correlates with the absence of IFN-β and IL-10 proteins. Although the anti-osteoclast mediators IL-10 and IFN-β were detectable in the ESO medium after 14 days, the induction of the osteoclastic differentiation and activity markers was still demonstrated. However, besides the presence of higher IL-6 protein concentrations, the clearly enhanced concentration of the TNF-α protein in particular seemed to be more inductive for osteoclastogenesis. Although IFN-β and IL-10 were no longer detectable in the 21 d ESO medium, the composition of the medium did not affect osteoclastogenesis. This could be due to the presence of other mediators in the medium, which we did not consider in our setup. However, in our previous work, we could show that, especially on day 21, the highest mineralization of osteoblasts was detectable following stimulation with alternating electric fields [30]. Since osteoclastogenesis is particularly inhibited by enhanced calcium ion levels [48] the accumulation of calcium in the 21 d ESO medium might have a greater inhibitory effect on osteoclastogenesis than the ESO media of the earlier time points.

4.2. Activation of Pre-Osteoclasts

Osteoclasts are the major antagonists for osteoblasts, and their interplay is essential for bone turnover and remodeling [36]. On the one hand, excessive activity of osteoclasts can lead to diseases such as osteoporosis, periprosthetic osteolysis, or bone tumors; on the other hand, reduced activity can lead to osteopetrosis [49]. Therefore, studying osteoclastic cell behavior under electric stimulation is important to understand bone remodeling processes. Before the pre-osteoclast cells were incubated with the specific osteoblast supernatants, they were first stimulated with RANKL and M-CSF. Both are essential factors that induce and promote osteoclastogenesis in vitro [50]. The subsequent change of cell culture conditions with the osteoblast media was intended to clarify whether the factors secreted by osteoblasts can maintain osteoclastogenesis.

As for the PBMCs, most of the changes were observed with the 7 d medium. *MMP9* and *CA2* were upregulated in pre-osteoclasts cultured with the ESO supernatant compared

to the NSO. *MMP9* plays an important role in bone resorption processes and remodeling by degrading the organic matrix and releasing the extracellular matrix proteins [51]. Oliveria et al. reported an upregulation of *MMP9* during the improved healing process of an amputated rat limb through electric stimulation [52]. This highlights the importance of *MMP9* and its role as a marker for osteoclastogenesis through electric stimulation. *CA2* is important for bone resorption as it regulates the pH through H^+ production, leading to an acidification of the extracellular environment [53]. The simultaneous upregulation of *MMP9* and *CA2* indicates an increased induction of osteoclast activity through the cultivation with 7 d ESO supernatants. This increase in activity can be related, as explained before, to the increased TNF-α concentration in the ESO medium compared to the NSO medium. Further, the medium of the NSO contained a higher concentration of the osteoclastic antagonists IFN-β and IL-10. This could have led to the higher activity of the pre-osteoclasts which were cultured with the ESO medium compared to the cells cultured with the NSO medium. In addition, a higher IL-6 protein release and *MCP1* expression were observed. IL-6 is known to trigger the expression of *MCP-1* in cells, and the resulting higher *MCP-1* expression may, in turn, further increase osteoclastogenesis [54–56], resulting in the enhanced recruitment of monocytic cells through the 7 d ESO supernatant. It can be postulated that the stimulation with electric fields alters the osteoblastic secretion of proteins, which in turn influence the differentiation and activity of osteoclastic cells and therefore affect remodeling processes. This fact might be more marked at the earlier stimulation time points than the later ones, as the induction and the maintenance of osteoclastogenesis were more prominent with 7 d ESO medium.

It was not possible to generate multinuclear osteoclasts through the pre-stimulation or through the cultivation with the ESO or NSO media. To improve the outcome in the generation of osteoclasts, the usage of mineralized surfaces or scaffolds can be implemented. Through the cultivation on apatite-containing materials, osteoclastogenesis is enhanced and more robust sealing zones are formed compared to the cultivation on plastic [57]. Further, resorption pits, as results from osteoclast activity, can be used to make assumptions about the resorption activity [57–59].

4.3. Influence on Cell Viability during Osteoclastogenesis

The ESO supernatants influenced the viability of both PBMCs and pre-osteoclasts. Thereby, the 7 d and 14 d ESO supernatants led to different changes in viability compared to the 21 d supernatants. The 7 d and 14 d supernatants reduced the viability of cultivated PBMCs but did not influence pre-osteoclasts. Supernatants from day 21 did not change PBMCs' viability but increased the viability of pre-osteoclasts. This reveals a cell stage-dependent influence on the viability through the released cytokines and chemokines from stimulated osteoblasts. PBMCs consist of multipotent progenitor cell populations with a high capacity to differentiate into different cell types [60]. In addition to this differentiation potential, PBMCs as precursors have a higher proliferation capacity than already differentiated cells [61]. ESO supernatants of 7 d and 14 d increased the differentiation potential of PBMCs compared to the fewer-differentiated cells cultivated with NSO. It is possible that the enhanced differentiation reduced the viability of the cells. This assumption can be strengthened by the reduced differentiation with 21 d and the simultaneous unchanged viability. Further investigations are necessary to confirm this assumption.

Compared to the PBMCs, the pre-osteoclasts were further differentiated, as actin ring structures were observed in all cultivation conditions. The 21 d supernatants did not enhance the osteoclasts' activation or differentiation but increased the viability of the cells. Further, the *CASP8* gene expression was downregulated by the 21 d supernatant. As *CASP8* is known to be an initiator for apoptosis, reduced apoptosis can be assumed, leading to higher viability [62]. Cell cycle analysis and live dead assays can provide further information about cell viability. Especially the cell cycle analysis can reveal the proliferation possibilities and provide more details on the differentiation state of the cells [61]. Moreover, other possible cytokines could have influenced the proliferation rate. Therefore, a more

comprehensive screening of the ESO supernatant can be implemented to increase the understanding of stimulation factors released from osteoblasts under electric stimulation.

4.4. Feedback Signaling on Osteogenesis and Bone Remodeling

Due to the differentiation and activation of PBMCs and pre-osteoclasts, feedback signals are assumed. Compared to the NSO media, lower amounts of IL-4, IL-23, and TNF-α were observed in the supernatants of pre-osteoclasts cultivated with ESO media. These proteins are known for their anti-osteoclastogenic properties, leading to reduced osteoblastic differentiation and activity [63,64]. As electric stimulation indirectly reduced the amount of released IL-4, IL-23, and TNF-α, promoting feedback on osteoblasts can be expected. The increase in IL-6 concentration supports this assumption, as IL-6 is known to be important for osteogenesis [65–67]. Moreover, a rise in IL-6 can also improve the recruitment of new osteoclastic progenitors, as it can act as a proinflammatory signal [68,69]. The analyzed BMP-2 concentration is in contrast to the previous hypotheses, as lower amounts of BMP-2, an inducer of osteoblast differentiation [70], were observed with ESO. Further studies on osteogenesis are necessary to observe the impact of the released cytokines. It can be expected that the indirect stimulation of PBMCs and pre-osteoclasts influences bone remodeling processes.

Therefore, analyses of the interaction between progenitor cells, osteoclasts, and osteoblasts are necessary. Co-cultures such as trans-well systems or 3D scaffolds would allow the observation of feedback signals and the resulting changes in cell differentiation simultaneously [71]. Moreover, 3D scaffolds with a matrix that is similar to bone tissue would give a more physiological environment and allow the study of osteoblastic and osteoclastic cells together in one culture setup. Further, it has been described that exosomes and apoptotic bodies as osteoclast-derived extracellular vesicles can carry different miRNAs, which can influence osteogenesis [72]. Therefore, a protein screening of the supernatant as well as the determination of extracellular vesicles might give a more detailed insight into the signaling and interplay between the different cell types.

5. Conclusions

The application of external electric fields is a method that is used to improve bone healing, but there are still open questions regarding the fundamental cellular mechanisms and how to improve clinical outcomes. For this reason, we have postulated the following question: Is there an influence of electrically stimulated osteoblasts on the induction of osteoclastogenesis? It could be shown that electrically stimulated human osteoblasts release signaling factors in a time-dependent manner which affects the viability, differentiation, and activity of PBMCs and pre-osteoclasts. In this context, different stimulation times of osteoblasts led to different cell responses in both PBMCs and pre-osteoclasts. Further studies with direct co-culture systems are necessary to understand the effect of electrical stimulation on osteoblasts and osteoclasts simultaneously and how their interaction affects cell behavior.

Supplementary Materials: The following supporting information can be downloaded at: https://www.mdpi.com/article/10.3390/app122211840/s1, Figure S1: Released cytokines of PBMCs after 48 h incubation with pooled supernatant of osteoblast stimulated over 7, 14, and 21 d and without electrical stimulation, Figure S2: *MCP1* expression of pre-osteoclasts after 48 h incubation with pooled supernatant of osteoblast stimulated over 7, 14, and 21 d and without electrical stimulation, Figure S3: Released cytokines of pre-osteoclasts after 48 h incubation with pooled supernatant of osteoblast stimulated over 7, 14, and 21 d and without electrical stimulation.

Author Contributions: Conceptualization: F.S. and A.J.-H.; methodology: A.J. and F.S.; resources: A.J.-H. and R.B.; data curation: A.J. and F.S.; writing—original draft preparation: F.S.; writing—review and editing: A.J., A.J.-H., R.D. and R.B.; visualization: A.J. and F.S.; supervision: A.J.-H., R.D. and R.B.; project administration: A.J.-H.; funding acquisition: A.J.-H. and R.D. All authors have read and agreed to the published version of the manuscript.

Funding: Funded by the Deutsche Forschungsgemeinschaft (DFG, German Research Foundation): JO 1483/1-1 and CRC ELAINE 1270/2-299150580.

Institutional Review Board Statement: The study was conducted in accordance with the Declaration of Helsinki and approved by the Institutional Ethics Committee of Rostock University Medical Centre (registration number: A 2010-0010, approval date: 27 January 2017; registration number: A2011-140, approval date: 24 November 2021).

Informed Consent Statement: Informed consent was obtained from all subjects involved in the study.

Data Availability Statement: The datasets generated during the current study are available from the corresponding author on reasonable request.

Acknowledgments: We gratefully acknowledge Doris Hansmann and Simone Krüger from the department of Orthopedics (Rostock University Medical Center) as well Wendy Bergmann and Michael Müller from the Core Facility for Cell Sorting and Cell Analysis (Rostock University Medical Center) for their technical support.

Conflicts of Interest: The authors declare no conflict of interest. The funders had no role in the design of the study; in the collection, analyses, or interpretation of data; in the writing of the manuscript; or in the decision to publish the results.

References

1. Balint, R.; Cassidy, N.J.; Cartmell, S.H. Electrical Stimulation: A Novel Tool for Tissue Engineering. *Tissue Eng. Part. B Rev.* **2013**, *19*, 48–57. [CrossRef] [PubMed]
2. Fukada, E.; Yasuda, I. On the Piezoelectric Effect of Bone. *J. Phys. Soc. Japan* **1957**, *12*, 1158–1162. [CrossRef]
3. deVet, T.; Jhirad, A.; Pravato, L.; Wohl, G.R. Bone Bioelectricity and Bone-Cell Response to Electrical Stimulation: A Review. *Crit. Rev. Biomed. Eng.* **2021**, *49*, 1–19. [CrossRef] [PubMed]
4. Ryan, C.N.M.; Doulgkeroglou, M.N.; Zeugolis, D.I. Electric Field Stimulation for Tissue Engineering Applications. *BMC Biomed. Eng.* **2021**, *3*, 1. [CrossRef] [PubMed]
5. Chen, C.; Bai, X.; Ding, Y.; Lee, I.-S. Electrical Stimulation as a Novel Tool for Regulating Cell Behavior in Tissue Engineering. *Biomater. Res.* **2019**, *23*, 25. [CrossRef]
6. Griffin, M.; Bayat, A. Electrical Stimulation in Bone Healing: Critical Analysis by Evaluating Levels of Evidence. *Eplasty* **2011**, *11*, e34.
7. Ercan, B.; Webster, T.J. The Effect of Biphasic Electrical Stimulation on Osteoblast Function at Anodized Nanotubular Titanium Surfaces. *Biomaterials* **2010**, *31*, 3684–3693. [CrossRef]
8. Srirussamee, K.; Xue, R.; Mobini, S.; Cassidy, N.J.; Cartmell, S.H. Changes in the Extracellular Microenvironment and Osteogenic Responses of Mesenchymal Stem/Stromal Cells Induced by in Vitro Direct Electrical Stimulation. *J. Tissue Eng.* **2021**, *12*, 2041731420974147. [CrossRef]
9. Sahm, F.; Ziebart, J.; Jonitz-Heincke, A.; Hansmann, D.; Dauben, T.; Bader, R. Alternating Electric Fields Modify the Function of Human Osteoblasts Growing on and in the Surroundings of Titanium Electrodes. *Int. J. Mol. Sci.* **2020**, *21*, 6944. [CrossRef]
10. Supronowicz, P.R.; Ajayan, P.M.; Ullmann, K.R.; Arulanandam, B.P.; Metzger, D.W.; Bizios, R. Novel Current-Conducting Composite Substrates for Exposing Osteoblasts to Alternating Current Stimulation. *J. Biomed. Mater. Res.* **2001**, *59*, 499–506. [CrossRef]
11. Creecy, C.M.; O'Neill, C.F.; Arulanandam, B.P.; Sylvia, V.L.; Navara, C.S.; Bizios, R. Mesenchymal Stem Cell Osteodifferentiation in Response to Alternating Electric Current. *Tissue Eng. Part A* **2013**, *19*, 467–474. [CrossRef] [PubMed]
12. Zhang, B.; Xie, Y.; Ni, Z.; Chen, L. Effects and Mechanisms of Exogenous Electromagnetic Field on Bone Cells: A Review. *Bioelectromagnetics* **2020**, *41*, 263–278. [CrossRef] [PubMed]
13. Detsch, R.; Boccaccini, A.R. The Role of Osteoclasts in Bone Tissue Engineering. *J. Tissue Eng. Regen. Med.* **2015**, *9*, 1133–1149. [CrossRef] [PubMed]
14. Chang, K.; Chang, W.H.-S.; Tsai, M.-T.; Shih, C. Pulsed Electromagnetic Fields Accelerate Apoptotic Rate in Osteoclasts. *Connect. Tissue Res.* **2006**, *47*, 222–228. [CrossRef]
15. Chang, K.; Chang, W.H.-S.; Wu, M.-L.; Shih, C. Effects of Different Intensities of Extremely Low Frequency Pulsed Electromagnetic Fields on Formation of Osteoclast-like Cells. *Bioelectromagnetics* **2003**, *24*, 431–439. [CrossRef] [PubMed]
16. Rubin, J.; McLeod, K.J.; Titus, L.; Nanes, M.S.; Catherwood, B.D.; Rubin, C.T. Formation of Osteoclast-like Cells Is Suppressed by Low Frequency, Low Intensity Electric Fields. *J. Orthop. Res.* **1996**, *14*, 7–15. [CrossRef]
17. Shankar, V.S.; Simon, B.J.; Bax, C.M.R.; Pazianas, M.; Moonga, B.S.; Adebanjo, O.A.; Zaidi, M. Effects of Electromagnetic Stimulation on the Functional Responsiveness of Isolated Rat Osteoclasts. *J. Cell Physiol.* **1998**, *176*, 537–544. [CrossRef]
18. Ferrier, J.; Ross, S.M.; Kanehisa, J.; Aubin, J.E. Osteoclasts and Osteoblasts Migrate in Opposite Directions in Response to a Constant Electrical Field. *J. Cell Physiol.* **1986**, *129*, 283–288. [CrossRef]
19. He, Z.; Selvamurugan, N.; Warshaw, J.; Partridge, N.C. Pulsed Electromagnetic Fields Inhibit Human Osteoclast Formation and Gene Expression via Osteoblasts. *Bone* **2018**, *106*, 194–203. [CrossRef]

20. Lei, Y.; Su, J.; Xu, H.; Yu, Q.; Zhao, M.; Tian, J. Pulsed Electromagnetic Fields Inhibit Osteoclast Differentiation in RAW264.7 Macrophages via Suppression of the Protein Kinase B/Mammalian Target of Rapamycin Signaling Pathway. *Mol. Med. Rep.* **2018**, *18*, 447–454. [CrossRef]
21. Pesce, M.; Patruno, A.; Speranza, L.; Reale, M. Extremely Low Frequency Electromagnetic Field and Wound Healing: Implication of Cytokines as Biological Mediators. *Eur. Cytokine Netw.* **2013**, *24*, 1–10. [CrossRef] [PubMed]
22. Chen, Y.; Menger, M.M.; Braun, B.J.; Schweizer, S.; Linnemann, C.; Falldorf, K.; Ronniger, M.; Wang, H.; Histing, T.; Nussler, A.K.; et al. Modulation of Macrophage Activity by Pulsed Electromagnetic Fields in the Context of Fracture Healing. *Bioengineering* **2021**, *8*, 167. [CrossRef] [PubMed]
23. Groiss, S.; Lammegger, R.; Brislinger, D. Anti-Oxidative and Immune Regulatory Responses of THP-1 and PBMC to Pulsed EMF Are Field-Strength Dependent. *Int. J. Environ. Res. Public Health* **2021**, *18*, 9519. [CrossRef] [PubMed]
24. Srirussamee, K.; Mobini, S.; Cassidy, N.J.; Cartmell, S.H. Direct Electrical Stimulation Enhances Osteogenesis by Inducing Bmp2 and Spp1 Expressions from Macrophages and Preosteoblasts. *Biotechnol. Bioeng.* **2019**, *116*, 3421–3432. [CrossRef] [PubMed]
25. Sun, Y.-S.; Peng, S.-W.; Cheng, J.-Y. In Vitro Electrical-Stimulated Wound-Healing Chip for Studying Electric Field-Assisted Wound-Healing Process. *Biomicrofluidics* **2012**, *6*, 34117. [CrossRef] [PubMed]
26. Detsch, R.; Mayr, H.; Seitz, D.; Ziegler, G. Is Hydroxyapatite Ceramic Included in the Bone Remodelling Proccess? An In Vitro Study of Resorption and Formation Processes. *Key Eng. Mater.* **2008**, *361–363*, 1123–1126. [CrossRef]
27. Zehnder, T.; Boccaccini, A.R.; Detsch, R. Biofabrication of a Co-Culture System in an Osteoid-like Hydrogel Matrix. *Biofabrication* **2017**, *9*, 025016. [CrossRef]
28. Borciani, G.; Montalbano, G.; Baldini, N.; Cerqueni, G.; Vitale-Brovarone, C.; Ciapetti, G. Co-Culture Systems of Osteoblasts and Osteoclasts: Simulating in Vitro Bone Remodeling in Regenerative Approaches. *Acta Biomater.* **2020**, *108*, 22–45. [CrossRef]
29. Wang, W.; Junior, J.R.P.; Nalesso, P.R.L.; Musson, D.; Cornish, J.; Mendonca, F.; Caetano, G.F.; Bartolo, P. Engineered 3D Printed Poly(Varepsilon-Caprolactone)/Graphene Scaffolds for Bone Tissue Engineering. *Mater. Sci. Eng. C Mater. Biol. Appl.* **2019**, *100*, 759–770. [CrossRef]
30. Sahm, F.; Freiin Grote, V.; Zimmermann, J.; Haack, F.; Uhrmacher, A.M.; van Rienen, U.; Bader, R.; Detsch, R.; Jonitz-Heincke, A. Long-Term Stimulation with Alternating Electric Fields Modulates the Differentiation and Mineralization of Human Pre-Osteoblasts. *Front. Physiol.* **2022**, *13*, 965181. [CrossRef]
31. Grunert, P.C.; Jonitz-Heincke, A.; Su, Y.; Souffrant, R.; Hansmann, D.; Ewald, H.; Krüger, A.; Mittelmeier, W.; Bader, R. Establishment of a Novel In Vitro Test Setup for Electric and Magnetic Stimulation of Human Osteoblasts. *Cell Biochem. Biophys.* **2014**, *70*, 805–817. [CrossRef] [PubMed]
32. Hiemer, B.; Krogull, M.; Bender, T.; Ziebart, J.; Krueger, S.; Bader, R.; Jonitz-Heincke, A. Effect of Electric Stimulation on Human Chondrocytes and Mesenchymal Stem Cells under Normoxia and Hypoxia. *Mol. Med. Rep.* **2018**, *18*, 2133–2141. [CrossRef] [PubMed]
33. Klinder, A.; Markhoff, J.; Jonitz-Heincke, A.; Sterna, P.; Salamon, A.; Bader, R. Comparison of Different Cell Culture Plates for the Enrichment of Non-Adherent Human Mononuclear Cells. *Exp. Ther. Med.* **2019**, *17*, 2004–2012. [CrossRef]
34. Livak, K.J.; Schmittgen, T.D. Analysis of Relative Gene Expression Data Using Real-Time Quantitative PCR and the $2^{-\Delta\Delta CT}$ Method. *Methods* **2001**, *25*, 402–408. [CrossRef] [PubMed]
35. Bhavsar, M.B.; Han, Z.; DeCoster, T.; Leppik, L.; Costa Oliveira, K.M.; Barker, J.H.; Oliveira, K.M.C.; Bhavsar, M.B.; Barker, J.H.; Han, Z.; et al. Electrical Stimulation-Based Bone Fracture Treatment, If It Works so Well Why Do Not More Surgeons Use It? *Eur. J. Trauma Emerg. Surg.* **2020**, *46*, 245–264. [CrossRef] [PubMed]
36. Sieberath, A.; Della Bella, E.; Ferreira, A.M.; Gentile, P.; Eglin, D.; Dalgarno, K. A Comparison of Osteoblast and Osteoclast In Vitro Co-Culture Models and Their Translation for Preclinical Drug Testing Applications. *Int. J. Mol. Sci.* **2020**, *21*, 912. [CrossRef]
37. Duncan, R.L.; Turner, C.H. Mechanotransduction and the Functional Response of Bone to Mechanical Strain. *Calcif. Tissue Int.* **1995**, *57*, 344–358. [CrossRef]
38. Ogle, M.E.; Segar, C.E.; Sridhar, S.; Botchwey, E.A. Monocytes and Macrophages in Tissue Repair: Implications for Immunoregenerative Biomaterial Design. *Exp. Biol. Med.* **2016**, *241*, 1084–1097. [CrossRef]
39. Anesi, A.; Generali, L.; Sandoni, L.; Pozzi, S.; Grande, A. From Osteoclast Differentiation to Osteonecrosis of the Jaw: Molecular and Clinical Insights. *Int. J. Mol. Sci.* **2019**, *20*, 4925. [CrossRef]
40. Wilson, S.R.; Peters, C.; Saftig, P.; Brömme, D. Cathepsin K Activity-Dependent Regulation of Osteoclast Actin Ring Formation and Bone Resorption. *J. Biol. Chem.* **2009**, *284*, 2584–2592. [CrossRef]
41. Kim, N.; Kadono, Y.; Takami, M.; Lee, J.; Lee, S.-H.; Okada, F.; Kim, J.H.; Kobayashi, T.; Odgren, P.R.; Nakano, H.; et al. Osteoclast Differentiation Independent of the TRANCE–RANK–TRAF6 Axis. *J. Exp. Med.* **2005**, *202*, 589–595. [CrossRef] [PubMed]
42. Mun, S.H.; Ko, N.Y.; Kim, H.S.; Kim, J.W.; Kim, D.K.; Kim, A.-R.; Lee, S.H.; Kim, Y.-G.; Lee, C.K.; Lee, S.H.; et al. Interleukin-33 Stimulates Formation of Functional Osteoclasts from Human CD14+ Monocytes. *Cell. Mol. Life Sci.* **2010**, *67*, 3883–3892. [CrossRef] [PubMed]
43. Kobayashi, K.; Takahashi, N.; Jimi, E.; Udagawa, N.; Takami, M.; Kotake, S.; Nakagawa, N.; Kinosaki, M.; Yamaguchi, K.; Shima, N.; et al. Tumor Necrosis Factor α Stimulates Osteoclast Differentiation by a Mechanism Independent of the Odf/Rankl–Rank Interaction. *J. Exp. Med.* **2000**, *191*, 275–286. [CrossRef] [PubMed]
44. Fuller, K.; Murphy, C.; Kirstein, B.; Fox, S.W.; Chambers, T.J. TNFα Potently Activates Osteoclasts, through a Direct Action Independent of and Strongly Synergistic with RANKL. *Endocrinology* **2002**, *143*, 1108–1118. [CrossRef]

45. Heiland, G.R.; Zwerina, K.; Baum, W.; Kireva, T.; Distler, J.H.; Grisanti, M.; Asuncion, F.; Li, X.; Ominsky, M.; Richards, W.; et al. Neutralisation of Dkk-1 Protects from Systemic Bone Loss during Inflammation and Reduces Sclerostin Expression. *Ann. Rheum. Dis.* **2010**, *69*, 2152–2159. [CrossRef]
46. Amarasekara, D.S.; Yun, H.; Kim, S.; Lee, N.; Kim, H.; Rho, J. Regulation of Osteoclast Differentiation by Cytokine Networks. *Immune Netw.* **2018**, *18*, e8. [CrossRef]
47. Evans, K.E.; Fox, S.W. Interleukin-10 Inhibits Osteoclastogenesis by Reducing NFATc1 Expression and Preventing Its Translocation to the Nucleus. *BMC Cell Biol.* **2007**, *8*, 4. [CrossRef]
48. Cho, H.; Lee, J.; Jang, S.; Lee, J.; Oh, T.I.; Son, Y.; Lee, E. Casr-Mediated Hbmscs Activity Modulation: Additional Coupling Mechanism in Bone Remodeling Compartment. *Int. J. Mol. Sci.* **2021**, *22*, 325. [CrossRef]
49. Bi, H.; Chen, X.; Gao, S.; Yu, X.; Xiao, J.; Zhang, B.; Liu, X.; Dai, M. Key Triggers of Osteoclast-Related Diseases and Available Strategies for Targeted Therapies: A Review. *Front. Med.* **2017**, *4*, 234. [CrossRef]
50. Xu, F.; Teitelbaum, S.L. Osteoclasts: New Insights. *Bone Res.* **2013**, *1*, 11–26. [CrossRef]
51. Zheng, X.; Zhang, Y.; Guo, S.; Zhang, W.; Wang, J.; Lin, Y. Dynamic Expression of Matrix Metalloproteinases 2, 9 and 13 in Ovariectomy-Induced Osteoporosis Rats. *Exp. Ther. Med.* **2018**, *16*, 1807–1813. [CrossRef] [PubMed]
52. Oliveira, K.M.C.; Barker, J.H.; Berezikov, E.; Pindur, L.; Kynigopoulos, S.; Eischen-Loges, M.; Han, Z.; Bhavsar, M.B.; Henrich, D.; Leppik, L. Electrical Stimulation Shifts Healing/Scarring towards Regeneration in a Rat Limb Amputation Model. *Sci. Rep.* **2019**, *9*, 11433. [CrossRef] [PubMed]
53. Lehenkari, P.; Hentunen, T.A.; Laitala-Leinonen, T.; Tuukkanen, J.; Väänänen, H.K. Carbonic Anhydrase II Plays a Major Role in Osteoclast Differentiation and Bone Resorption by Effecting the Steady State Intracellular PH and Ca^{2+}. *Exp. Cell Res.* **1998**, *242*, 128–137. [CrossRef] [PubMed]
54. Arendt, B.K.; Velazquez-Dones, A.; Tschumper, R.C.; Howell, K.G.; Ansell, S.M.; Witzig, T.E.; Jelinek, D.F. Interleukin 6 Induces Monocyte Chemoattractant Protein-1 Expression in Myeloma Cells. *Leukemia* **2002**, *16*, 2142–2147. [CrossRef] [PubMed]
55. Biswas, P.; Delfanti, F.; Bernasconi, S.; Mengozzi, M.; Cota, M.; Polentarutti, N.; Mantovani, A.; Lazzarin, A.; Sozzani, S.; Poli, G. Interleukin-6 Induces Monocyte Chemotactic Protein-1 in Peripheral Blood Mononuclear Cells and in the U937 Cell Line. *Blood* **1998**, *91*, 258–265. [CrossRef]
56. Miyamoto, K.; Ninomiya, K.; Sonoda, K.-H.; Miyauchi, Y.; Hoshi, H.; Iwasaki, R.; Miyamoto, H.; Yoshida, S.; Sato, Y.; Morioka, H.; et al. MCP-1 Expressed by Osteoclasts Stimulates Osteoclastogenesis in an Autocrine/Paracrine Manner. *Biochem. Biophys. Res. Commun.* **2009**, *383*, 373–377. [CrossRef]
57. Takahashi, N.; Ejiri, S.; Yanagisawa, S.; Ozawa, H. Regulation of Osteoclast Polarization. *Odontology* **2007**, *95*, 1–9. [CrossRef]
58. Azari, A.; Schoenmaker, T.; de Souza Faloni, A.P.; Everts, V.; de Vries, T.J. Jaw and Long Bone Marrow Derived Osteoclasts Differ in Shape and Their Response to Bone and Dentin. *Biochem. Biophys. Res. Commun.* **2011**, *409*, 205–210. [CrossRef]
59. Detsch, R.; Schaefer, S.; Deisinger, U.; Ziegler, G.; Seitz, H.; Leukers, B. In Vitro-Osteoclastic Activity Studies on Surfaces of 3D Printed Calcium Phosphate Scaffolds. *J. Biomater. Appl.* **2011**, *26*, 359–380. [CrossRef]
60. Zhang, M.; Huang, B. The Multi-Differentiation Potential of Peripheral Blood Mononuclear Cells. *Stem Cell Res. Ther.* **2012**, *3*, 48. [CrossRef]
61. Ruijtenberg, S.; van den Heuvel, S. Coordinating Cell Proliferation and Differentiation: Antagonism between Cell Cycle Regulators and Cell Type-Specific Gene Expression. *Cell Cycle* **2016**, *15*, 196–212. [CrossRef] [PubMed]
62. Fritsch, M.; Günther, S.D.; Schwarzer, R.; Albert, M.-C.; Schorn, F.; Werthenbach, J.P.; Schiffmann, L.M.; Stair, N.; Stocks, H.; Seeger, J.M.; et al. Caspase-8 Is the Molecular Switch for Apoptosis, Necroptosis and Pyroptosis. *Nature* **2019**, *575*, 683–687. [CrossRef] [PubMed]
63. Amarasekara, D.S.; Kim, S.; Rho, J. Regulation of Osteoblast Differentiation by Cytokine Networks. *Int. J. Mol. Sci.* **2021**, *22*, 2851. [CrossRef]
64. Gilbert, L.; He, X.; Farmer, P.; Boden, S.; Kozlowski, M.; Rubin, J.; Nanes, M.S. Inhibition of Osteoblast Differentiation by Tumor Necrosis Factor-Alpha. *Endocrinology* **2000**, *141*, 3956–3964. [CrossRef] [PubMed]
65. Bastidas-Coral, A.P.; Bakker, A.D.; Zandieh-Doulabi, B.; Kleverlaan, C.J.; Bravenboer, N.; Forouzanfar, T.; Klein-Nulend, J. Cytokines TNF-α, IL-6, IL-17F, and IL-4 Differentially Affect Osteogenic Differentiation of Human Adipose Stem Cells. *Stem Cells Int.* **2016**, *2016*, 1318256. [CrossRef]
66. Xie, Z.; Tang, S.; Ye, G.; Wang, P.; Li, J.; Liu, W.; Li, M.; Wang, S.; Wu, X.; Cen, S.; et al. Interleukin-6/Interleukin-6 Receptor Complex Promotes Osteogenic Differentiation of Bone Marrow-Derived Mesenchymal Stem Cells. *Stem Cell Res. Ther.* **2018**, *9*, 13. [CrossRef]
67. Park, Y.-T.; Lee, S.-M.; Kou, X.; Karabucak, B. The Role of Interleukin 6 in Osteogenic and Neurogenic Differentiation Potentials of Dental Pulp Stem Cells. *J. Endod.* **2019**, *45*, 1342–1348. [CrossRef]
68. Ishimi, Y.; Miyaura, C.; Jin, C.H.; Akatsu, T.; Abe, E.; Nakamura, Y.; Yamaguchi, A.; Yoshiki, S.; Matsuda, T.; Hirano, T. IL-6 Is Produced by Osteoblasts and Induces Bone Resorption. *J. Immunol.* **1990**, *145*, 3297–3303.
69. Feng, W.; Liu, H.; Luo, T.; Liu, D.; Du, J.; Sun, J.; Wang, W.; Han, X.; Yang, K.; Guo, J.; et al. Combination of IL-6 and SIL-6R Differentially Regulate Varying Levels of RANKL-Induced Osteoclastogenesis through NF-KB, ERK and JNK Signaling Pathways. *Sci. Rep.* **2017**, *7*, 41411. [CrossRef]
70. Yamaguchi, A.; Sakamoto, K.; Minamizato, T.; Katsube, K.; Nakanishi, S. Regulation of Osteoblast Differentiation Mediated by BMP, Notch, and CCN3/NOV. *Jpn. Dent. Sci. Rev.* **2008**, *44*, 48–56. [CrossRef]

71. Remmers, S.J.A.; de Wildt, B.W.M.; Vis, M.A.M.; Spaander, E.S.R.; de Vries, R.B.M.; Ito, K.; Hofmann, S. Osteoblast-Osteoclast Co-Cultures: A Systematic Review and Map of Available Literature. *PLoS ONE* **2021**, *16*, e0257724. [CrossRef] [PubMed]
72. Yuan, F.-L.; Wu, Q.; Miao, Z.-N.; Xu, M.-H.; Xu, R.-S.; Jiang, D.-L.; Ye, J.-X.; Chen, F.; Zhao, M.-D.; Wang, H.; et al. Osteoclast-Derived Extracellular Vesicles: Novel Regulators of Osteoclastogenesis and Osteoclast–Osteoblasts Communication in Bone Remodeling. *Front. Physiol.* **2018**, *9*, 628. [CrossRef] [PubMed]

Bioelectrochemistry 151 (2023) 108395

Contents lists available at ScienceDirect

Bioelectrochemistry

journal homepage: www.journals.elsevier.com/bioelectrochemistry

Experimental and numerical methods to ensure comprehensible and replicable alternating current electrical stimulation experiments

Julius Zimmermann [a,*], Franziska Sahm [b], Nils Arbeiter [a], Henning Bathel [a], Zezhong Song [b], Rainer Bader [b,c], Anika Jonitz-Heincke [b,*], Ursula van Rienen [a,c,d,*]

[a] Institute of General Electrical Engineering, University of Rostock, D-18051 Rostock, Germany
[b] Department of Orthopaedics, Biomechanics and Implant Technology Research Laboratory, Rostock University Medical Center, D-18057 Rostock, Germany
[c] Department Life, Light & Matter, University of Rostock, D-18051 Rostock, Germany
[d] Department of Ageing of Individuals and Society, Interdisciplinary Faculty, University of Rostock, D-18051 Rostock, Germany

ARTICLE INFO

Keywords:
Electrical stimulation
Computational modelling
Computational electromagnetics
Electrochemical impedance spectroscopy
Regenerative medicine
Replicability

ABSTRACT

Electrical stimulation has received increasing attention for decades for its application in regenerative medicine. Applications range from bone growth stimulation over cartilage regeneration to deep brain stimulation. Despite all research efforts, translation into clinical use has not yet been achieved in all fields. Recent critical assessments have identified limited documentation and monitoring of preclinical in vitro and in vivo experiments as possible reasons hampering clinical translation. In this work, we present experimental and numerical methods to determine the crucial quantities of electrical stimulation such as the electric field or current density. Knowing the stimulation quantities contributes to comprehending the biological response to electrical stimulation and to finally developing a reliable dose–response curve. To demonstrate the methods, we consider a direct contact electrical stimulation experiment that stands representative for a broad class of stimulation experiments. Electrochemical effects are addressed and methods to integrate them into numerical simulations are evaluated. A focus is laid on affordable lab equipment and reproducible open-source software solutions. Finally, clear guidelines to ensure replicability of electrical stimulation experiments are formulated.

1. Introduction

Electrical stimulation has been investigated for use in different fields of regenerative medicine. Examples are wound healing [1], bone growth stimulation [2], cartilage regeneration [3], and deep brain stimulation [4]. Except for deep brain stimulation with more than 160,000 treated patients [5], electrical stimulation has not yet been widely implemented for clinical use. One reason may be that systematic reviews of clinical studies have not led to clear recommendations, for example, for the treatment of bone fractures [6,7] or osteoarthritis [8]. Nicksic et al. [2,9] have identified another reason: insufficient device specifications that prevents replication of electrical stimulation experiments. In this work, we will not consider pulsed electromagnetic fields and instead focus on direct electrical stimulation (i.e., electric fields evoked by an applied voltage). Furthermore, we will not consider direct current (DC) stimulation (i.e., stimulation with constant, zero-frequency voltages or currents). For a discussion of this case, we refer to [10]. Please note that challenges for accurate 3D simulation models, which we will present in this work, lie in the case of DC stimulation in a lack of knowledge of the electrochemical state of the electrode and multiple scales that must be bridged in the modelling approach [11]. Thus, we will restrict ourselves to alternating current (AC) applications, which include sine wave stimulation or rectangular pulses as the most popular types.

In general, it has not yet been established which quantities have to be known to compare different stimulation approaches. Often, the electric field strength is compared in literature reviews [1,12–14]. In contrast, Nicksic et al. [2,9] suggest to consider, among others, the current density and the electrode material. We suggested to report the measured current and voltage [15], which also permits to estimate the prevailing electric field and current density upon initial experimental calibration

* Corresponding authors at: Institute of General Electrical Engineering, University of Rostock, D-18051 Rostock, Germany (U. van Rienen and J. Zimmermann). Department of Orthopaedics, Biomechanics and Implant Technology Research Laboratory, Rostock University Medical Center, D-18057 Rostock, Germany (A. Jonitz-Heincke).

E-mail addresses: julius.zimmermann@uni-rostock.de (J. Zimmermann), anika.jonitz-heincke@med.uni-rostock.de (A. Jonitz-Heincke), ursula.van-rienen@uni-rostock.de (U. van Rienen).

https://doi.org/10.1016/j.bioelechem.2023.108395
Received 27 September 2022; Received in revised form 27 January 2023; Accepted 29 January 2023
Available online 3 February 2023

[11]. In the aforementioned works, measurements of the electric field or current density have been suggested but not implemented. Already in the 1980 s, Gundersen and Greenebaum [16] presented three methods to measure the electric field in a relatively simple system that generated a mostly homogeneous field. The field strength of a homogeneous field can be estimated by an analytical formula. However, in real stimulation experiments often inhomogeneous fields are applied. These fields usually require numerical simulations. We consider a stimulation device that has originally been developed to study the interaction of an electrical stimulation implant with chondrocytes and mesenchymal stem cells [17]. The electric field strength delivered by the stimulation device has been estimated using numerical simulations [17]. In previous research, it has been attempted to validate the numerical simulations by manually moving a reference electrode to different positions. The recorded voltages have then been compared to experimental data [18]. A good agreement of the simulated electric potential and the measured electric potential has only been observed at particular points. The numerical simulations have predicted a higher field strength than actually measured. Thus, it has only been possible to estimate an upper bound of the applied field strength by scaling the numerical simulations to match the measured values [17]. In this work, we will improve on that and outline how the numerical simulations are related to the different measurement approaches. With this, we would like to contribute to bridging the gap between guidelines focused mostly on experiments [9,19] and works on the numerical simulations [20,21].

We will use two methods described by Gundersen and Greenebaum [16]. One method requires measurement of the applied voltage, resulting current and conductivity of the stimulated sample. The other method scans the local voltage distribution in the stimulation chamber. Both methods can be used to validate numerical simulations and permit to estimate the prevailing local electric field and current density. Frequency-dependent electrochemical effects occur at stimulation electrodes in direct contact with the sample [19,22]. We compare two methods that are frequently used to integrate electrochemical effects into numerical models. Moreover, we present how an initial calibration of the stimulation electrode over a wide frequency range can be used to detect electrochemical ageing. Finally, we discuss the general applicability of the suggested workflow to electrical stimulation in vitro and in vivo.

2. Materials and methods

2.1. Electrical stimulation device

The considered electrical stimulation device (see Fig. 1) is based on the clinically used ASNIS IIIs screw system, which is used among others for the treatment of avascular femoral head necrosis [23,24]. It consists of two titanium pieces separated by an insulator. It has been developed to work with standard 6-well plates [17]. An earlier version of the stimulation device had been used to study the effect of electrical stimulation on bone cells and bacteria but had required custom-built chambers [18]. Different waveforms, frequencies and stimulation voltages, currents or field strengths are of interest in electrical stimulation [13]. Both devices have been used exclusively with sine waves. Parameter combinations have been considered that are typically chosen for applications in bone or cartilage regeneration. Chondrocytes and mesenchymal stem cells have been stimulated with this device using 1 kHz sine waves [17] with voltages of a root mean square (RMS) value of 0.7 V. With the earlier version of the device, osteoblasts and bacteria have been exposed to 20 Hz sine waves with RMS values of 0.2 V to 2.8 V [18,25]. With other devices, a frequency of 60 kHz has been considered for the stimulation of chondrocytes [3,26] and bone cells [27]. In this case, the applied voltage had, for example, a fixed root mean square (RMS) value of less than 1 V [26] or was chosen such that an estimated field strength of 2 Vm ^{1} was achieved [3]. However, the field strength has, to the least of our knowledge, never been measured but has been estimated using analytical or numerical models. We would like to mention that varying the applied voltage to achieve a certain field strength is very similar to current-controlled stimulation. In current-controlled stimulation, the voltage is varied until a pre-set current is reached.

In Schematic 1, the general stimulation experiment and the corresponding model are shown. The electrode was connected to a signal generator (or the output of a power amplifier that stabilises the signal provided by the signal generator). An oscilloscope was used to record the stimulation input signal and the voltage drop across a shunt resistor R , which is used to estimate the current. Both the input signal and the current were measured with respect to a common ground (GND). Hence, the total impedance can be computed from the amplitudes and phase shift of the signals. An equivalent circuit model can be employed to account for the interface impedance and integrate experimental data into numerical simulations [11]. When a reference electrode (depicted in blue and black in Schematic 1) was used, the local voltage in the cell culture medium was also recorded with the oscilloscope.

Moreover, a digital representation of the device geometry is shown in Schematic 1, which is required for numerical models. The 3D geometry was prepared using *SolidWorks*[1] and *SALOME*[2]. The electrode can be placed in two configurations in the culture well: the 'high configuration corresponds to a spacing of 3 mm between the well bottom and the electrode, and the 'low configuration to a spacing of 1 mm between the well bottom and the electrode. We prepared a computer model for both geometries.

Due to capillary forces, there was a meniscus of the cell culture medium visible (i.e., the medium is more elevated close to the wall of the well) [28]. However, due to the electrode holder and also the electrode placement, it appeared to be impossible to estimate the shape of the meniscus reliably for all volumes used in actual in vitro experiments. For a low volume of 5 mL, which has been used for in vitro experiments, the medium barely covered the electrode and did not cover the electrode holder. Microscope images of the electrode immersed in liquid did not help to create a better geometry model. Hence, the cell culture medium was modelled as a cylinder. Only for volumes greater than 10 mL, which covered the entire electrode and the holder, the meniscus was modelled. Then, the parameters c 2 0 and h_0 2 0 for the meniscus model of Schuderer and Kuster [28] were used. The height of the medium in the centre of the well was measured manually (and later also using a 3D printer, see Section 2.3.4). For 10 mL, it was about 11 mm to 12 mm. A volume of about 7 mL marks a special case as the height of the medium is then approximately equal to the height of the electrode holders. The final geometry for the individual models was prepared using the *OCCT*[3] kernel in *NGSolve* for computer-aided design (CAD) modelling.

2.2. Modelling approach

2.2.1. Lumped-element model

The entire stimulation device can be described by an equivalent circuit comprising lumped elements (see also Fig. 1). The elements correspond to the properties of the individual parts of the system. The model can be reduced to three elements.

1. the impedance of external circuitry, which is usually known a priori. This includes also a shunt resistor, which can be used to measure the current or to limit the current.
2. the impedance of the cell culture medium or, more general, the sample to be stimulated. This impedance will be discussed in the next section.
3. the impedance of the electrode electrolyte interface (EEI).

[1] https://www.solidworks.com/
[2] https://www.salome-platform.org/
[3] https://www.opencascade.com/open-cascade-technology/

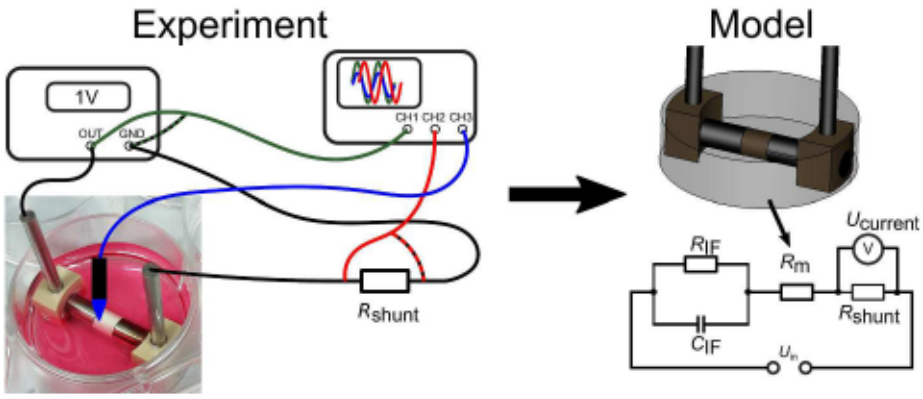

Schematic 1. A schematic of the experimental and numerical approach is shown. The electrode (two titanium bars separated by a polyether ether ketone (PEEK) insulator and supported by PEEK electrode holders) was placed in a cell culture well filled with cell culture medium. A geometrical model of the entire stimulation setup was prepared and used to compute the electric field in and the resistance of the cell culture medium R_m. For the field computation, the model was integrated into an equivalent circuit model (see also [11]).

The EEI can be understood as a thin ionic double layer. Upon electrical stimulation (the application of an external voltage signal), capacitive charging of the double layer and charge transfer through the double layer occur at the interface [29]. The charge transfer is due to faradaic processes, i.e. oxidation/reduction reactions and can be described by a charge transfer resistance (e.g., R_{IF} in Fig. 1). The capacitive charging manifests itself in a phase shift of the current with respect to the input voltage.

There exist methods to account for the electrode–electrolyte interface in numerical models [11,21,22]. The EEI impedance is then described by either a lumped or distributed element. Its value is derived from experimental data (e.g., from [29]) and rescaled according to the size of the actual electrode [21,22]. Thus, they are only valid for the electrode, temperature and voltage range considered in the original experiment.

2.2.2. Finite element model

For low frequencies (i.e, DC to MHz range), the electromagnetic fields due to the applied electrical stimulation can be regarded as slowly varying. This means that the magnetic field can be neglected and an estimate of the electric field can be obtained from the electroquasistatic field equation [20]. When time-harmonic fields are used, all electric properties can be described by phasors (i.e., they are complex-valued with characteristic amplitude and phase at the given frequency). The electroquasistatic field equation reads

$$\nabla\cdot(\sigma^*\nabla\Phi) = 0, \mathbf{E} = -\nabla\Phi. \tag{1}$$

Here, Φ is the electric potential, $\mathbf{E}$ the electric field and σ^* is the complex conductivity. The complex conductivity is computed from the dielectric properties, which are the real conductivity σ and permittivity ϵ, as $\sigma^* = \sigma + j\omega\epsilon$. The dielectric properties used in this work are summarised in Table 1.

Hence, it is required to know the dielectric properties of all components to build a meaningful simulation model. Moreover, the applied voltage amplitude U is set as a boundary condition. For that, one electrode is assigned 0 V (i.e., ground potential) and the other electrode is assigned the non-zero input voltage U_{in}. Because Eq. (1) is linear, a fixed voltage of 1 V is usually applied unless otherwise stated. If any other voltage is applied in the experiment or the ground level is not 0 V, the numerical solution can be scaled and shifted to match the experimental reality.

Under certain conditions, a reduced model can be used. When the conductivity σ is much greater than the capacitive term $\omega\epsilon_0\epsilon_r$, a capacitive behaviour of the cell culture medium is not to be expected. Thus, only the cell culture medium has to be considered. Because we then have only one domain (cell culture medium), the numerical solutions for the potential and electric field are independent of the conductivity and it suffices to solve Laplace's equation. This means that $\Delta\Phi = 0$ is solved instead of Eq. (1). From a physics point of view, the reduced model assumes that there occur no dielectric losses in the wall of the Petri dish, the polyether ether ketone (PEEK) insulator between the two metal electrodes or the air above the cell culture medium. This assumption implies that there is no significant current flow through these structures.

As the electrode is in direct contact with an insulator, electric field enhancement is expected at this point. Thus, we employed a Zienkiewicz-Zhu error estimator for adaptive mesh refinement [30]. All computations were performed using the finite element method (FEM) library *NGSolve* [31] with *NETGEN* as the mesher [32]. Unless otherwise stated, the FEM systems of equations were solved using a conjugate gradient (CG) solver with a balanced-domain decomposition (BDDC) preconditioner combined with an algebraic multigrid (AMG) preconditioner. More details on the modelling approach can also be found in [11].

Even though the conductivity does not need to be known to obtain the numerical solution of Laplace's equation, it has to be known to estimate the current through the medium (and thus the resistance of the medium) and the current density. In the electroquasistatic regime, the current density equals the complex conductivity times the electric field, which can be computed according to Eq. (1).

The EEI impedance can be included in the FEM model by a Robin boundary condition [22]. Then, the EEI impedance is assumed to be equally distributed on the electrode surface. The specific impedance of the electrode surface is $z_s = ZA$, where Z is the (lumped) EEI impedance and A is the electrode surface area. The Robin boundary condition takes the normal component of the current density J_n

$$-J_n = \frac{1}{z_s}(\Phi - U). \tag{2}$$

Here, U is the stimulation voltage, which is usually imposed, and Φ the unknown potential to be computed. The impedance can in principle be distributed on both electrodes. We considered two options: (1) an asymmetric distribution with the impedance distributed only on the high-side electrode and (2) a symmetric distribution where both the electrodes were assigned half of the impedance. An example of this choice can also be found in [11].

Table 1
Assumptions for the dielectric properties of the different materials considered in this work. The conductivity of the KCl solution was changed depending on the temperature as specified by the manufacturer.

Domain	Conductivity/ Sm^{-1}	Permittivity
DMEM at 37°C	1.84	80
KCl at room temperature	1.22	80
Plastic	10^{-14}	2
Air	10^{-14}	1

2.2.3. Integrating a reference electrode

When using a reference electrode to measure the local voltage, this electrode should also be included in the model. The reference electrode also has a finite surface impedance and is polarised in the external field [33]. Moreover, the input impedance of the recording device (in our case an oscilloscope) should be much greater than the sample impedance to avoid current flow. The treatment of measuring electrodes in an external field is of great relevance in the field of electrical impedance tomography. Somersalo et al. [34] have shown that experimental data is best matched if the electrode is assigned a boundary condition as described in Eq. (2). The only difference to the aforementioned boundary condition is that the fixed value of the voltage on the electrode is not known a priori but treated as an additional unknown. This value corresponds to the expected measurement value. In the case of a vanishing surface impedance, the floating potential problem has to be solved. Mathematical details of this approach can, for example, be found in [35].

To gain an understanding of the system with a measurement electrode, an approximate model of a cannula (a needle) was used. It had been considered as it is available in every medical laboratory and is easy to handle. The geometry is standardised. For a typical cannula type 21G, the diameter is 0.8 mm and it has a sharp tip. To avoid numerical artefacts, we modelled the cannula by a cylinder of matching diameter with a semi-sphere of the same diameter as the measurement tip. Then, different configurations of the cannula-like probe were considered: straight, tilted in one direction (tilted #1) and tilted in two directions (tilted #2) as well as a mirror of this configuration (tilted #3, see Schematic 2).

In a second step, the shaft of the probe was insulated and only the tip was left floating. Subsequently, a thinner probe with a diameter of 200 m was considered. All these simulations were performed for a medium height of 5 mL. The measurement points were chosen along a line in x-direction at the bottom of the well (0.5 mm distance between the tip and the bottom, see Schematic 2). This setup aimed at resembling the manual measurement of local voltages during a cell culture experiment.

The floating part of the electrode was also modelled using a surface impedance. As the exact value of the surface impedance is not known, we chose two numerical values that represent an intermediate (10^3 mm^2) and a large surface (10^6 mm^2) impedance.

The arising linear system was solved using the direct solver *MUMPS* [36] available in *NGSolve* and the *FieldSplit* block preconditioner [37] together with the flexible GMRES solver, both implemented in *PETSc* [38 40] and available in *NGSolve* through the *ngs-petsc* interface[4]. When considering the surface impedance, CG with an AMG preconditioner was used as an iterative solver.

2.3. Experimental approach

To characterise the device, an electrolyte solution with known properties is used. We used KCl solution of known conductivity (Hanna Inst.) at ambient conditions (22 to 25 C). To predict the in vitro behaviour, cell culture medium (DMEM, without calcium, containing 10% fetal calf serum (PAN-Biotech, Aidenbach, Germany), 1% amphotericin B, 1% penicillin streptomycin, and 1% HEPES buffer (Sigma-Aldrich, Munich, Germany)) was used at a temperature of 37 C. The cell culture medium has a conductivity of about 1.84 Sm ^{1} at 37 C (measured with a handheld conductivity meter, LF 325-A, Wissenschaftlich Technische Werkstatten, Weilheim, Germany). Different volumes according to the experimental specifications were used and will be stated in the following.

2.3.1. Electrochemical impedance spectroscopy

Electrochemical Impedance Spectroscopy (EIS) was performed with the Gamry Reference 600 potentiostat. The impedance was measured over a broad frequency range using small voltage amplitudes (25 mV and 50 mV). As the Gamry potentiostat is relatively expensive, we also used field-programmable gate array (FPGA) based frequency response analysers (Moku:Go and RTB2004 with frequency response analyser R&S(C) RTB-K36, Rohde&Schwarz, Munich, Germany), which are more affordable. The measured impedance spectra were fitted against lumped-element models using the open-source package *ImpedanceFitter* [41].

2.3.2. Current and voltage measurements

The current was recorded by measuring the voltage drop across a shunt resistor (1 or 10 , see also Fig. 1) with an Rigol MSO5104 oscilloscope. The other channels of the oscilloscope were used to record the applied voltage and the voltage of the reference electrode. The voltage was supplied by a frequency generator (Metrix GX310, Chauvin Arnoux, Annecy, France). As the frequency generator has a limited power output, we used a linear amplifier (F30PV, FLC, Gothenburg, Sweden) with a gain of 10. The voltage drop across the shunt and the voltage of the reference electrode were also amplified if necessary (with F10A, FLC, Gothenburg, Sweden with a gain of 10 or an Agilent 33502a, Santa Clara, CA, USA with a gain of 5). Importantly, the amplifiers have a high bandwidth that permits to measure signals up to at least 60 kHz.

2.3.3. Local voltage measurements

To measure the local voltage, a measurement electrode is inserted in the cell culture medium. We performed preliminary measurements of the voltage inside KCl solution using a manually positioned cannula (hollow needle) with and without an insulated shaft. For the final measurements, a 3D printer (MP Select Mini Pro, Monoprice, Berlin, Germany) was modified such that a small measurement probe could be moved along defined grid points. We used a customised unipolar microelectrode with a diameter of 370 m and a few m of the metal tip uninsulated (PI2PT33.0B10, Microprobes, Gaithersburg, MD, USA) and a Ag/AgCl wire of diameter 200 m with only the tip uninsulated.

The measurement probe was manually positioned in the holder such that the bottom of the well corresponded to the zero level of the tip. This position served as the calibration point, where z 0 . It is required to perform a calibration for each positioning device to be able to replicate the experiments. We give a more detailed description of the modified 3D printer, measurement electrodes and calibration procedure in the Supplementary Material (Figs. S1 and S2). Throughout the measurements with the reference electrode we recorded the input voltage and current to ensure stable conditions and detect possible variations due to the electrode or temperature changes. The exact data acquisition and data analysis will be described in the following.

2.3.4. Data acquisition and analysis workflow

The goal of the presented approach is to validate numerical simulations. Thus, experimental and numerical data should be compared in a well-defined and automated fashion. For that, we developed the following workflow to automate data acquisition and analysis:

1. Measure the height of the medium in the centre of the well. Switch on the stimulation voltage and move down the electrode until a sinusoidal signal with the stimulation frequency appears on the oscilloscope screen.
2. Prepare the geometry model. Load the standard electrode geometry and add a cylinder with the radius of the well and the measured height. Reshape the cylinder to account for the meniscus using the model of Schuderer and Kuster [28].
3. Compute the expected current or impedance and estimate the voltage drop across the shunt resistor. Choose the dimensions of the shunt resistor such that the voltage drop is within the measurement range of the oscilloscope.
4. Choose the measurement grid along which the measurement probe should be moved.

[4] https://github.com/NGSolve/ngs-petsc

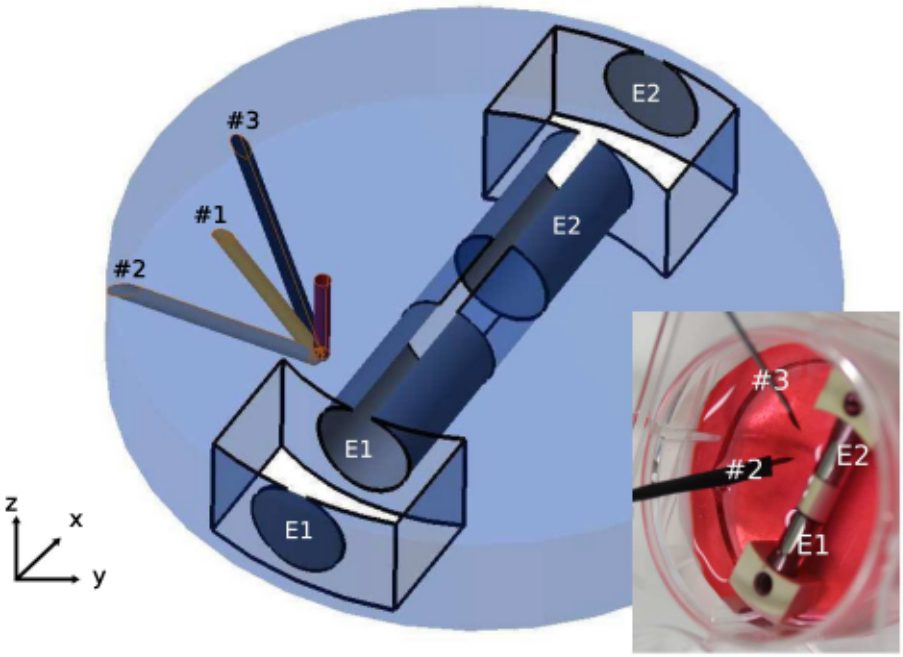

Schematic 2. Positioning of the measurement probe in the cell culture medium (blue, transparent). The surfaces E1 and E2 belonging to the active electrodes are shown in grey. Four configurations of the measurement electrode were considered: a straight probe (named straight, brown), tilted in one direction (named tilted #1, golden), tilted in two directions (named tilted #2, light grey) and a mirror of tilted #2 (named tilted #3, dark grey). The measurement probe was moved along the x-axis at fixed y- and z-positions. For comparison, a photograph with two cannulae placed roughly at postions #2 and #3 is shown. To make the comparison between the model and reality easier, the photograph was rotated.

5. Apply the stimulation voltage and scan the voltage distribution inside the medium. The measurement result at each point is written to a YAML-file. *Python* scripts for synchronising the 3D printer movements and the oscilloscope readings can be found on *GitHub*[5].
6. Use automated *Python* scripts to extract the input amplitude, current and measured voltage from fits to sine functions.
7. The expected voltage is computed from the benchmark simulation results by shifting and scaling. To account for the shunt resistor, a voltage divider equation is used to compute the effective voltage drop across the chamber. For that, the absolute value of the impedance of the entire system Z is computed by dividing the voltage amplitude by the current. Then, the voltage at the low side of the chamber is computed by $U_{\mathrm{low}} = U_{\mathrm{in}}\frac{R_{\mathrm{shunt}}}{Z}$. The benchmark simulation result is scaled by the voltage drop across the chamber $U_{\mathrm{in}} - U_{\mathrm{low}}$ and shifted by adding U_{low}.
8. The expected voltage is evaluated at the measurement points. Both expected and measured voltage are interpolated on a triangulation of the grid using *Matplotlib* [42] and their interpolated values are compared (e.g., by computing and visualising the absolute and relative difference).

If the comparison of the expected and measured voltage reveals a difference, more detailed analysis is required, which we will discuss in the Results section.

3. Results

3.1. Numerical modelling

The numerical modelling can be subdivided into two parts: the initial modelling to determine physically crucial parts of the experiment and to reduce the complexity of the model and the subsequent productive modelling process ideally using measured data.

[5] https://github.com/j-zimmermann/PyVISAScope/tree/master/examples/3DPrinter

3.1.1. Initial numerical analysis—gaining insight into the experiment

The first step of the numerical analysis is to formulate hypotheses. To estimate, if the full electroquasistatics field Eq. (1) has to be solved, the upper frequency limit of the impedance analysis, 5 MHz, was considered. Particularly, it is of interest if the insulating PEEK piece separating the metal pieces of the electrode acts similar to a dielectric in a capacitor and influences the expected impedance.

The analysis was performed for the high and low electrode configurations with 5 mL, 7 mL and 10 mL of medium. When using 5 mL, a spherical domain representing air was added. With this, it was accounted for the fact that the electrode was not fully covered by medium. The full model for the low configuration after adaptive mesh refinement had 2,764,910 degrees of freedom. The computed impedance had a magnitude of 56.258 Ω and a phase of 0.013°. The reduced model had 532,348 degrees of freedom and the computed resistance was 56.259 Ω. For the high configuration, similar results could be obtained. The full model yielded an impedance magnitude of 65.637 Ω with a phase of 0.013° having 2,913,918 degrees of freedom, while the reduced model yielded an impedance magnitude of 65.646 Ω with a phase of 0.013° having 432,204 degrees of freedom. Evidently, the system behaves mainly as a resistor and is fully characterised by its resistance. A similar result was obtained for the other volumes. For a volume of 7 mL, both the low and the high configuration yielded a resistance of 38.57 Ω. This was to be expected as both configurations are geometrically equal if the meniscus is neglected. For a volume of 10 mL, the low configuration yielded a resistance of 33.35 Ω. Using the same volume but the high configuration yielded a resistance of 31.7 Ω, i.e. about 5% less than for the low configuration. To put it in a nutshell, the electric field in the cell culture medium can be modelled using Laplace's equation instead of the full electroquasistatics equation. Hence, the number of degrees of freedom can be reduced significantly compared to the full electroquasistatic model. Moreover, the fast and reliable preconditioned CG solver can be used.

The electric field distribution for a volume of 10 mL is shown for representative cut planes in Fig. 1. The electric field is highest in the area below the insulator, which separates the electrodes, and can reach values up about 150 Vm^{-1}. For the low configuration, electric field strengths of similar order can be reached at the bottom of the well, where usually the cells are located. In contrast, the field is only about

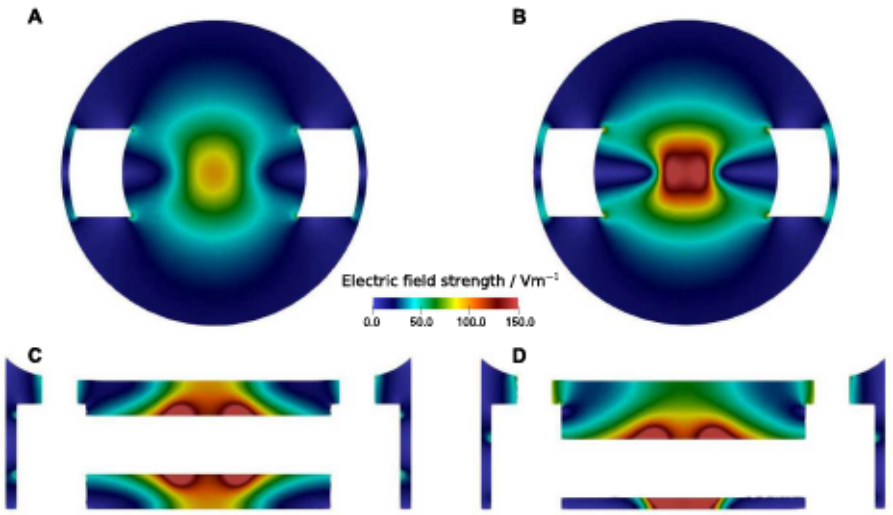

Fig. 1. The electric field strength is compared at the bottom plane of the well for high (**A**) and low (**B**) configuration with a volume of 10 mL. Furthermore, the field is shown on the center plane for high (**C**) and low (**D**) configuration. In **C** and **D**, the electrode is cut out to support the identification of the center plane from Fig. 1.

100 Vm^{-1} at the bottom in the high configuration. Please note that the values for the electric field were computed for a voltage drop across the well of 1 V. This should not be mistaken with the applied voltage amplitude of 1 V. The applied voltage in the experiment may be divided due to the different elements in the circuit (e.g., the shunt resistor) so that the voltage drop across the well is not equal to the applied voltage amplitude. Then, the voltage drop across the well has to be adjusted in the simulations. In this case, the electric field can be scaled linearly with regard to the adjusted voltage drop. The electric field below the electrode did not significantly depend on the volume, which is in line with the results of our previous work [11].

In addition, the resistance of the cell culture medium can be easily scaled according to the medium conductivity without re-running the simulations (see detailed explanation in [11]). For EIS measurements, this result means that a real-valued impedance is predicted. As it can be expected that an EEI impedance will also be present for this electrode, a real-valued impedance is to be expected at frequencies greater than the cutoff frequency. A definition of the cutoff frequency can be, for example, found in [19]. The cutoff frequency can be understood as the frequency from which the EEI impedance is not dominant anymore. Instead, the impedance of the sample begins to dominate from this frequency on. The cutoff frequency is to be determined by EIS. Moreover, there should not be a significant difference between the high and low configurations if a volume of 10 mL is used. For smaller volumes, e. g. 5 mL, a notable difference should be measured. However, it must be mentioned that the impedance of the configurations with a small volume strongly depends on the height of the medium. As mentioned before, it was not possible to accurately measure the height of the medium and thus no automated uncertainty quantification analysis to quantify the variation of the impedance was performed. An example of uncertainty quantification analysis for an electrical stimulation device can be found in [11].

3.1.2. *Productive simulations—interacting with the experiment*

The productive simulation runs should take into account the experimental reality. As only Laplace's equation has to be solved, no complex numbers have to be considered and the simulations will be performed only for the absolute values of, for example, the current. Potential phase shifts will be neglected. In reality, they correspond to a time shift of the applied sinusoidal signals, which should have no effect on the biological response as they are small compared to the total stimulation time. *Python* scripts were prepared to take into account the applied voltage, shunt resistor and conductivity of the medium. Moreover, scripts were prepared to consider the EEI impedance in the FEM model by the lumped- and distributed-element approaches (compare Section 2.2.2).

In a last step, the local voltage measurements should be prepared. For that, the measurement electrode was integrated as described in Section 2.2.3. The simulations revealed that the positioning of the measurement electrode is the most crucial parameter if the shaft of the measurement probe is not insulated (Fig. 2). If the probe is not kept straight, the measured value can deviate significantly (i.e., up to about 50%) from the expected benchmark value. This means that the numerical simulations could not be validated correctly using this approach. However, when the probe was kept straight, the relative deviation between benchmark and measured value were below 1.2% at all measurement points. In our preliminary experiments, we observed exactly this behaviour: if the cannula was not kept straight, the measurement value changed.

Based on the simulation results, it can be expected to detect the deviation introduced by the measurement probe. Introducing a fully uninsulated metal probe in the system leads to a change in the total current under the assumption that there is no surface impedance on the electrode (Fig. 3). As this change is position-dependent for configurations that lead to a perturbed measurement result, recording the current during experiment can help to detect this unwanted influence of the measurement probe. Unfortunately, the change did not exceed 1.6%, which suggests a high-resolution current measurement to be required for successful detection. Nevertheless, the straight configuration led to a small change in the current of not more than 0.2%, which is most likely not detectable in a real experiment. If a surface impedance was considered, the current did not deviate significantly (Fig. 3).

These first results could be improved by insulating the shaft of the electrode, which led to a deviation of less than 1.5% for all configurations. The accuracy could be further improved by reducing the diameter of the electrode.

In sum, the measurement probe should be widely insulated and only the tip should be left uninsulated to sense the local voltage. Then, the positioning of the electrode has a negligible influence and instead of running multiple simulations for the different probe locations, the expected measurement value can be extracted from the benchmark simulation. Nevertheless, a straight positioning is expected to yield the most accurate measurement results. The surface impedance of the measurement probe is in general unknown but did not appear to influence the expected measurement value. Thus, it does not have to be determined a priori for the chosen probe geometry.

The validation of the simulation results shown in Fig. 1 requires

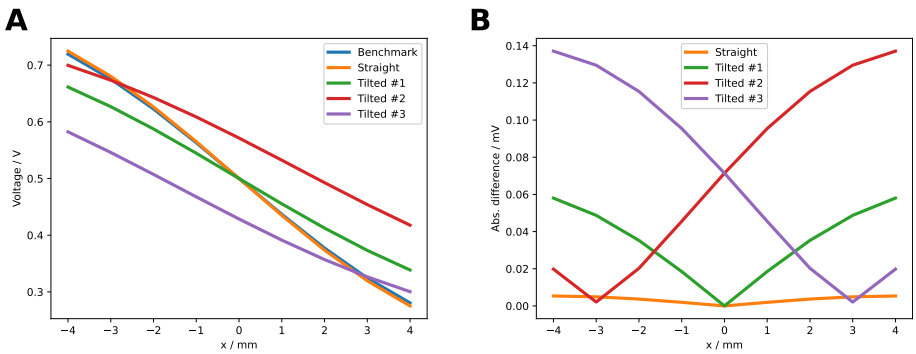

Fig. 2. Comparison of the benchmark values derived from a simulation without inserted measurement probe and simulation results for different configurations of a floating measurement probe. In **A**, the measured voltage extracted from the simulations is compared. In **B**, the deviation between measured and expected benchmark values is shown. For more details regarding the naming, please see Schematic 2.

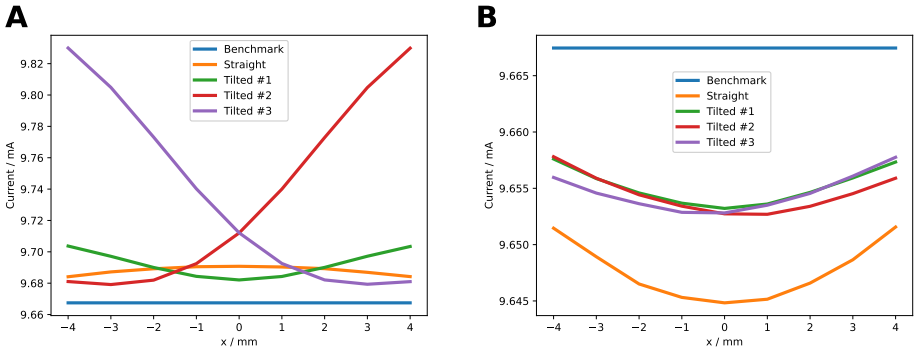

Fig. 3. Comparison of the computed current through a well with and without measurement probe. Different configurations of a floating measurement probe were studied. For more details regarding the naming, please see Schematic 2. In **A**, a perfectly conducting probe without a surface impedance was considered, while in **B** a surface impedance of 10^3 mm^2 was considered. Note that the scales are different for the sake of better comparability between the benchmark and the results for different probe configurations.

scanning the local voltage at many points to successfully resolve the inhomogeneity of the field. The negative gradient of the recorded local voltage serves as an estimate of the electric field. As the area under the electrode is not easily accessible, a small probe shall be used to scan the area above the electrode using a volume of 10 mL. A grid was constructed using 330 points with a spacing of 1 mm in x- and y-direction at two planes 1 mm and 3 mm above the electrode. The electrode was moved to the grid points in straight configuration. As for the previous example (Schematic 2), the measurement probe could successfully reproduce the benchmark simulation without significant differences.

When modelling the probe configurations, the iterative solver failed for 4 out of the 330 configurations while the direct solver could always solve the problem. It is unclear why it happened only for these configurations. In future research, it is desirable to use a projection-based preconditioner such that the indefinite linear system can also be solved by conjugate gradient [43].

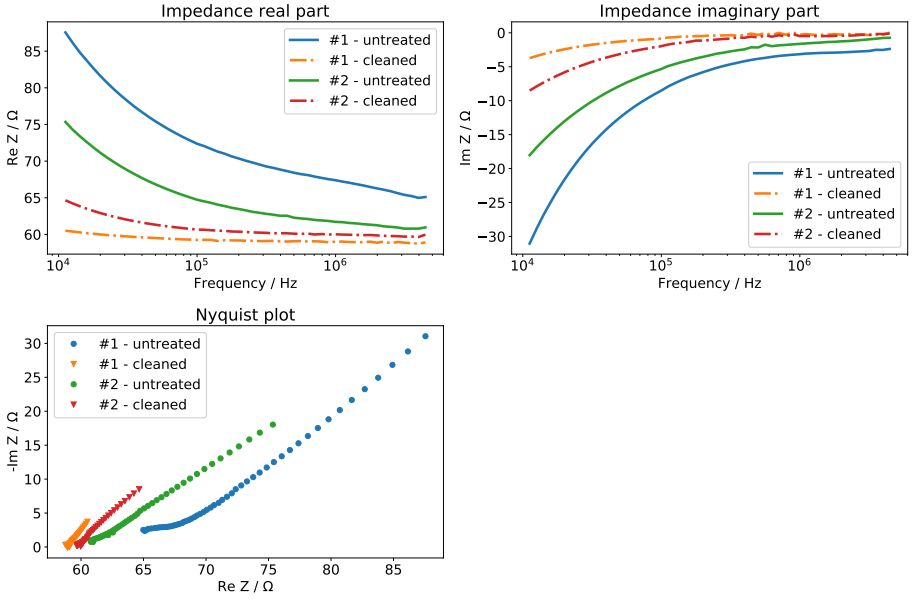

Fig. 4. Comparison of two electrodes before and after a cleaning treatment with 10% acetic acid for about 20 min. The impedance was measured for the low configuration using 7 mL KCl conductivity standard at 19 C with a conductivity of 1.143 Sm ^{1}. To highlight the high-frequency behaviour, the impedance is shown only for frequencies above 10 kHz. The electrodes were used in stimulation experiments before the treatment. Evidently, the untreated electrodes show capacitive behaviour, i.e. a non-zero imaginary part, up to very high frequencies. This stands in contrast with the simulation result that predicted purely resistive behaviour, i.e. an imaginary part tending to zero, at high frequencies. After the cleaning treatment, both electrodes show resistive behaviour at high frequencies. By fitting a constant-phase element in series with a resistor, the resistance at high frequencies could be determined. The resistance of electrode #1 was estimated to be 58.9 , while electrode #2 had a resistance of 59.7 . For the setup here, the simulations predicted 62.1 . This is in good agreement with the measured values (deviation not significantly greater than 5%) particularly given the fact that the meniscus was ignored.

3.2. Experimental results

3.2.1. Electrochemical impedance spectroscopy initial assessment

Initially, the goal was to validate the setup for the volume used in the in vitro experiments, 5 mL. During these investigations, a fresh electrode was compared to an electrode that had been in use multiple times. The impedance measurements revealed significant differences between the two electrodes (data not shown). The predicted purely resistive impedance was not observed at high frequencies. Instead, unexpected capacitive behaviour appeared with the multiply used electrodes in the MHz-range (Fig. 4). An elemental analysis of the electrode surface using energy-dispersive X-ray spectroscopy revealed that a layer of calcium and phosphorus covered the electrode surface. We speculated that a layer of calcium phosphate must have built on the titanium surface; most likely due to corrosive processes. It is known that titanium implants in aqueous environment corrode [44] and that calcium phosphate forms on titanium in electrolyte solution [45]. This process can potentially be enhanced by active electrical stimulation as titanium can be coated by calcium phosphate by electrochemical deposition [46]. However, the focus did not lie on the determination of the exact mechanism behind the corrosion. Instead, the removal of the calcium phosphate layer was paramount to regenerate the electrical properties of the electrode. For that, 10% acetic acid was employed successfully (Fig. 4). Hence, the experimental lab protocol could be successfully updated to ensure reproducible stimulation conditions. Most importantly, the corrosion of the electrode could not be easily identified by visual inspection as the calcium phosphate layer is probably only a few hundred nm thick. Instead of thinking of corrosion, we first assumed that the electrode surface was scratched. Evidently, the electrode corrosion could not have been detected without the numerical prediction.

3.2.2. Electrochemical impedance spectroscopy validation measurements

We measured the impedance of the two configurations using liquids of different conductivity (Table 2). The relative error between the predicted and fitted resistance was usually below 5%. This indicates a very good agreement between theory and experiment. The uncertainty of the numerical prediction due to the assumed conductivity can be estimated to about 2% (see detailed reasoning in [11]). Two different electrodes were compared using 7 mL (Fig. 4). The fitted resistance deviated by less than 1 . This deviation corresponds to a relative error of about 1 4%, which is close to the accuracy of the potentiostat (1%). Thus, the manufacturing uncertainty was assumed to be negligibly small. Furthermore, this result permits to define a reference state for performance assurance. Every manufactured electrode can be tested using the presented experimental approach. If, for example, the fitted resistance or measured impedance at high frequencies significantly deviates (e.g., more than 5%) from the expected value, the electrode should not be used for stimulation experiments until the reason for the deviation has been found and eliminated.

Aside of the manufacturing uncertainty the height of the cell culture medium can be expected to be the main source of uncertainty. Particularly at low volumes (5 mL and 7 mL) it cannot be extracted accurately and the meniscus was therefore not included. At a volume of 10 mL, we could estimate its height using an uncertainty of about 1 mm with a median height of 11 mm. Moreover, the meniscus was modelled. Changing the height from the assumed 11 mm to 12 mm, yielded a resistance of 31.67 , which deviates about 5% from the predicted value. Furthermore, it yields a value closer to the measured resistance of 31.92 . In sum, this rough estimate of the uncertainty of the numerical prediction demonstrates the agreement of measured and predicted values. Hence, the chosen geometrical model appeared to be valid.

Yet, the influence of the EEI has to be considered. In principle, it can be modelled by an equivalent circuit as, for example, done in the fitting of the resistance. However, the electrode has been used only for stimulation at a single frequency. Thus, no information on the frequency-dependent behaviour of the impedance can be extracted from the stimulation signal. Instead, only the impedance magnitude and phase at one frequency can be obtained from the stimulation voltage and resulting current signals. To extract the impedance of the EEI at this frequency, the cell culture medium resistance is subtracted from the measured impedance. By monitoring the impedance over time, electrochemical changes and temperature changes can be detected. However, unlike in the example in [11], the contributions from electrochemistry and temperature cannot be distinguished. For that, EIS measurements would have to be conducted regularly as, for example, done in [47]. An economic possibility to realise such a setup could be FPGA-based frequency response analysers. The two different frequency response analysers could reproduce the spectra recorded with the by-far more expensive potentiostat with reasonable accuracy. As both frequency response analysers can also just provide the stimulation signal, they might be a viable option for future integrated experimental solutions. Currently, efforts to automate the approach using easy-to-understand *Python* scripts are underway. In the following, we want to explore if the numerical simulations can be validated by local voltage measurements.

Table 2
Comparison of the fitted resistance from EIS measurements (see Fig. 4 for more details) and the resistance predicted by numerical simulations. To reduce the fitting error, the impedance was considered at frequencies greater than 1 kHz. In this range, a constant-phase element in series with a resistor yielded a relative difference of usually less than 2% between the fitted resistance and the measured impedance modulus (which at high frequencies is equal to the resistance). Different configurations were compared. The different conductivities are due to the different ambient temperatures.

Configuration	Conductivity / Sm ^{1}	Fitted resistance/	Predicted resistance/	Relative difference/ %
5 mL, low	1.84	55.20	56.26	1.9
5 mL, low	1.191	88.1	86.99	1.3
5 mL, high	1.264	91.29	95.56	4.5
7 mL, low	1.143	58.90	62.09	5.1
7 mL, low	1.143	59.70	62.09	3.9
10 mL, low	1.84	31.92	33.35	4.3

3.3. Local measurements

We chose three frequencies, which have both biological and electrical relevance, to study the voltage distribution in the well:

1. 20 Hz: This frequency has been considered for bone regeneration [18,21]. Similar frequencies are considered for other applications [14]. The impedance of the EEI is expected to be very large such that the electric field is much smaller than predicted from the raw simulations.
2. 1 kHz: This frequency has been considered for chondrocytes and mesenchymal stem cells [17], but frequencies in this range have also found application in, for example, neural stimulation [13]. Here, the EEI impedance is expected to have only a small influence.
3. 60 kHz: This frequency has been used for the stimulation of chondrocytes [26] and bone cells [27]. At this frequency, the EEI impedance becomes negligible and a good agreement between raw simulation and measurement is to be expected.

As expected, the measurement results at 60 kHz are in good agreement with the simulation results (Fig. 5). The relative difference is below 10% for most of the measurement points (Fig. 6). However, it is evident that the positioning by the 3D printer might not be sufficiently accurate as fluctuations are visible in the recorded values. Sometimes the positioning failed and shifts occurred in the recorded voltages. Currently, it is investigated how to make the experimental approach more robust.

The electric field can be estimated from the local voltage distribution (Fig. 7) by taking the gradient of the voltage. The general field

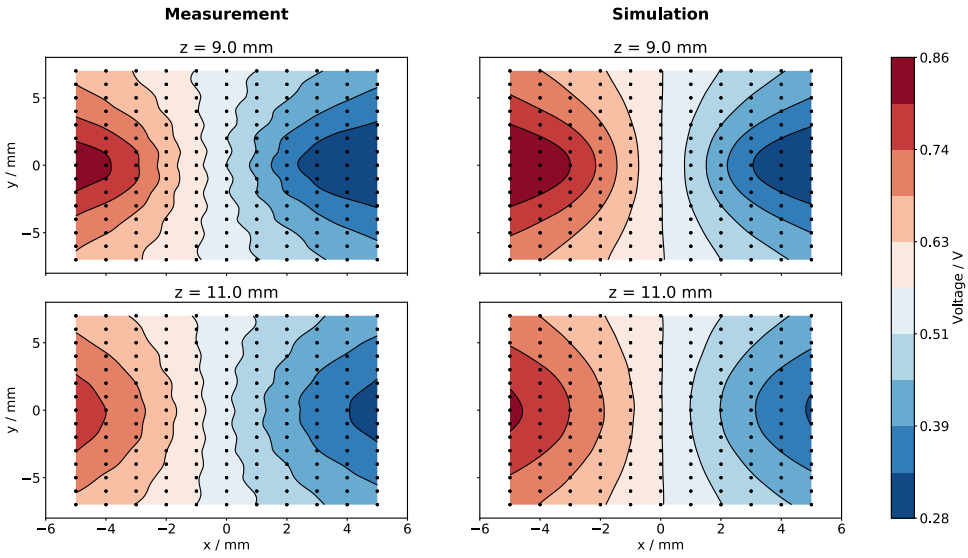

Fig. 5. Local voltage recording in cell culture medium at 60 kHz and 37 C for the high configuration and 1 V input voltage amplitude. The left side shows the measured values at two different heights relative to the well bottom, which corresponds to z 0 . The black dots indicate the measurement points. The measured values were interpolated to generate a heatmap. The right side shows the corresponding expected values, which were numerically computed. The relative difference between measured and expected values is shown in Fig. 6.

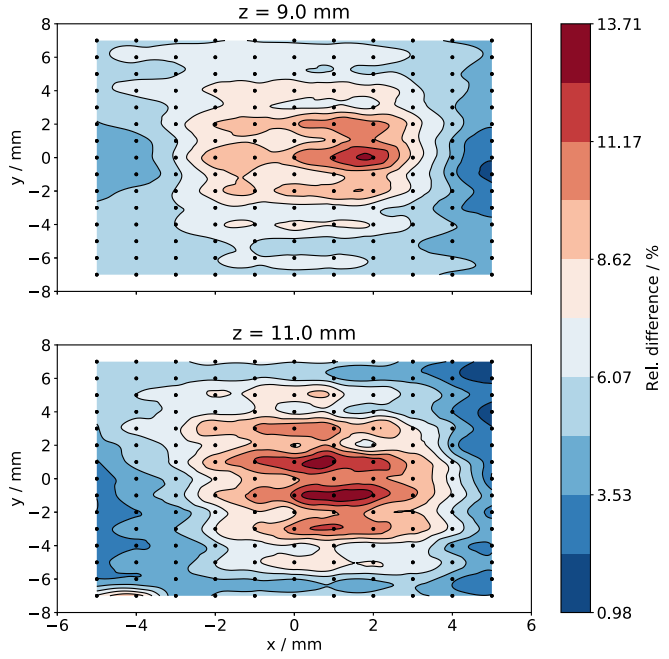

Fig. 6. The relative difference between measured and expected values at two different heights relative to the well bottom, which corresponds to z 0 . The measured and expected values are shown in Fig. 5. The measurements were performed in cell culture medium at 60 kHz and 37 C for the high configuration and 1 V input voltage amplitude. The corresponding absolute difference between measured and expected values is in the range of a few mV.

distribution is in agreement with the numerical predictions. Nevertheless, the uncertainty of the positioning propagates. Hence, the field distribution is, for example, not symmetric as predicted and fluctuates. Nevertheless, the expected and measured field strength agree well.

It takes about 30 min to scan the voltage distribution in the well. In contrast, global properties such as the current can be measured in a couple of seconds. At 60 kHz, the measured current has a phase shift of about 1 (1) with respect to the stimulation voltage and deviates less than 5% from the expected current. This result was expected and indicates that it is sufficient to record the current (both amplitude and phase shift) to validate the numerical simulations. Moreover, current recordings throughout a stimulation experiment can be used to monitor the status of the stimulation electrodes. Hence, for high frequencies such as 60 kHz, a digital twin was successfully established for the considered stimulation setup. This means that there is a clear relation between measurement data (in this case the electric current) and the numerical simulations. With that it becomes feasible to, for example, estimate the temperature of the electrolyte or identify electrochemical ageing. More details are described in [11].

In contrast, the results at 20 Hz and 1 kHz were less promising. At 20 Hz, the voltage drop across the medium was only a few mV, which is close to the measurement resolution. The measurement results at 20 Hz can be found in the Supplementary Material (Figs. S3 and S4). Due to the noise in the recordings and the limited measurement resolution, we will only show the results at 1 kHz for the high configuration and cell culture medium to demonstrate the general approach. At 1 kHz, the general shape of the recorded local voltage looks similar (Fig. 8) to the expected result (Fig. 5). However, the voltage drop across the medium is smaller than expected. Moreover, the measured current has a phase shift of about 22 and is also about 21 5% smaller than expected.

Instead of the expected impedance of about 31.1 , an impedance of about 42.6 was measured after subtracting the shunt resistor. This suggests that the EEI impedance is about 11.5 . With this information, the EEI can be taken into account. In the lumped-element approach, the benchmark result is scaled to match the voltage drop across the medium that is estimated using the EEI impedance. In the distributed-element approach, the EEI impedance is distributed across the electrode surface (see Section 2.2.2 for more details).

It must be noted that the computed current using the distributed-element approach deviates slightly from the measured value, which was used to calibrate the simulation model. Instead of the expected 17.87 mA, the computed current was 16.38 mA (symmetrically distributed impedance) and 16.85 mA (asymmetrically distributed impedance). A possible reason for these observations could be the assumption that the surface impedance z equals the global EEI impedance Z multiplied by the surface area A. However, the global impedance (if considered in) is in general related to the surface integral of the local impedance [48]

$$Z \quad \left(\int_S \overline{z \quad \mathbf{x}} \quad S \right) \tag{3}$$

where S is the electrode surface and z x the position-dependent local impedance. Evidently, the surface impedance z can be computed reliably from the global impedance Z only under the assumption that the surface impedance is not position-dependent. This assumption is not

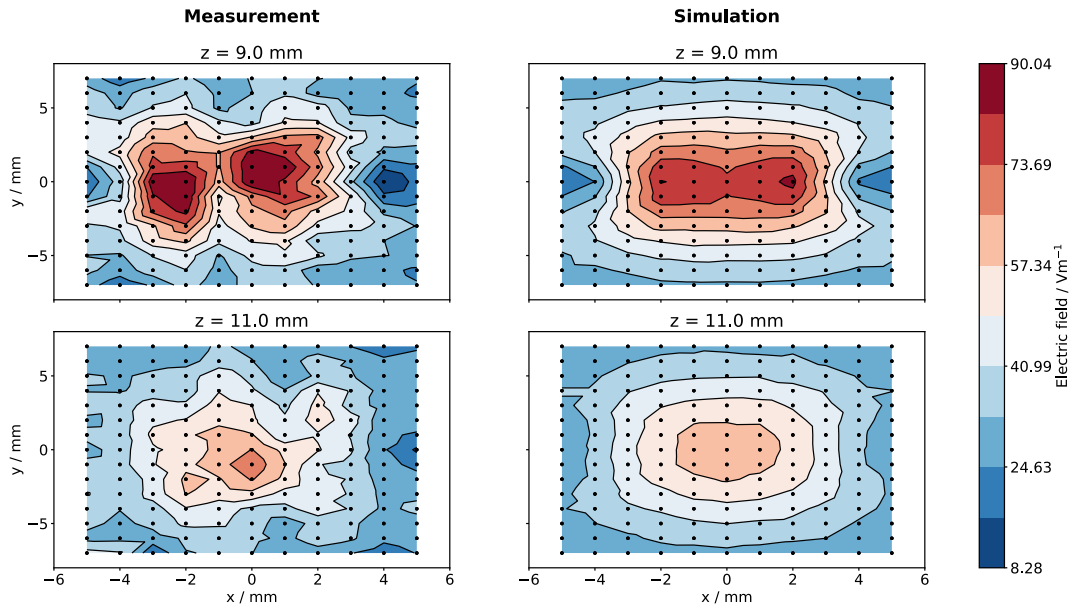

Fig. 7. The electric field strength was estimated from the voltages recorded in cell culture medium at 60 kHz and 37 C (shown in Fig. 5) by computing the gradient. Again, the measured values are shown on the left for two different heights relative to the well bottom, which corresponds to z 0 . On the right, the expected electric field is shown.

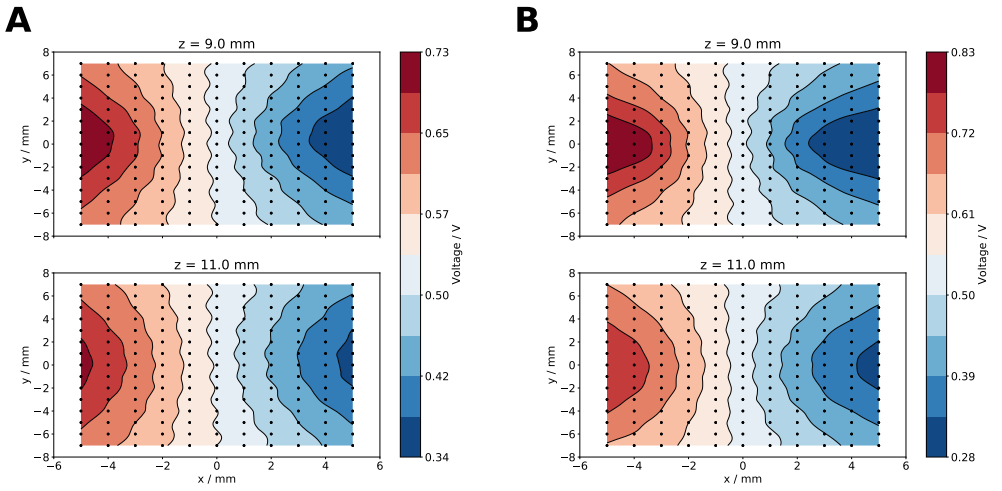

Fig. 8. Local voltage recording in cell culture medium at 1 kHz and 37 C for the high configuration and 1 V input voltage amplitude (**A**). The voltage was measured at two different heights relative to the well bottom, which corresponds to z 0 . For comparison, the voltage distribution at 60 kHz is shown in **B**. Please note the different voltage scales, which arise due to the EEI impedance present at 1 kHz. Moreover, the EEI impedance changes the shape of the voltage distribution. This evidences that the voltage-divider approach is not suitable to integrate the EEI impedance into the model. The voltage-divider approach would only lead to a scaled and shifted voltage but not to a different shape of the distribution.

justified in general. Indeed, we observed a position-dependent phase shift between the recorded local voltage and the stimulation voltage when the EEI impedance had a significant influence (Fig. 9). This result was also confirmed using a different reference electrode made of Ag/AgCl (not shown). At 60 kHz, where the EEI impedance has no significant effect, a position-dependent phase could not be observed (not shown). This result suggests that the choice of a fixed surface impedance is not perfectly reflecting reality. Nevertheless, the predicted and observed field distributions agree well. By visual inspection, the asymmetric distributed-element approach yielded the best agreement between measurement and simulation (Fig. 10). Still, the symmetric distributed-element approach did not deviate considerably. The lumped-element approach overestimated the field. Moreover, there was no constant ratio between the measured and the expected voltage (not shown). This result suggests that the lumped-element approach based on a voltage divider is not applicable as it would employ a linear scaling of the voltage drop across the medium. In comparison to the electric field strength predicted without the influence of the EEI, the maximal observed field strength is about 30% smaller.

4. Discussion

In this work, experimental and numerical methods to characterise electrical stimulation devices were presented. The goal was to establish reliable estimates of the prevailing electric field and thus also current density. Furthermore, a clear relation between numerical simulations and experimental approaches should be outlined. This is required to remove roadblocks on the way to clinical translation of electrical stimulation approaches [2,9]. Unfortunately, many studies cannot be replicated at the moment due to an insufficient amount of documentation [2,9,10,12,49] or yield different estimated field strengths than initially reported [11]. To overcome this limitation, we suggest a workflow that in our opinion suits the results of the presented methods (Fig. 11).

Initially, the geometry of the electrode, surrounding parts and biological sample(s) (here only the cell culture medium) have to be known precisely. For the considered electrode, the height and surface shape of the cell culture medium are expected to carry the largest uncertainty. Hence, they should be quantified with the best possible accuracy. The geometric dimensions are together with the dielectric properties at the

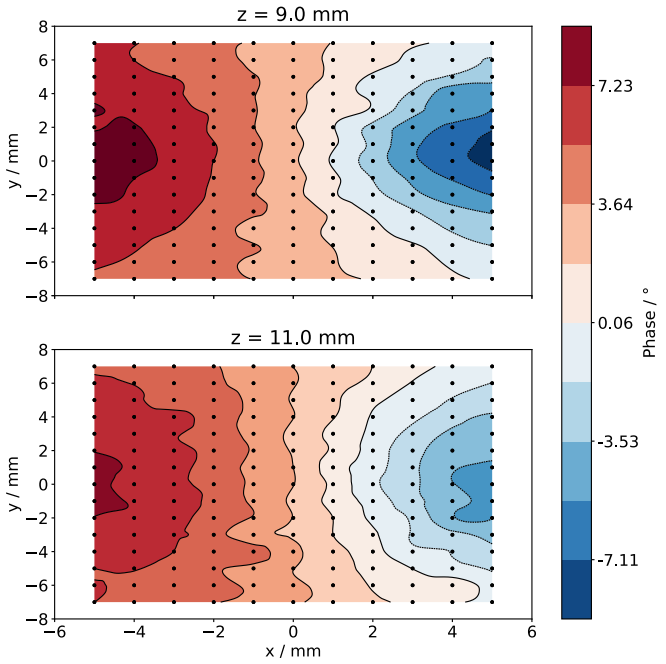

Fig. 9. Phase shift between the local voltage recorded in cell culture medium at 1 kHz and 37 C for the high configuration (shown in Fig. 8) and the applied input voltage of 1 V amplitude. The voltage was recorded at two different heights relative to the well bottom, which corresponds to z 0 .

desired stimulation frequency and temperature the key ingredient to developing the initial numerical model. The stimulation voltage does not necessarily have to be known as the models are initially linear. At this point, the first challenge of the approach arises with regard to a translation to an in vivo setting. The dielectric properties of tissue at relevant frequencies for regenerative medicine applications are not known unambiguously [50]. Moreover, the dielectric properties of many materials are to our knowledge not tabulated for a broader temperature range. Thus, it is recommended to always perform the initial characterisation with an electrolyte solution or phantom of known conductivity. Nevertheless, the workflow is supposed to work for in vivo settings once the input information is reliable.

Using the provided initial information, a detailed initial numerical model can be developed. The focus of this model should lie on the reduction of the complexity. Thus, parts that do not contribute to the measured impedance should be removed. For the device considered here, this applied to the insulators and the air. A simple measure to determine these parts is the current density: whenever it is much smaller than in other parts of the domain, these parts do not contribute to the total impedance of the device. With this information, it should be possible to reduce the initially complex-valued system of equations to a purely real-valued system. The real-valued system can be solved by the reliable preconditioned conjugate gradient method. In addition to the detailed model, lumped-element or circuit models should be developed. However, in contrast to the FEM-based models presented here and in [11], circuit models cannot resolve the spatial distribution of the electric field [51]. Detailed numerical simulations based on the real geometry drastically improve the understanding of the stimulation device.

From the initial numerical models, hypotheses are derived to be tested in validation experiments. The first method to be considered is EIS. It yields the cutoff frequency and also the device impedance, which is predicted by the initial model. In agreement with the results of Zimmermann et al. [11], the numerical models are only predictive at frequencies above the cutoff frequency. Once the numerical models are validated by EIS, they can be extended to include, for example, reference electrodes for local voltage measurements. We demonstrated that from the numerical simulations valuable information about the positioning and dimensions of the reference electrode can be obtained.

Furthermore, corrosive processes can be clearly identified by changes of the impedance and thus the cutoff frequency. The numerical models helped to unambiguously identify these processes. With this result, we extend the guideline of Boehler et al. [19] who in greater detail explain electrochemical characterisation methods of electrical stimulation electrodes. At frequencies below the cutoff frequency, the electrochemical effects have to be considered and integrated into the numerical model. While an electrode system previously studied by us has revealed no significant difference between the lumped- and distributed element approach [11], we identified significant differences between the approaches in this work. They were revealed by local voltage recordings, which agreed better with the distributed-element approach. However, the resolution of the experiments has to be improved to obtain a general best practice. The focus of this work was on practical and economic solutions, which are not suitable to measure

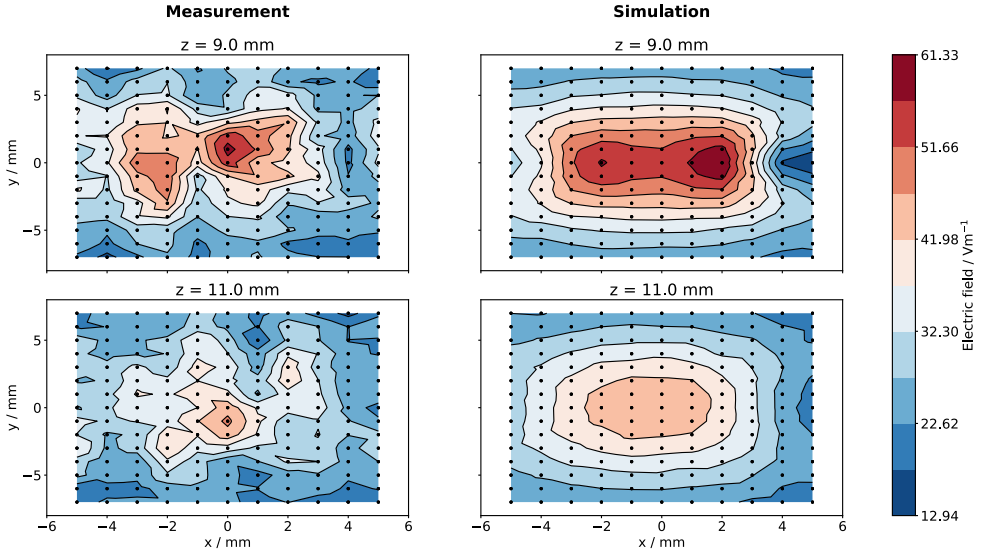

Fig. 10. The electric field strength was estimated from the voltage recorded in cell culture medium at 1 kHz and 37 C for the high configuration (shown in Fig. 8) by computing the gradient. The measured values are shown on the left for two different heights relative to the well bottom, which corresponds to z 0 . On the right, the expected electric field is shown computed using the asymmetric distributed-element approach.

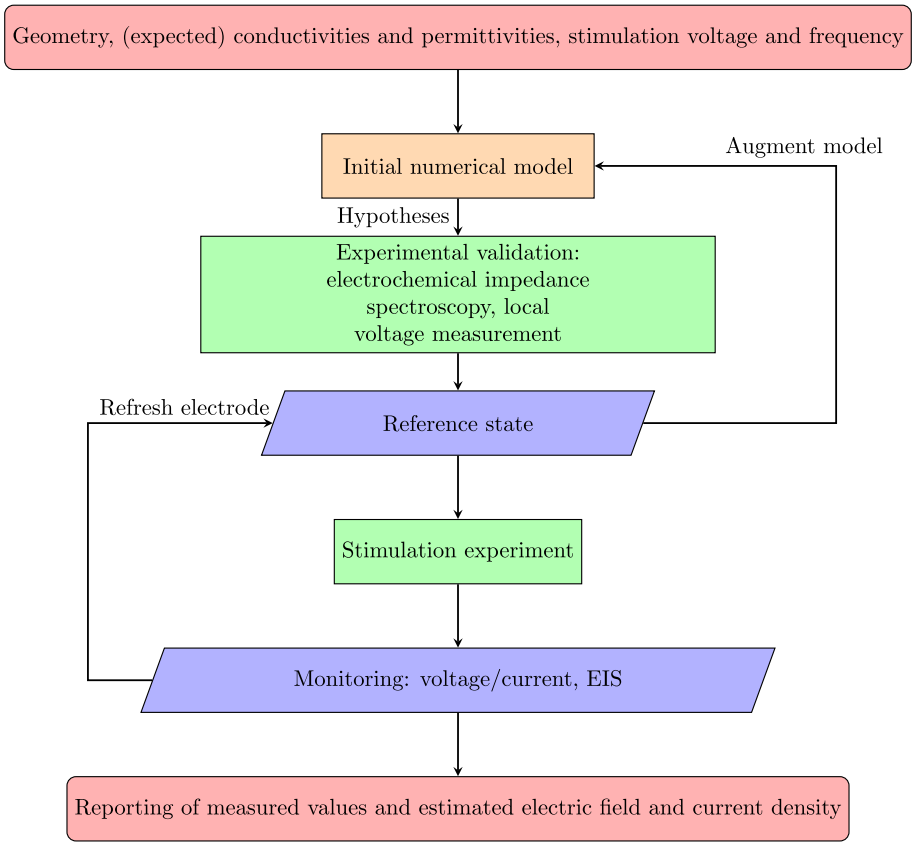

Fig. 11. Suggested workflow to obtain a controlled and monitored electrical stimulation experiment with reliable electric field and current density estimates.

electrochemical processes with the required accuracy. Still, it is, in our opinion, possible to use the presented setup to obtain reliable estimates of the electric field and current density. The simulations were calibrated using only the measured current, input voltage and conductivity of the medium. Nevertheless, the electric field predicted by the simulations using a distributed-element approach agreed well with the local voltage recordings (Fig. 10). A limitation of this approach is that the temperature of the medium and thus its conductivity have to be accurately known and that the geometry of the electrode must not change during the experiment. Thus, additional sensors should be used during a stimulation experiment. We speculate that the assumption of a fixed surface impedance is not realistic as we observed local phase shifts (Fig. 9). Probably, empirical nonlinear models that use a surface impedance depending on the overpotential could help to contribute [22]. However, such models require much more detailed knowledge of the surface electrochemistry and are thus possibly too detailed for a use in lab practice. Hence, we recommend to compare the lumped- and distributed-element approaches using measured values for each stimulation electrode. Attention should be paid to the predicted current in the distributed-element approach: if it deviates significantly from the measured current, it indicates that the model is not reliable. For the electrode specified in this work and at a frequency of 1 kHz, we observed a deviation of only about 5%, which is acceptable given the experimental accuracy. At lower frequencies, such as 20 Hz, the EEI impedance was about 10 times the impedance of the medium. Nevertheless, the computed current did not deviate more than a few percent from the measured current. This result is however only valid for the considered electrode geometry and cannot be generalised.

For meaningful local voltage recordings, it is paramount to choose the measurement points such that effective voltage differences in the measurement range of the used instrumentation can be expected. For example, the results in the centre of the well (at x 0 mm) are always about 0.5 V for the considered stimulation voltage of 1 V (compare Figs. 5 and 8) irrespective of the frequency and height of the measurement probe. This is mostly for geometrical reasons. If one measured only along this line at x 0 mm, one will find very good agreement between simulation and experiment. Nevertheless, this is not sufficient for validation as the measurement at different x-positions would reveal frequency-dependent deviations and also the current would not match the expectations for certain frequencies. Furthermore, the EEI impedance at 20 Hz was so large that the voltage drop across the medium became so small that it could not be well resolved with the used oscilloscope. Advanced instrumentation has to be considered for this case. For now, the field strength can only be estimated using the numerical approach estimated at 1 kHz. This result also poses a problem for the DC case. In previous research, we found that the resistance of the EEI of a Pt electrode is about a hundred times larger than the resistance of the medium [11]. Likewise, the voltage drop across the medium is small. Moreover, the resistance changes with time due to electrochemical reactions unlike in the AC application considered here. This problem must be addressed in future research. Ideally, electrochemically stable electrodes will be employed.

After the initial experimental and numerical characterisation, a reference state has been obtained. Whenever a stimulation experiment is performed, the monitored voltage and current or impedance can be compared to the reference state to identify changes in the stimulation device. In this work, we did not consider faradaic reactions during the stimulation [52]. They manifest themselves in nonlinear properties of the EEI in the low-frequency region (roughly below 1 kHz) [29,53,54]. In this range, the EEI impedance decreases with increasing voltage [29,54]. We expect this nonlinear behaviour to be identifiable by comparison to the reference state at the respective frequency. For a detailed investigation, a harmonic analysis of the nonlinear processes has to be conducted [29,54]. As faradaic reactions indicate corrosive processes, a

procedure to refresh the electrode such that it reaches the reference state again should be considered. Here, we cleaned the electrode for about 20 min with 10% acetic acid to remove possible calciumphosphate layers from the electrode surface. Ideally, a digital twin of the stimulation device can be designed to help identify various processes already during the stimulation experiment.

The presented workflow is deterministic in its nature because the electric field can be described by Maxwell s equations. No stochastic processes are expected to influence the physics. Hence, it is sufficient that we considered only a few electrodes with a few configurations. Nevertheless, it is desirable to obtain a better overview of the manufacturing accuracy. For that, every employed electrode should be characterised and its properties saved in a database. We are working on the realisation of this idea. Furthermore, the influence of surface roughness and other manufacturing-related aspects on the EEI impedance are to be investigated. This information can then be used to refine the accuracy estimates and possibly improve the digital twin.

5. Conclusion

The presented numerical and experimental methods contribute to an improved documentation of electrical stimulation experiments. We provide a software that automates the suggested workflow (Fig. 11) based on open-source software. All in all, a data set is generated that can be shared, for example, in the supplementary material of a publication. As the required hardware equipment is relatively affordable (in sum less than 5000 EUR if FPGA-based frequency response analysers are used), it should pose no problem to adapt the suggested workflow. The numerical simulations and data evaluations can be run on a standard PC or laptop with at least 12 GB memory. Hence, we expect the use of the presented methods to greatly contribute to a better understanding of the electrical stimulation experiments and help to overcome the limitations pointed out in various critical assessments [2,9 11,15,49].

Author contributions

JZ: Conceptualisation, Data curation, Formal Analysis, Investigation, Methodology, Software, Validation, Visualisation, Writing original draft. FS: Investigation, Methodology, Writing review & editing. NA: Investigation, Methodology, Writing review & editing. HB: Investigation, Methodology, Writing review & editing. ZS: Investigation, Writing review & editing. RB: Funding acquisition, Project administration, Resources, Supervision, Writing review & editing. AJH: Funding acquisition, Project administration, Resources, Supervision, Writing review & editing. UvR: Funding acquisition, Project administration, Resources, Supervision, Writing review & editing.

Declaration of Competing Interest

The authors declare that they have no known competing financial interests or personal relationships that could have appeared to influence the work reported in this paper.

Data availability

The datasets generated and analyzed for this study can be found online. The name of the repository and accession number can be found below: Zenodo (10.5281/zenodo.6937096).

Acknowledgment

This work was funded by the Deutsche Forschungsgemeinschaft (DFG, German Research Foundation) SFB 1270/1,2 299150580 and JO1483/1 1 384148830. We would like to thank Sylvia Speller s group, in particular Ingo Barke and Regina Lange, for providing the Gamry potentiostat and the amplifier. Moreover, we would like to thank Mario Jackszis and Ingo Barke for their support of the modification of the 3D printer. We also thank Regina Lange for performing the EDX measurements.

Appendix A. Supplementary material

Supplementary data associated with this article can be found, in the online version, at https://doi.org/10.1016/j.bioelechem.2023.108395.

References

[1] L.P. da Silva, S.C. Kundu, R.L. Reis, V.M. Correlo, Electric phenomenon: a disregarded tool in tissue engineering and regenerative medicine, Trends Biotechnol. 38 (1) (2020) 24 49, https://doi.org/10.1016/j.tibtech.2019.07.002.
[2] P.J. Nicksic, D.T. Donnelly, N. Verma, A.J. Setiz, A.J. Shoffstall, K.A. Ludwig, A. M. Dingle, S.O. Poore, Electrical stimulation of acute fractures: a narrative review of stimulation protocols and device specifications, Front. Bioeng. Biotechnol. 10 (2022) 879187, https://doi.org/10.3389/fbioe.2022.879187.
[3] J.J. Vaca-González, J.M. Guevara, M.A. Moncayo, H. Castro-Abril, Y. Hata, D. A. Garzón-Alvarado, Biophysical stimuli: a review of electrical and mechanical stimulation in hyaline cartilage, Cartilage 10 (2) (2019) 157 172, https://doi.org/10.1177/1947603517730637.
[4] J.K. Krauss, N. Lipsman, T. Aziz, A. Boutet, P. Brown, J.W. Chang, B. Davidson, W. M. Grill, M.I. Hariz, A. Horn, M. Schulder, A. Mammis, P.A. Tass, J. Volkmann, A. M. Lozano, Technology of deep brain stimulation: current status and future directions, Nat. Rev. Neurol. 17 (2) (2020) 75 87, https://doi.org/10.1038/s41582-020-00426-z.
[5] A.M. Lozano, N. Lipsman, H. Bergman, P. Brown, S. Chabardes, J.W. Chang, K. Matthews, C.C. McIntyre, T.E. Schlaepfer, M. Schulder, Y. Temel, J. Volkmann, J.K. Krauss, Deep brain stimulation: current challenges and future directions, Nat. Rev. Neurol. 15 (3) (2019) 148 160, https://doi.org/10.1038/s41582-018-0128-2.
[6] M. Griffin, A. Bayat, Electrical stimulation in bone healing: critical analysis by evaluating levels of evidence, Eplasty 11 (2011) e34.
[7] B. Schmidt-Rohlfing, J. Silny, K. Gavenis, N. Heussen, Elektromagnetische Felder, elektrischer Strom und Knochenheilung: Was ist gesichert? Z. Orthop. Unfall. 149 (3) (2011) 265 270, https://doi.org/10.1055/s-0030-1250518.
[8] S. Li, B. Yu, D. Zhou, C. He, Q. Zhuo, J.M. Hulme, Electromagnetic fields for treating osteoarthritis, Cochrane Database Syst. Rev. (12). doi:10.1002/14651858.CD003523.pub2.
[9] P.J. Nicksic, D.T. Donnelly, M. Hesse, S. Bedi, N. Verma, A.J. Seitz, A.J. Shoffstall, K.A. Ludwig, A.M. Dingle, S.O. Poore, Electronic Bone Growth Stimulators for Augmentation of Osteogenesis in In Vitro and In Vivo Models: A Narrative Review of Electrical Stimulation Mechanisms and Device Specifications, Front. Bioeng. Biotechnol. 10 (2022) 793945, https://doi.org/10.3389/fbioe.2022.793945.
[10] S. Guette-Marquet, C. Roques, A. Bergel, Theoretical analysis of the electrochemical systems used for the application of direct current/voltage stimuli on cell cultures, Bioelectrochemistry 139 (2021) 107737, https://doi.org/10.1016/j.bioelechem.2020.107737.
[11] J. Zimmermann, K. Budde, N. Arbeiter, F. Molina, A. Storch, A.M. Uhrmacher, U. van Rienen, Using a Digital Twin of an Electrical Stimulation Device to Monitor and Control the Electrical Stimulation of Cells in vitro, Front. Bioeng. Biotechnol. 9 (2021) 765516, https://doi.org/10.3389/fbioe.2021.765516.
[12] L.A. Portelli, K. Falldorf, G. Thuróczy, J. Cuppen, Retrospective estimation of the electric and magnetic field exposure conditions in in vitro experimental reports reveal considerable potential for uncertainty, Bioelectromagnetics 39 (3) (2018) 231 243, https://doi.org/10.1002/bem.22099.
[13] G. Thrivikraman, S.K. Boda, B. Basu, Unraveling the mechanistic effects of electric field stimulation towards directing stem cell fate and function: A tissue engineering perspective, Biomaterials 150 (2018) 60 86, https://doi.org/10.1016/j.biomaterials.2017.10.003.
[14] C.N.M. Ryan, M.N. Doulgkeroglou, D.I. Zeugolis, Electric field stimulation for tissue engineering applications, BMC Biomed. Eng. 3 (1) (2021) 1 9, https://doi.org/10.1186/s42490-020-00046-0.
[15] K. Budde, J. Zimmermann, E. Neuhaus, M. Schroder, A.M. Uhrmacher, U. van Rienen, Requirements for Documenting Electrical Cell Stimulation Experiments for Replicability and Numerical Modeling, in: in: 2019 41st Annual International Conference of the IEEE Engineering in Medicine and Biology Society (EMBC), 2019, pp. 1082 1088, https://doi.org/10.1109/embc.2019.8856863.
[16] R. Gundersen, B. Greenebaum, Low-voltage ELF electric field measurements in ionic media, Bioelectromagnetics 6 (2) (1985) 157 168, https://doi.org/10.1002/bem.2250060207.
[17] B. Hiemer, M. Krogull, T. Bender, J. Ziebart, S. Krueger, R. Bader, A. Jonitz-Heincke, Effect of electric stimulation on human chondrocytes and mesenchymal stem cells under normoxia and hypoxia, Mol. Med. Rep. 18 (2018) 2133 2141, https://doi.org/10.3892/mmr.2018.9174.
[18] T.J. Dauben, J. Ziebart, T. Bender, S. Zaatreh, B. Kreikemeyer, R. Bader, A Novel In Vitro System for Comparative Analyses of Bone Cells and Bacteria under Electrical Stimulation, Biomed Res. Int. 2016 (2016) 1 12, https://doi.org/10.1155/2016/5178640.
[19] C. Boehler, S. Carli, L. Fadiga, T. Stieglitz, M. Asplund, Tutorial: guidelines for standardized performance tests for electrodes intended for neural interfaces and bioelectronics, Nat. Protoc. 15 (11) (2020) 3557 3578, https://doi.org/10.1038/s41596-020-0389-2.

[20] U. van Rienen, J. Flehr, U. Schreiber, S. Schulze, U. Gimsa, W. Baumann, D. G. Weiss, J. Gimsa, R. Benecke, H.W. Pau, Electro-quasistatic simulations in bio-systems engineering and medical engineering, Adv. Radio Sci. 3 (2005) 39 49, https://doi.org/10.5194/ars-3-39-2005.
[21] H. Raben, P.W. Kämmerer, R. Bader, U. van Rienen, Establishment of a numerical model to design an electro-stimulating system for a porcine mandibular critical size defect, Appl. Sci. 9 (10). doi:10.3390/app9102160.
[22] D.R. Cantrell, S. Inayat, A. Taflove, R.S. Ruoff, J.B. Troy, Incorporation of the electrode-electrolyte interface into finite-element models of metal microelectrodes, J. Neural Eng. 5 (1) (2008) 54 67, https://doi.org/10.1088/1741-2560/5/1/006.
[23] P.C. Grunert, A. Jonitz-Heincke, Y. Su, R. Souffrant, D. Hansmann, H. Ewald, A. Krüger, W. Mittelmeier, R. Bader, Establishment of a Novel In Vitro Test Setup for Electric and Magnetic Stimulation of Human Osteoblasts, Cell Biochem. Biophys. 70 (2) (2014) 805 817, https://doi.org/10.1007/s12013-014-9984-6.
[24] B. Hiemer, J. Ziebart, A. Jonitz-Heincke, P.C. Grunert, Y. Su, D. Hansmann, R. Bader, Magnetically induced electrostimulation of human osteoblasts results in enhanced cell viability and osteogenic differentiation, Int. J. Mol. Med. 38 (1) (2016) 57 64, https://doi.org/10.3892/ijmm.2016.2590.
[25] F. Sahm, J. Ziebart, A. Jonitz-Heincke, D. Hansmann, T. Dauben, R. Bader, Alternating electric fields modify the function of human osteoblasts growing on and in the surroundings of titanium electrodes, Int. J. Mol. Sci. 21 (18) (2020) 1 13, https://doi.org/10.3390/ijms21186944.
[26] S. Krueger, S. Achilles, J. Zimmermann, T. Tischer, R. Bader, A. Jonitz-Heincke, Re-Differentiation Capacity of Human Chondrocytes in Vitro Following Electrical Stimulation with Capacitively Coupled Fields, J. Clin. Med. 8 (11) (2019) 1771, https://doi.org/10.3390/jcm8111771.
[27] M. Hronik-Tupaj, W.L. Rice, M. Cronin-Golomb, D.L. Kaplan, I. Georgakoudi, Osteoblastic differentiation and stress response of human mesenchymal stem cells exposed to alternating current electric fields, Biomed. Eng. Online 10 (1) (2011) 9, https://doi.org/10.1186/1475-925X-10-9.
[28] J. Schuderer, N. Kuster, Effect of the Meniscus at the Solid/Liquid Interface on the SAR Distribution in Petri Dishes and Flasks, Bioelectromagnetics 24 (2) (2003) 103 108, https://doi.org/10.1002/bem.10066.
[29] A. Richardot, E.T. McAdams, Harmonic analysis of low-frequency bioelectrode behavior, IEEE Trans. Med. Imaging 21 (6) (2002) 604 612, https://doi.org/10.1109/TMI.2002.800576.
[30] O.C. Zienkiewicz, J.Z. Zhu, A simple error estimator and adaptive procedure for practical engineerng analysis, Int. J. Numer. Methods Eng. 24 (2) (1987) 337 357, https://doi.org/10.1002/nme.1620240206.
[31] J. Schöberl, C 11 implementation of finite elements in NGSolve, Tech. Rep. ASC-2014-30. URL https://www.asc.tuwien.ac.at/ schoeberl/wiki/publications/ngs-cpp11.pdf.
[32] J. Schöberl, An advancing front 2D/3D-mesh generator based on abstract rules, Comput. Vis. Sci. 1 (1) (1997) 41 52, https://doi.org/10.1007/s007910050004.
[33] H.P. Schwan, Alternating current electrode polarization, Biophysik 3 (2) (1966) 181 201, https://doi.org/10.1007/BF01191612.
[34] E. Somersalo, M. Cheney, D. Isaacson, Existence and uniqueness for electrode models for electric current computed tomography, SIAM J. Appl. Math. 52 (4) (1992) 1023 1040, https://doi.org/10.1137/0152060.
[35] G. Brandstetter, S. Govindjee, A high-order immersed boundary discontinuous-Galerkin method for Poisson s equation with discontinuous coefficients and singular sources, Int. J. Numer. Methods Eng. 101 (11) (2015) 847 869, https://doi.org/10.1002/nme.4835.
[36] P.R. Amestoy, I.S. Duff, J.Y. L Excellent, J. Koster, A fully asynchronous multifrontal solver using distributed dynamic scheduling, SIAM Journal on Matrix Analysis and Applications 23 (1) (2002) 15 41, https://doi.org/10.1137/S0895479899358194.
[37] J. Brown, M.G. Knepley, D.A. May, L.C. McInnes, B. Smith, Composable linear solvers for multiphysics, in: Proceedings - 2012 11th International Symposium on Parallel and Distributed Computing, ISPDC 2012, IEEE, 2012, pp. 55 62. doi: 10.1109/ISPDC.2012.16.
[38] S. Balay, S. Abhyankar, M.F. Adams, J. Brown, P. Brune, K. Buschelman, L. Dalcin, A. Dener, V. Eijkhout, W.D. Gropp, D. Karpeyev, D. Kaushik, M.G. Knepley, D.A. May, L.C. McInnes, R.T. Mills, T. Munson, K. Rupp, P. Sanan, B.F. Smith, S. Zampini, H. Zhang, H. Zhang, PETSc Web page, https://www.mcs.anl.gov/petsc (2019). https://www.mcs.anl.gov/petsc.
[39] S. Balay, S. Abhyankar, M.F. Adams, J. Brown, P. Brune, K. Buschelman, L. Dalcin, A. Dener, V. Eijkhout, W.D. Gropp, D. Karpeyev, D. Kaushik, M.G. Knepley, D.A. May, L.C. McInnes, R.T. Mills, T. Munson, K. Rupp, P. Sanan, B.F. Smith, S. Zampini, H. Zhang, H. Zhang, PETSc users manual, Tech. Rep. ANL-95/11 - Revision 3.14, Argonne National Laboratory (2020). https://www.mcs.anl.gov/petsc.
[40] S. Balay, W.D. Gropp, L.C. McInnes, B.F. Smith, Efficient management of parallelism in object oriented numerical software libraries, in: E. Arge, A. M. Bruaset, H.P. Langtangen (Eds.), Modern Software Tools in Scientific Computing, Birkhäuser Press, 1997, pp. 163 202.
[41] J. Zimmermann, L. Thiele, j-zimmermann/impedancefitter: v2.0.2 (Jul. 2021). doi: 10.5281/zenodo.5116618. doi: 10.5281/zenodo.5116618.
[42] J.D. Hunter, Matplotlib: A 2d graphics environment, Computing in Science & Engineering 9 (3) (2007) 90 95, https://doi.org/10.1109/MCSE.2007.55.
[43] M. Clemens, M. Wilke, G. Benderskaya, H. De Gersem, W. Koch, T. Weiland, Transient electro-quasistatic adaptive simulation schemes, IEEE Trans. Magn. 40 (2) (2004) 1294 1297, https://doi.org/10.1109/TMAG.2004.824582.
[44] R.A. Gittens, R. Olivares-Navarrete, R. Tannenbaum, B.D. Boyan, Z. Schwartz, Electrical implications of corrosion for osseointegration of titanium implants, J. Dent. Res. 90 (12) (2011) 1389 1397, https://doi.org/10.1177/0022034511408428.
[45] T. Hanawa, M. Ota, Calcium phosphate naturally formed on titanium in electrolyte solution, Biomaterials 12 (8) (1991) 767 774, https://doi.org/10.1016/0142-9612(91)90028-9.
[46] R. Narayanan, S.K. Seshadri, T.Y. Kwon, K.H. Kim, Calcium phosphate-based coatings on titanium and its alloys, J. Biomed. Mater. Res. Part B Appl. Biomater. 85B (1) (2008) 279 299. doi:10.1002/jbm.b.30932.
[47] S. Abasi, J.R. Aggas, N. Venkatesh, I.G. Vallavanatt, A. Guiseppi-Elie, Design, fabrication and testing of an electrical cell stimulation and recording apparatus (ECSARA) for cells in electroculture, Biosens. Bioelectron. 147 (October 2019) (2020) 111793, https://doi.org/10.1016/j.bios.2019.111793.
[48] M.E. Orazem, B. Tribollet, Electrochemical impedance spectroscopy, 2nd Edition, The Electrochemical Society series, John Wiley & Sons Inc, Hoboken, New Jersey, 2017.
[49] M. Cemazar, G. Sersa, W. Frey, D. Miklavcic, J. Teissié, Recommendations and requirements for reporting on applications of electric pulse delivery for electroporation of biological samples, Bioelectrochemistry 122 (2018) 69 76, https://doi.org/10.1016/j.bioelechem.2018.03.005.
[50] J. Zimmermann, U. van Rienen, Ambiguity in the interpretation of the low-frequency dielectric properties of biological tissues, Bioelectrochemistry 140 (2021) 107773, https://doi.org/10.1016/j.bioelechem.2021.107773.
[51] N. Hlavac, D. Bousalis, R.N. Ahmad, E. m. Pallack, A. Vela, Y. Li, S. Mobini, E. Patrick, C.E.S chmidt, Effects of Varied Stimulation Parameters on Adipose-Derived Stem Cell Response to Low-Level Electrical Fields, Annals of Biomedical Engineeringdoi:10.1007/s10439-021-02875-z.
[52] D.R. Merrill, M. Bikson, J.G. Jefferys, Electrical stimulation of excitable tissue: Design of efficacious and safe protocols, J. Neurosci. Methods 141 (2) (2005) 171 198, https://doi.org/10.1016/j.jneumeth.2004.10.020.
[53] B. Onaral, H.P. Schwan, Linear and nonlinear properties of platinum electrode polarisation. Part 1: frequency dependence at very low frequencies, Med. Biol. Eng. Comput. 20 (3) (1982) 299 306. doi:10.1007/BF02442796.
[54] M. Moussavi, H.P. Schwan, H.H. Sun, Harmonic distorition caused by electrode polarisation, Med. Biol. Eng. Comput. 32 (2) (1994) 121 125, https://doi.org/10.1007/BF02518907.

9 Anhang

Manuelle Messung der Spannung

Um das elektrische Feld manuell zu messen, wurde die Elektrode in der 1 mm Konfiguration in das Well platziert und eine Spannung von 0,7 V_{eff} und 20 Hz angelegt. 5 ml Medium wurden in das Well gefüllt und unterhalb des Wells ein Raster platziert, welches zur Orientierung bei der Messung diente (Ergänzende Abb. 1A). Die Elektrode wurde mit einem Generator (Metrix 310) sowie einem Oszilloskop (Tektronix, TDS 2012B) verbunden. Der schematische Schaltplan ist der ergänzenden Abb. 1D zu entnehmen.

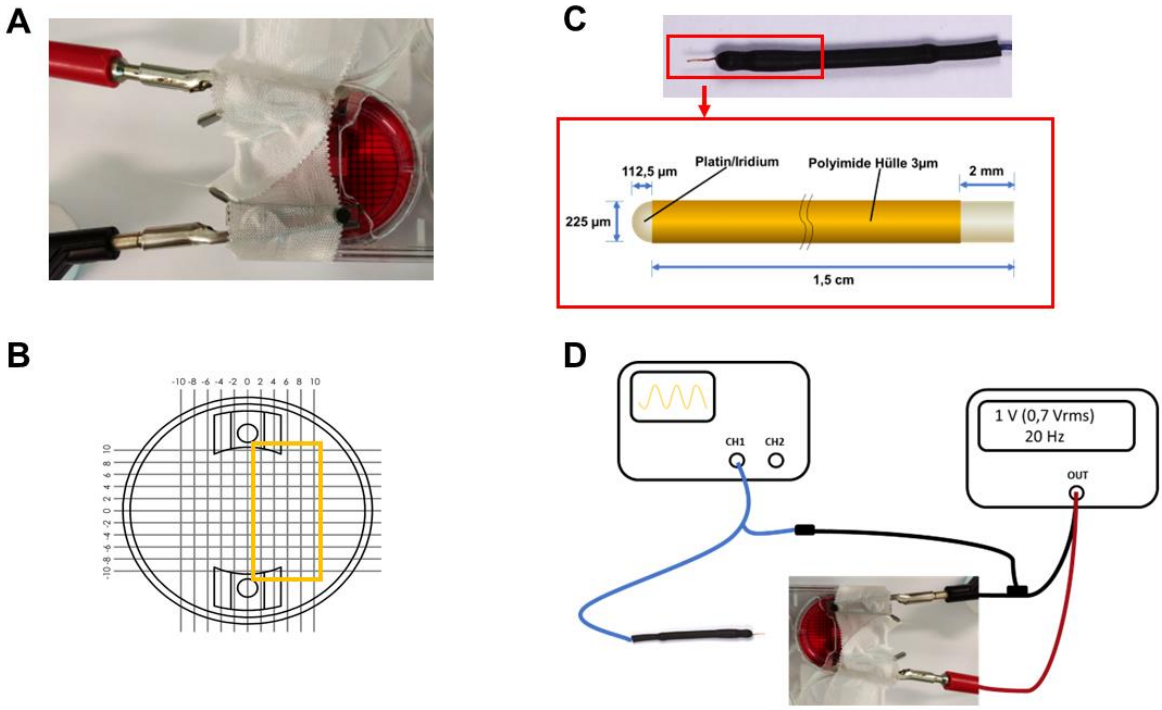

Ergänzende Abbildung 1: Manuelle Messung des Spannungsverteilung auf dem Boden einer Zellkulturplatte. (**A**) Elektrode in einem Well einer 6-Well-Platte mit Medium und Messraster, wobei an den Kontaktstäben der Elektrode Krokodilsklemmen befestigt wurden. (**B**) Messraster, welches unter ein Well der 6-Well Zellkultuplatte gelegt wurde. Orange umrahmt ist der Abschnitt, welcher manuell gemessen wurde. (**C**) Verwendete Messelektrode mit schematischer Darstellung und Abmessungen der Messelektrode. (**D**) Schematischer Messaufbau mit dem Funktionsgenerator, Oszilloskop, Messelektrode und Stimulationselektrode im 6-Well. Das Oszilloskop ist mit dem blauen Kabel zur Messelektrode und zur zum Erdungskabel (in schwarz) verbunden. Die Erdung (schwarz) erfolgt zwischen dem Funktionsgenerator, der Stimulationselektrode und der Messelektrode. Das rote Kabel verbindet die Messelektrode mit dem Funktionsgenerator.

Da die Elektrode symmetrisch aufgebaut ist, wurden die Spannungsmessungen nur auf einer Seite des Wellbodens durchgeführt. Es wurde ein Bereich von 10 mm x 8 mm mit Messpunkten alle 2 mm neben der Elektrode gemessen (ergänzende Abb. 1B). Als Messelektrode wurde eine monopolare, speziell angefertigte Platin/Iridium Elektrode verwendet (Microprobes, Gaithersburg, MD, Vereinigte Staaten) (ergänzende Abb. 1C). Insgesamt wurden 9 Messungen bei Raumtemperatur durchgeführt und dabei wurden die Frequenz, V_{ss} und V_{eff} und die

Sinuskurve zu jedem Messpunkt aufgenommen. Der Mittelwert der gemessenen Spannungen an jedem Punkt wurde bestimmt. Durch den Abstand von 2 mm war es möglich, ein elektrisches Feld zu berechnen.

Abkürzungsverzeichnis

%	Prozent
°C	Grad Celsius
µm	Mikrometer
3D	Drei Dimensional
ACP5	Tartratresistente saure Phosphatase Typ 5b
ALPL	Alkalische Phosphatase (Gen)
CA2	Caboanhydrase II
Ca^{2+}	Calcium-Ionen
$CaCl_2$	Calciumchlorid
CASP8	Caspase-8
cDNA	komplementäre Desoxyribonukleinsäure
CICP	Typ I C-terminal Collagen Propeptide
cm	Zentimeter
CO_2	Kohlenstoffdioxid
COL1A1	Collagen Type I Alpha 1 Kette
CSF1R	Colony stimulating factor 1 receptor
CTSK	Cathepsin K
d	Tag
DKK-1	Dickkopf-verwandtes Protein 1
ELISA	Enzyme-linked Immunosorbent Assay
ES	Elektrische Stimulation
ESO	Elektrisch stimulierte Osteoblasten
GO	Gene Ontology
GPCR	G-Protein-gekoppelten Rezeptoren
h	Stunde
HEF	High electrical field – hohes elektrisches Feld
Hz	Herz
IL-6	Interleukin-6
l	Liter
LEF	Low electrical field – niedriges elektrisches Feld
M-CSF	Macrophage colony-stimulating factor
MCP1	Monocyte chemoattractant protein 1
m	Meter
min	Minute
ml	Milliliter
mm	Millimeter
mM	Millimolar
MMP-9	Matrix Metallopeptidase 9
ng	Nanogramm
nm	Nanometer

nM	Nanomolar
NSO	nicht elektrisch stimulierte Osteoblasten
O_2	Sauerstoff
OPG	Osteoprotegerin
OPN	Osteopontin
PBMCs	Mononukleäre Zellen des peripheren Blutes
qPCR	quantitative Echtzeit Polymerase-Kettenreaktion
RANK	Receptor activator of NF-κB
RANKL	Receptor activator of NF-κB ligand
RNA	Desoxyribonukleinsäure
Rz	Rautiefe
Ti6Al4V	Titan-Aluminium-Vanadium
V	Volt
V_{SS}	Volt Spitze Spitze
V_{eff}	Volt Effektivwert
WST-1	Wasserlösliches Tetrazoliumsalz
ΔΔCt	delta-delta Cycle of Threshold

Danksagung

Ich möchte mich bei den verschiedenen Menschen bedanken, die mich in der Zeit meiner Promotion begleitet und unterstützt haben.
Zunächst bedanke ich mich bei Frau PD Dr. rer. hum. habil. Dipl. Biol. Anika Jonitz-Heincke und Herrn Prof. Dr. med. Dipl.-Ing. Rainer Bader für die Chance, dieses interessante Projekt in dem Forschungslabor für Biomechanik und Implantattechnologie zu bearbeiten und für die Begleitung während dieses Projektes. Die gemeinsamen konstruktiven Besprechungen sowie hilfreichen Vorschläge leiteten mich durch meine Promotionszeit. Besonderer Dank gilt dabei meiner Doktormutter Frau PD Dr. rer. hum. habil. Dipl. Biol. Jonitz-Heincke für ihre konstante Betreuung, die wissenschaftliche Anleitung und wertvolle Unterstützung bei allen Fragestellungen in den letzten Jahren.
Weiterhin möchte ich Dr.-Ing. Rainer Detsch und Thomas Kreller für ihre Kooperationsarbeit und den Austausch danken. Die Zusammenarbeit mit dem Department Werkstoffwissenschaften der Friedrich-Alexander-Universität hat essentiell zu dem Erfolg dieser Arbeit beigetragen. Ich danke Herrn Dr.-Ing. Rainer Detsch zudem für die hilfreichen Ratschläge und die Zusammenarbeit in der Endphase meiner Promotion.
Besonders möchte ich mich auch bei allen Mitarbeitern des Forbiomits bedanken. Ein großer Dank gilt dabei Frau Simone Krüger, die durch Gespräche, den aktiven Austausch von Ideen und Problemstellungen, und durch die Kontakte zum Sonderforschungsbereiches 1270 – ELAINE zu meiner fachlichen sowie persönlichen Weiterentwicklung beigetragen hat. Ebenso danke ich Frau Doris Hansmann, welche immer mit Rat und Tat für ein gutes Gelingen der Experimente zur Seite stand und Herrn Mario Jackszis für seine Unterstützung und Ideen in allen technischen Fragestellungen. Auch gilt mein Dank Frau Vivica Freiin Grote und Frau Ana Jakovljevic für ihre Beiträge während ihren Abschlussarbeiten bzw. Tätigkeiten als wissenschaftliche Hilfskräfte.
Ferner möchte ich mich bei Dr. Julius Zimmermann, Nils Arbeiter und Henning Bathel aus dem Institut für allgemeine Elektrotechnik bedanken, die bei Messungen und physikalischen Fragestellungen immer geholfen haben. Besonderer Dank gilt Dr. Julius Zimmermann für die intensive Zusammenarbeit und das Anfertigen der numerischen Simulationen. Ebenso bedanke ich mich bei Dr. Ingo Barke aus der Gruppe Oberflächen- und Grenzflächenphysik für die Unterstützung bei dem Umbau und Programmierung des automatischen 3D-Messsystems. Dank gilt auch Dr.-Ing. Fiete Haack aus dem Lehrstuhl für Modellierung und Simulation für die Auswertung der Transkriptomanalyse.
Zuletzt möchte ich mich bei meiner Familie, meine Eltern und meinen Geschwistern sowie bei meinen Freunden für ihre Unterstützung in den letzten Jahren bedanken. Sie haben mich stets auf meinem Weg unterstützt und mir in schweren Zeiten den Rücken gestärkt. Besonders möchte ich mich bei meinem Lebenspartner Peter Stange bedanken für seinen konstanten

Beistand, Hilfe und seine Zuversicht, dass ich diese Promotion und alle Hürden auf dem Weg dahin bewältigen werde.

Selbstständigkeitserklärung

Ich versichere hiermit, dass ich die vorliegende Dissertation mit dem Thema: „Untersuchungen zu den Einflüssen von niederfrequenten elektrischen Wechselfelder auf die Differenzierung humaner Osteoblasten und dessen indirekter Effekt auf die Osteoklastogenese“ selbstständig verfasst und keine anderen Hilfsmittel als die angegebenen benutzt habe. Die Stellen, die anderen Werken dem Wortlaut oder dem Sinn nach entnommen sind, habe ich in jedem einzelnen Fall durch Angabe der Quelle kenntlich gemacht. Ich erkläre hiermit weiterhin, dass ich meine wissenschaftlichen Arbeiten nach den Prinzipien der guten wissenschaftlichen Praxis gemäß der gültigen "Regeln zur Sicherung guter wissenschaftlicher Praxis und zur Vermeidung wissenschaftlichen Fehlverhaltens" an der Universität Rostock angefertigt habe.

Rostock, 09.02.2023

Unterschrift: ……..
(Franziska Sahm)